Integrated motions of light driven molecular motors at macroscopic scale

Quan Li

UNIVERSITÉ DE STRASBOURG

THÈSE

présentée pour obtenir le grade de

DOCTEUR de l'UNIVERSITÉ DE STRASBOURG

Discipline : Chimie

Par

Quan Li

Integrated motions of light driven molecular motors at macroscopic scale

Soutenue publiquement le 03 Février 2015 devant le jury composé de:

Professeur Ludovic Jullien (CNRS UMR 8640, Ecole Normale Supérieure, Paris)-Rapporteur

Professeur Patrice Woisel (CNRS UMR 8207- Université Lille 1)-Rapporteur

Professeur Jean-Pierre Sauvage (ISIS UMR 7006-CNRS, Université de Strasbourg)-Examinateur

Professeur Nicolas Giuseppone(ICS, Université de Strasbourg, Strasbourg)-Directeur de thèse

Table of Contents

Abstract in English

Molecular motors in nature such as ATP synthase, myosin, kinesin and dynein can convert conformational changes, due to chemical energy input, into directed motion for catalysis and transport. A limited number of artificial molecules which may mimic these natural motors have been synthesized during the last three decades.[1] Among these fully synthetic motors, light driven rotary motors designed by Feringa *et al* have shown high performance at the molecular level.[2]

Despite last two decades have witnessed this motor's improvements, many challenges still exist. In particular, the integration of such motors in a collective system to amplify and make use of their motions at macroscopic scale remains unachieved and this has been the focus of this PhD work.

Inspired by Feringa's work, particularly by the development of a second generation of light-driven motors which can rotate with high frequencies, we have synthesized a highly functionalized motor with different functional groups in its upper and lower part, in order to make it more versatile towards polymer modifications and targeted applications (Schemes A1, A2 and A3). Importantly, this motor can be obtained for the first time on gram scale in its enantiopure form. With the help of single X-ray diffraction techniques, the stereochemistry of key compounds **15**, **1** and **18** was assigned unambiguously (Figure A1).

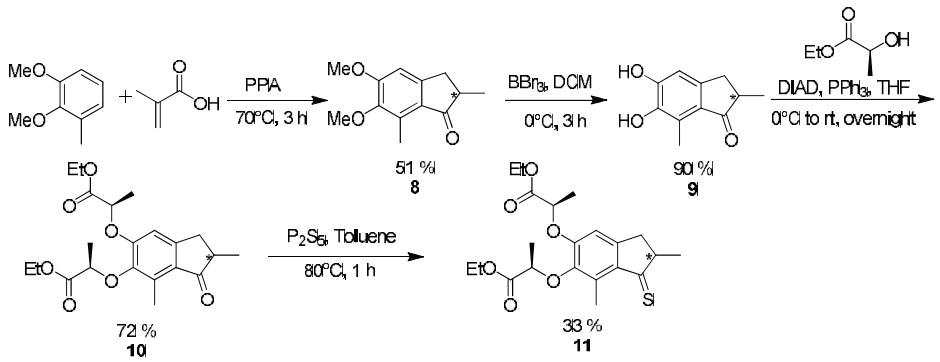

Scheme A1 | Synthesis of diastereoisomers of **11** constituting the upper part of the motor unit

[1] E. R. Kay.; D. A. Leigh.; F. Zerbetto. Synthetic molecular motors and mechanical machines. *Angew. Chem. Int. Ed.*, **46**, 72-191 (2007).
[2] W. R. Brown.; B. L. Feringa. Making molecular machines work. *Nat. Nanotechnol.* **1**, 25-35 (2006).

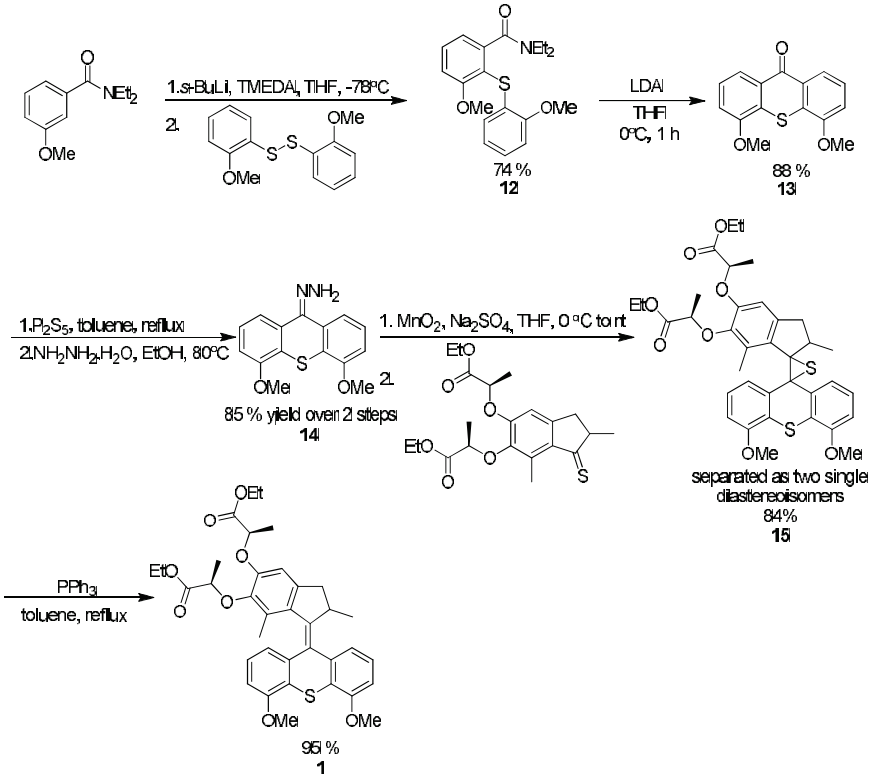

Scheme A2 | Synthesis of methoxy protected motor **1**

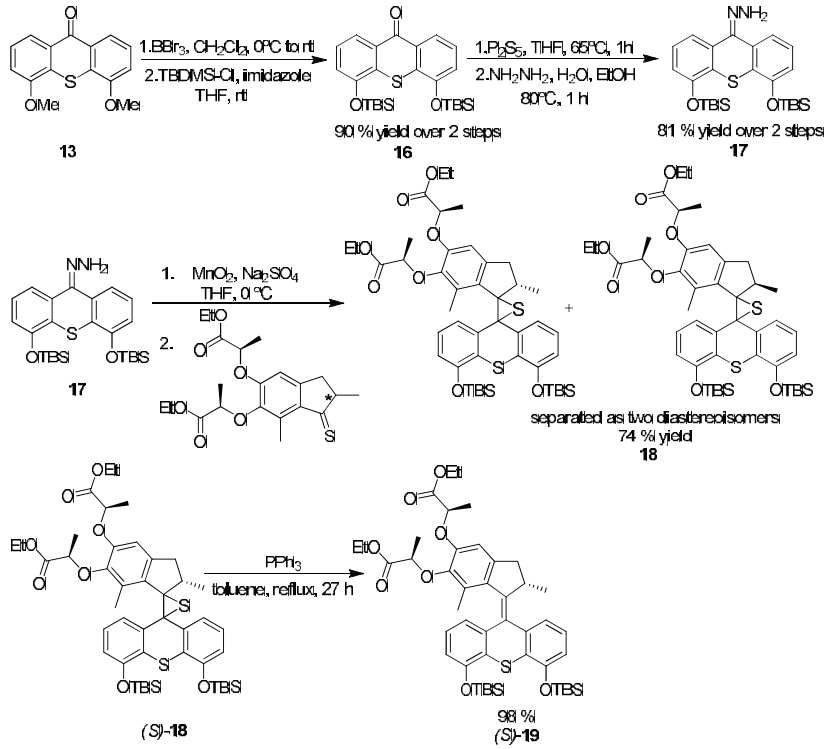

Scheme A3 | Synthesis of enantiopure TBS protected motor **19**

We further integrated this motor into several kinds of entangled polymer systems. First, "8" shaped macrocyclic motor-polymer conjugates were produced by using a very efficient Cu-catalyzed azide-alkyne cycloaddition (CuAAC) under highly diluted conditions (Figure A1). Their structures were clearly evidenced by ^{1}H NMR, AFM, SAXS experiments (Figure A2). Upon UV irradiation, the morphology and dimension of those macrocyclic polymers were changed towards collapsed (spherical or more elongated) coils with smaller radius of gyration values (R_g), indicating the polymer chains were entangled by the rotating motion of the motor (Figure A2c and A2e).

Then, following the same CuAAC reaction but under more concentrated conditions, a gel-like motor-polymer conjugate system was prepared (Figure A1). This gel demonstrated strong macroscopic contracting properties upon UV irradiation. The contracting process was characterized both at macroscopic scale by a digital recording camera (Figure A3), and at microscopic scale by AFM and SAXS techniques (Figure A4). With the UV light energy input, the individual motions from single molecular motor at nanoscale were integrated and amplified to generate macroscopic contractions.

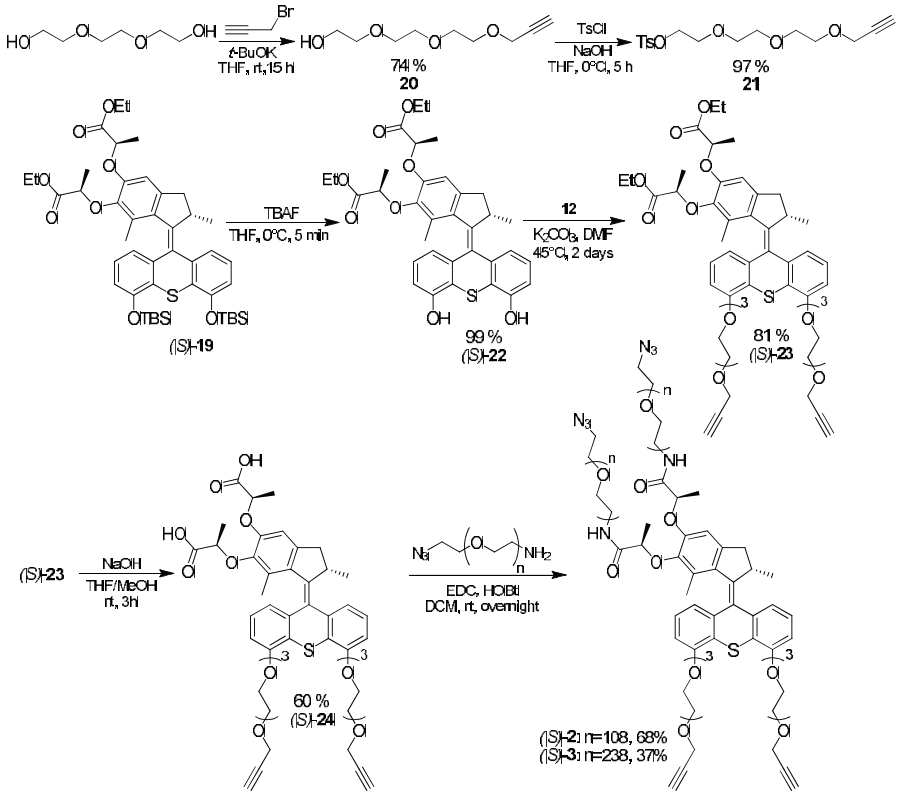

Scheme A4 | Synthesis of motor-polymer conjugates **2** and **3**

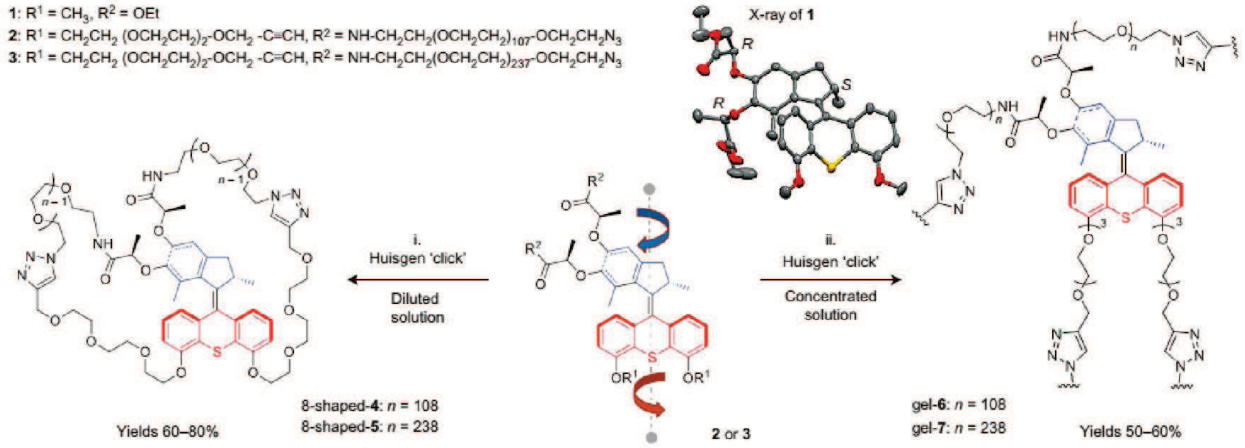

Figure A1 | General chemical design to access enantiopure polymer-motor conjugates. Key molecular motor intermediates **2** or **3** can be engaged either (*i*) in a double intramolecular "click" cyclisation catalyzed by Cu(I) yielding 8-shaped compounds **4** and **5** which incorporate the rotary unit in their cores; or (*ii*) in a intermolecular "click" cross-linkage catalyzed by Cu(I) to yield chemical gels **6** and **7** which incorporate rotary units as mechanically active reticulating nodes.

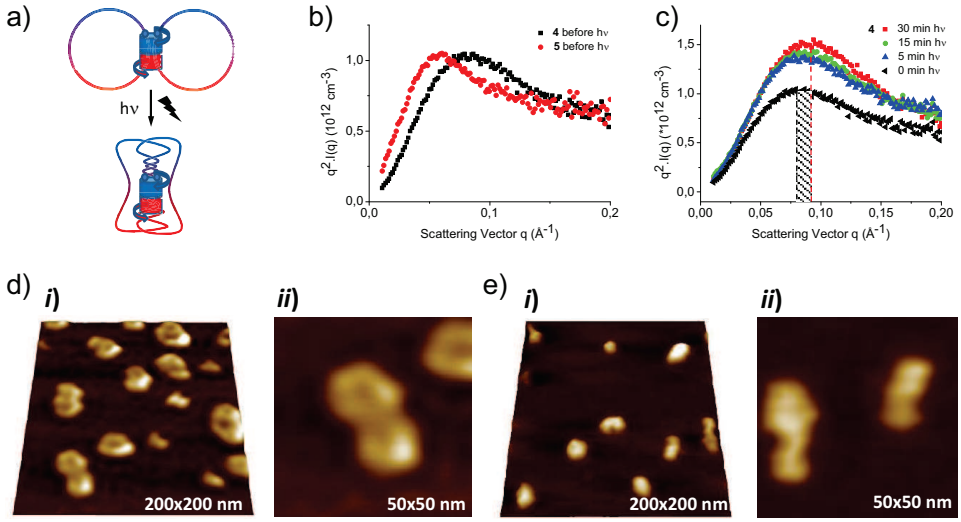

Figure A2 | Characterization of mechanically active 8-shaped polymer-motor conjugates. **a)** Schematic representation of an 8-shaped polymer-motor conjugate which, due to its self-entangled topology, coils up the rings and reduces its size upon light-activated rotation. **b)** Kratky plot representation of the scattered intensities of 8-shaped compounds **4** and **5** ($c = 10^{-2}$ g·cm^{-3} in toluene) before light irradiation. **c)** Kratky plot representation of the scattered intensities of 8-shaped compound **4** upon light irradiation. **d)** AFM images of isolated uncoiled 8-shaped **5** on a mica surface before light irradiation. **e)** AFM images of isolated coiled 8-shaped **5** on a mica surface after 15 minutes of light irradiation.

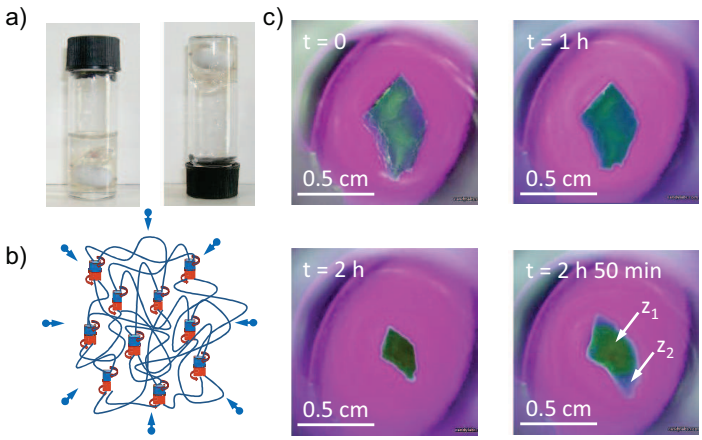

Figure A3 | Macroscopic behaviour of a mechanically active gel based on a chemically cross-linked polymer-motor conjugate system. **a)** Gel **6** at 10% w/w in toluene. **b)** Schematic representation of a cross-linked polymer-motor conjugate which, due to its mechanically active entangled topology, coils up the polymer chains and reduces the entire size of the network upon light-activated rotation. **c)** Snapshots taken from a movie (see Supplementary Information) showing time-dependent macroscopic contraction of a piece of gel **6** immersed in toluene and upon UV light irradiation. At t= 2 h 50 min, z_1 corresponds to a region still contracted and z_2 corresponds to a region which starts disrupting.

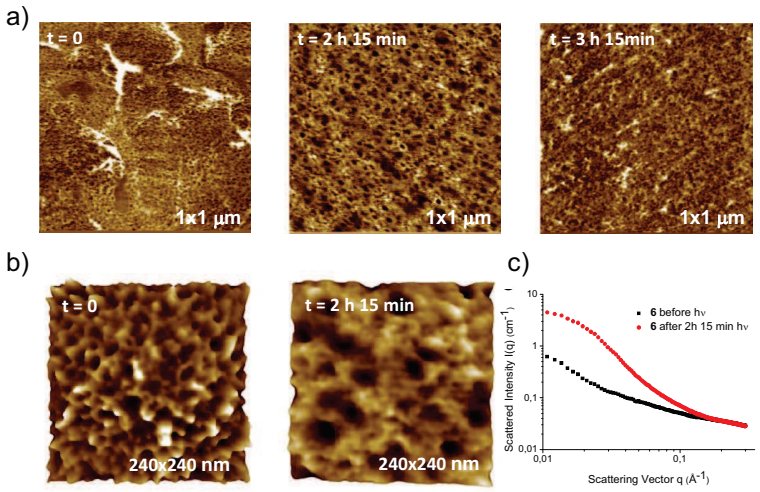

Figure A4 | Micro- and nanoscopic characterizations of mechanically active gels based on chemically cross-linked polymer-motor conjugates. **a)** AFM images of gel **6** submitted to different UV light irradiation times: before contraction (t = 0), after contraction (t = 2 h 15min), and after rupture (t = 3 h 15 min). **b)** Detailed AFM images before and after contraction of gel **6** upon UV light irradiation, showing an increase of the average pore sizes from 8 nm to 20 nm. **c)** SAXS data obtained before and after irradiation of gel **6**.

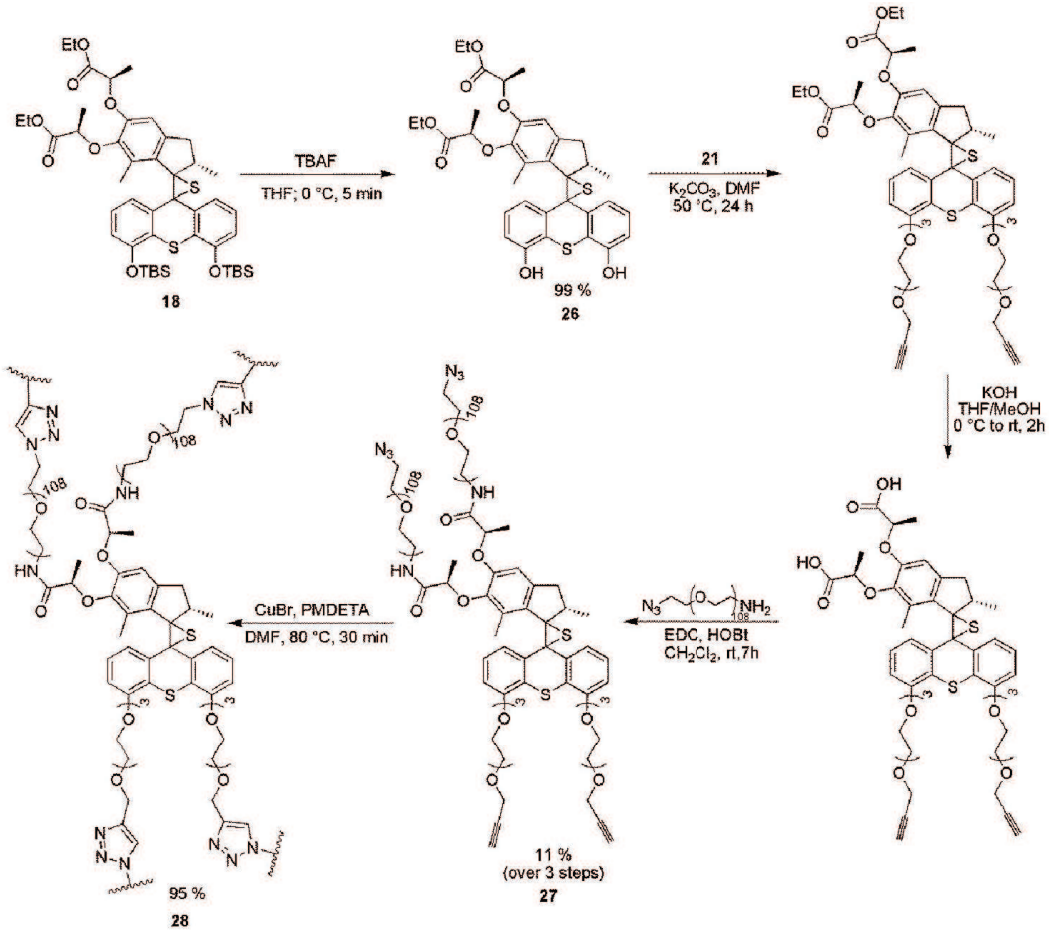

Scheme A5 | Synthesis of non-motor gel for control experiment

To verify the gel contraction was indeed due to the rotation of a motor in which the central double bond plays a key role, we then synthesized a similar gel but without the function of motor for control experiment (Scheme A5). Since the central double bond was essential for the rotation of motor, its episulfide version should not rotate due to the central sulfur bridge. Upon UV irradiation, no significant contraction was observed even after long irradiation time, proving that the gel contraction originates from the rotation of the motor.

To gain more insight into the motor's rotation dynamics and mechanism, density functional theory (DFT) was used to calculate the transition state for the rate limiting thermal helix inversion step. As indicated in Figure A5, the free motor has a $\Delta G^{\neq}_{free}$=31.9 kJ/mol for transition state when the unstable form undergoes thermal helix inversion to stable form. This $\Delta G^{\neq}_{free}$ corresponds to a $t_{1/2}$=43 ns and a frequency of 8.05 MHz for motor's rotation at 25 ˚C. For gel **6** in which the motor is bound to polymer, $\Delta G^{\neq}$ value increased to 81.5 kJ/mol. This value was estimated from a simplified physical model as well as by plotting the contraction volume with the irradiation time (Figure A6). It was shown that the

maximum frequency for the motor' rotation in gel **6** was 3.16×10^{-2} Hz which corresponds a $t_{1/2}$=22 s at 25 ˚C for the thermal helix inversion step.

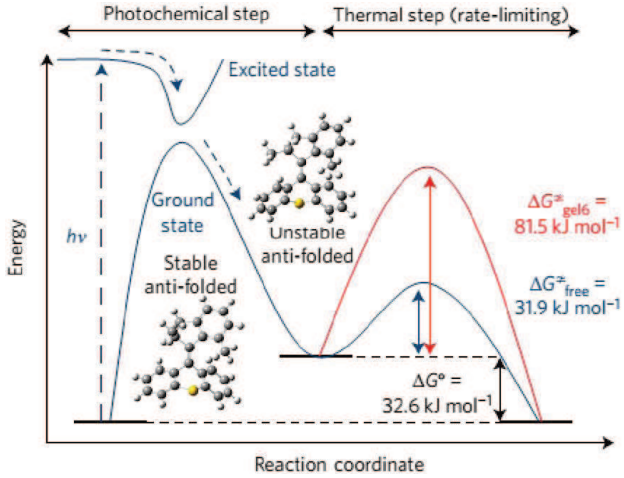

Figure A5 | Energy profile along the reaction coordinate for non-substituted free motor (model compound) obtained by DFT calculation (deep blue curve); The red curve shows the increase of the transition state in the gel by 50 kJ/mol for the rate determining thermal step.

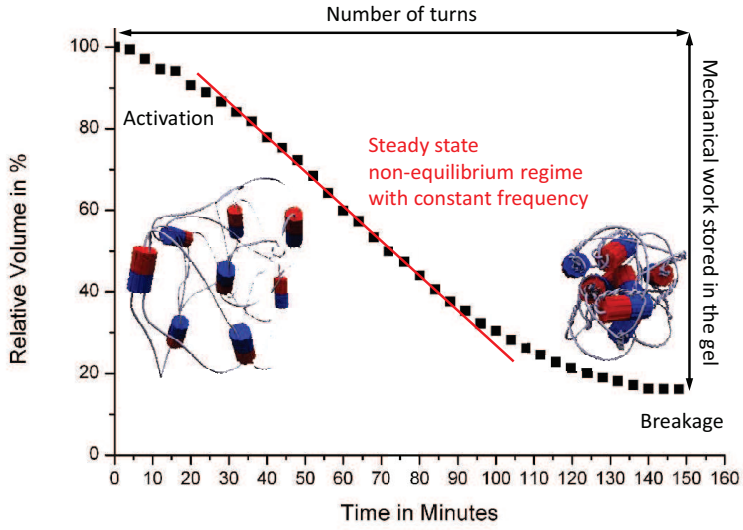

Figure A6 | Overview of the gel contraction percentage as a function of irradiation time.

In summary, we have successfully synthesized highly functionalized and enantiopure rotary molecular motors on gram scale through state of the art organic synthetic strategies. Our synthetic route is expected to be applicable to many light driven molecular motors with a straightforward access to large amount of enantiopure materials.

After this unit was coupled to entangled polymer chains as reticulating points, our results demonstrated for the first time that the unidirectional rotations of molecular motors fuelled by light are

able to perform useful work from nanoscale to macroscopic scale by operating together in a fully integrated system. We demonstrated that the motions of molecular motor could be amplified from nanometers to centimeters with 8 orders of magnitude.

Unlike other materials based on switch type machines which works only stepwise by multi-stimulus and only between two thermodynamic minima states, our motor-containing system can work continuously far from equilibrium in a metastable material by using just a single energy input. It is also able to perform a useful work in an isotropic system in the presence of Brownian motion, something impossible for switches as described up to now. In addition, in such twisted polymer chains, the energy from UV light can be stored in the gel via the motor's rotation which gives unique properties to this material.[3]

[3] Q. Li.; G. Fuks.; E. Moulin.; M. Maaloum.; M. Rawiso.; I. Kulic.; J. T. Foy.; N. Giuseppone. Macroscopic contraction of a gel induced by the integrated motion of light-driven molecular motors. *Nat. Nanotechnol*. **10**, 161-165 (2015).

Résumé en Français

Dans les organismes vivants, des moteurs moléculaires tels que la myosine et la kinésine sont capables en consommant de l'énergie chimique de convertir des changements de conformations en mouvement dirigé afin de transporter des vésicules, des organelles… Ces trente dernières années, des chercheurs ont essayé de synthétiser des molécules capables de mimer les mouvements de ces moteurs naturels.[1] Parmi ces moteurs moléculaires synthétisés, les moteurs rotatifs unidirectionnels consommant de l'énergie sous forme de lumière décrits par le groupe du Professeur Feringa se sont révélés être très prometteurs en vue d'applications futures.

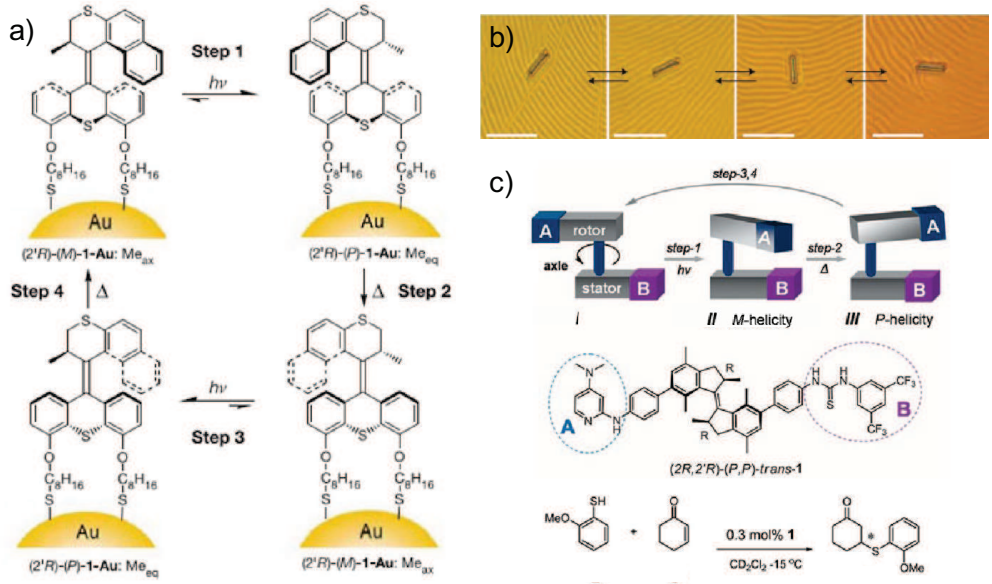

Figure A1 | (a) Un moteur moléculaire seconde génération greffé sur la surface de nanoparticules d'or. (b) Rotation d'un batônnet de verre micrométrique sur un cristal liquid dope par un moteur seconde génération sous l'effet d'une irradiation UV. Barre d'échelle: 50 µm. (c) Une réaction d'addition de Michael assymétrique catalysée par un catalyseur bifonctionnel couple à un moteur moléculaire rotatif.

Jusqu'à présent, deux générations de ces moteurs ont été synthétisées avec notamment des fréquences de rotation qui peuvent atteindre 3 MHz à température ambiante.[2] L'équipe de Feringa a montré qu'il était possible d'immobiliser des moteurs sur des surfaces sans compromettre le mouvement de rotation ce qui représente une étape cruciale dans l'optique d'une application macroscopique des

[1] W. R. Brown.; B. L. Feringa. Making molecular machines work. *Nat. Nanotechnol.* **1**, 25-35 (2006).
[2] M. Klok.; N. Boyle.; M. T. Pryce.; A. Meetsma.; W. R. Browne.; B. L. Feringa. MHz unidirectional rotation of molecular rotary motors. *J. Am. Chem. Soc*. **130**, 10484-10485 (2008).

moteurs (Figure A1a). [3] Il a également été démontré que ces moteurs étaient en mesure d'induire le mouvement unidirectionnel d'un bâtonnet de verre microscopique placé sur un film de type cristal liquide (Figure A1b).[4] De plus, en couplant un catalyseur bifonctionnel à un moteur moléculaire rotatif, cette équipe a montré qu'il était possible de catalyser une réaction assymétrique de Michael de manière dynamique(Figure A1c).[5] En effet, au cours d'un cycle de rotation de l'unité rotative, les sites catalytiques se positionnent de manière à favoriser la formation soit d'un mélange racémique, soit d'un énantiomère ou de l'autre. Malgré les innovations majeures développées pendant ces deux dernières décennies sur ces moteurs moléculaires rotatifs unidirectionnels, de nombreux défis restent à relever dans ce domaine.

En premier lieu, la synthèse de ces moteurs à grande échelle n'a encore jamais été réalisée. Le caractère unidirectionnel de la rotation des moteurs est garanti par la pureté énantiomérique de ces derniers. Or, il est bien difficile de préparer de grandes quantités de moteurs énantiopurs car il faut soit avoir recours à des techniques de chromatographie chirale, soit utiliser des voies de synthèse énantiosélectives. Enfin, afin de relever le défi majeur qu'est l'intégration de moteurs rotatifs afin d'obtenir une réponse macroscopique, il est nécessaire d'être en mesure de les fonctionnaliser de manière orthogonale afin de pouvoir coupler de nombreux moteurs. Nous avons donc développé une nouvelle voie de synthèse de moteur moléculaire basés sur les voies de synthèse décrites par l'équipe du Pr. Feringa[6,7]. L'étape clé de cette synthèse est le passage du composé **9** au composé **10** (Schéma A1). Lors de cette étape, un ester énantiomériquement pur est additionné via une réaction de Mitsunobu. Grâce au greffage de cette partie chirale, le couplage des composés **11** et **14**, **17** via une réaction de Barton-Kellog conduit à la formation de deux diastéréoisomères (sans l'ester chiral, un mélange d'énantiomères serait obtenu) qui peuvent être séparés par des techniques de chromatographie classique à l'échelle du gramme (Schéma A2, A3).

[3] R. A. van Delden.; M. K. J. ter Wiel.; M. M. Pollard.; J. Vicario.; N. Koumura.; B. L. Feringa. Unidirectional molecular motor on a gold surface. *Nature* **437**, 1337-1340 (2005).
[4] J. Vicario.; N. Katsonis.; B. S. Ramon.; C. W. M. Bastiaansen.; D. J. Broer.; B. L. Feringa. Nanomotor rotates microscale objects. *Nature* **440**, 163 (2006).
[5] J. B. Wang.; B. L. Feringa. Dynamic control of chiral space in a catalytic asymmetric reaction using a molecular motor. *Science* **331**, 1429-1432 (2011).
[6] G. London.; G. T. Carroll.; T. F. Landaluce.; M. M. Pollard.; P. Rudolf.; B. L. Feringa. Light-driven altitudinal molecular motors on surfaces. *Chem. Commun.*, 1712-1714 (2009).
[7] M. M. Pollard.; M. K. J. ter Wiel.; R. A. van Delden.; J. Vicario.; N. Koumura.; C. R. van den Brom.; A. Meetsma.; B. L. Feringa. Light-driven rotary molecular motors on gold nanoparticles. *Chem. Eur. J.* **14**, 11610-11622 (2008).

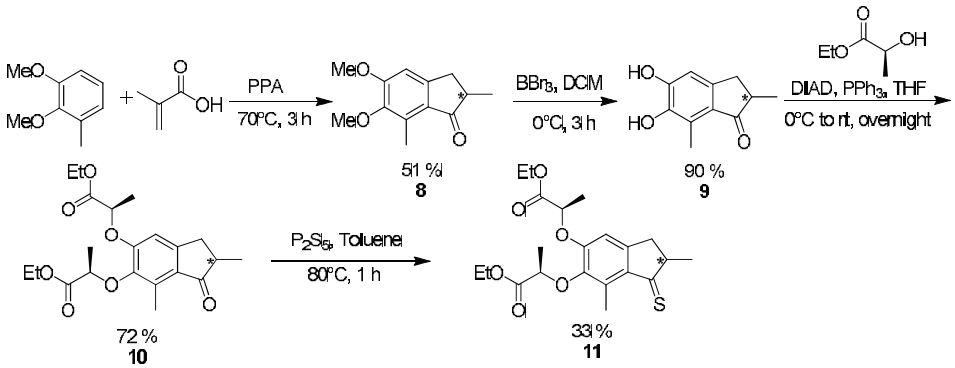

Schéma A1 | Synthèse de la partie haute du moteur

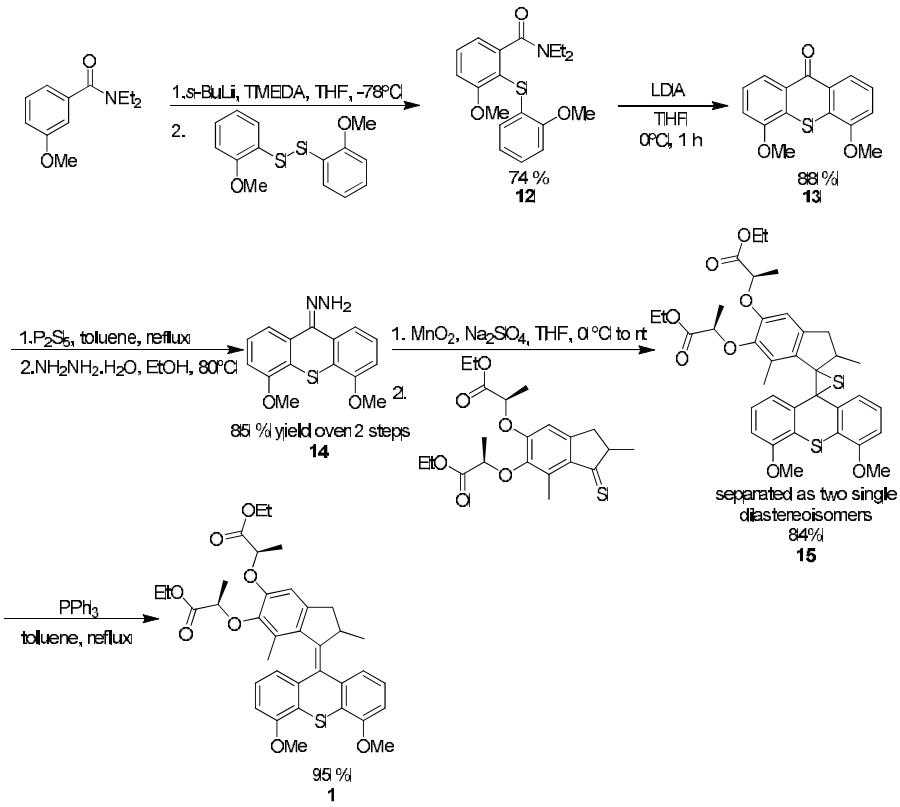

Schéma A2 | Synthèse du moteur protégé par des groupes -OMe

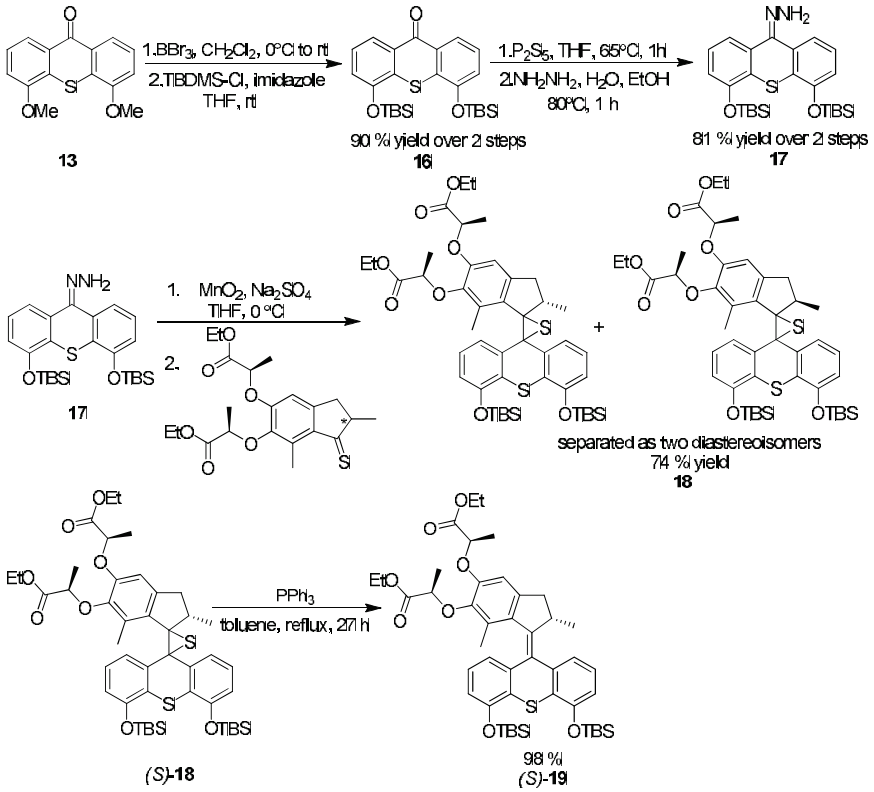

Schéma A3 | Synthèse du moteur protégé par des groupes TBS

Une fois la synthèse réalisée, nous avons greffé des chaines de PEG (Polyethylene glycol) aux moteurs afin de pouvoir coupler les unités rotatives de deux manières distinctes (Figure A2). La première approche a consisté en une cyclisation intramoléculaire à haute dilution via une cycloaddition de Huisgen résultant en l'obtention d'un macrocycle de la forme du chiffre 8. La seconde approche consiste elle en la formation d'un gel par couplage intermoléculaire à haute concentration des moteurs fonctionnalisés. Ensuite, l'effet de la rotation des moteurs a été étudié sur ces deux systèmes grâce à des analyses par diffusion des rayons X aux petits angles puis à de la microscopie à force atomique.

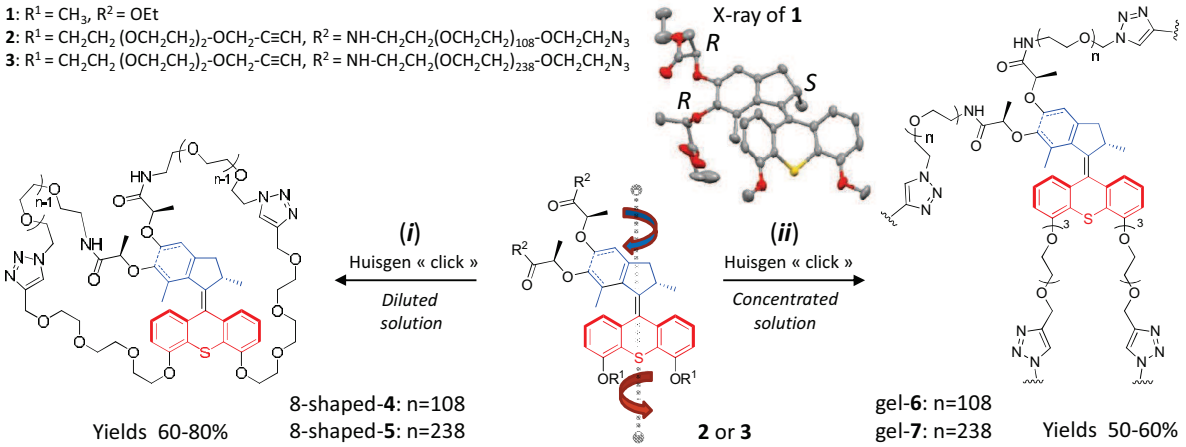

Figure A2 | Voie d'accès générale aux conjugués moteur polymers énantiopures. Les intermédiaires clé **2** or **3** peuvent être engages soit (*i*) dans une double reaction "click" intramoléculaire catalysée par du Cu(I) menant aux composes à forme de 8 **4** et **5** comprenant une unité rotative en leur coeur; ou (*ii*) dans une réaction de réticulation « click » intermoléculaire catalysée par du Cu(I) menant aux gels chimiques **6** et **7** qui contiennent des unités rotatives mécaniquement actives aux points de réticulation des gels.

Dans le premier cas, suite à une irradiation dans le domaine de l'UV (λ=365 nm), l'AFM a permis d'observer que la morphologie ainsi que les dimensions des macrocycles à forme de 8 avaient évolué significativement vers des pelotes agrégées avec des rayons de gyration diminués résultant de l'enroulement des chaines de polymère autour des unités rotatives (Figure A3). Les études par diffusion des rayons X aux petits angles ont également permis de mettre en évidence la diminution des rayons de gyration ainsi que l'augmentation de la densité interne du polymère résultant de l'enroulement des chaines de polymères pendant la rotation du moteur moléculaire.

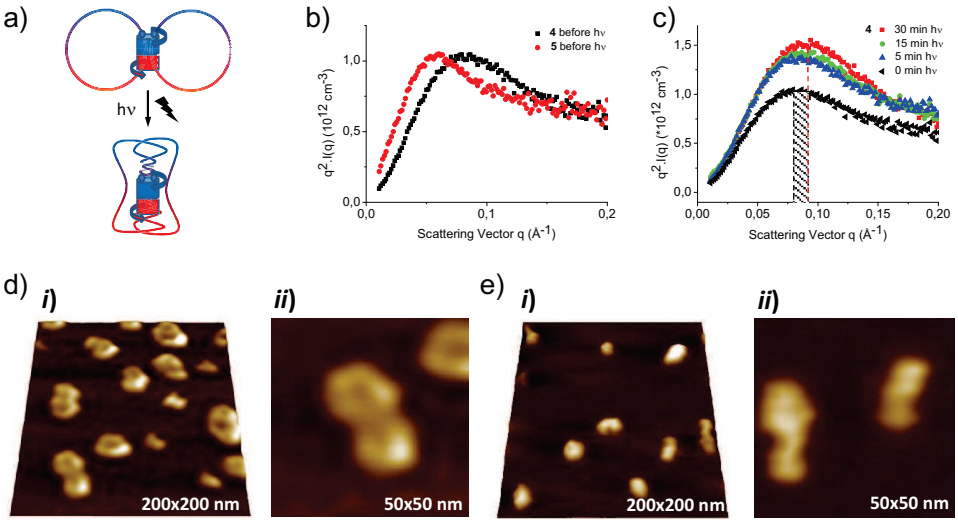

Figure A3 | Caractérisation des conjugués moteur-polymère en forme de 8. **a)** Représentation schématique d'un conjugué en forme de 8 dont la taille caractéristique diminue suite à

l'enchevêtrement des chaines induit par la rotation des moteurs sous UV. **b)** Représentation de Kratky des intensités diffusées par les conjugués **4** et **5** (PEG 5000 et 10000 respectivement, c = 10^{-2} g.cm^{-3} dans le toluène) avant irradiation UV. **c**) Représentation de Kratky des intensités diffusées par le conjugué **4** (PEG 5000, c = 10^{-2} g.cm^{-3} dans le toluène) au cours d'une irradiation UV. **d)** Images AFM du conjugué **4** isolé avant irradiation. **e)** Images AFM du conjugué **4** isolé après 15 minutes d'irradiation UV.

Dans le second cas, une réaction de cycloaddition de Huisgen « click » en milieu concentré a mené à la formation d'un gel chimique de PEG dont les points de réticulation sont des unités rotatives. En soumettant ce gel à de la lumière UV, une contraction macroscopique du gel a pu être visualisée à l'échelle macroscopique grâce à une caméra USB (Figure A4).

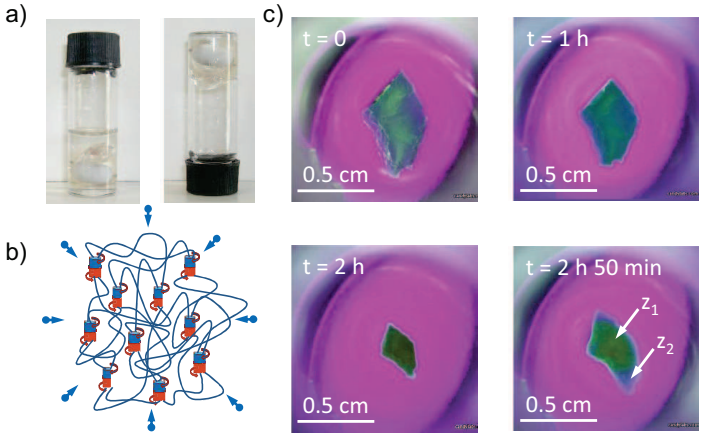

Figure A4 I Comportement macroscopique d'un gel comprenant des unités rotatives aux points de réticulation. **a**) Photos du gel **6** (PEG 5000) à 10% dans le toluène. **b**) Représentation schématique du gel comprenant des moteurs moléculaires aux points de réticulation ; à cause de sa topologie, ce dernier enroule les chaines de polymère et réduit considérablement la taille du réseau suite à la rotation des moteurs sous irradiation UV. **c**) Instantanés tirés d'une vidéo montant la contaction macroscopique du gel **6** (PEG 5000) immergé dans le toluène sous irradiation UV. A t= 2 h 50 min, z_1 correspond à une region en core contractée tandis que z_2 correspond à une region qui commence à éclater.

En effet, après 2 heures d'irradiation UV le volume du gel représente 20% du volume initial du gel. Pour la première fois, des moteurs moléculaires ont été couplés et leur mouvement a été amplifié afin d'être visualisable à l'échelle macroscopique. Après la contraction, le gel retrouve rapidement sa forme initiale. Ce phénomène est attribué à l'augmentation de la tension des chaines qui rend les doubles liaisons suffisamment actives pour réagir avec l'oxygène présent dans le milieu. Suite à cette oxydation, les doubles liaisons sont redevenues des simples liaisons et les moteurs peuvent alors tourner en sens inverse ce qui permet de dérouler les chaines de polymère et de retrouver la forme initiale du gel.

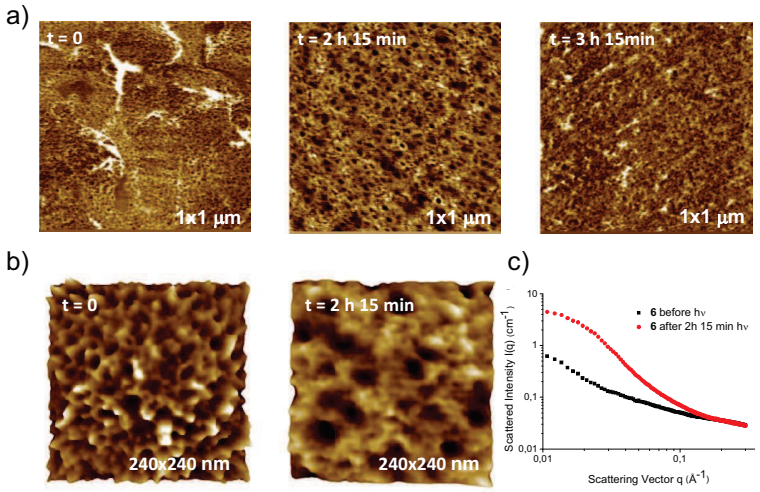

Figure A5 I Caractérisations micro- et nanoscopiques du gel **6** (PEG 5000). **a)** Images AFM du gel **6** soumis à différents temps d'irradiation UV: avant contraction (t = 0), après contraction (t = 2 h 15min), et après éclatement du gel (t = 3 h 15 min). **b)** Images AFM détaillées avant et après contraction du gel **6** mettant en évidence l'augmentation de la taille moyenne des pores du gel de 8 nm à 20 nm. **c)** Données obtenues par diffusion des rayons X aux petits angles avant et après irradiation du gel **6**.

L'effet de la contraction du gel a également été étudié à l'échelle microscopique par diffusion des rayons X aux petits angles. Dans la figure A5, on observe qu'après irradiation UV, l'intensité diffusée augmente signe d'une augmentation de la densité interne des polymères. A l'échelle nanoscopique, la microscopie à force atomique nous montre que l'irradiation UV s'accompagne par une augmentation de la taille des pores du gel qui passent de 8 nm à 20 nm en moyenne. Cet effet corrèle très bien avec l'augmentation de la densité interne des chaines observée en diffusion des rayons X aux petits angles.

Afin de s'assurer que la contraction du gel observée est bien liée à la rotation des moteurs moléculaires, nous avons décidé de synthétiser un gel témoin dont les points de réticulation sont des épisulfures précurseurs des moteurs moléculaires (Schéma A4). Ces derniers ne peuvent tourner car ils ne contiennent pas la double liaison responsable de la rotation des moteurs. Suite à une irradiation UV, aucune contraction significative n'a pu être observée, ce résultat est bien la preuve que la contraction observée était liée à la rotation des unités mécaniquement actives placées aux points de réticulation du gel (Figure A6).

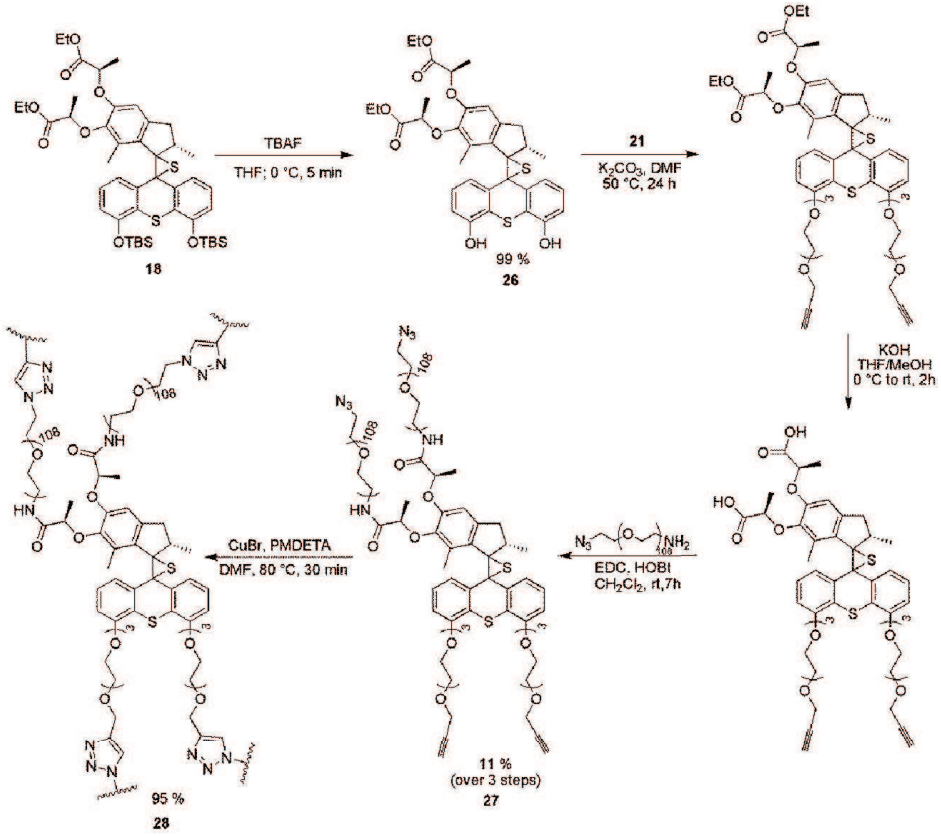

Schéma A4 | Synthèse d'un gel témoin sans unites rotatives

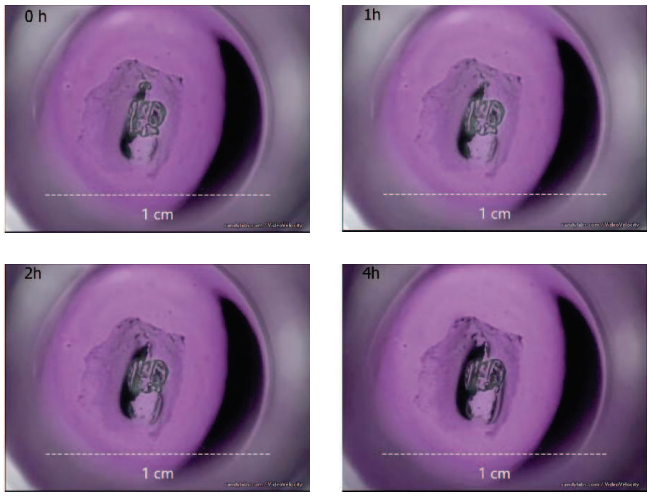

Figure A6 | Instantanés tires de la video montrant l'absence de contraction significative du gel témoin immerge dans le toluene sous irradiation UV.

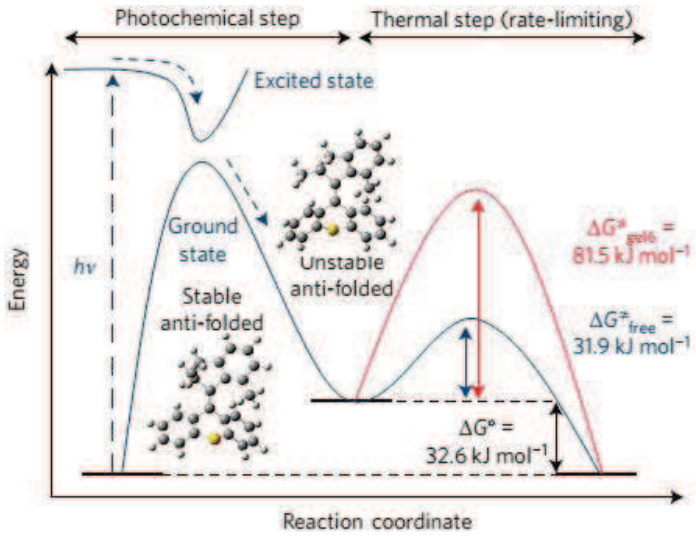

Figure A7 | Profil énergétique pour le moteur non substitué obtenue par DFT (courbe bleue); La courbe rouge correspond au profil énergétique du gel **6** et met en évidence l'augmentation de 50 kJ/mol de l'énergie d'activation nécessaire à l'étape thermique d'inversion d'hélicité cinétiquement déterminante.

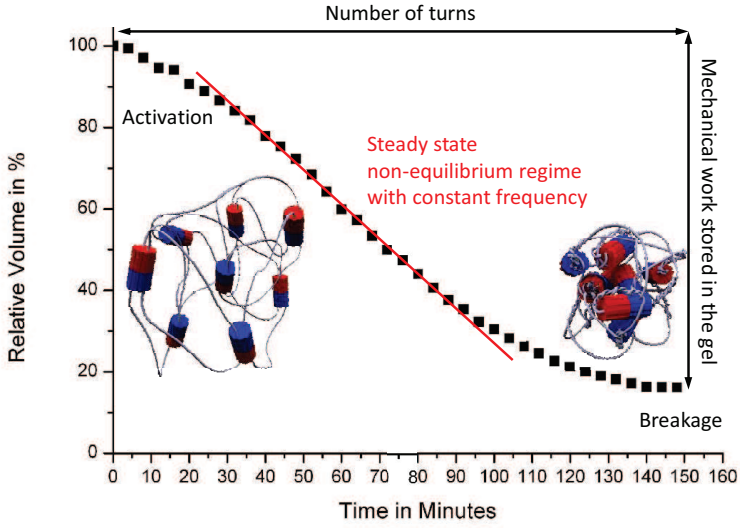

Figure A8 | Evolution temporelle du volume de gel soumis à une irradiation UV.

Des études théoriques par DFT ont également été menées afin de déterminer le mécanisme de l'étape cinétiquement déterminante d'inversion d'hélicité. Comme on peut le voir sur la figure A7, la forme instable du moteur non greffé a une énergie $\Delta G^{\neq}_{libre}$=31.9 kJ/mol. Cette énergie correspond à une fréquence de rotation de 8.05 MHz et $t_{1/2}$=43 ns à 25°C.

En représentant l'évolution temporelle du volume de gel **6** (PEG 5000) soumis au rayonnement UV (Figure A8), nous avons pu déterminer qu'une fois les chaines de polymère greffées, la fréquence de rotation diminue considérablement pour atteindre 3.16×10^{-2} Hz à température ambiante. Cette vitesse

correspond à une barrière de 81.5 kJ/mol. Cette augmentation de 50 kJ/mol correspond au prix à payer pour faire tourner les chaines de polymère. L'étude du gel comprenant des chaines de polymères plus longues (PEG 10000 Da) a permis de confirmer cette tendance au ralentissement du moteur lié à la présence de chaines polymères plus longues.

En conclusion, grâce à un long travail de synthèse organique, nous avons réussi développer une voie de synthèse stéréosélective qui permet d'accéder à des moteurs moléculaires hautement fonctionnalisés à l'échelle du gramme. Nous avons pu tirer profit de cette nouvelle voie de synthèse pour coupler des moteurs moléculaires à des chaines de polymère. Par le biais d'une réaction de cycloaddition « click », nous avons pu obtenir un gel chimique dont les points de réticulation sont des unités rotatives. La rotation des moteurs dans ce gel a résulté en un enchevêtrement des chaines de polymère ce qui permet d'observer à l'échelle macroscopique la contraction du gel. Il s'agit du premier exemple d'intégration de moteurs moléculaires fonctionnant hors équilibre et dont le mouvement est amplifié jusqu'à l'échelle macroscopique. Cette avancée permet d'ouvrir la voie à de nouvelles applications des moteurs moléculaires synthétiques avec notamment la possibilité de stocker de l'énergie lumineuse sous forme d'énergie mécanique. Notre équipe travaille désormais sur la possibilité de rendre le système réversible afin de réutiliser cette énergie.

Acknowledgements

First I would like to thank my PhD supervisor Professor Nicolas Giuseppone who accepted me to work in the SAMS group. I have been grateful to work on this fantastic project he designed for me. During my PhD studies, Professor Nicolas has showed his magic organic chemistry knowledge which helped me advancing step by step. I also thank him for his patience, trust, encouragement and humor.

I greatly appreciated Dr. Gad Fuks who is my co-supervisor for his help, advices, and the chemistry skills he taught to me. I also thank him for correcting my thesis with great patience.

I want to thank Dr. Emilie Moulin for her advices on organic synthesis. Her intelligence in organic synthesis impressed me deeply.

Then I want to thank Prof. Michel Rawiso and Dr. Fleith Guillaume for their helps in performing SAXS experiments as well as data treatment. I want to thank Prof. Mounir Maaloum for his help in AFM experiment.

I am grateful to Viginie Oberlé, Odile Lemblé, Lea Koch and Magali Meyer for the administrative support during my PhD period in ICS.

I appreciated the technical support from Mélodie Archimbaud and Odile Gavat and I thank them for the daily work and maintaining of the SAMS laboratories.

I fully appreciated my labmates Antoine Goujon and Joseph Armao, I enjoy working and joking with them and the comfortable feeling in the lab. I appreciated my officemates Valentina Garavini, Artem Osypenko and Dr. Thomas Ellis. I will never forget the funny time we shared together. I also want to thank the whole SAMS members and thank all the people who has worked, discussed and played with me.

I thank Prof. Jean-Pierre Sauvage, Prof. Ludovic Jullien, Prof. Patrice Woisel for reviewing my thesis.

I would greatly thank my parents, my sister and all the people in my family who encouraged me to finish this PhD.

Finally, I want to thank the University of Strasbourg where I registered for my PhD studies, and China Scholarship Council (CSC) for funding my PhD studies for 3.5 years.

Abbreviations and Symbols

Ac	Acetyl
AFM	Atomic Force Microscopy
Å	Angström
aq	aqueous
Bn	Benzyl
°C	Celsius degree
DCE	Dichloroethane
DCM	Dichloromethane
DFT	Density function theory
DMF	Dimethylformamide
DMSO	Dimethylsulfoxide
EDC	1-Ethyl-3-(3-dimethylaminopropyl)carbodiimide
eq.	equivalent
MS (ESI)	Mass Spectrometry with Electro Spray Ionisation
EtOAc	Ethyl acetate
h.	hour
HOBt	Hydroxybenzotriazole
HPLC	High Performance Liquid Chromatography
J	Coupling constant
K	Kelvin
L_c	Contour length
LC/MS	Liquid Chromatography coupled to Mass Spectrometry
L_p	Persistense length
λ_{max}	Maximum of emission/absorption wavelength
MALDI-TOF	Matrix-assisted laser desorption/ionization -Time of Flight
µL	microliter
µm	micrometer
mL	milliliter
MS	Mass Spectrometry

nm	nanometer
NMR	Nuclear Magnetic Resonance
PEG	Polyethylene glycol
PMDETA	N,N,N',N',N'-pentamethyldiethylenetriamine
ppm	Parts per million
R_f	Retardation factor
R_g	Radius of gyration
rt	room temperature
SAXS	Small Angle X-ray Scattering
T	Temperature
TEA	Triethylamine
THF	Tetrahydrofuran
TLC	Thin Layer Chromatography
Ts	Tosyl (p-$CH_3C_6H_4SO_2$)
UPLC	Ultra Performance Liquid Chromatography
UV	Ultra-violet

General Introduction and Purpose of This Work:

Nanotechnologies are believed to hold great promises in many domains. It is expected that the availability of nanosized systems will find applications in various fields such as medicine or materials science for instance. In particular, the development of molecular machines could be a major breakthrough in nanotechnology like the development of macroscopic machines was an essential part of the industrial revolution in the 19th century. In the last 30 years, several molecular devices have been designed by chemists and were often described in analogy with their macroscopic counterparts. Indeed, the development of molecular topology and the progresses in the control of isomerizable bonds have opened the way for molecular systems that could display molecular scale motions. Molecular machines, in the form of switches or motors, have since been synthesized and some of them have already been implemented in larger scale systems in order to perform different functions. However, molecular machines generate molecular scale motions and low amounts of work which are difficult to embed in systems that should perform macroscopic functions. This issue has been solved by evolution in nature which has designed nanoscopic devices that can perform macroscopic motions. For instance, the process of muscle contraction is the result of the integration and cooperation of thousands of thin myosin filaments sliding over thick actin ones yielding a macroscopic motion. Up to now, there has been only a few examples of integration of molecular motions that allowed to cross length scales. For instance, our group has shown that it was possible to integrate the motion from bistable rotaxanes that can switch between two thermodynamic minima generating a nanoscopic translation by supramolecular polymerization through coordination chemistry. It resulted in a wormlike chain consisting in thousands of daisy chains which could generate a micrometric elongation.[1] However, only three orders of magnitude have been crossed and the applicability of such a system remains limited by the fact that it works at equilibrium and thus cannot generate a continuous work.

This Ph. D. project aims at designing an analogous system where the translational switch is replaced by a unidirectional light driven rotary motor working out of equilibrium in order to access a machine that can perform useful functions at the macroscopic scale just like nature does.

[1] G. Du.; E. Moulin.; N. Jouault.; E. Buhler. ; N. Giuseppone. Muscle-like supramolecular polymers: integrated motion from thousands of molecular machines. *Angew. Chem. Int. Ed.*, **51**, 12504-12508 (2012).

Theoretical Part

Chapter 1: Bibliography

1/ Biological motors

A motor is a device which is able to convert repetitively various forms of energy such as chemical, electrical, thermal energy into mechanical work.[2] Biological molecular motors are quite abundant in living systems, which are the result of evolution over millions of years. All cells use protein motors to move and position their organelles. Cytoplasmic motors can be mainly divided into three types known as: myosin,[3] which moves on the actin filaments; dynein[4] and kinesin,[5] which use microtubules as tracks. In these motors, ATP hydrolysis triggers a small conformational change in a globular motor domain that is amplified and translated into movement with the aid of accessory structural motifs. Dimerization, regulation and interactions with other molecules are controlled by accessory domains in proximity with the motor domain.[6] These motors operate in a consortium, in which their actions are coordinated to perform useful tasks. In the following section, we will first give a brief introduction of these three types of cytoplasmic motor as well as ATP synthase.

a) Myosin

Myosin can move unidirectionally along actin filaments using ATP as fuel. It is used in several different cellular activities such as muscle contraction, vesicle transport, membrane trafficking and signal transduction.

[2] (a) V. Balzani.; A. Credi.; M. Venturi. Molecular Devices and Machines, Second Edition, 2008 WILEY-VCH Verlag GmbH & Co. KGaA, Weinheim. (b) J. P. Sauvage.; P. Gaspard. From non-covalent assemblies to molecular machines. 2011 WILEY-VCH Verlag GmbH & Co. KGaA, Weinheim.
[3] A. D. Mehta.; M. Rief.; J. A. Spudich.; D. A. Smith.; R. M. Simmons. Single-molecule biomechanics with optical methods. *Science* **283**, 1689-1695 (1999).
[4] S. M. Block. Kinesin motor mechanics: binding, stepping, tracking, gating, and limping. *Biophys. J.*, **92**, 2986-2995 (2007).
[5] S. A. Burgess.; P. J. Knight. Is the dynein motor a winch? *Curr. Op. Struct. Biol.*, **14**, 138-146 (2004).
[6] M. Schliwa.; G. Woehlke. Molecular motors. *Nature* **422**, 759-765 (2003).

Generally, myosin consists of three domains (Figure 1a). The first one is the motor domain or head which contains the nucleotide- and actin-binding sites.[7a] The motor domain is mechanically linked to a second domain consisting of an α-helix segment. The third one is the tail domain consisting of a coiled-coil-forming domain with periodic interruptions. It can dimerize the heavy chains and two globular tail chains which bind cargo.

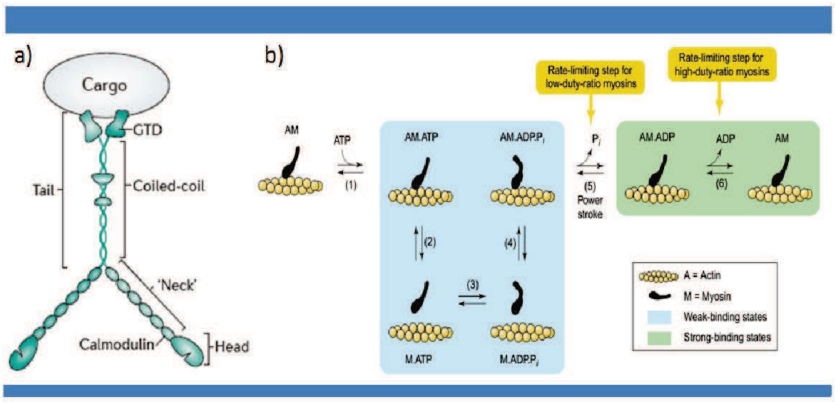

Figure 1 | a) Domain structure of myosin V_a. [7a] b) Mechanism of the actomyosin ATPase pathway coupled to a mechanical model [7b]

The minimum mechanism needed to describe the myosin ATPase cycle consists of at least six nucleotide-linked biochemical reactions (Figure 1b).[7b] In the absence of ATP, myosin binds tightly to actin. ATP binding (step 1) will cause a conformational change in myosin, the actin affinity is then weakened and myosin consequently detaches from actin (step 2). A second conformational change will allow the hydrolysis of ATP to ADP and inorganic phosphate (Pi) (step 3); the hydrolysis products remain bound to myosin. The M.ADP.Pi state will then bind again to the actin filament (step 4) and a force-generating power-stroke occurs as well as a phosphate release (step 5). ADP is released (step 6) and the cycle repeats upon ATP binding. The actin-detached M and M.ADP states are omitted for clarity and to illustrate that these states are not populated during enzymatic cycling in the presence of saturating actin and ATP.

b) Dynein

Cytoplasmic dynein is a large, microtubule-dependent molecular motor (1.2 MDa) which can move processively along microtubules (Figure 3). Its many functions include spindle formation and

[7] (a) J. A. Hammer III.; J. R. Sellers. Walking to work: roles for class V myosins as cargo transporters. *Nat. Rev. Mol. Cell Biol.***13**, 13-26 (2012). (b) Enrique M De La Cruz.; E. M. Ostap. Relating biochemistry and function in the myosin superfamily. *Curr. Opin. Cell Biol.***16**, 61-67 (2004).

chromosome segregation and the transport of numerous cargoes including viruses, RNA, signaling molecules, and organelles. [8]

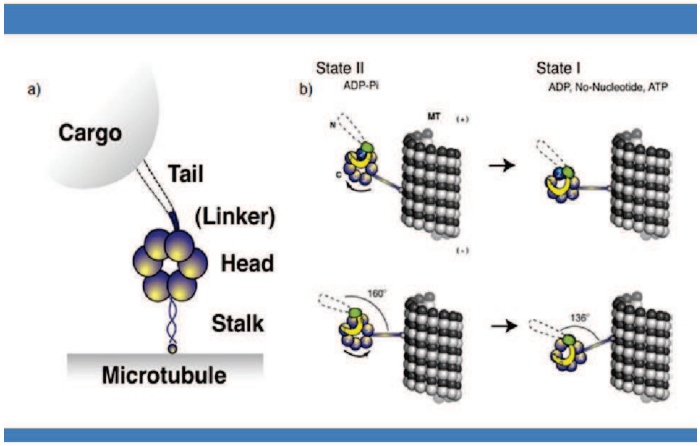

Figure 3 | a) Schematic diagrams of the dynein constructs. b) Models showing how a conformational change in the dynein domain could generate movement along a microtubule.[9]

Unlike the two other cytoskeletal motor protein families, kinesin and myosin, for which detailed structural and mechanistic models exist, relatively little is known about the mechanism of dynein motility. Dynein motion most frequently consists in 8 nm steps, although longer as well as side and backward steps have sometimes been observed. Individual motor domains showed a different stepping pattern. This is best explained by the two motor domains shuffling alternatively between rear and forward positions. This suggests that the coordination of its two motor domains allows cytoplasmic dynein to move in a processive manner, but its variable step size and direction suggest the importance of diffusion in its step.[10]

c) Kinesin

Kinesins were discovered as intracellular transport motors which move on microtubules. This transportation is powered by the hydrolysis of ATP. Numerous cellular functions including mitosis, meiosis and transport of cellular cargo, such as in axonal transport depend on the active movement of kinesins. Usually kinesins walk towards the plus end of a microtubule, which, in most cells, consists in a

[8] R. B. Vallee.; J. C. Williams.; D. Varma.; L. E. Barnhart. Dynein: An ancient motor protein involved in multiple modes of transport. *J. Neurobiol*. **58**, 189-200 (2004).
[9] N. Mizuno.; A. Narita.; T. Kon.; K. Sutoh.; M. Kikkawa. Three-dimensional structure of cytoplasmic dynein bound to microtubules. *PNAS*, **104**, 20832-20837 (2007).
[10] S. L. Reck-Peterson.; A. Yildiz.; A. P. Carter.; A. Gennerich.; N. Zhang.; R. D. Vale. Single-molecule analysis of dynein processivity and stepping behavior. *Cell* **126**, 335-348 (2006).

transport of cargo from the centre of the cell towards the periphery.

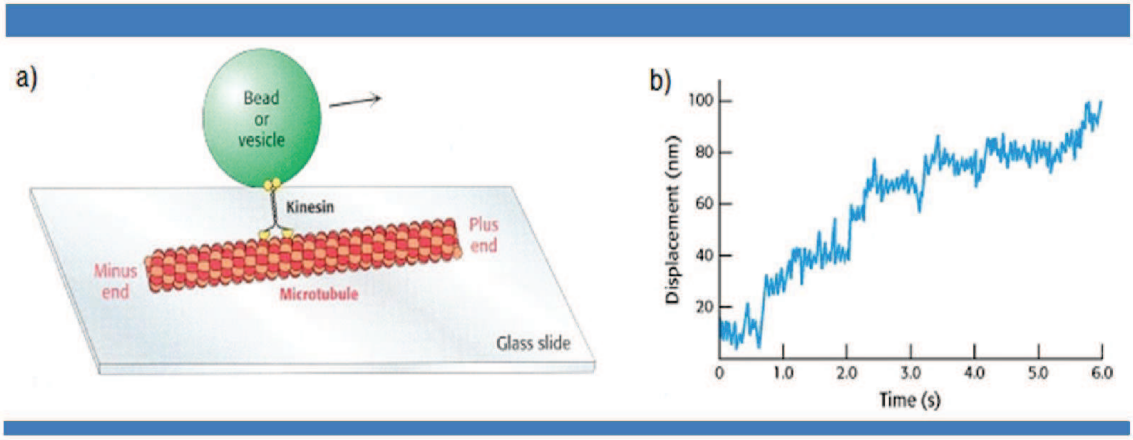

Figure 4 | a) Kinesin moving along a microtubule. The movement of beads or vesicles, carried by individual kinesin dimers along a microtubule, can be directly observed. b) A trace shows the displacement of a bead carried by a kinesin molecule. Multiple steps are taken in the 6-s interval. The average step size is about 8 nm.[11]

A kinesin molecule may take many steps before both heads groups are dissociated at the same time. A single kinesin molecule will typically "walk" 100 or more steps toward the plus end of a microtubule in a period of seconds before the molecule is detached from the microtubule.

d) ATP synthase

Another ubiquitous and abundant biological motor is ATP synthase. It plays a vital role in our cells, producing most of the ATP that powers nearly all our cellular processes.

ATP synthase is a large protein complex which is made from ~3500 amino acids (~500 KDa). It consists of two regions: the membrane-embedded portion F_0; and the F_1 portion which is above the membrane, inside the matrix of the mitochondria (Figure 5a).[12] The F_0 domain is a motor which is embedded in a membrane and is powered by the flow of proton across the membrane. It contains three kinds of transmembrane subunit with a stoichiometry $a_1b_1c_{10\sim15}$ (the number of *c* subunits varies from 10 to 15 in different species). As the protons flow through domain F_0, they drive a circular rotor (*c* subunit in Figure 5b) to rotate. Currently, the structural basis and detailed mechanism for this proton translocation pathway is not clear. But Asp or Glu residues of the *c* subunit and Arg of the *a* subunit

[11] K. Svoboda.; C. F. Schmidt.; B. J. Schnapp.; S. M. Block. Direct observation of kinesin stepping by optical trapping interferometry. *Nature* **365**, 721 (1993).
[12] M. Yoshida.; E. Muneyuki.; T. Hisabori. ATP synthase-a marvellous rotary engine of the cell. *Nat. Rev. Mol. Cell Biol.*, **2**, 669-677 (2001).

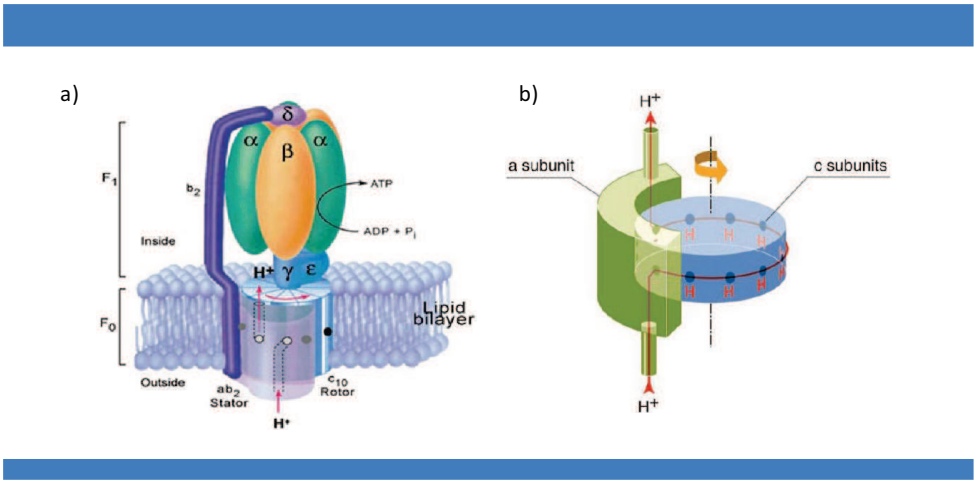

Figure 5 | a) Structure of ATP synthase.[13a] b) Hypothetical model for the generation of rotation by proton transport through the F_0 domain of ATP synthase.[13b]

were found to be the proton binding sites and directly involved in proton translocation. The most widely accepted model on proton translocation in F_0 is the so-called two-channel model. In this model, it is assumed that *a* subunit possesses two proton pathways each of which spans half of the membrane, but towards different sides; the channels ensure the connection between the proton-binding site of the *c* subunit with the periplasmic or cytoplasmic space.[14] A proton enters the half channel exposed to the periplasmic side (or intermembrane space of mitochondria) and is then transferred to the carboxy residue of the *c* subunit. This protonation results in the neutralization of the negative charge from the residue, allowing the *c* subunit to rotate apart from the *a* subunit towards the surrounding lipid layer. At the same time, the neighbouring *c* subunit at the anticlockwise side returns from the lipid layer to form contacts with the other half which has a hydrophilic environment that promotes the deprotonation of the carboxyl residue. The released proton then enters into the cytoplasmic space.

The rotor F_0 is connected to the second motor, termed F_1 which contains five kinds of subunits with a stoichiometry $\alpha_3\beta_3\gamma_1\delta_1\varepsilon_1$. The three α and β subunits are alternatively arranged and form a hexameric stator ring. The rotor shaft is the γ subunit, which is located in the central cavity of the $\alpha_3\beta_3$ ring. When F_0 turns, driven by the power from a proton gradient, it also drives the reverse rotation of the γ subunit rotor in F_1 while synthesizing ATP.

The classic model for synthesizing ATP in F_1 domain is the "binding-change mechanism" proposed by Paul Boyer.[15] The catalytic reaction centers for ATP synthesis reside at the three α-β interfaces. As

[13] (a) R. H. Fillingame. Molecular Rotary Motors. *Science* **286**, 1687-1688 (1999). (b) D. Stock.; A. G. W. Leslie.; J. E. Walker. *Science* **286**, 1700-1705 (1999).
[14] D. Okuno.; R. Iino.; H. Noji. Rotation and structure of FoF_1-ATP synthase. *J. Biochem*. **149** (6): 655-664 (2011).
[15] P. D. Boyer. The ATP synthase-a splendid molecular machine. *Annu. Rev. Biochem*. **66**, 717-749 (1997).

the axis rotates, the conformation of the α and β subunits in the F_1 complex's active site is altered such that it switches from an "open" state (where ADP and phosphate can enter the active site) to a "closed" state (where ADP and phosphate are bound loosely) to a "tight" state (where the ADP and phosphate molecules are forced together, covalently bonding to form ATP). The active site then undergoes another conformational change, resulting in the breaking of the hydrogen bonds that were stabilizing the ATP in the active site (releasing the newly-formed molecule), and reverting back to the original open state, ready for another reaction cycle. In our cells, food is broken down and used to pump hydrogen ions across the mitochondrial membrane. The F_0 portion of ATP synthase allows them to flow back, turning the rotor in the process. As the rotor turns, it turns the axle and the F_1 motor becomes a generator, creating ATP as it turns.

2/ Synthetic molecular machines and motors

Obviously, nature has successfully harnessed the work from the above motors to perform numerous useful tasks. The learning and inspiration from nature has always enabled the chemists to design and construct synthetic molecular systems. During the past three decades, chemists have demonstrated their fantastic imagination and considerable skills towards these smart artificial machineries. In such smart molecular complexes, the submolecular components could move between different positions due to the varying environmental stimuli which provide energy input. [16]

a) Definitions and concepts

People who newly enter into this field are often confused by molecular devices, machines, switches, motors, etc. In general, for artificial molecular motions, they are classified by the direct comparison with the motions occurring in our macroscopic world (e.g., braking, locking, shuttling, rotation). Such a comparison helps us to understand molecular devices easily by just drawing vivid cartoons that clearly explain their mechanical functions. However, it may ignore the essential differences between the macroscopic and molecular scale worlds.[2] In many reviews, authors are usually quite cautious when dealing with these definition issues. In this bibliography, we would like to cite the definitions from reference **2** because it is much easier to understand and seems more reasonable from our point of view.

A mechanical device is a particular type of device designed to perform mechanical movements.

[16] E. R. Kay.; D. A. Leigh.; F. Zerbetto. Synthetic molecular motors and mechanical machines. *Angew. Chem. Int. Ed.*, **46**, 72-191 (2007).

These movements can drive the corresponding system either far away from equilibrium or stay at equilibrium (motors or switches respectively). A machine is a particular type of mechanical device designed to perform a specific mechanical movement with a defined energy input. Compared with a device, a machine needs energy input to move. Then when it comes to a motor, it is defined as a machine capable of using an energy input to produce useful work. In addition, this motion should and can be used to do useful work. So the relationship among these systems can be generally summarized as: "a motor is a machine, and a machine is also a mechanical device, but a mechanical device might not be a machine or a motor and a machine might not be a motor."[2]

Currently, most synthetic molecular systems are just switch type machines rather than motors. It should be noted that "motor" and "switch" are descriptors of very different types of behavior at molecular nanoscales.[16] A "switch" just works as a function of state and most importantly, there is no net energy that can be stored in the system because of the "back and forth" style motion. However, a "motor" can work as a function of the trajectory of its components or the substrate. A motor can use an energy input to drive a system away from equilibrium repetitively and progressively, whereas a switch cannot. However, a switch is a minimal component from a machine as it is the basis for molecular positional displacement (Figure 6).

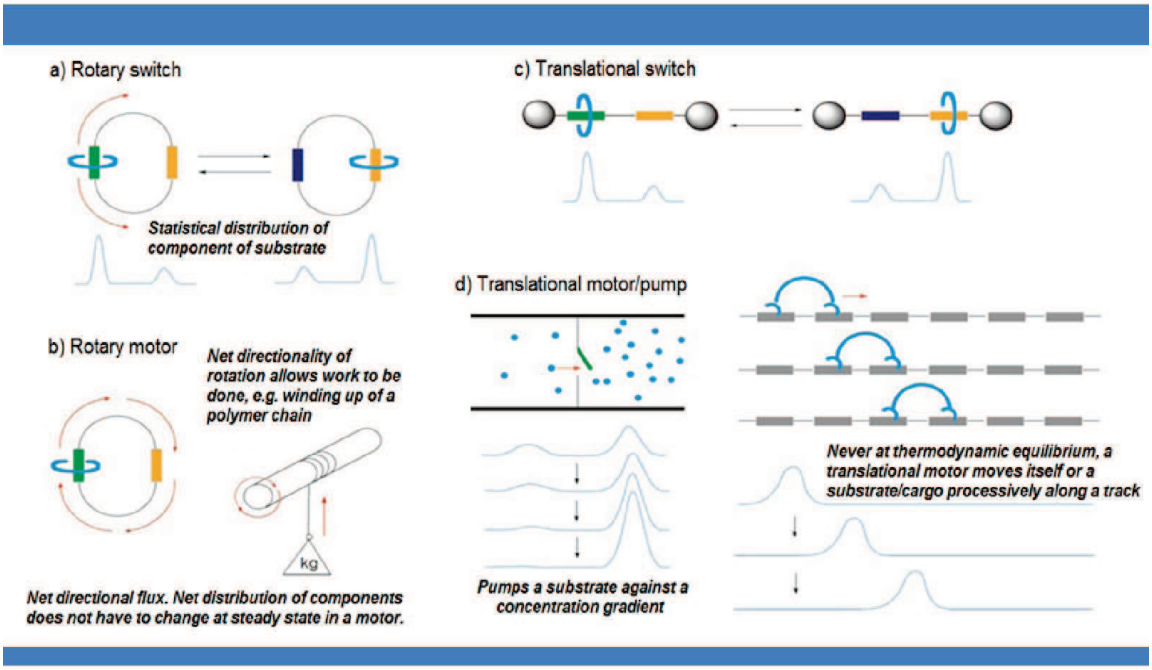

Figure 6 | The fundamental difference between a "switch" and a "motor" at the molecular level. Both translational and rotary switches influence a system as a function of the switch state. They switch between two or more, often equilibrium, states. Motors, however, influence a system as a function of the trajectory of their components or a substrate. Motors function repetitively and progressively on a

system; the affect of a switch is undone by resetting the machine. a) Rotary switch. b) Rotary motor. c) Translational switch. d) Translational motor or pump.[16]

There are already numerous reviews and books on molecular machines and motors.[2,16-18] Upon distinguishing those definitions, we would like to focus more on rotary synthetic molecular motors that work out of equilibrium as it is the purpose of this Ph.D. project.

b) Bioengineered machines

In the field of synthetic molecular machines, nature's building blocks have provided us many advantages to produce bioengineered machines. DNA is a very versatile building block and a series of systems which use DNA hybridization as an energy source to control molecular motion and translocation have been developed.

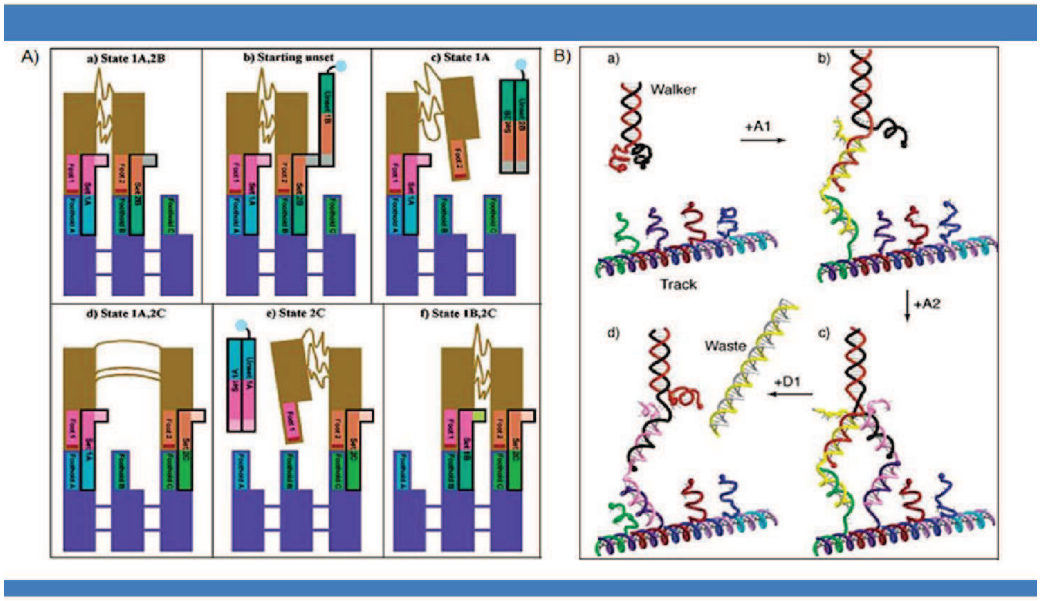

Figure 7 | A) Demonstration of biped system taking a full step.[19] B) A processive bipedal DNA nanomotor that moves by advancing the trailing foot to the lead at each step.[20]

The first synthetic DNA walking device on a DNA track was produced by Seeman (Figure 7A). [19] The device consists of a biped and a well-defined track where it walks. The biped region consists of two double-helical domains connected by three flexible, 9-nucleotide linker strands of DNA and the track is

[17] V. Balzani. ; A. Credi.; B. Ferrer.; S. Silvi.; M. Venturi. Artificial molecular motors and machines: Design principles and prototype systems. *Top Curr Chem* **262**, 1-27 (2005).
[18] E. R. Kay.; D. A. Leigh. Beyond switches: Rotaxane- and catenane-based synthetic molecular motors. *Pure Appl. Chem.*, **80**, 17-29 (2008).
[19] W. B. Sherman.; N. C. Seeman. A precisely controlled DNA biped walking device. *Nano Lett.* **4**, 1203-1207 (2004).

essentially a rigid structure with three single stranded "Footholds" on its left side. Two psoralen molecules were attached to the ends of the feet allowing to determine the state of walker by gel electrophoresis. The set strands complimentary to a foot and a foothold enable the linking of a foot on the track. While unset strands with better complementarity or affinity for set strands will trigger the detachment of the foot from the foothold and produce a duplex as waste products. The total distance traveled by the biped relative to the footpath is approximately 2 nm.

Similarly, another DNA walker that moves by advancing the trailing foot to the lead yielding a 5 nm motion at each step was reported by Pierce *et al* (Figure 7B).[20] The track is also made of DNA and the step is triggered by the addition of set strands that are complementary to the track and the feet. Dyes connected to the legs and the branches of the track allow monitoring the walking motion of the biped on the track through fluorescence experiments.

A new biodevice that displays a true motor behavior was produced again by Seeman in 2009.[21] It is an autonomous bipedal walker made of DNA that walks along a directionally polar DNA track. By covalently cross-linking aliquots of the walker to its track in successive walking states it has been demonstrated that this Brownian motor could complete a full walking cycle on a track whose length could be extended for longer walks. This study helps to uncover principles behind the design of unidirectional devices that can function without intervention. It is expected that this device should be able to fulfill roles that entail the performance of useful mechanical work on the nanometer scale (Figure 8).

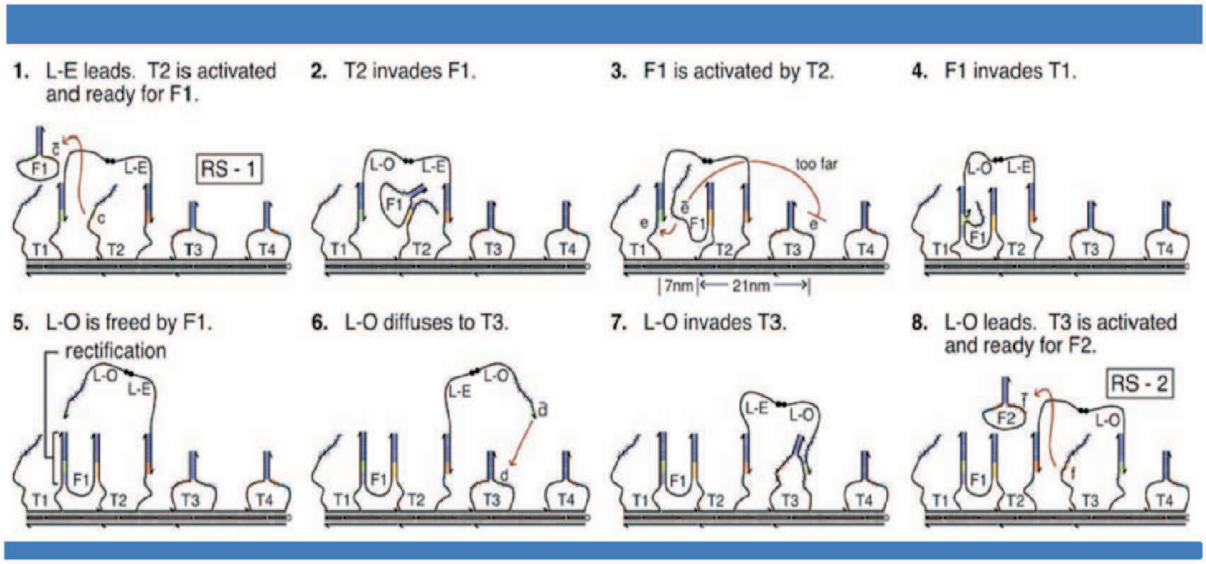

Figure 8 | Demonstration of bipedal DNA brownian motor with coordinated legs.[21]

[20] J. S. Shin.; N. A. Pierce. A synthetic DNA walker for molecular transport. *J. Am. Chem. Soc*. **126**, 10834-10835 (2004).
[21] T. Omabegho.; R. Sha.; N. C. Seeman. A bipedal DNA brownian motor with coordinated legs. *Science* **324**, 67-71 (2009).

c) Chemically powered molecular motors

In search of the Feymann's ratchet, Kelly synthesized the first molecular ratchets in 1997.[22] They have successfully incorporated triptycene[4]helicene into a single molecule which is the essential components of a simple ratchet: the asymmetric combination of a ratchet wheel, a pawl, and a spring. But the experiment demonstrated that this molecular ratchet rotated equally in both directions when no external source of energy was supplied. Then in 1999, they achieved 120° unidirectional motion using a similar ratchet structure coupled with a chemical reaction to supply energy (Figure 9).[23]

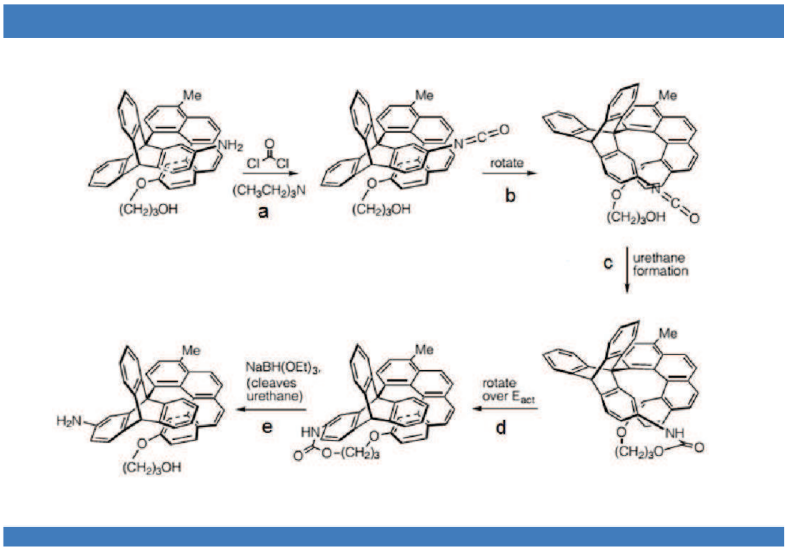

Figure 9 | The chemically driven molecular motor designed by Kelly *et al.*[23]

This rotation takes place in five steps. The amine group present on the triptycene moiety is converted to an isocyanate group by condensation with phosgene. Thermal or spontaneous rotation around the central bond then brings the isocyanate group in proximity of the hydroxyl group located on the helicene moiety, thereby allowing these two groups to react with each other. This reaction irreversibly traps the system as a strained cyclic urethane that is highly energetic (enough to overcome the rotational energy barrier). A relatively small amount of thermal activation is sufficient in order to overcome this barrier, thereby releasing the strain. Finally, cleavage of the urethane group allows recovering the initial amine and alcohol functionalities of the molecule.

The result of this sequence is a unidirectional 120° rotation of the triptycene moiety with respect to the helicene moiety. The unidirectionality of the system is a result from both the asymmetric design of

[22] T. R. Kelly.; I. Tellitu.; J. P. Sestelo. In search of molecular ratchets. *Angew. Chem. Int. Ed.*, **36**, 1866-1868 (1997).
[23] T. R. Kelly.; H. D. Silva.; R. A. Silva. Unidirectional rotary motion in a molecular system. *Nature* **401**, 150-152 (1999).

the helicene moiety as well as the strain of the cyclic urethane which is formed in **c**. The only way to lower this strain is to perform a clockwise rotation of the triptycene rotor in **d**, as both counterclockwise rotation as well as the inverse process of **d** are energetically unfavorable. In this respect the preference for the rotation direction is determined by both the positions of the functional groups and the shape of the helicene allowing chemists to determine the directionality of the rotation through an elegant design.

Another impressive example was reported by Feringa *et al* (Figure 10).[24] The full rotation of this molecular motor takes place in four stages. In stages A and C, the rotation of the aryl group is prevented by the ester bond, although helix inversion is possible. In stages B and D, the ester bond is cleaved and the aryl can now rotate with respect to the naphtalene with steric interactions preventing the aryl from passing the naphthalene. This molecular motor is the first example of a fully artificial chemically driven rotary molecular motor that is capable of 360° rotation (Kelly's motor has only achieved 120° unidirectional rotation).

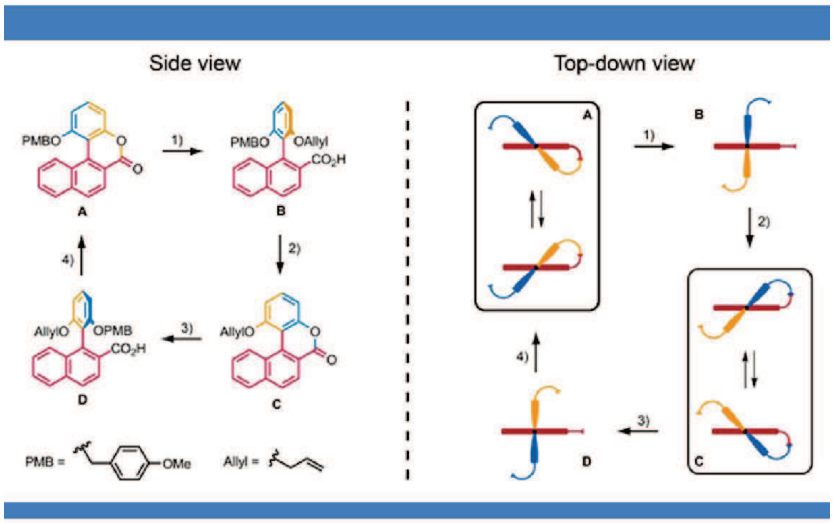

Figure 10 | The Chemically driven molecular motor designed by Feringa *et al*.[24]

Another multi-stimuli driven unidirectional motor was designed by David Leigh's group in 2003 (Figure 11).[25a] This motor was prepared by the synthesis of a [3]catenane[25b] in which two small rings move along a larger one. These two small rings can interact with different stations on the lager trajectory via hydrogen bonds between amides and carbonyl groups. By applying a specific sequence of light and

[24] S. P. Fletcher.; F. Dumur.; M. M. Pollard.; B. L. Feringa. A reversible, unidirectional molecular rotary motor driven by chemical energy. *Science* **310**, 80-82 (2005).
[25] (a) D. A. Leigh, J. K. Y. Wong, F. Dehez.; F. Zerbetto. Unidirectional rotation in a mechanically interlocked molecular rotor. *Nature* **424**, 174-179 (2003). (b) J. P. Sauvage.; C. Dietrich-Buchecker. Molecular catenanes, rotaxanes and knots. 1999 VCH-Wiley, Weinheim.

chemical energy input, the small shuttles can move in a preferred direction. The presence of the second macrocycle is necessary to ensure the unidirectionnality of the process. It is noteworthy that no chirality is required in this system to control the direction of rotation.

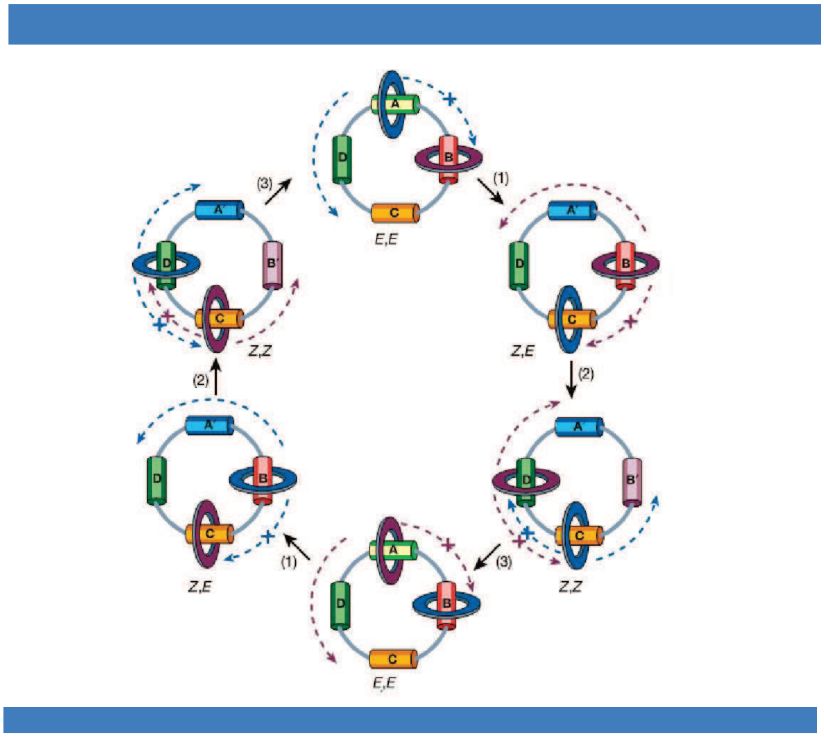

Figure 11 | Stimuli-induced unidirectional rotation in a four-station [3]catenane. (1) 350 nm, CH_2Cl_2, 5 min, 67 %; (2) 254 nm, CH_2Cl_2, 20 min, 50 %; (3) heat, 100 °C, $C_2H_2Cl_4$, 24 h,100 %; catalytic ethylenediamine, 50 °C, 48 h, 65 %; or catalytic Br_2, 400-670 nm, CH_2Cl_2, -78 °C, 10 min,100 %. [25a]

d) Light driven unidirectional molecular motors

Compared with chemically driven molecular motors, light driven molecular motors are more stimulating due to the simplification of the energy input. The pioneer of this field is undoubtedly the group of B. L. Feringa. Since the first light driven unidirectional molecular motor reported in 1999 [26] (the same publishing time as Kelly's motor), they have developed two generations of light driven unidirectional molecular motors with accelerated rotation speeds.

[26] N. Koumura.; R. W. J. Zijlstra.; R. A. van Delden.; N. Harada.; B. L. Feringa. Light-driven monodirectional molecular rotor. *Nature* **401**, 150-152 (1999).

I. The first generation motors

The first light driven unidirectional molecular motor was reported by Feringa's group in 1999 (Figure 12).[26] This type of motor is called first generation motor because it features two identical parts connected by a central overcrowded carbon-carbon double bond, which acts as the axis of rotation. The molecule features two stereogenic centers whose configuration will dictate the direction of rotation of the upper half relative to the lower half of the molecule.

The rotary cycle of this motor can be divided into four successive steps:

Step 1: Irradiation of stable (*P*, *P*)-*trans*-**1** with UV light (λ≥280 nm) triggers a *trans*→*cis* photoisomerization around the central double bond (Figure 12). This isomerization also results in the molecular helix inversion (*P*, *P*→*M*, *M*). In the unstable form (*M*, *M*)-*cis*-**2**, the methyl substituents are forced to adopt a strained pseudo-equatorial orientation, in which they experience steric crowding with the naphthalene rings.

Step 2: Since (*M*, *M*)-*cis*-**2** is a highly energetic intermediate, an energetically favorable thermal helix inversion step will occur spontaneously at room temperature, releasing the strain in the molecule. In this step, the methyl groups slip past the naphthalene rings of the opposite half and regain their energetically favored pseudo-axial conformation, thus generating another stable form (*P*, *P*)-*cis*-**2**. After this step, the motor completes the first 180° of the rotary cycle of the upper half relative to the lower half of the molecule.

Step 3: Similar to step 1, irradiation (λ≥280 nm) of stable (*P*, *P*)-*cis*-**2** triggers another *cis*→*trans* photoisomerization to generate the unstable form (*M*, *M*)-*trans*-**1**. As in the unstable form (*M*, *M*)-*cis*-**2**, the methyl groups at the stereogenic center in the unstable form (*M*, *M*)-*trans*-**1** are locked in a highly strained pseudo-equatorial conformation.

Step 4: Slightly different from step 2, the strained molecule (*M*, *M*)-*trans*-**1** needs mild heating (60 °C) to facilitate the last step of the rotary cycle. A thermal helix inversion releases the conformational strain and regenerates the stable form (*P*, *P*)-*trans*-**1** with the methyl substituents at the favored axial position.

The rotation speed is strongly dependent on the steric hindrance in the fjord region (Figure 13a). Since the photoisomerisation usually occurs on the picoseconds timescale, the thermal helix inversion becomes the rate limiting step during the whole rotation cycle of the molecule. To accelerate the rotation speed, synthetic efforts have been made towards changing the size of the group bound to the stereogenic center as well as the size of the ring connected to the central double bond. For example, the smallest

light driven molecular motor, compound **3** which features two five-membered ring in the two halves of the molecule was prepared (Figure 13b).[27] It was expected that the presence of a smaller five-membered ring bearing a stereogenic center as in **3** (Figure 13b) would allow a faster unidirectional 360°

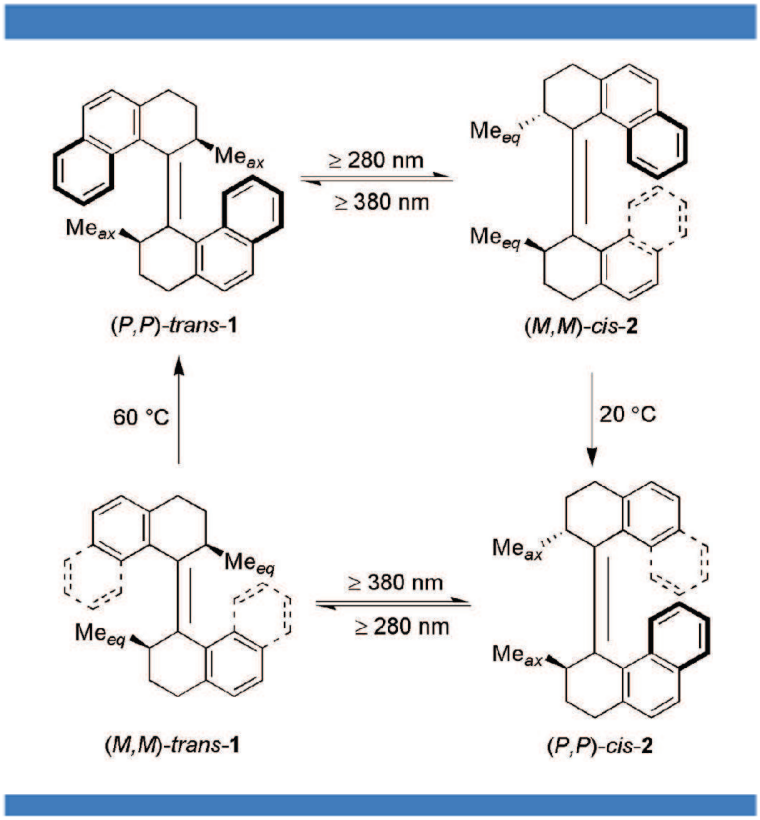

Figure 12 | Typical rotation cycle of the first generation motor.[26]

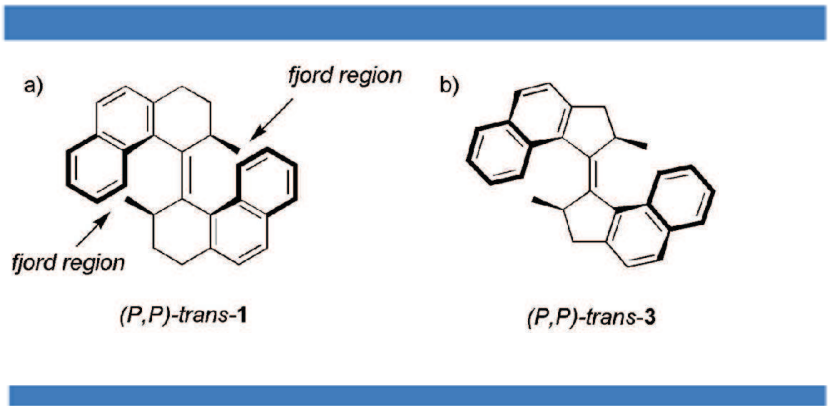

Figure 13 | Structure of a) the first generation motor with six-membered ring bearing the stereogenic center; b) Motor **3** with five-membered ring bearing the stereogenic center.[27]

[27] M. K. J. ter Wiel.; R. A. van Delden.; A. Meetsma.; B. L. Feringa. Increased speed of rotation for the smallest light-driven molecular motor. *J. Am. Chem. Soc.,***125**, 15076-15086 (2003).

rotation. The full rotary cycle comprises four consecutive steps: two photoisomerisations each followed by a thermal helix inversion. Both photo *cis-trans* isomerizations proceed with a preference for the unstable diequatorial isomers over the stable diaxial isomers. The barriers for thermal helix inversion of this motor molecule have decreased dramatically compared to its six-membered ring analogue, the half-life of the fastest step being only 18 s at room temperature (compared with 439 hours for the six-membered ring).

Due to the high the steric hindrance around the central double bond, it is always challenging to synthesize the first generation motors. The most crucial step to produce the first generation motor is to use the McMurry reaction to form the overcrowded central olefinic bond by coupling two identical ketone halves (Scheme 1). The key intermediate ketone **4** was obtained from the acid precursor **5** via Friedel-Crafts acylation (Scheme 2). Since the configuration of the stereogenic center determines the direction of rotation, it is mandatory to prepare enantiopure compounds.

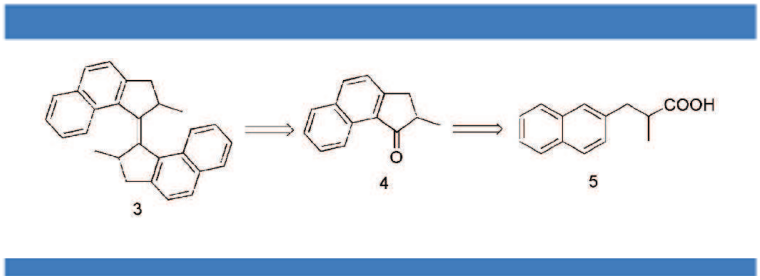

Scheme 1 | Retrosynthesis of motor **3** [27]

For this purpose, chiral resolution methods or asymmetric synthetic routes are usually employed. For chiral resolution, preparative chiral HPLC is required, however, this method is quite time-consuming, the yield is dramatically lowered and the scale of synthesis is limited.[27] The use of an enantiopure ketone (Scheme 3) as the precursor was not satisfying neither as under the reaction conditions used, the chiral ketone racemized completely.

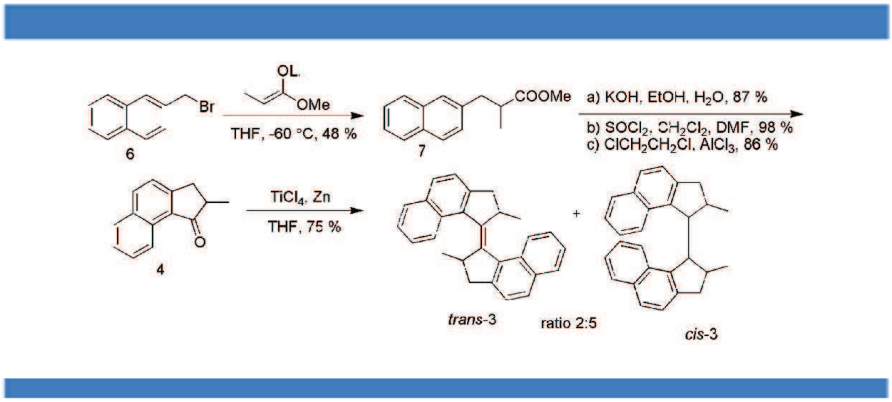

Scheme 2 | Typical synthetic route towards first generation motor **3**, enantiopure motor requires chiral resolution by preparative chiral HPLC.[27]

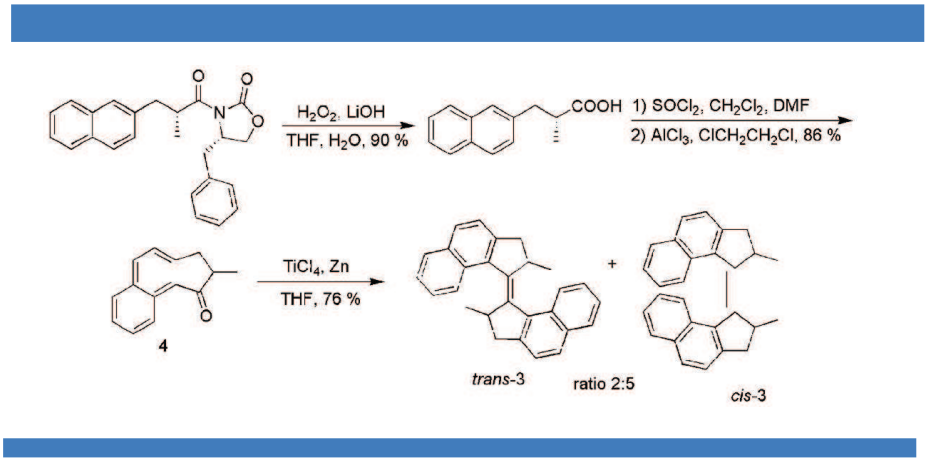

Scheme 3 | Asymmetric synthetic method toward motor **3**.[27]

In addition, further functionalization of this type of motor is another bottle neck concerning its applications, e.g, integration into even more complex materials system. The tolerance ability to the McMurry reaction has limited the substituents range. The most common method to functionalize the motor is to introduce a stable substituent on the benzene ring, such as -OMe, -Br before the McMurry coupling reaction (Figure 14).[28,29]

[28] M. K. J. ter Wiel.; B. L. Feringa. Synthesis of functionalized molecular motors. *Synthesis* **11**, 1789-1796 (2005).
[29] J. Wang.; A. Kulago.; W. R. Browne.; B. L. Feringa. Photoswitchable intramolecular H-stacking of perylenebisimide. *J. Am. Chem. Soc*. **132**, 4191-4196 (2010).

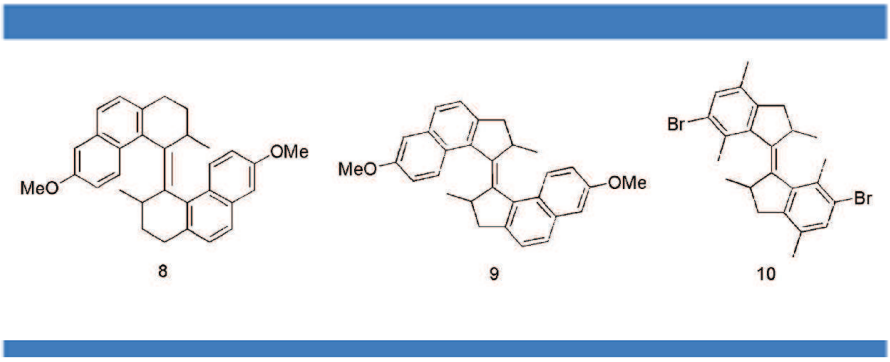

Figure 14 | Functionalized first generation motors.

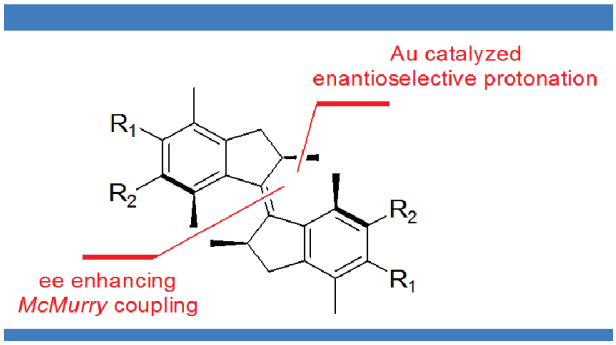

Figure 15 | Asymmetric synthesis of functionalized first generation motors.[30]

More recently, Feringa *et al* reported a novel enantioselective route to functionalized first generation molecular motors (Figure 15).[30] The key features of this approach are the use of the catalytic enantioselective protonation of silyl enol ethers by a cationic Au(I)BINAP complex giving access to the enantiomeric enriched ketones (81% ee~98% ee) followed by a highly diastereoselective McMurry coupling with an ee amplification step yielding overcrowded alkenes with up to >98% ee.

II. The second generation motors

Unlike their macroscopic counterparts, in the nanoscale world, molecular motors must overcome the "Brownian storm" of molecular collisions and vibrations while converting energy into controlled motion and further to do useful work.[31] With this goal in mind, Feringa *et al* designed a second generation

[30] T. M. Neubauer.; T. van Leeuwen.; D. Zhao.; A. S. Lubbe.; J. C. M. Kistemaker.; B. L. Feringa. Asymmetric synthesis of first generation molecular motors. *Org.Lett*. **16**, 4220-4223 (2014).
[31] (a) M. M. Pollard.; M. Klok.; D. Pijper.; B. L. Feringa. Rate acceleration of light-driven rotary molecular motors. *Adv. Funct. Mater*., **17**, 718-729 (2007). (b) D. A. Leigh, E. M. Pérez, Dynamic chirality: molecular shuttles and motors. *Top. Curr. Chem.*, **265**, 185-208 (2006).

motor in which the lower half is now derived from a symmetric tricyclic molecule.[32] Unlike the first generation motor, there is only one single stereogenic center which determines the direction of rotation for a second generation motor. Also from the synthetic point of view, the asymmetric two halves make it possible to functionalize the motor in an asymmetric manner.

The key step to synthesize second generation motors is the Barton-Kellogg reaction (Scheme 4) in which a diazo compound reacts with a thioketone through an episulfide intermediate to ultimately yield the overcrowded alkene.[33-35] The diazo compound can be obtained via oxidation of a hydrazone. Many reagents exist for this oxidation such as silver oxide and [bis(trifluoroacetoxy)iodo]benzene.[36] The thioketone required for this reaction can be obtained by reacting the corresponding ketone with phosphorus pentasulfide. Desulfurization of the episulfide can be accomplished by many phosphines and also by copper powder.[37] Unlike the McMurry reaction in which the steric hindrance of the two halves around the central double bond was introduced directly in just one step, the Barton-Kellogg reaction offers a milder alternative by forming a low strain sulfur bridge first, then releasing this strain via the formation of the final double bond. In addition, Barton-Kellogg reaction also avoids the strong Lewis acid conditions used in the McMurry reaction which can reveal problematic for functionalized motors.

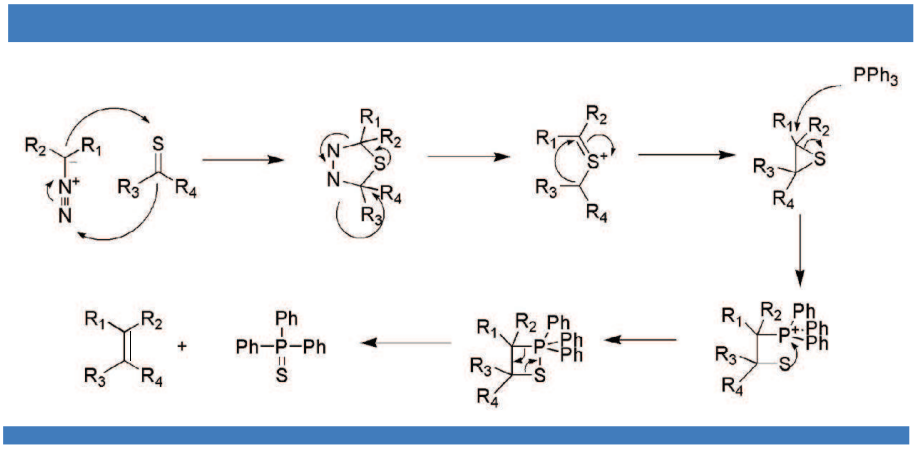

Scheme 4 | Mechanism of Barton-Kellogg reaction

[32] N. Koumura.; E. M. Geertsema.; A. Meetsma.; B. L. Feringa. Light-driven molecular rotor: unidirectional rotation controlled by a single stereogenic center. *J. Am. Chem. Soc*., **122**, 12005-12006 (2000).
[33] D. H. R. Barton.; B. J. Willis. Olefin synthesis by twofold extrusion processes. *J. Chem. Soc. D*, **19**, 1225 (1970).
[34] R. M. Kellogg.; S. Wassenaar. Thiocarbonyl ylides. An approach to "tetravalent sulfur" compounds. *Tetrahedron Lett.* **11** (23): 1987 (1970).
[35] R. M. Kellogg. The molecules R2CXCR2 including azomethine, carbonyl and thiocarbonyl ylides. Their syntheses, properties and reactions. *Tetrahedron* **32** (18): 2165 (1976).
[36] M. K. J. ter Wiel.; J. Vicario.; S. G. Davey.; A. Meetsma.; B. L. Feringa. New procedure for the preparation of highly sterically hindered alkenes using a hypervalent iodine reagent. *Org. Biomol. Chem.,* **3**, 28-30 (2005).
[37] M. M. Pollard.; M. K. J. ter Wiel.; R. A. van Delden.; J. Vicario.; N. Koumura.; C. R. van den Brom.; A. Meetsma.; B. L. Feringa. Light-driven rotary molecular motors on gold nanoparticles. *Chem. Eur. J*., **14**, 11610-11622 (2008).

For the second generation motors, the rotation cycle is similar to the first generation ones in which two photoisomerization steps each followed by a thermal helix inversion are involved. Due to the symmetry of the lower part, proving the unidirectionality of the rotation usually requires to desymmetrize the lower part by introducing one more group (e.g.-OMe) on one of benzene rings (Figure 16) in order to differentiate the *cis* and *trans* isomers.[32]

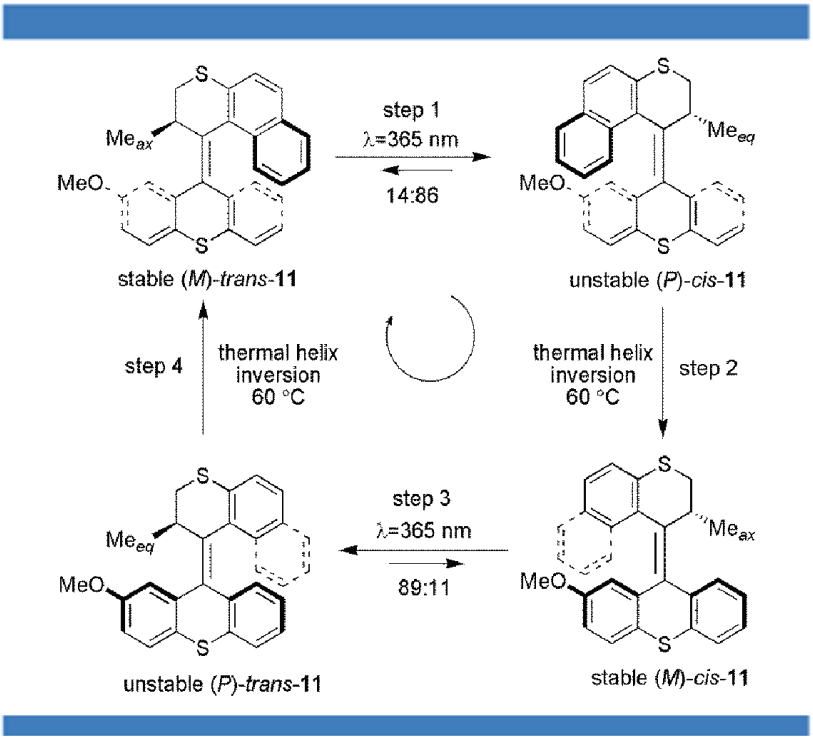

Figure 16 | Typical unidirectional rotation cycle of second generation motor.[32]

As it was shown in Figure 16, the stable form (*M*)-*trans*-**11** adopts a helical shape, in which the upper and lower parts distort from planarity due to the significant steric repulsion between them. The methyl group at the stereogenic center adopts a pseudo-axial conformation to diminish the steric hindrance with the lower benzene ring of the molecule. Irradiation of stable (M)-*trans*-**11** at 355 nm induces a *trans*→*cis* photoisomerization affording the unstable form (*P*)-*cis*-**11**. Now the stereogenic methyl group is forced to adopt a pseudo-equatorial conformation, which causes large strain in this molecule due to the steric crowding between this pseudo-equatorial methyl group and the lower half. This large strain can be released in step 2 by thermal induced isomerization. During this step, the upper naphthalene moiety slips past the benzene ring of the lower half, allowing the methyl group to readopt an axial conformation while inverting the helicity of the molecule. Step 3 is analogous to step 1 and regenerates the unstable form (*P*)-*trans*-**11**. Another thermal helix inversion follows in step 4 affording

the original stable form (*M*)-*trans*-**11**, thus completing a full 360° rotation of the upper "rotor" with respect to the lower "stator" of the molecule.

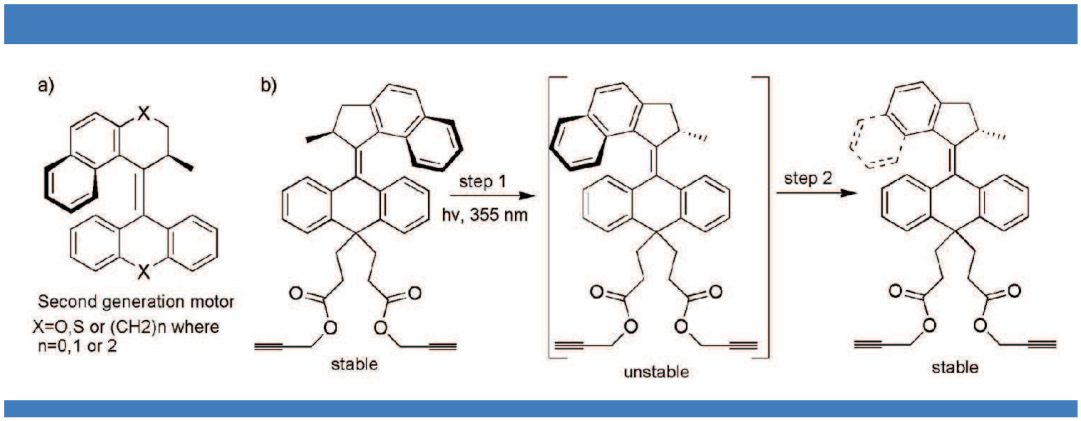

Figure 17 | a) Typical structure of second generation motors.[31a,38] b) The fastest motor up to now designed by Feringa *et al*.[39b] Step 1 is a photoisomerization step which is followed by a thermal helix inversion step.

It has been shown that changing the bridging atoms X and Y would result in a dramatic effect on the thermal isomerization barriers and thus a great increase in the rate of thermal isomerization was achieved (Figure 17a).[31a,38] Up to now, the fastest molecular motor prepared displays a half-life of the rate determining thermal step of the rotary cycle in solution of 38±1 ns (Figure 17b).[39b]

As mentioned above, the configuration of the methyl group at the stereogenic center determines the direction of rotation, either clockwise or anticlockwise. Biological rotary motors such as adenosine triphosphatase and the bacterial flagella motor have the ability to reverse the direction of the rotation.[40] Similarly, reversal of the direction of rotation for these molecular motors was also achieved by a smart design from Feringa *et al* (Figure 18).[41] The direction of light-driven rotation can be reversed by base-catalysed epimerization. To achieve this, the authors designed a new motor where the methyl group at the stereogenic centre was replaced by an electron withdrawing group (an amide). During the rotary cycle, after the first photoinitiated isomerization from *(3'S)-(M)*, the unstable isomer formed *(3'S)-(P)* can be deprotonated leading to the more stable *(3'R)-(P)*. This isomer displays a configuration at the

[38] W. R. Brown.; B. L. Feringa. Making molecular machines work. *Nat. Nanotech*. **1**, 25-35 (2006).
[39] (a) M. Klok.; N. Boyle.; M. T. Pryce.; A. Meetsma.; W. R. Browne.; B. L. Feringa. MHz unidirectional rotation of molecular rotary motors. *J. Am. Chem. Soc*., **130**, 10484-10485 (2008). (b) J. Vachon.; G. T. Carroll.; M. M. Pollard.; E. M. Mes.; A. M. Brouwer.; B. L. Feringa. An ultrafast surface-bound photo-active molecular motor. *Photochem. Photobiol. Sci*., **13**, 241-246 (2014).
[40] (a) D. J. De Rosier. The turn of the screw: the bacterial flagellar motor. *Cell*, **93**, 17-20 (1998). (b) K. Kinosita.; R. Yasuda.; H. Noji.; S. Ishiwata.; M. Yoshida. F-ATPase: a rotary motor made of a single molecule. *Cell*, **93**, 21-24 (1998).
[41] N. Ruangsupapichat.; M. M. Pollard.; S. R. Harutyunyan.; B. L. Feringa. Reversing the direction in a light-driven rotary molecular motor. *Nature Chem.* **3**, 53-60 (2011).

sterogenic centre opposite to the initial isomer and can then undergo anticlockwise rotation. This work represents an essential step towards mechanical molecular systems with adaptive functional behavior.

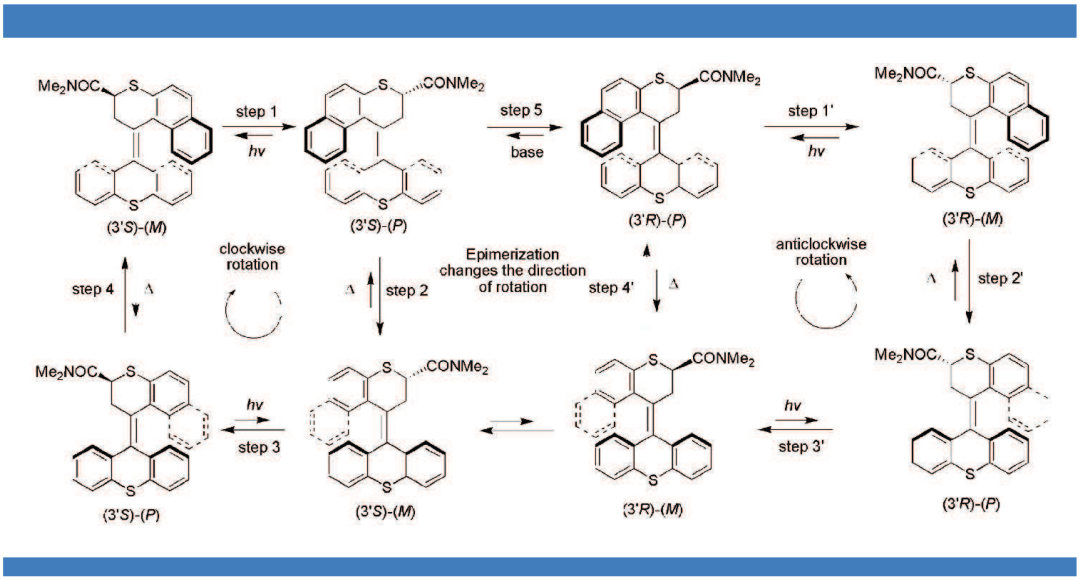

Figure 18 | Controlled clockwise and anticlockwise rotary cycles of molecular motor.[41]

In analogy with the first generation motors, functionalization of second generation motors still needs to be addressed.[42-49] Since the upper and lower parts are not symmetric, it is possible to introduce two different functional groups on both sides improving the versatility of the system.

[42] J. Vicario.; A. Meetsma.; B. L. Feringa. Controlling the speed of rotation in molecular motors. Dramatic acceleration of the rotary motion by structural modification. *Chem. Commun.*, 5910-5912 (2005).
[43] R. A. van Delden.; M. K. J. ter Wiel.; H. de Jong.; A. Meetsma.; B. L. Feringa. Exploring the boundaries of a light-driven molecular motor design: new sterically overcrowded alkenes with preferred direction of rotation. *Org. Biomol. Chem.*, **2**, 1531-1541 (2004).
[44] R. A. van Delden.; N. Koumura.; A. Schoevaars.; A. Meetsma.; B. L. Feringa. A donor-acceptor substituted molecular motor: unidirectional rotation driven by visible light. *Org. Biomol . Chem* ., **1**, 33-35 (2003).
[45] M. M. Pollard.; M. Lubomska.; P. Rudolf.; B. L. Feringa. Controlled rotary motion in a monolayer of molecular motors. *Angew. Chem. Int. Ed*., **46**, 1278-1280 (2007).
[46] A. Cnossen.; D. Pijper.; T. Kudernac.; M. M. Pollard.; N. Katsonis.; B. L. Feringa. A trimer of ultrafast nanomotors: synthesis, photochemistry and self-Assembly on graphite. *Chem. Eur. J.*, **15**, 2768-2772 (2009).
[47] G. London.; G. T. Carroll.; T. F. Landaluce.; M. M. Pollard.; P. Rudolf.; B. L. Feringa. Light-driven altitudinal molecular motors on surfaces. *Chem. Commun.*, 1712-1714 (2009).
[48] D. Pijper.; R. A. van Delden.; A. Meetsma.; B. L. Feringa. Acceleration of a nanomotor: electronic control of the rotary speed of a light-driven molecular rotor. *J. Am. Chem. Soc*., **127**, 17612-17613 (2005).
[49] D. Qu.; B. L. Feringa. Controlling molecular rotary motion with a self-complexing lock. *Angew. Chem. Int. Ed.*, **49**, 1107-1110 (2010).

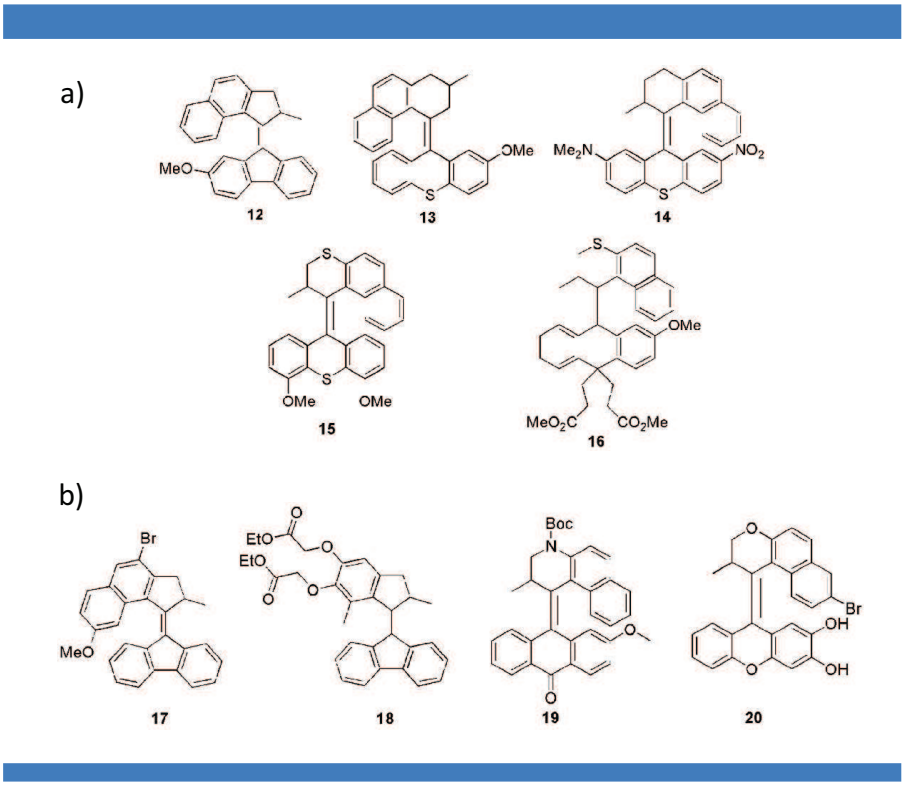

Figure 19 | a) Functionalized lower parts of second generation motors.[42-45] b) Functionalized upper part and both parts of some second generation motors.[46-49]

For the lower and upper part, -OMe, -NO_2, ester groups have been successfully introduced (Figure 19a). Methoxy was often used due to its high stability but this may also make its cleavage difficult. Ester in **16** and **18** was a "milder" protecting group which can be easily converted without touching the motor's other moiety. In motor **19** and **20**, both halves were functionalized. In particular, motor **20** is more suitable for creating complex materials system (Figure 19b).

During this PhD work, a new type of rotary motor based on imines was reported by Lehn.[50] This new motor was featured by the central C=N double instead of C=C double bond. By tuning the conformational flexibility of the stator part (the carbonyl residue) and the nitrogen inversion barrier of the rotor part (the amine residue) in the molecule, unidirectional rotation could be achieved followed by two photoisomeization and thermal induced ring inversion steps (Figure 20).

[50] L. Greb. ; J. M. Lehn. Light-driven molecular motors: imines as four-step or two-step unidirectional rotors. *J. Am. Chem. Soc.*, **136,** 13114-13117 (2014).

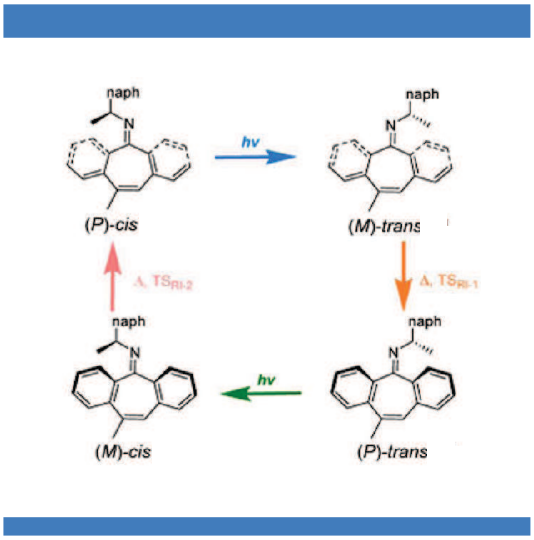

Figure 20 | Unidirectional rotation of chiral *N*-alkyl imines induced by light and heat.[50]

e) Applications of light-driven molecular motors

After the successful syntheses of different molecular motors, the group of Feringa tried to implement them in systems that would allow to harness the work produced by nanoscale motors like in natural systems. Indeed, in nature, the work provided by biological motors can be used to serve different functions such as ATP synthesis, cargo transport…

I. Motors on surface

Synthetic light driven molecular motors have been successfully immobilized on a surface without compromising their functions, which is a crucial step to be able to interface them with the macroscopic world. In this example, two attachment points at the stator are introduced in order to anchor the motor on the surface through a gold-thiol interaction. This can prevent the uncontrolled thermal rotation of the entire motor with respect to the surface while leaving the propeller function intact (Figure 21).[51]

The altitudinal molecular motors in which the rotor part is functionalized can also be attached on the surface (Figure 22a).[52] A hydrophobic perfluorobutyl chain and a relatively hydrophilic cyano group were introduced on the rotor part of the motors. Molecular motors were then attached to quartz

[51] R. A. van Delden.; M. K. J. ter Wiel.; M. M. Pollard.; J. Vicario.; N. Koumura.; B. L. Feringa. Unidirectional molecular motor on a gold surface. *Nature* **437**, 1337-1340 (2005).
[52] G. London.; K. Y. Chen.; G. T. Carroll.; B. L. Feringa. Towards dynamic control of wettability by using functionalized altitudinal molecular motors on solid surfaces. *Chem. Eur. J.* **19**, 10690-10697 (2013).

surfaces by using "click" cycloaddition method. These substituents have no significant effect on the thermal and photochemical processes of the motor, and the functionalized motors preserved their rotary function both in solution and on the quartz surface. The introduction of hydrophobic or hydrophilic substituents on the rotor part allowed controlling the wettability of the surface upon the motor's rotation as evidenced by the shape of water droplets deposited on the surface. However, efforts to control the wettability of the surface *in situ* did not show substantial effects. This could be due to the observed lower photoconversion in the case of monolayers than in solution.[53] It has already been shown that the increased steric crowding at the interface could influence the dynamic behavior of the surface-bound motors by slowing down the thermal isomerization step considerably.

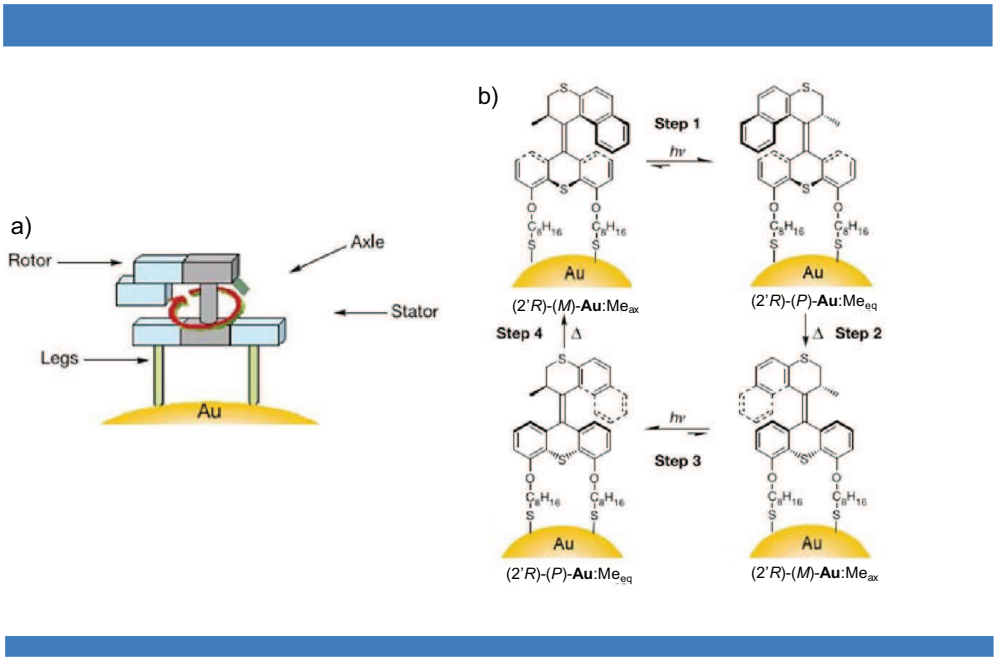

Figure 21 | a) Schematic illustration of attaching the motor on gold nanoparticles. b) Four steps rotation cycle of motor on the gold nanoparticles.[51]

To improve switching efficiency of the surface-bound motors and control the surface wettability in a dynamic manner, monolayers of fluorinated light-driven molecular motors were synthesized and immobilized on gold films in an altitudinal orientation via tripodal stators (Figure 22b).[54] Herein a tripod was chosen as the surface anchoring group because of its rigidity which was expected to anchor the motor in a fixed altitudinal orientation with respect to the surface. It also allows binding of the motor to gold in a rigid manner that is expected to sufficiently isolate the motor from the surface, allowing

[53] G. T. Carroll.; G. London.; T. F. Landaluce.; P. Rudolf.; B. L. Feringa. Adhesion of photon-driven molecular motors to surfaces *via* 1, 3-dipolar cycloadditions: effect of interfacial interactions on molecular motion. *ACS Nano*, **5**, 622-630 (2011).

efficient photoinduced isomerization. In addition, the attachment of overcrowded alkenes to surfaces via two-legs leads to a high density of packing resulting in an increase of the half-life time of the thermal helix inversion step thus yielding a decrease in the overall speed of the rotary cycle.[53] This system can modify the contact angle of a water droplet by up to 16° upon irradiation of the motor-water interface. In the present system the thermal helix inversion is not inhibited, showing that the tripod is an ideal surface anchoring group to prevent the motors from interacting with each other and from interacting directly with the underlying gold substrate.

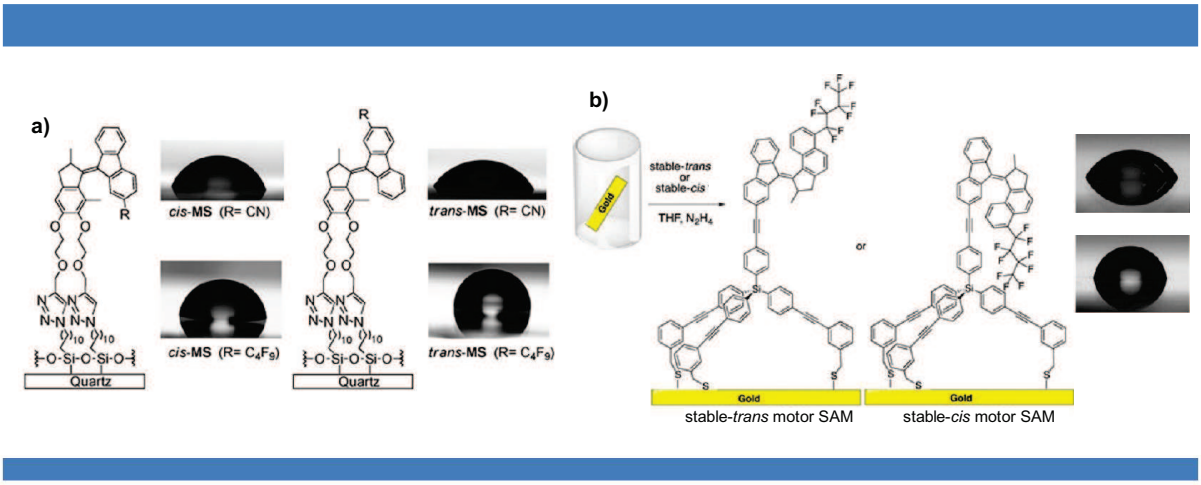

Figure 22 | a) Pictures of water droplets on altitudinal motor modified quartz **s**urfaces (**MS**).[52] b) stable-*trans* and -*cis* motor on gold surface. Water droplet on stable-*cis* motor SAM (top) and stable-*trans* motor SAM (bottom).[54]

Driving single molecules along a surface in a controlled manner remains extremely challenging because it requires molecules that can use an energy input to modulate their interaction with the surface in a way that generates motion. Based on previously reported rotary motors, Feringa *et al* designed a four-wheeled nanocar which contains four molecular motors (Figure 23).[55] Upon sequential electronic and vibrational excitation the reported nanocar undergoes continuous and defined conformational changes. Scanning tunneling microscopy has been used to monitor the activation of the conformational changes of the rotors through inelastic electron tunneling which results in a unidirectional motion of the nanocar across a Cu (111) surface. Depending on the chirality of the motor units, the system will follow either linear or random surface trajectories or remain stationary. This elegant design paves the way for

[54] K. Y. Chen.; O. Ivashenko.; G. T. Carroll.; J. Robertus.; J. C. M. Kistemaker.; G. London.; W. R. Browne.; P. Rudolf.; B. L. Feringa. Control of surface wettability using tripodal light-activated molecular motors. *J. Am. Chem. Soc.*, **136**, 3219-3224 (2014).
[55] T. Kudernac.; N. Ruangsupapichat.; M. Parschau.; B. Macia.; N. Katsonis.; S. R. Harutyunyan.; K. H. Ernst.; B. L. Feringa. Electrically driven directional motion of a four-wheeled molecule on a metal surface. *Nature* **479**, 208-211 (2011).

the exploration of molecular mechanical systems that display directed motion.

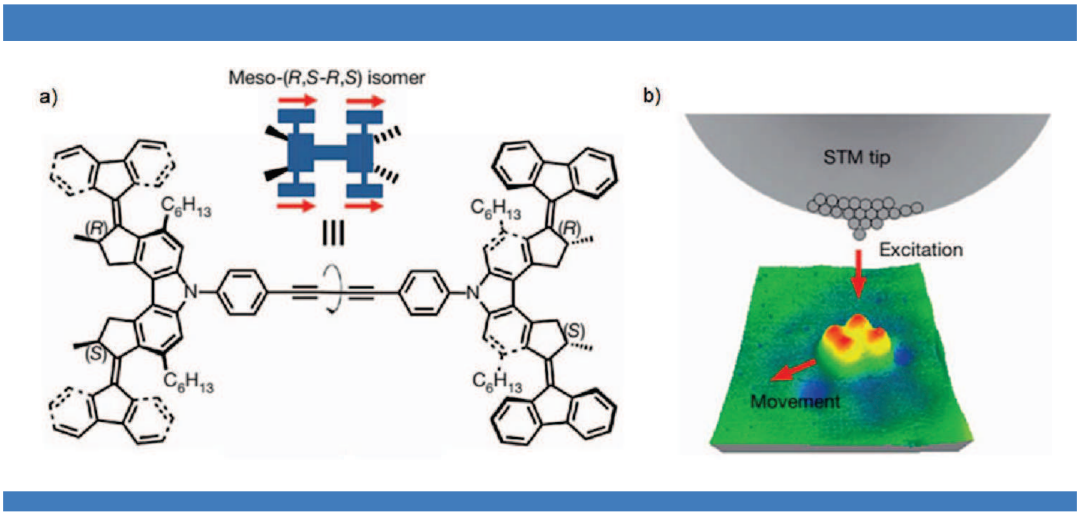

Figure 23 | a) Structure and cartoon representation of the *meso*-(*R,S-R,S*) isomer. Red arrows indicate the direction in which the rotary action of the individual motor units propels the molecule. b) Electrons tunneling through the molecule excite vibrational and electronic states and induce translational movement on the surface.[55]

II. Molecular chirality transmission

As the motor itself is chiral and its chirality can be controlled upon UV irradiation, amplifying its chirality from molecular to the macro- and supramolecular level may provide a new manner to produce smart materials. In this purpose, Feringa *et al* introduced a modified version of the light-driven molecular motors at the α-chain-end of a poly-(*n*)-hexylisocyanate (PHIC) via polymerization between benzamide functionalized motor and *n*-hexylisocyanate (Figure 24).[56]

Upon UV irradiation, the motor will undergo photoisomerization resulting in a different chirality, which leads to a preferred helical sense of the polymer backbone. Then the thermal helix inversion will induce a helicity change in the polymer chain. A subsequent photochemical and thermal isomerization step establishes the original situation with a random helicity of the polymer backbone. The transmission of chirality, from a single chiral photochromic switch unit-a rotary molecular motor-to the backbone of a dynamically racemic helical polyisocyanate, allows for reversible induction and inversion of a preferred helical sense of the polymer.

[56] D. Pijper, B. L. Feringa. Molecular transmission: controlling the twist sense of a helical polymer with a single light-driven molecular motor. *Angew. Chem. Int. Ed.*, **46**, 3693-3696 (2007).

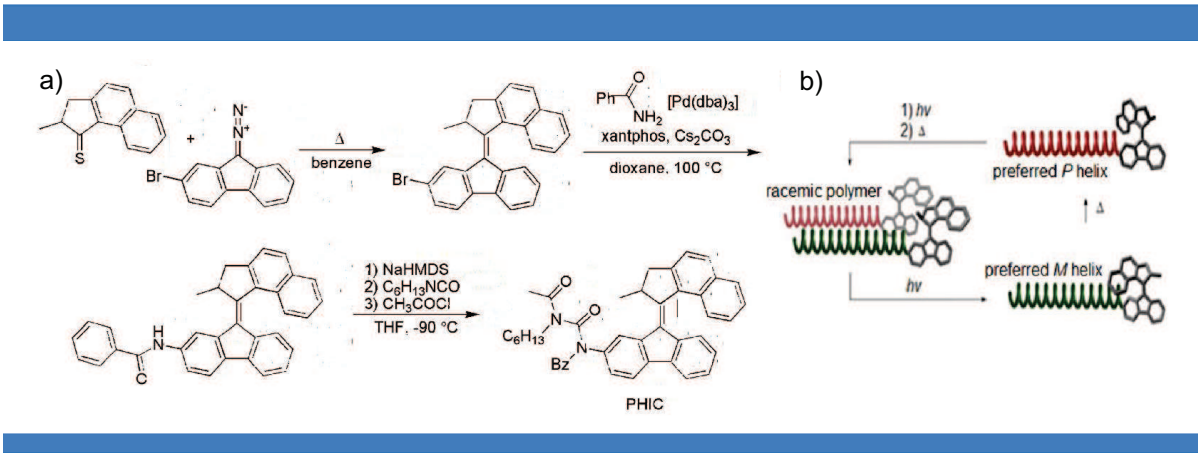

Figure 24 | a) Synthesis of motor functionalized polymers. b) Schematic illustration of the reversible induction and inversion of the helicity of a polymer backbone by a single light-driven molecular motor positioned at the terminus.[56]

Furthermore, this system can be incorporated into liquid crystals to control the supramolecular helicity of a lyotropic cholesteric liquid crystalline phase (Figure 25).[57]

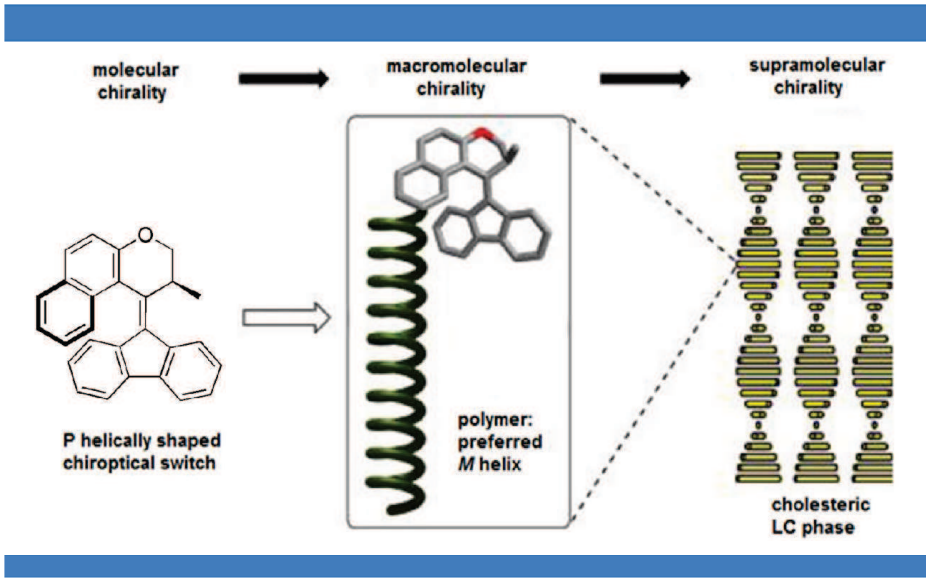

Figure 25 | Schematic demonstration of the hierarchical chirality transmission from the molecular level of a single chiroptical switch molecule, via the macromolecular level of a polyisocyanate, to the supramolecular level of a cholesteric LC phase.[57]

[57] D. Pijper.; M. G. M. Jongejan.; A. Meetsma.; B. L. Feringa. Light-controlled supramolecular helicity of a liquid crystalline phase using a helical polymer functionalized with a single chiroptical molecular switch. *J. Am. Chem. Soc.*, **130**, 4541-4552 (2008).

III. Motor used as organocatalysts

In 2011, the group of Feringa reported an example of light being used used to provide control over the chiral space in which a catalytic reaction takes place. By using a first-generation molecular motor modified with two distinct moieties that together can catalyze an asymetric reaction, it was possible to obtain both enantiomers of the Michael adduct of 2-methoxythiophenol and 2-cyclohexen-1-one by using the two pseudoenantiomeric *cis* states of the motor during its rotary cycle (Figure 26).[58] When switched to *trans* state, only racemic adduct can be obtained which means that the bifunctional activation of this catalyst was lost.

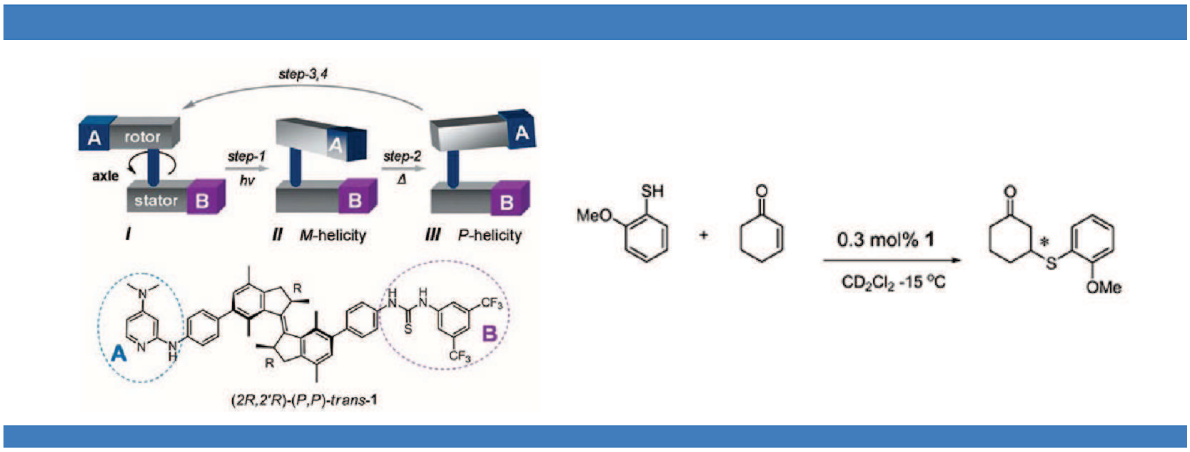

Figure 26 | A asymmetric Michael addition catalyzed by an integrated light driven molecular motor acting as a bifunctional organocatalyst.[58]

The above organocatalyst bears a 2-aminopyridine base and a weakly acidic thiourea functionality that engage in bidentate coordination to the substrate. However, this catalyst displayed poor catalytic performance in Henry and related reactions both in terms of activity and stereoselectivity. So a novel molecular motor-based catalyst, in which the phenyl spacers between the motor core and the catalytic functionalities were removed was prepared (Figure 27).[59] It was expected that bringing the catalytically active groups (thiourea and DMAP) in greater proximity would result in a more effective cooperative action between these two functionalities. Indeed, two *cis* forms of motor catalyst could direct the stereochemical outcome of this reaction with an improved yield compared to the original catalyst. As expected, the *trans* form of motor catalyst in which the two groups are far away in space, led to very

[58] J. Wang.; B. L. Feringa. Dynamic control of chiral space in a catalytic asymmetric reaction using a molecular motor. *Science* **331**, 1429-1432 (2011).
[59] M. Vlatkovic.; L. Bernardi.; E. Otten.; B. L. Feringa. Dual stereocontrol over the Henry reaction using a light- and heat-triggered organocatalyst. *Chem. Commun.*, **50**, 7773-7775 (2014).

poor conversion and stereoselectivity.

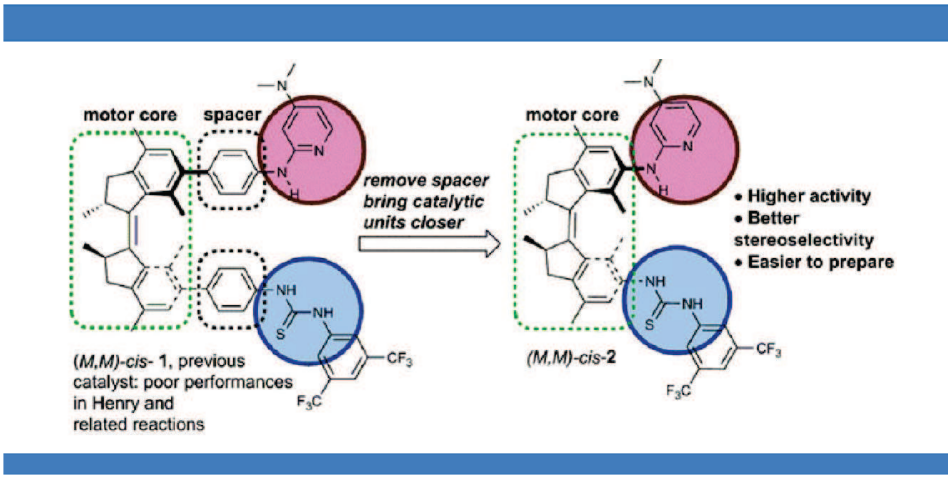

Figure 27 | A new design of motor organocatalyst.[59]

IV. Utilizing the motion of motor to perform useful work

Feringa *et al* have also showed that their motor was able to induce microscopic movements in doped liquid crystal films (Figure 28).[60] Indeed, on a liquid crystal film doped with unidirectional molecular motors (1 % in weight), it was reported that the photochemically or thermally induced isomerization steps of the motor result in reorganization of the polygonal LC texture. A surface relief of 20 nm was observed on top of this film by using AFM and optical profilometry. The rotational change in surface relief generates sufficient torque to rotate a microscopic object (a glass rod) placed on top of the film in a unidirectional manner. It should be mentioned that in this case, the rotation of the glass rod was induced by the helical reorganization of the liquid-crystal film which served as a "transfer station" between the motor and the glass rod. Driving a microscopic object motion directly by the collective action of several motor units like in natural systems still remains a challenge. This will represent a new milestone in the area of nanotechnology.

[60] J. Vicario.; N. Katsonis.; B. S. Ramon.; C. W. M. Bastiaansen.; D. J. Broer.; B. L. Feringa. Nanomotor rotates microscale objects. *Nature* **440**, 163 (2006).

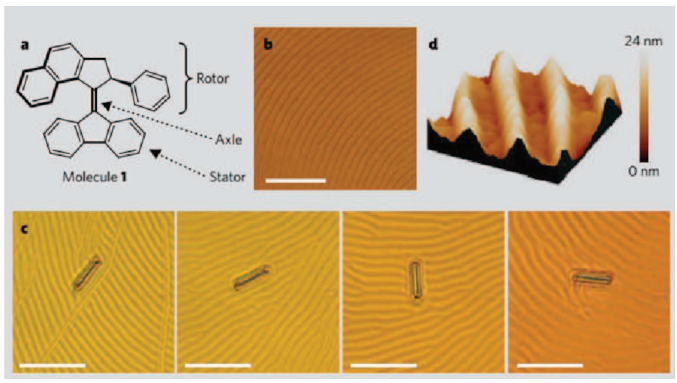

Figure 28 | a) Structure of the motor. b) Polygonal texture of a liquid-crystal film doped with motor (1 % by weight). c) Glass rod rotating on the liquid crystal during irradiation with ultraviolet light. Frames 1-4 (from left) were taken at 15-s intervals and show clockwise rotations of 28° (frame 2), 141° (frame 3) and 226° (frame 4) of the rod relative to the position in frame 1. Scale bars, 50 μm. d) Atomic force microscopy image of surface structure of the liquid-crystal film.[60]

3. Conclusion

Although Kelly reported their motor at the same time as Feringa, applications of his motor were limited by non-continuous rotation, the inconvenient manner of energy input as well as the rotation speed. On the contrary, by rational design and fine synthetic strategy, Feringa *et al* have improved their light driven unidirectional molecular motor from first to second generation motors that have achieved MHz unidirectional rotation. It has been demonstrated that light and chemical energy input could be used to induce controlled and unidirectional rotation. In addition, they have shown great and promising potential of these molecular motors. Anchoring molecular motors to surfaces without loss of function was a significant step towards future nanomachines and devices. Also it has been shown that rotary motors could perform useful work and move microscopic objects (it should be mentioned that the movement of microscopic object is not driven directly by the motor). It has been proven that they could be used as dynamic catalysts to provide control over the chiral space of a reaction. Furthermore, motors could be integrated into a nanocar system which is capable of converting an external energy input into unidirectional movement along a surface. Although some applications of molecular motors have been realized, the whole area is still at very early stage. More challenges still exist, such as how to efficiently synthesize enantiopure motors on large scale; how to control the directional motion especially on a specific trajectory; how to integrate motors into larger and more complicated machines and devices as

well as more complex systems, etc. Those challenges and especially the integration of motors working out of equilibrium to provide macroscopic motion represent the foundation of this Ph. D. work. As biological systems can successfully harness work from nano-scaled motors to perform tasks freely and efficiently, though this is the result of natural evolution and selection over billions of years, understanding these biological processes and mechanism will undoubtedly help us to design artificial molecular motors more rationally. Thus learning from nature should always be kept in mind. The above examples will obviously be a continuous inspiration for chemists to pave the way for useful synthetic molecular motors and machines.

Chapter 2: Synthesis and Characterization of Highly Functionalized Rotary Molecular Motors

In the first chapter, an overview was given concerning synthetic rotary molecular motors. Certain aspects of these molecular motors have been explored, however, synthetic improvements still need to be focused on because there has not been an efficient route to highly functionalized motors, and particularly the development of an enantiopure synthetic strategy remains a challenge. Thus, this situation has spurred us to develop a new molecular motor that is easily accessible and highly functionalized, and which can provide motors with more applications in materials science. Specifically, our aim was to design a new second generation motor with different functional groups in the upper and lower parts. These different functional groups should be easily tunable as well as tolerant towards specified reaction conditions. We also expect that this new motor could be used in materials science for performing some useful tasks directly by coordinating the motions in polymer networks.

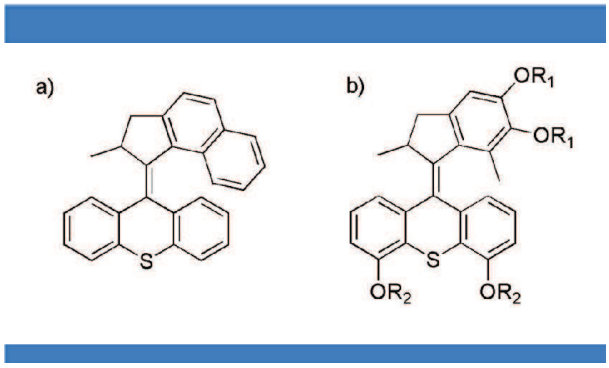

Figure 29| a) Reported molecular motor with 3 MHz rotational frequencies at ambient temperature.[39a] b) Our synthetic target molecule.

As the cyclopentane-based molecular rotary motor (Figure 29a) displayed even less steric hindrance and could accomplish unidirectional rotary motion with MHz rotational frequencies at ambient temperature, [39a] our synthesis was directed towards a new functionalized cyclopentane-based molecular rotary motor (Figure 29b). By replacing the benzyl ring with a small methyl group, it was anticipated that it could further diminish the steric hindrance during the thermal helix inversion step thus enhancing the rotation speed.

1/ Retrosynthetic approach

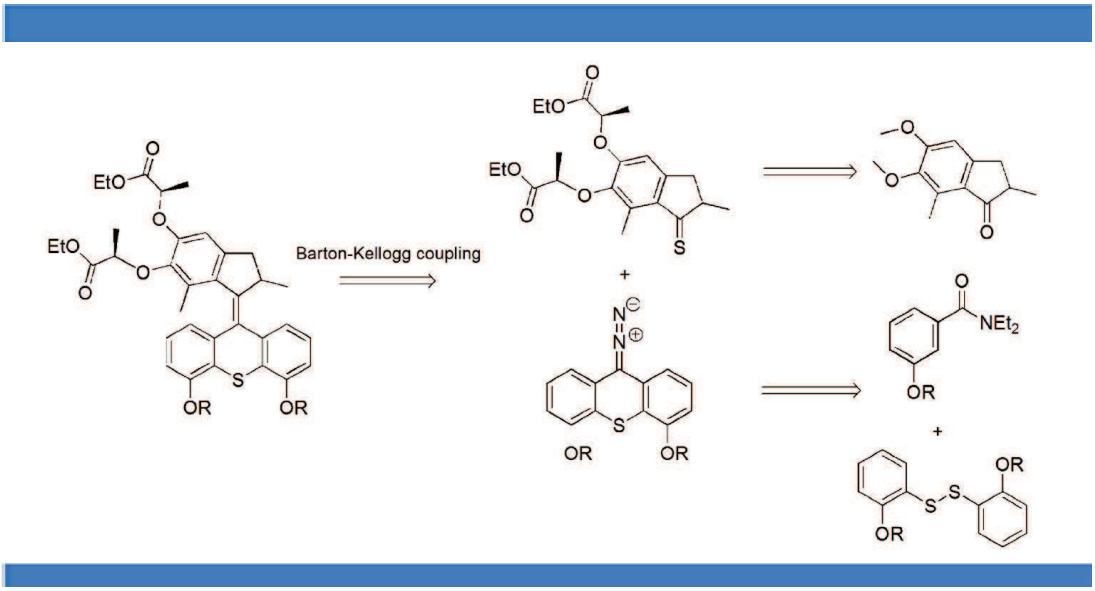

Figure 30 | Retrosynthetic analysis of the target motor

Generally, the second generation motors can be divided into two parts: an upper and a lower part. The upper and lower parts are usually connected using the Barton-Kellogg coupling method (Figure 30).[33-35] In this method, the hydrazone are first oxidized (MnO_2, Ag_2O, etc) into a diazo compound. This active diazo intermediate is then reacted with a thioketone forming the episulfide which undergoes desulfurization affording the final motor (see Chapter 1). For the upper part, a survey of the literature indicates that using ester as the functional or protecting group may be reliable as some related syntheses of this part have been reported in the literature.[47] The most challenging section is the synthesis of the lower part. First, the protecting group for the phenol should be compatible with the ester cleavage conditions. Secondly, the central double bond should also be tolerant to the deprotection conditions.

During the course of our strive towards highly functionalized molecular motor, we tried different phenol protecting groups. We will detail this synthesis in the following discussions.

2/ Synthesis of molecular motor

a) Synthesis of the upper part

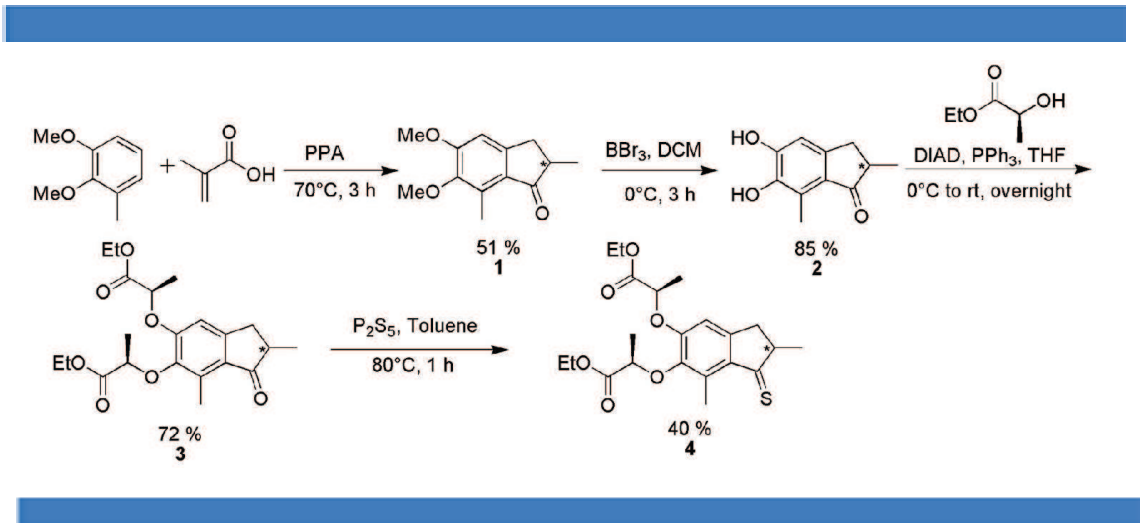

Scheme 5 | Synthesis of the upper part

First, our synthesis started from the upper part (Scheme 5). 2,3-dimethoxytoluene and methacrylic acid underwent a Friedel-Crafts type reaction in PPA at 70 °C to form methoxy protected indanone **1** with 51 % yield. Then methoxy groups were removed by boron tribromide in DCM at 0 °C affording bis-phenol indanone **2** as a racemic mixture in 85 % yield. As the configuration of the carbon atom next to ketone group in **2** will determine the direction of rotation of the final motor, it was highly required that the upper part could be separated and used as enantiopure compounds. So in the next step, we introduced a chiral auxiliary which is (-)-lactic ethyl ester to the indanone giving bis-ester indanone **3** via a Mitsunobu reaction in THF. As it is well known, the configuration of the alcohol is inverted under these conditions and thus, compound **3** will be obtained as a diastereomeric mixture which could be separated by classical chromatography method. Another advantage is that we also introduced a functional group-ester into the upper part. Although in the following synthetic steps, we found that when we started with a diastereoisomeric mixture, we could still get optically pure motors after the Barton-Kellogg coupling reaction. From the synthetic strategy point of view, there is no doubt that trying to introduce a chiral auxiliary to facilitate the separation is still highly valuable. Indanone **3** was then converted to thioketone **4** using P_2S_5 in toluene at 80 °C with 40 % yield. This thioketone was obtained as a purple oil but was not stable towards air and the yield of this step was usually no more than 50 %. Therefore we only prepared it freshly just before the next reaction step. With the upper part in hand, we

will now focus on the lower part.

b) Synthesis of the lower part

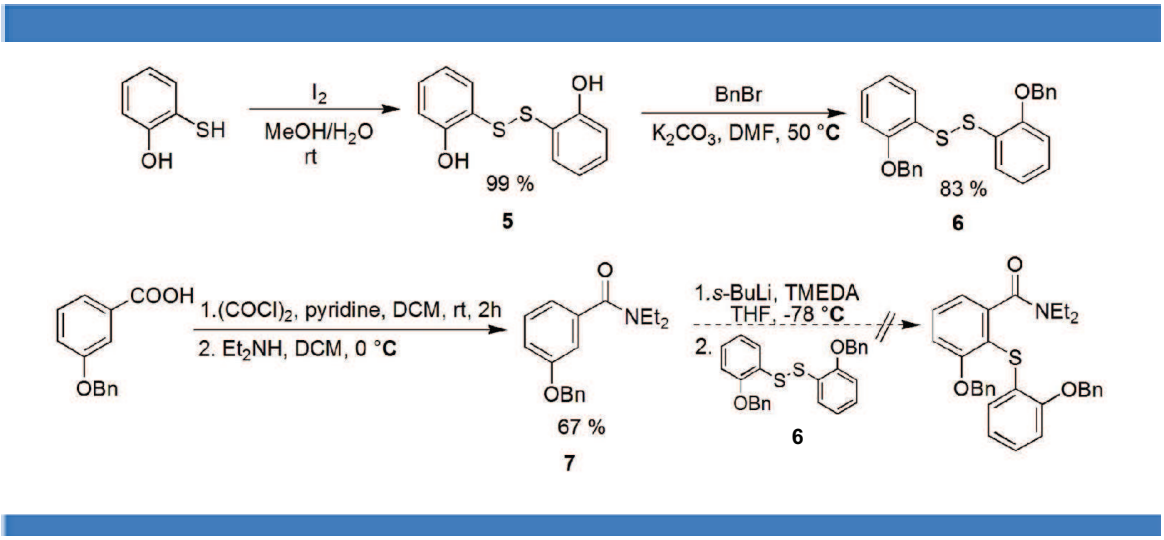

Scheme 6 | Synthesis of -OBn protected lower part

For the lower part, we first tried benzyl group (-OBn) as the protecting group (Scheme 6). 2-mercaptophenol was oxidized using I_2 to the disulfide bis-phenol **5** in quantitative yield. Then bis-phenol **5** was reacted with benzyl bromide in DMF affording benzyl protected disulfide **6** with 83 % yield. In the parallel route, the benzyl protected amide **7** was produced from 3-benzylbenzoic acid by using oxalyl chloride and diethyl amine. The amide **7** was first lithiated with *s*-BuLi at the *ortho*-position. Then disulfide **6** was coupled to form the thioether-amide. Unfortunately, this reaction was unsuccessful. Probably because of the weak positional directing ability of the benzyl group. Another possibility is that the acidity of the benzylic hydrogen may cause the failure of this reaction as it introduces a strong base.

So we decided to change the protecting group. Silyl ether was chosen as it is a classical protecting group orthogonal to esters and only requiring mild cleavage condition (Scheme 7). TBS-protected disulfide **8** was then produced from phenol **5** by reacting with TBS-Cl and imidazole in DMF at room temperature with 96 % yield. 3-hydroxy benzoic acid was first converted to 3-hydroxyl benzamide **9** which was then protected by TBS group affording compound **10** with quantitative yield. We then tried to couple TBS protected amide **10** and disulfide **8**, but still the expected product was not obtained. One possible reason is that TBS group may be sensitive to the strong basic condition used (*s*-BuLi).

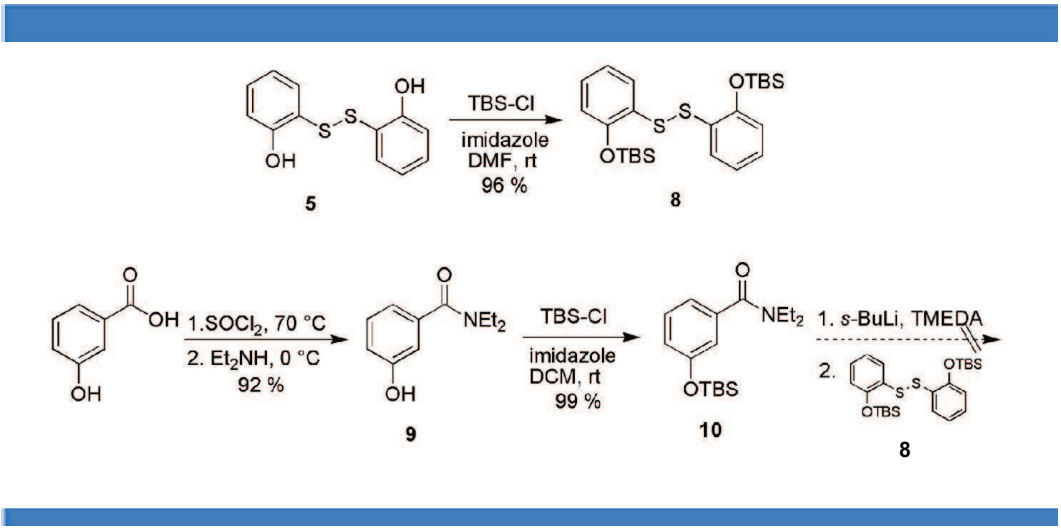

Scheme 7 | Synthesis of TBS protected lower part

Although the above results were frustrating, we decided to test -OMe as a protecting group which was previously used on other motors (Figure 31).[37] Furthermore for amide compounds like **7**, examples in the literature have reported that methoxy was a good directing group for *ortho*-lithiation.[61a,b]

Following the method from Feringa, we started with 3-methoxybenzamide which was first coupled with methoxy protected disulfide **11a**[61c] giving the thioether-amide **11** (Scheme 8). Then this amide underwent a ring closing reaction using LDA and affording a key intermediate ketone **12**. To convert this ketone into hydrazone **13** directly, we refluxed it with hydrazine monohydrate in EtOH, but no product was obtained maybe because of the low activity of this conjugated ketone (reduced electrophilic character). Thus hydrazone **13** had to be prepared over 2 steps via a more reactive thioketone intermediate. Then the most important step is the Barton-Kellogg coupling reaction. By using MnO_2 as the oxidant, the hydrazone **13** was first converted to a very reactive diazo intermediate which was then reacted with thioketone **4** to form episulfide **14**.

[61] (a) A. I. Meyers.; K. Lutomski. O. Metalations. Intermolecular competition between various substituents. *J. Org. Chem*. **44**, 4464-4466 (1979). (b) D. W. Slocum.; C. A. Jennings. Directed metalation reactions. 6. Competition of substituents for ortho direction of metalation in substituted anisoles. *J. Org. Chem*. **41**, 3653-3664 (1976). (c) J. D. Warren.; J. S. Miller.; S. J. Keding.; S. J. Danishefsky. Toward fully synthetic glycoproteins by ultimately convergent routes: a solution to a long-standing problem. *J. Am. Chem. Soc*. **126**, 6576-6578 (2004).

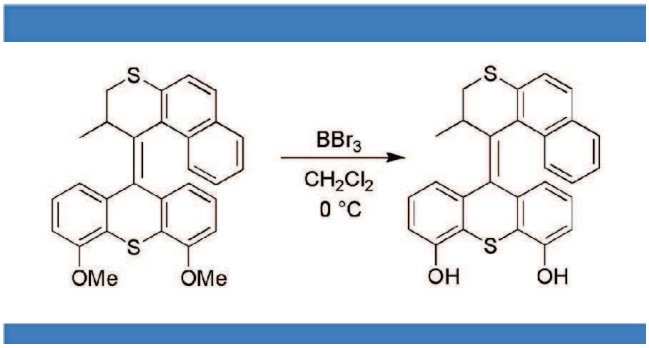

Figure 31 | Feringa's method for the cleavage of methoxy on the motor[37]

To our satisfaction, starting from a racemic mixture of **4**, only two single isomers of episulfide **14** were obtained which could even be separated with classical chromatography techniques (silica column). In addition, these two isomers could be prepared on a large scale which is crucial for the following materials research. Fortunately, we also obtained single crystals for one isomer which were suitable for X-ray analysis (*vide infra*).

With the two episulfides in hand, we could work with the single isomer in the following synthesis. The episulfide **14** was submitted to desulfurization by using PPh_3 affording the overcrowded alkene **15**. One of this two isomeric alkenes was obtained as single crystals which were suitable for X-ray analysis.

At that stage, we already have a fully protected motor in which the upper part is protected by an ester and the lower part is protected by a methoxy group. Thanks to the choice of orthogonal protecting groups, it is possible to selectively deprotect motor **15**. We first succeeded to saponify the motor giving the bis-acid **16** under classical conditions with 77 % yield (Scheme 9). Then we tried to remove the methoxy groups in the lower part.

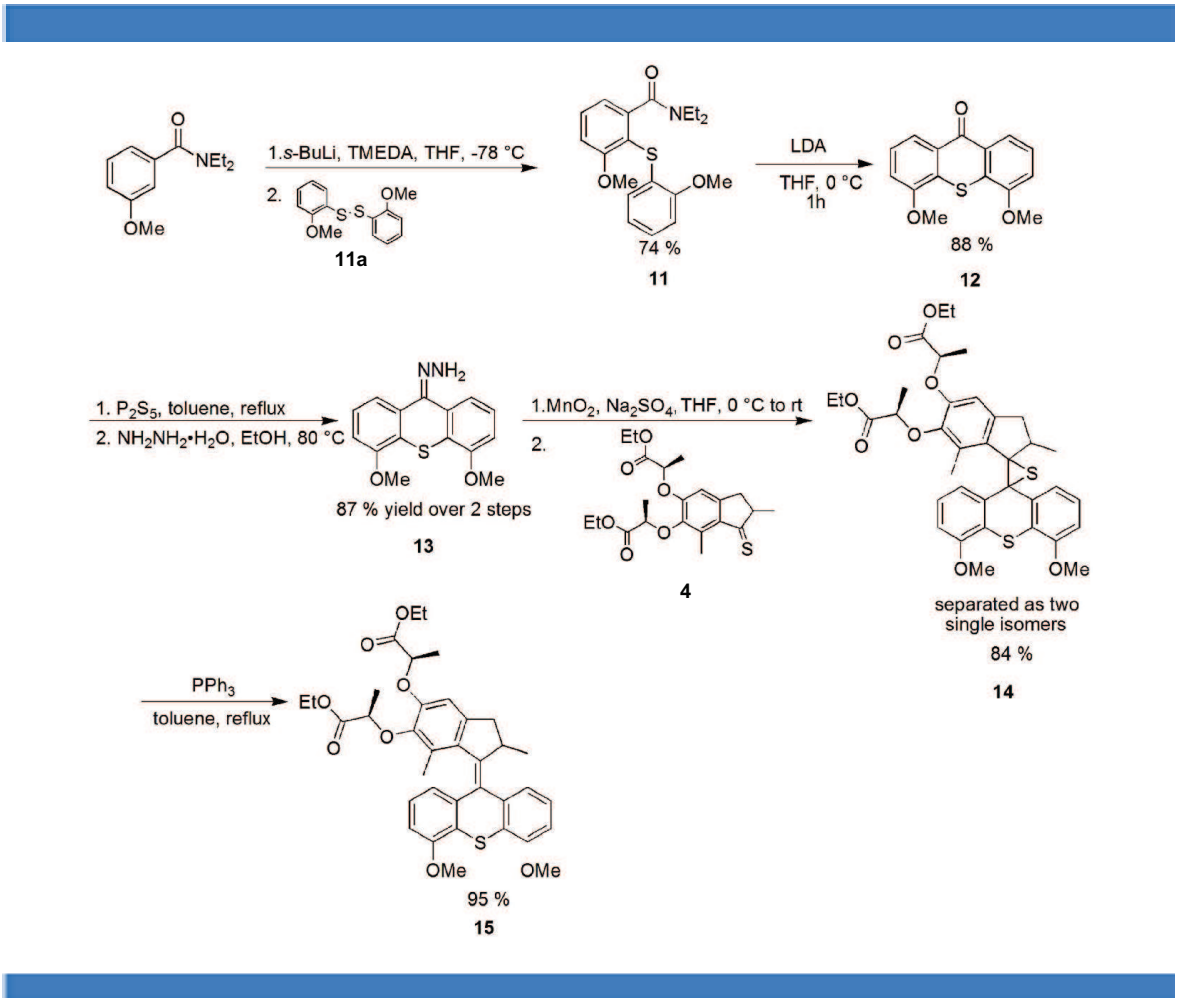

Scheme 8 | Synthesis of **-OMe** protected motor

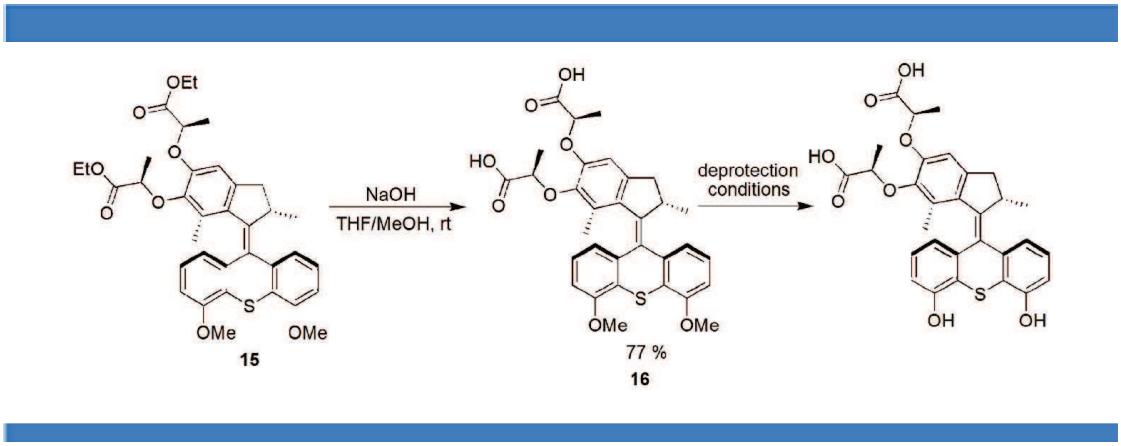

Scheme 9 | Selective deprotection of methoxy protected motor

Although many methods were used to remove the methoxy group (see Table 1), the results were not satisfying. With boron tribromide, the methoxy could be removed but there were always many side

products and tedious purification usually afforded limited amount of materials. Obviously it was not a practical method for further use in materials research. The methoxy is too stable to be removed in this case while the ester on the motor is affected by the methyl deprotection conditions.

Table 1 | Method for cleavage of -OMe

Method	Result
48 % HBr (3 eq.), HOAc, reflux	No target compound, unknown species
LiBr (2 eq.), DMF, reflux	Only starting materials
$AlCl_3$ (≥3 eq.), CH_2Cl_2, -10 to 80 °C	Low yield and unknown species
BBr_3, CH_2Cl_2, -70 °C to rt	Tedious purification, 5 % yield

However, during this synthetic stage, some points were quite informative and helpful. One extremely important thing was that by using Barton-Kellogg coupling method, we could determine the reaction conditions for the final overcrowded alkene. Another encouraging thing was that the motor could be prepared on a large scale (gram scale). This problem had never been resolved before and to the best of our knowledge, there was no literature reporting the synthesis of this type motor on large scale (it usually requires time-consuming preparative chiral HPLC to separate this kind of motor and only a few milligrams of materials can be obtained).[31,36] Last but not least, we had two crystal structures containing one episulfide isomer and one motor isomer. This will allow us to unambiguously determine the configuration and conformation of this new motor.

c) Synthesis of –OBn and –TBS protected motor

The above non-perfect synthesis has spurred us to reconsider the synthetic strategy seriously. Since the upper part in which the ester group is fixed, the core of this problem is to introduce a proper protecting group to the lower part that can be removed easily in the presence of ester or acid group on the motor. In scheme 2 and 3, we expected to introduce -OBn and -TBS by directly coupling with corresponding disulfide via *ortho*-lithiation. However, our results showed that only methoxy can be used in this step. So we considered the possibility to introduce the protecting groups in an "indirect" way by avoiding or even skipping the *ortho*-lithiation step. The strategy consisted in the conversion of methoxy ketone **12** to benzyl or TBS protected ketone before coupling to the upper part.

Ketone **12** was deprotected with BBr_3 and reprotected with -OBn over two steps affording ketone **17** with 95 % yield (Scheme 10). Hydrazone **18** was obtained from ketone **17** over two steps with 60 % yield. Then hydrazone **18** was oxidized by MnO_2 in THF at 0 °C followed by coupling with the upper part. Episulfide **19** was also obtained as two isomers as methoxy protected episulfide **14** but with only 28 % yield and the separation of these two isomers proved to be extremely tedious. Therefore we did not continue with this protecting group.

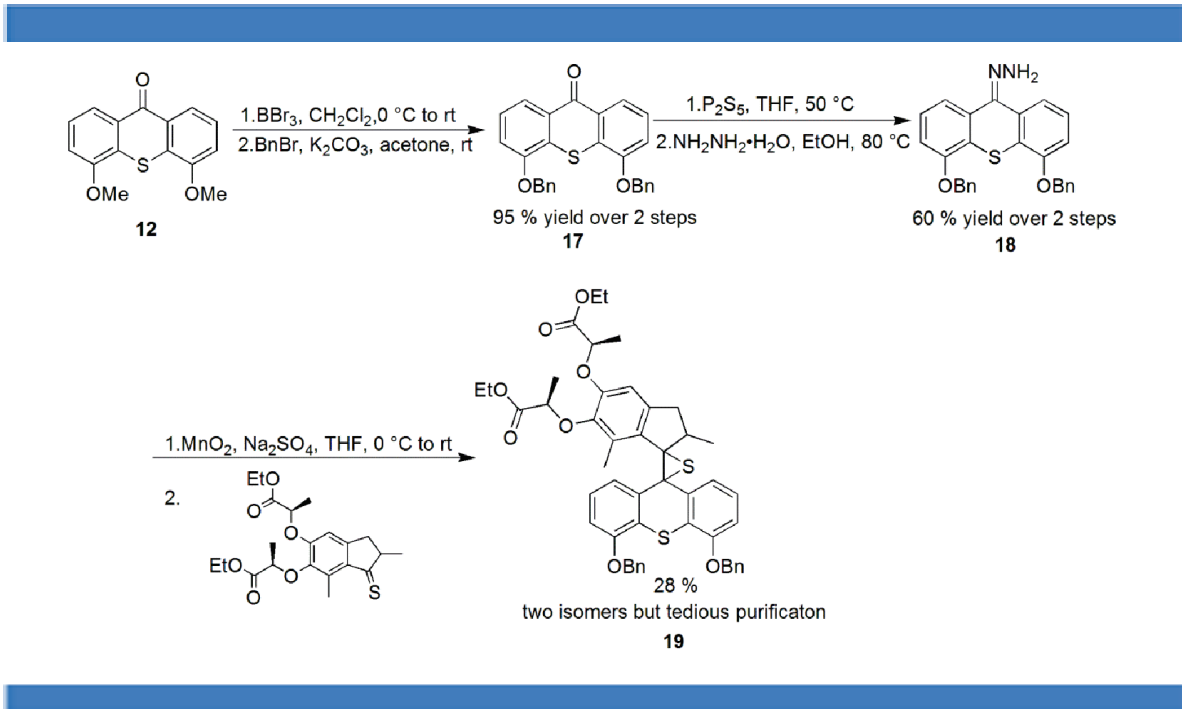

Scheme 10 | Synthesis of **-OBn** protected motor

Another choice is the -TBS group (Scheme 11). In the same manner, TBS protected ketone **20** was prepared from **12** over two steps in an almost quantitative yield. Then ketone **20** was converted to hydrazone **21** also over two steps with 89 % yield. The procedure from **12** to **21** always goes smoothly and even provides a better yield compared with the "direct" way in scheme 4. Finally, Barton-Kellogg coupling reaction was performed giving two isomers of TBS protected episulfide **22**. The most thing is that these two isomers could be separated on silica flash column, and could also be prepared on gram scale! Fortunately, we also obtained crystals of one isomer which were suitable for X-ray analysis. The NMR spectra of these two isomers and -OMe protected episulfide **14** showed similarities. Combining the NMR and X-ray data we could determine the configuration of each isomer (*vide infra*). Working with a single isomer, the episulfide underwent desulfurization with PPh_3 in toluene at 130 °C affording the final fully functionalized and enantiopure motor **23** with 95 % yield.

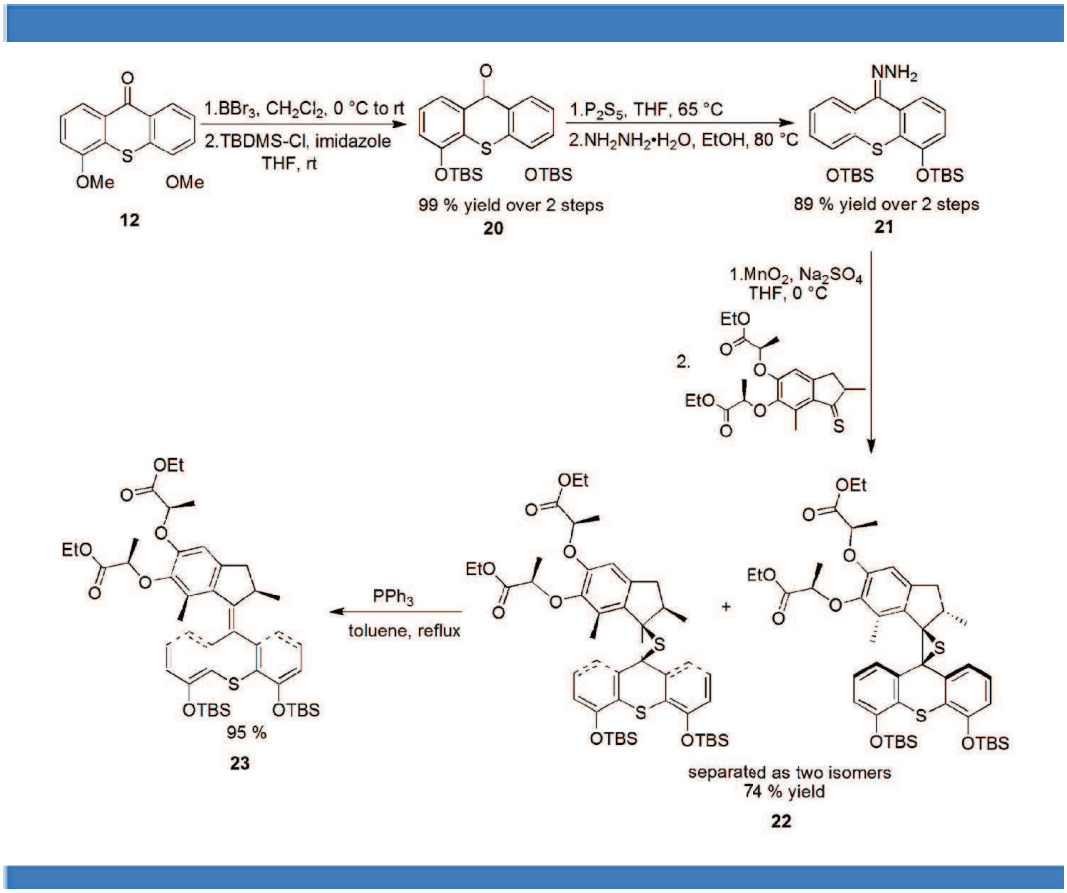

Scheme 11 | Synthesis of **TBS** protected motor

Since there are ester and TBS groups on the motor, we expect that these two groups can be removed in a selective manner irrespective to the sequence of cleavage (Scheme 12). First, TBAF was used to remove the TBS in the presence of ester. This step went smoothly almost in a quantitative manner at 0 °C within 5 min. Then the ester-phenol **24** underwent saponification yielding the fully deprotected motor **26**.

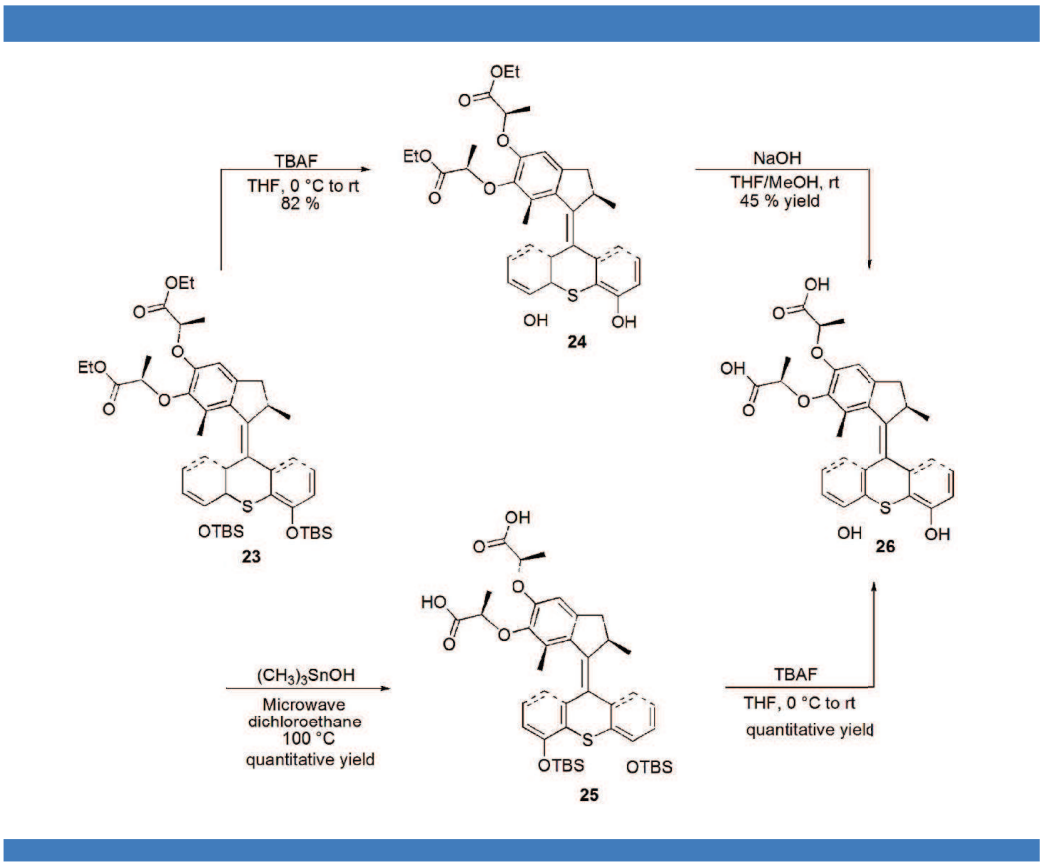

Scheme 12 | Selective deprotection of the motor

Meanwhile we tried to saponify the ester in the presence of TBS (Table 2). This step seemed more challenging since TBS is sensitive to basic condition. We first used some classical conditions to remove the ester. Under these conditions, TBS proved to be not tolerant and usually the fully deprotected motor was obtained. A survey of literature showed that $(CH_3)_3SnOH$ as a much milder reagent could remove the ester in the presence of many other functional groups including TBS.[62] Refinement of this method conditions allowed to optimize the reaction. Finally, bis-acid **25** could be prepared in quantitative yield under microwave irradiation at 100 °C for 9 h. Subsequently cleavage of TBS with TBAF worked very well as expected.

[62] K. C. Nicolaou.; A. A. Estrada.; M. Zak.; S. H. Lee.; B. S. Safina. A mild and selective method for the hydrolysis of esters with trimethyltin hydroxide. *Angew. Chem. Int. Ed.* **44**, 1378-1382 (2005).

Table 2 | Optimization of the saponification in the presence of TBS

Method	Result
NaOH (2 eq.) , MeOH/THF, rt	Cleavage of TBS
$Ba(OH)_2$ (2 eq.), THF, rt, 5h	Fully deprotected motor
$(CH_3)_3SnOH$ (2.2 eq), dichloroethane, 70 °C, 25 days	Single desired compound quantitative yield
$(CH_3)_3SnOH$ (2.2 eq), dichloroethane, 80 °C, 25 days	
$(CH_3)_3SnOH$ (5 eq), dichloroethane, 80 °C, one week	
$(CH_3)_3SnOH$ (2.5 eq), dichloroethane, 100 °C, microwave, 150w, 29h	
$(CH_3)_3SnOH$ (6 eq), dichloroethane, 100 °C, microwave, 150w, 11h	
$(CH_3)_3SnOH$ (8 eq), dichloroethane, 100 °C, microwave, 150w, 9h	

At this point, a fully functionalized molecular motor had been synthesized. Compared with the related motor systems reported before,[31a,63] this is the first motor which is highly functionalized both in the upper and lower parts with different functional groups making this motor more versatile with respect to future applications in materials science. Although elaborated synthetic steps are required, the motor can still be prepared on gram scale.

3/ Integrating the motor into the polymer system

With highly functionalized motor **23** in hand, we next tried to integrate this motor into the polymer system. Herein, polyethylene glycol (PEG) (Mw=5000 $g \cdot mol^{-1}$ and $g \cdot 10000^{-1}$) was chosen as the model polymer due to its commercial availability along with its various derivatives.

But before using these long chain polymers, short PEG chain molecules were used to explore the reaction conditions as polymeric reactions are quite different from ordinary organic reactions (reaction activities, dynamics, etc.). Therefore a short functionalized PEG chain molecule with Mw=750 $g \cdot mol^{-1}$ was used first (Scheme 13).

Following the classic peptide synthetic method, EDC was used as coupling reagent. During the synthesis, we found that the reaction could not be finished completely. There was always the mono-amide products in the mixture even by heating up the mixture. It was deduced that the problem may be coming from the stability or activity of the intermediate-EDC activated ester (O-acylurea (Scheme 14).

[63] Ben. L. Feringa. The art of building small: from molecular switches to molecular motors. *J. Org. Chem*. **72**, 6635-6652 (2007).

Thus HOBt which is a quite efficient additive was used since it usually can suppress the racemization of single-enantiomer chiral molecules and also improve the efficiency of peptide synthesis. After HOBt was used as additive for this reaction, the yield was improved significantly. By using excessive amounts of EDC (typically 8 eq.) and 2.5 eq. of HOBt, compound **28** could be made efficiently in dichloromethane at room temperature with 76 % yield. Then -TBS group in compound **28** was removed quantitatively by using TBAF in THF at 0 ˚C usually within only 5 min. Finally, NHS functionalized PEG was reacted with phenol **29** using DMAP as the base affording the four-armed motor-polymer conjugate **30**.

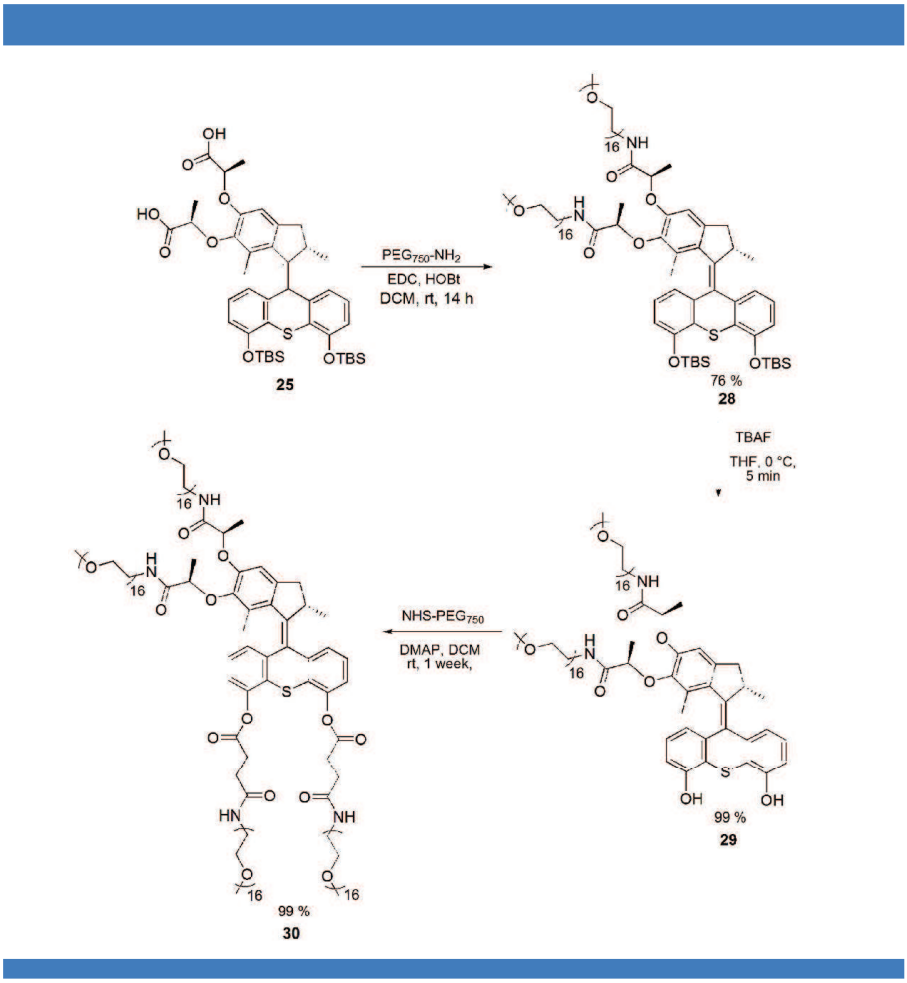

Scheme 13 | Model reaction using PEG_{750}

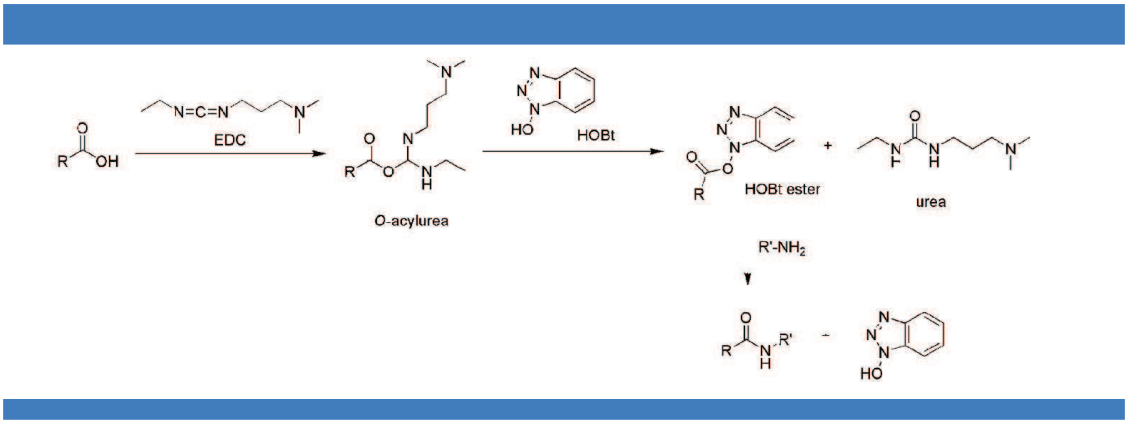

Scheme 14 | Reaction mechanism mediated by EDC and HOBt for peptide synthesis

Upon finishing the above model reaction, we applied the same conditions to PEG_{5000} (Scheme 15). First, compound **25** was reacted with N_3-PEG_{5000}-NH_2 (2 eq.) in dichloromethane using EDC (8 eq.) and HOBt (2.5 eq) as the coupling reagents at room temperature. After 163 h, the reaction was complete. Due to its large polarity, compound **31** could be purified by preparative HPLC, but strangely the yield was only 37 %. In the next step, TBS groups from compound **31** were removed in THF using TBAF at 0 ˚C within 5-10 minutes giving phenol **32**. Then compound **32** was purified by preparative HPLC. At this stage, the yield for the synthesis of compound **32** was a little bit unsatisfying (40 % yield) although the purity was guaranteed. To prepare the key precursor **33**, DMAP was used as the base, however we never managed to synthesize this compound because this reaction was difficult to monitor on the UPLC-MS (It seems that the starting material and the product have the same retention time) or the reaction advanced very slowly due to the limited accessibility of the reaction sites on the large polymer chain.

These issues have spurred us to find a more efficient alternative. In the above synthesis, two polymers with the same length were chosen to be connected to the motor's two halves. But it would be equivalent to connect a much longer chain (with terminal azide group and the length doubled) to the upper part while in the lower part a short linker (e.g. with terminal alkyne) could be introduced.

Therefore we decided to first modify the lower part with a short terminal alkyne linker. Starting from triethylene glycol, tosylated alkyne **35** was made via two steps in 72 % total yield (Scheme 16). Then phenol **24** was reacted with this short linker in DMF using K_2CO_3 as the base, heating up to 45 ˚C for 48 hours afforded the alkyne functionalized motor **36** in 86 % yield. Then motor **36** underwent saponification using NaOH giving a bis-acid motor **37** in 60 % yield. By using the classical peptide synthesis method, motor **37** was connected with azide modified-polyethylene glycol (Mw=10000 $g \cdot mol^{-1}$ or 5000 $g \cdot mol^{-1}$) via an amide bond formed through a combination of EDC (8 eq.) and HOBt (2.5 eq.) in dichloromethane at room temperature. Compound **38** could be separated by reverse phase column

chromatography with C18 as the packing materials. The yield was 60 % and 37 % for PEG 5000 and PEG 10000, respectively.

At this stage, by using the peptite synthesis method, the motor could be connected to polymers successfully. Since these motor-polymer conjugates contain terminal azide and alkyne groups, they will be used to prepare novel polymeric materials thanks to click chemistry in the following chapter in which the applications of molecular motor will be discussed.

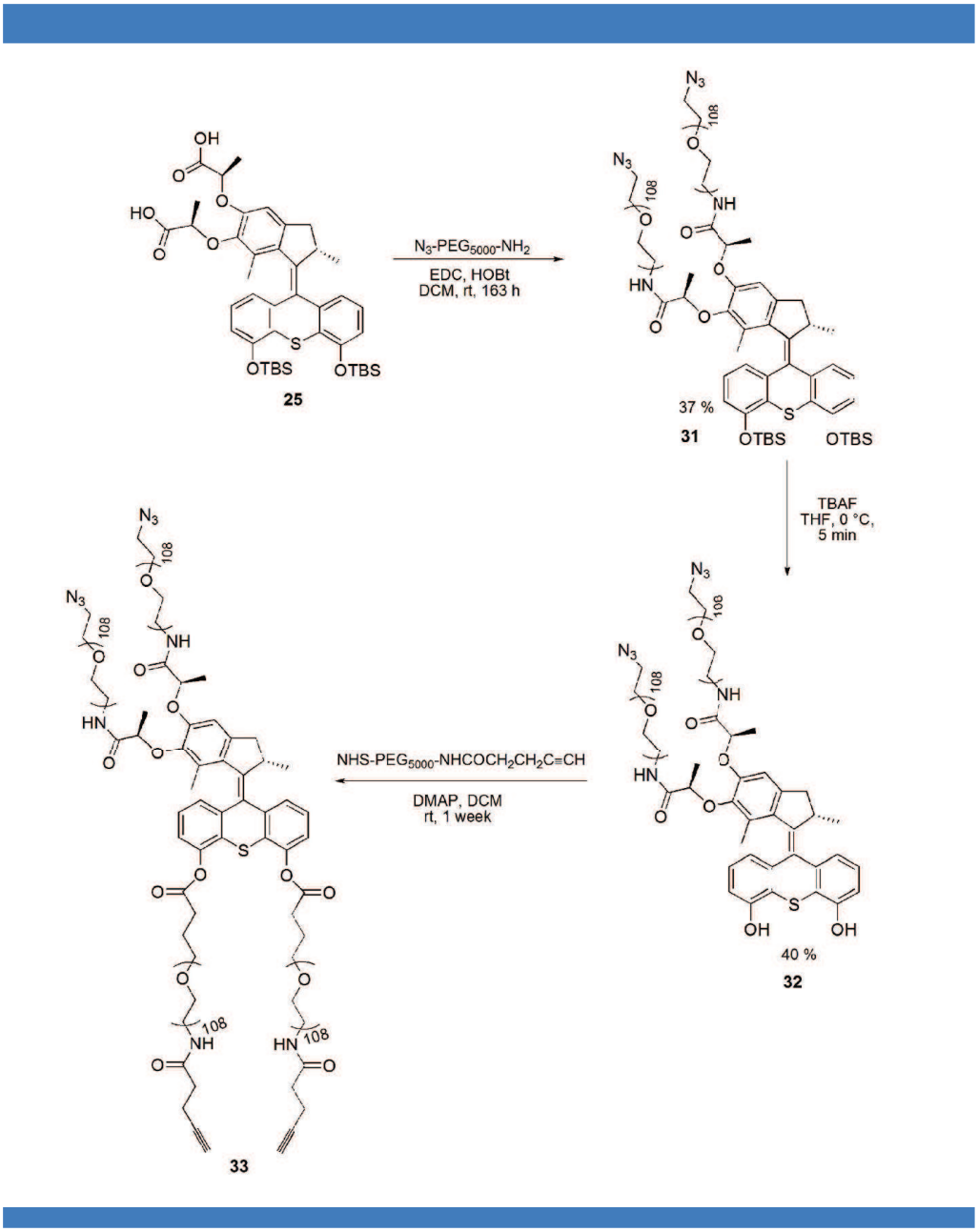

Scheme 15 | Synthesis of star shaped polymer using PEG_{5000}

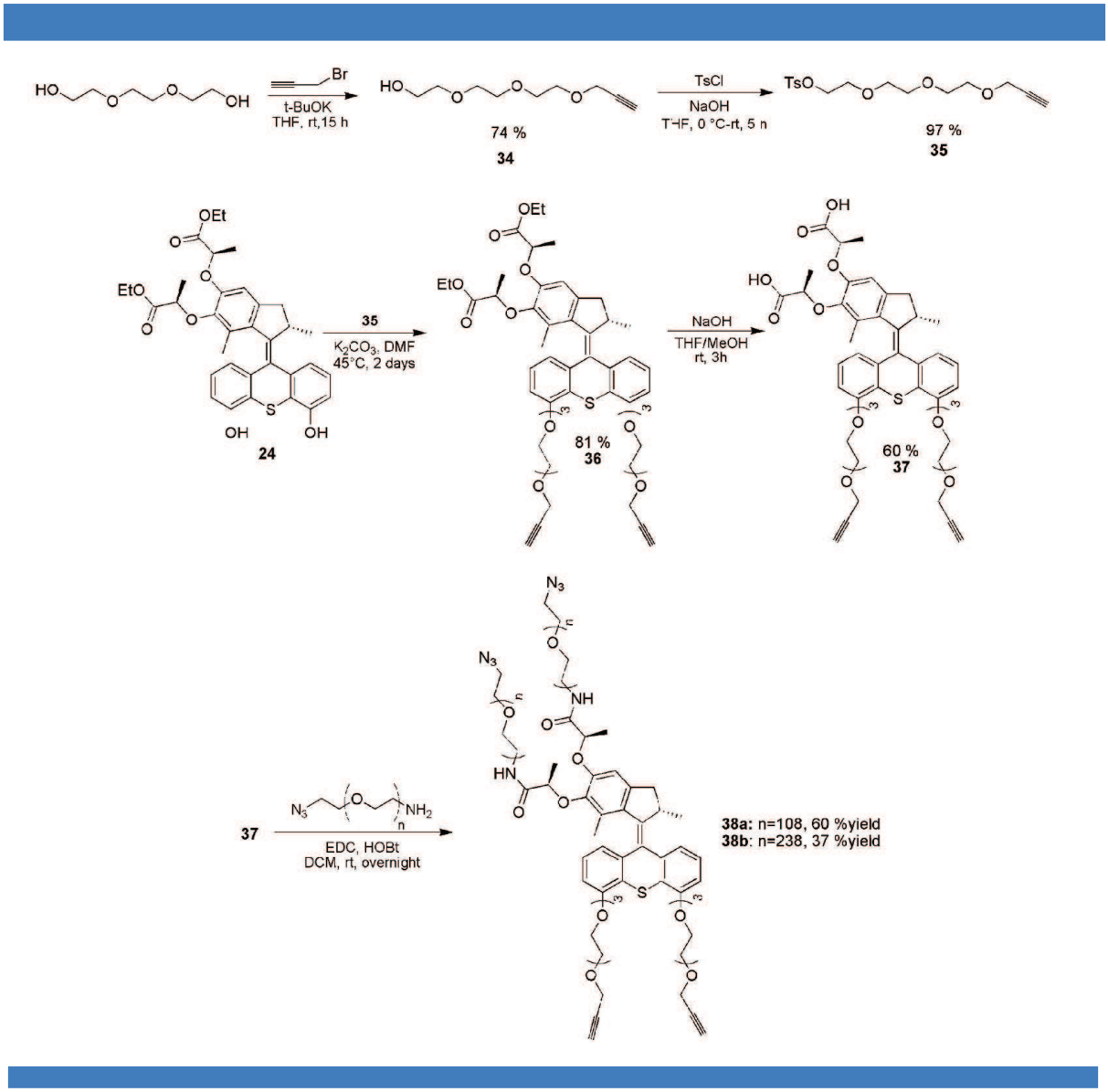

Scheme 16 | Alternative way of synthesis of star shaped motor-polymer. n=108 for PEG_{5000} and n=238 for PEG_{10000}

4/ X-ray analysis

Since the direction of the motor's rotation is determined by the configuration at the stereogenic center, X-ray crystallographic studies are strongly needed. Besides, the crystal structure of the motor can provide further insight into the conformation and the helical shape of these sterically overcrowded alkenes. In our studies, we have obtained three single crystals including either the overcrowded alkene or its precursor episulfide. In this section, the X-ray structures of **14**-(*R*), **15**-(*S*), **23**-(*R*) will be discussed.

Crystals of **14**-(*R*) were obtained by slow diffusion of *n*-heptane into a solution of **14**-(*R*) in EtOH at room temperature. This episulfide crystallized as tiny white crystals in the P $2_12_12_1$ space group. The unit cell dimensions are: a=8.84990(10) Å, b=11.3067(3) Å, c=33.4574(9) Å, α=90.00˚, β=90.00˚, γ=90.00˚ and V=3347.85 $Å^3$. The R-factor is 0.0574 which shows the accuracy and dependability of these data (Figure 32).

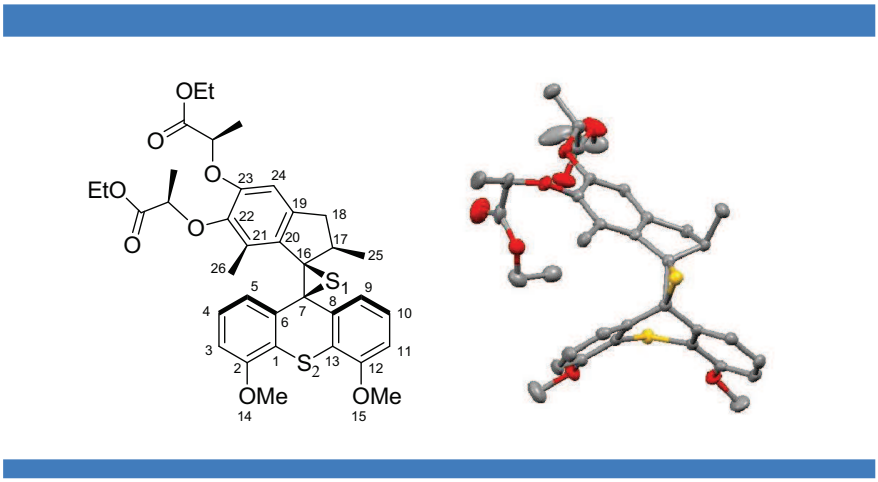

Figure 32 | The adopted numbering scheme of **14**-(*R*) (left) and its capped sticks drawing (right)

The molecular structure of **14**-(*R*) clearly shows the highly folded conformation (*syn*-folded) for the upper part with respect to the lower thioxanthene part around the central episulfide bridge. Most importantly, the methyl group (C_{25}) at the stereogenic center adopts a pseudoaxial orientation which can decrease the steric hindrance between C_{25} and the lower benzene plane. In addition, S1 atom adopts a *syn*-orientation with respect to the C_{25} which may generate some steric repulsion, but this orientation can result from the reaction mechanism as described in the literature.[36]

The C-S bond lengths of the central three-membered ring are 1.828 Å for S_1-C_{16} bond and 1.825 Å for S_1-C_7 bond. The central C_{16}-C_7 bond length is 1.526 Å. For sterically hindered episulfides, there are similar examples (1.857 Å, 1.819 Å and 1.550 Å, respectively;[64] or 1.848 Å, 1.822 Å and 1.550 Å).[65]

Here, the length of the central C_{16}-C_7 (1.526 Å) is slightly longer than the corresponding C-C bond length in ethylene sulfide itself (1.492 Å),[66] which may indicate the tension from the upper and lower halves.

The cyclopentylidene in the upper part adopts a chair-like conformation. The two benzene ring in

[64] Ben de Lange, PhD thesis, University of Groningen, 1993.
[65] A.Mugnoli.; M. Simonetta. The crystal structure of the monoclinic phase of 2,2-di-*tert*-butyl-3,3-diphenylthiirane at -140 °C. *Acta Cryst*., B**32**, 1762 (1976).
[66] G. L. Cunningham Jr.; A. W. Boyd.; R. J. Myers.; W. D. Gwinn.; W. I. Le Van. The microwave spectra, structure, and dipole moments of ethylene oxide and ethylene sulfide. *J. Chem. Phys.* **19**, 676 (1951).

the lower part are bended and deviate largely from the planarity which can be shown by the dihedral angle C_1-C_6-C_7-C_8=-51.7 °.

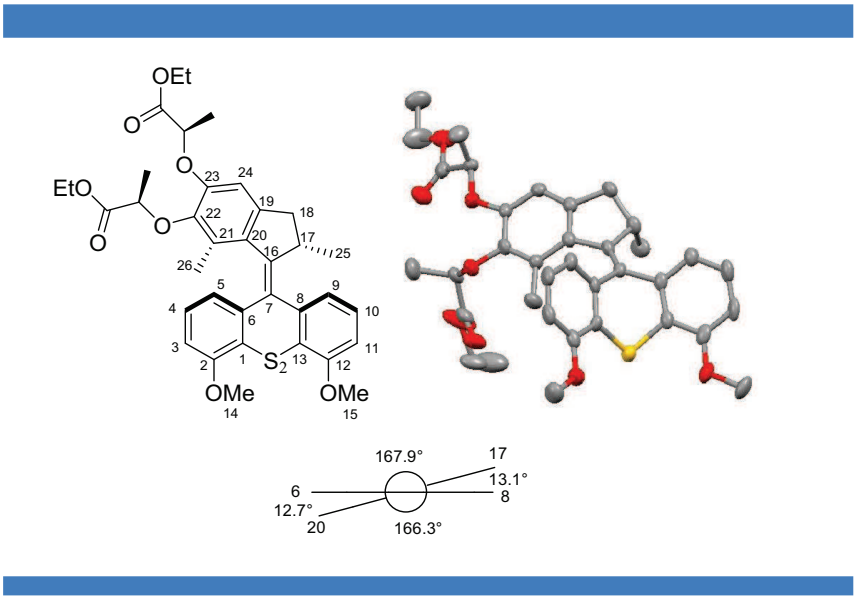

Figure 33 | The adopted numbering scheme of **15**-(*S*) (left) and its capped sticks drawing (right). Newman projection of the conformation around the central double bond (bottom).

After desulfurization, we obtained the overcrowded alkene which is the motor **15**. Fortunately, we have obtained the crystals for one motor isomer in which the configuration of the key carbon was determined as *S* (Figure 33). The unit cell was found to contain four residues. From the X-ray data, it is evident that the methyl group at the stereogenic center has a pseudo-axial orientation. And this pseudo-axial orientation can also diminish the steric hindrance with respect to the lower aromatic rings.

The key feature of this motor is the central double bond with a typical length of 1.360 Å which is slightly increased compared with a common carbon-carbon double bond 1.33 Å. This elongation may be due to the steric repulsion between the two halves around the double bond. Similarly, for other related second generation motor with a five membered ring in the upper part, the lengths of the central double bond were found as 1.360 Å. [67]

Although the configuration of C17 in this motor is different from the above episulfide, the comparison is still meaningful concerning the length of the central double bond. Obviously, the central bond length decreased after removing the sulfide atom, from 1.526 Å to 1.360 Å. This central double bond is considerably twisted which can be seen from the dihedral angles, C_6-C_7-C_{16}-C_{17}=167.9°, C_6-C_7-C_{16}-C_{20}=-12.7°, C_8-C_7-C_{16}-C_{17}=-13.1°, C_8-C_7-C_{16}-C_{20}=166.3° (see Newman projection in figure 33). The

[67] A. A. Kulago.; E. M. Mes.; M. Klok.; A. Meetsma.; A. M. Brouwer.; B. L. Feringa. Ultrafast light-driven nanomotors based on an acridane stator. *J. Org. Chem*. **75**, 666-679 (2010).

helical shape of the molecule is also clearly evidenced by the data, in which C_{26} is bent away from the lower aromatic ring. Thus the helicity of this molecule can be assigned as *M* (left handed).

In our later synthesis, we obtained the crystals of TBS protected episulfide, in which the stereogenic center has the same configuration as the above episulfide. This result can further prove the reliability of our NMR comparison and analysis between TBS protected and -OMe protected episulfide (see Experimental Part 3).

The key features of this episulfide can be characterized as follows: This episulfide crystallized as tiny white crystals in the P $2_12_12_1$ space group. The unit cell dimensions are: a=11.8751 (7) Å, b=18.7850(12) Å, c=43.388(3) Å, α=90.00°, β=90.00°, γ=90.00° and V=9678.72 $Å^3$. The R-factor is 0.0707 which shows the accuracy and dependability of these data. The C-S bond lengths of the central three-membered ring are 1.849 Å for S_1-C_{16} bond and 1.816 Å for S_1-C_7 bond. The central C_{16}-C_7 bond length is 1.535 Å. The upper and lower halves were bent and therefore making the central three membered ring looks like a "roof" (Figure 34).

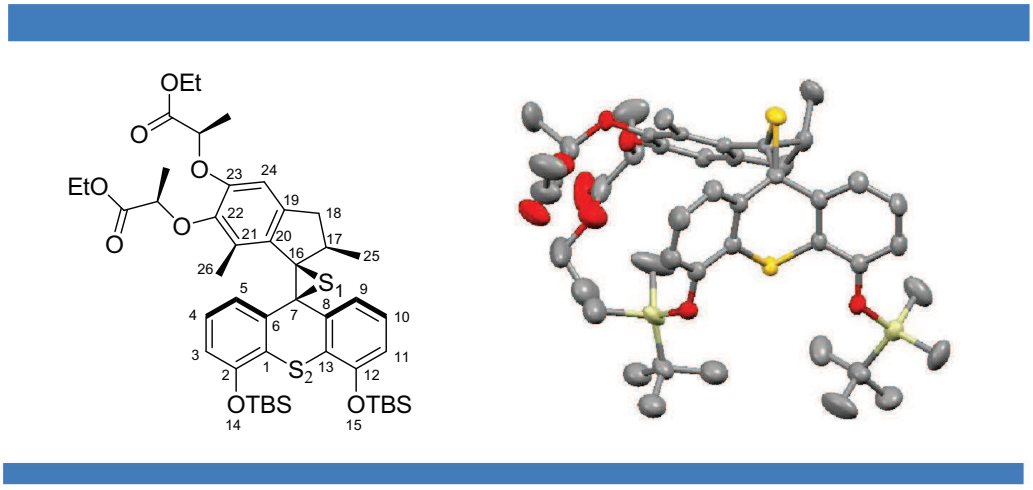

Figure 34 | The adopted numbering scheme of **23**-(*R*) (left) and its capped sticks drawing (right)

5/ Monitoring the rotation process: photochemical and thermal behavior of the motor

Since we have prepared the overcrowded alkene, the next important step is to study the unidirectional rotation cycle. As we have described before, for these second generation motors, the rotation cycle usually undergoes a photochemical isomerization which will generate a thermally unstable form, then followed by a thermal helix inversion;n step affording the original stable form (Figure 35).

As it is shown in Figure 35, the half life time $t_{1/2}$ for the unstable form is 38±1 ns which makes it the fastest light driven rotary molecular motor reported so far.[39b] Figure 36 also shows some ultrafast rotating motors reported rencently.[39a,67]

On the basis of the structurally related molecular motors, our motor was also expected to exhibit similar photochemical and thermal isomerization processes. It is also anticipated that the life time for our motor's unstable form should be at the ns time scale. To characterize this rotation process, cryogenic techniques are usually required to trap the unstable form at very low temperature. However, to reach such low temperatures, one needs to work in very apolar solvents like isopentane and due to its polarity, our motor cannot be solubilized in such apolar solvents. Considering the solubility of our motor, we first tried low temperature NMR techniques at -78 °C in CD_3OD to monitor the rotation process.

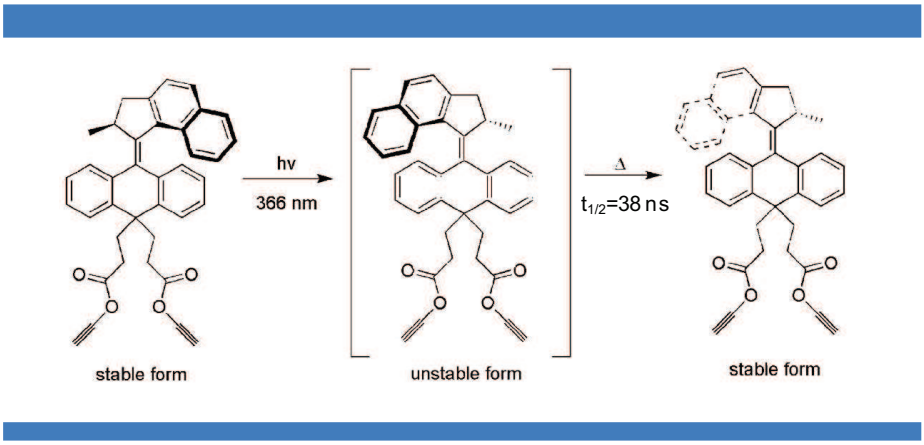

Figure 35 | Photochemical and thermal isomerization of a MHz motor.[39b]

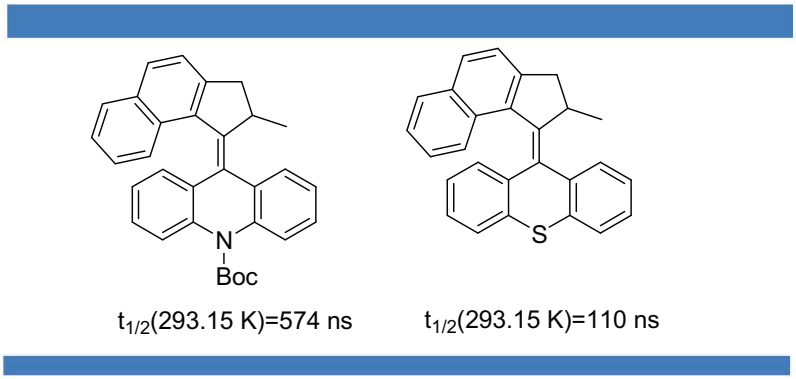

Figure 36 | Reported examples of the fastest motors.[39a,67]

Since the lower half is symmetric, during the rotation process, only two (*R*)-isomers exist, but here a four-step cycle is still used to illustrate the overall rotary process (Scheme 17). Starting from stable (*R*)-(*P*) isomer, irradiation with UV light at 365 nm will result in the formation of energetically unfavorable

(*R*)-(*M*) isomer in which the methyl will adopt an equatorial orientation (step 1). Upon thermal helix inversion, the stable (*R*)-(*P*) isomer is formed again (step 2). A second irradiation (step 3) and heating step (step 4), identical to step 1 and 2, will complete total 360˚ rotation of the upper part of the molecule with respect to the lower part.

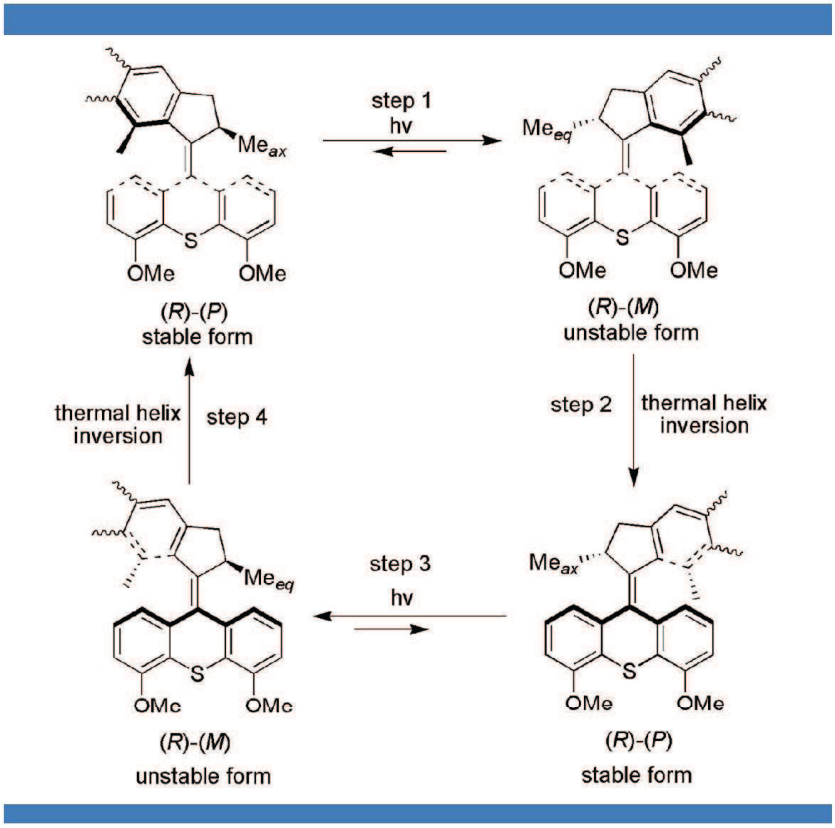

Scheme 17 | Proposed rotation cycle of motor with "symmetric" lower half (*R*-isomer is shown as an example).

We first irradiated motor **16**-(*R*) at -78 °C in a dry ice acetone bath for 16 h. Then we analyzed by ^{1}H NMR at -78 °C.We wanted to check at -78 °C after irradiation, the unstable form could be trapped, but during our experiment, we never found any signals of this unstable form (Figure 37). And, at -78 °C, the proton signals became very broad due to shimming problems. Although there was a little shift for aromatic protons, no new isomeric signals appeared, which indicated that even at -78 °C the thermal helix inversion step was too fast to be "frozen". Obviously lower temperature is needed but due to the solubility issues of our motor, we couldn't perform NMR experiment below -78 °C.

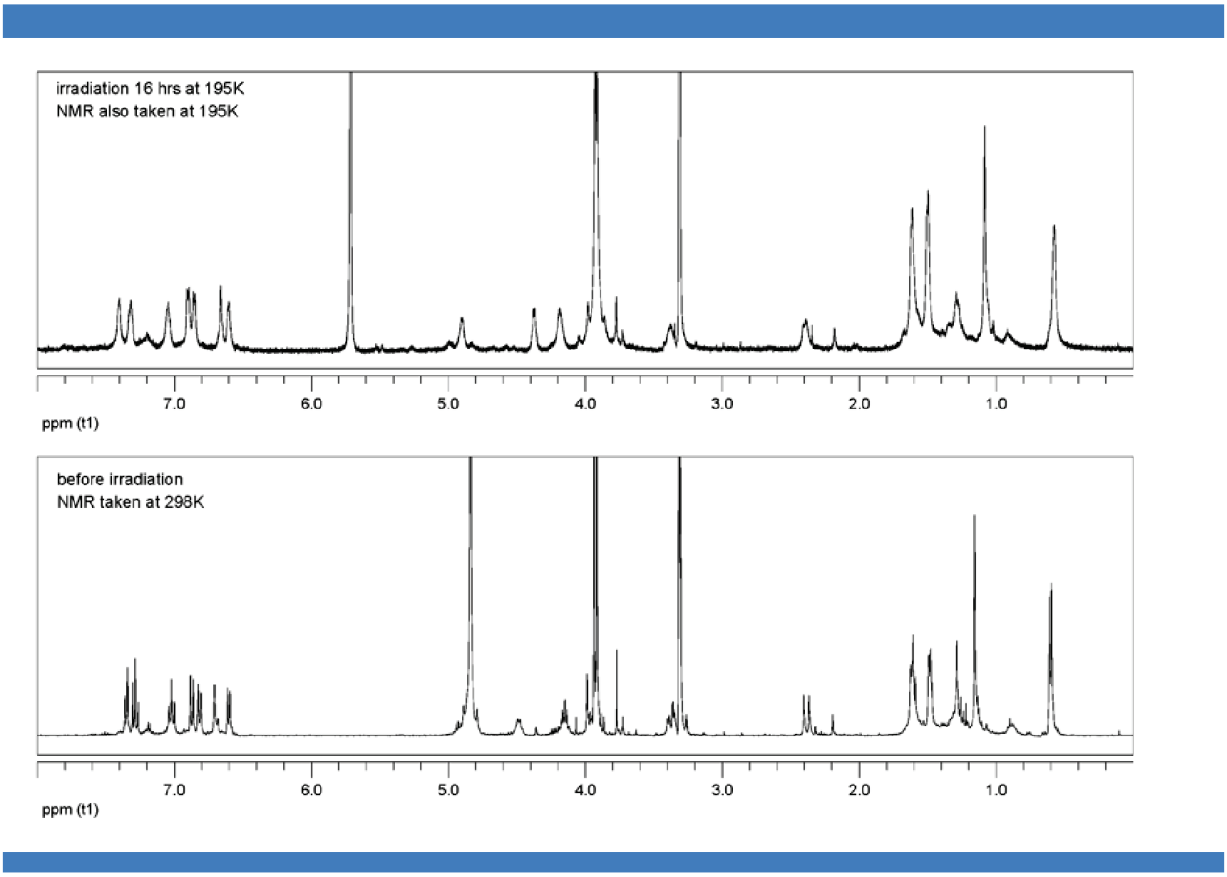

Figure 37 | ^{1}H NMR of motor **16**-(*R*) before (bottom) and after irradiation (top). Solvent: CD_3OD

Another alternative to probe the rotation cycle is to synthesize a molecular motor with an asymmetric lower part. Since the lower half is asymmetric, it is expected that we should have four different isomers during the rotation cycle (Scheme 18). From the above irradiation experiment we know that even at -78 °C, the unstable form cannot be trapped during the irradiation. So for the asymmetric motor, it is expected that there would be only two stable isomers (*cis* and *trans*) after UV irradiation at room temperature if we start with only *cis* or *trans* isomer.

Thus, an asymmetric molecular motor was synthesized from compound **24** which is reacted with TBDMS-Cl affording two different isomers *cis* or *trans* (Scheme 19). Separation of this two isomers proved to be extremely tedious and difficult. With repeated column, preparative TLC or preparative HPLC, we were finally able to isolate each isomer with around 90 % purity. Herein we cannot distinguish the *cis* and *trans* of these two isomers, but if we start irradiation from one pure isomer (*cis* or *trans*), a mixture of these two stable isomers should be obtained finally according to scheme 18. The NMR results proved our assumption (Figure 38).

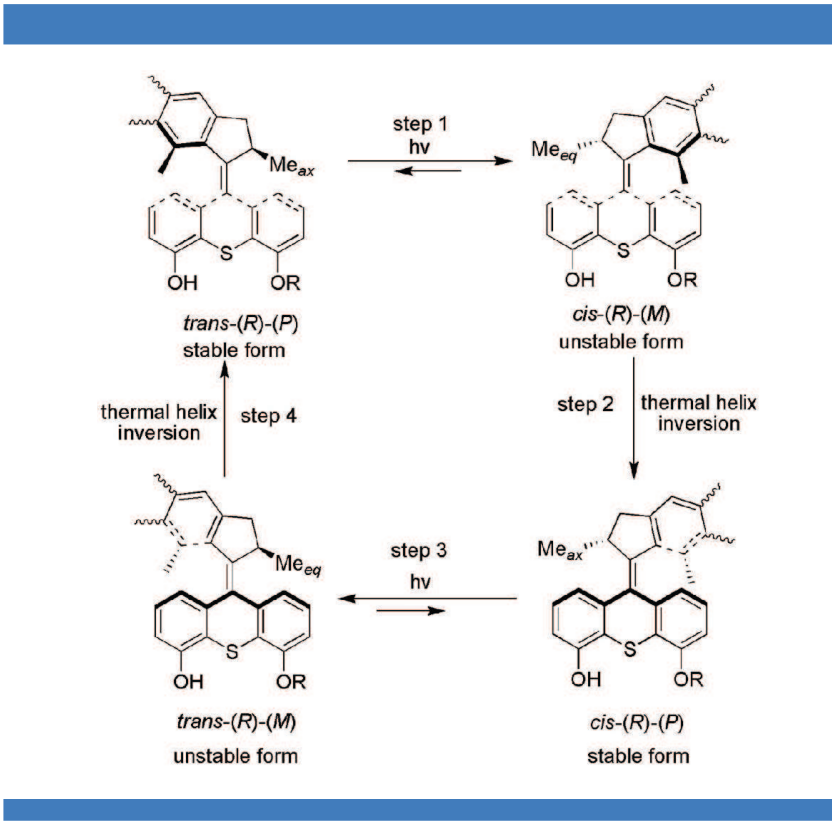

Scheme 18 | Proposed rotation cycle of motor with "nonsymmetric" lower half (*cis*-(*R*) isomer is shown as an example)

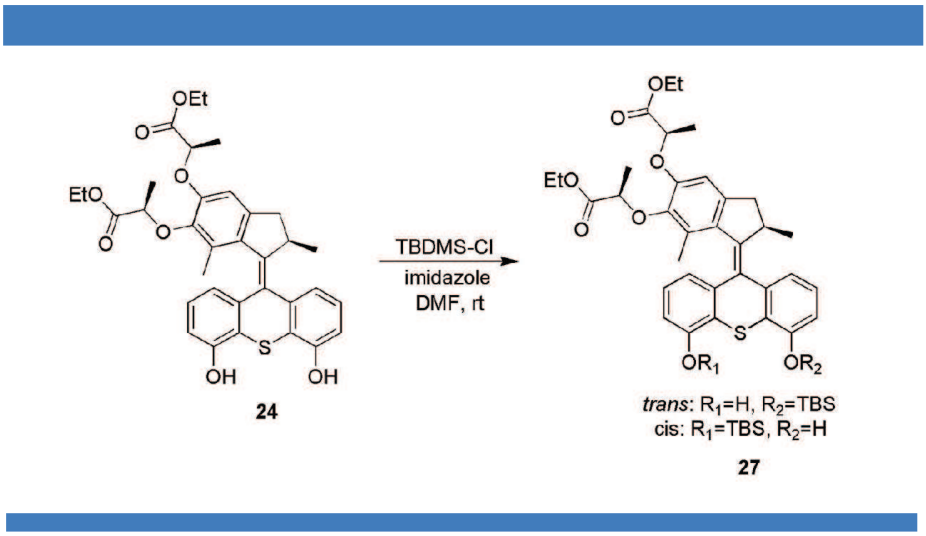

Scheme 19 | Synthesis of "asymmetric" motor

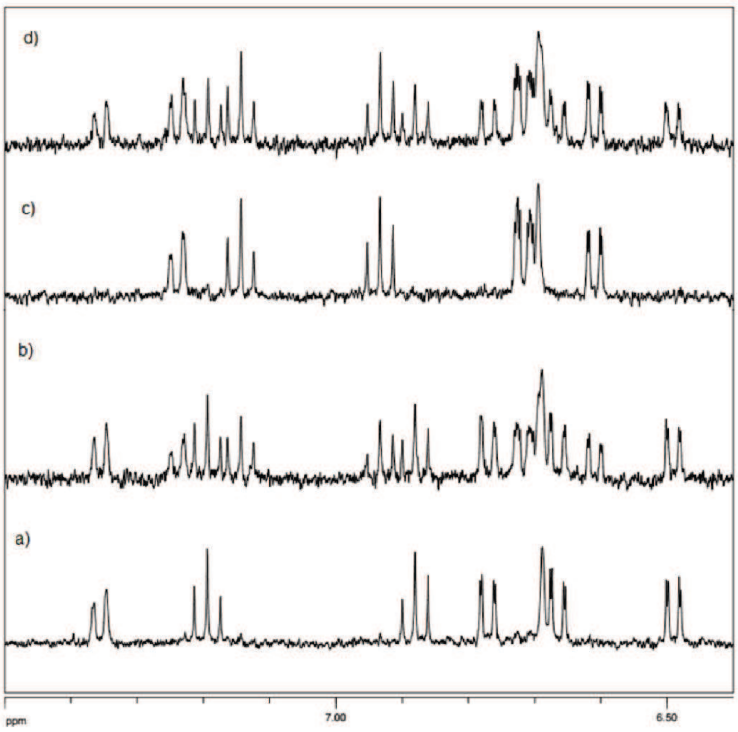

Figure 38 | ^{1}H NMR of asymmetric motor **27** (t_R=30.87 min) before irradiation (a), irradiation at 366 nm at room temperature for 30 min (b); and asymmetric motor **27** (t_R=30.17 min) before irradiation (c), irradiation under sunlight for 30 min (d). Solvent: CD_3OD

In figure 38, it is clearly shown that after irradiation of one pure isomer, a mixture of two isomers was obtained. In addition, even after irradiation for 24 h, the integration ratio for each isomer was still around 1:1, which means that in the rotation cycle the two thermal helix inversion steps are ultrafast steps at room temperature resulting in the equal distribution of two stable forms. By using UPLC-MS techniques, we could also follow the irradiation process. Figure 39 unambiguously showed the integration shift of each stable isomer upon the irradiation. Another quite important point is that the sunlight can also serve as energy input to drive this motor to rotate. This implies that all the motor related products should be shielded from light.

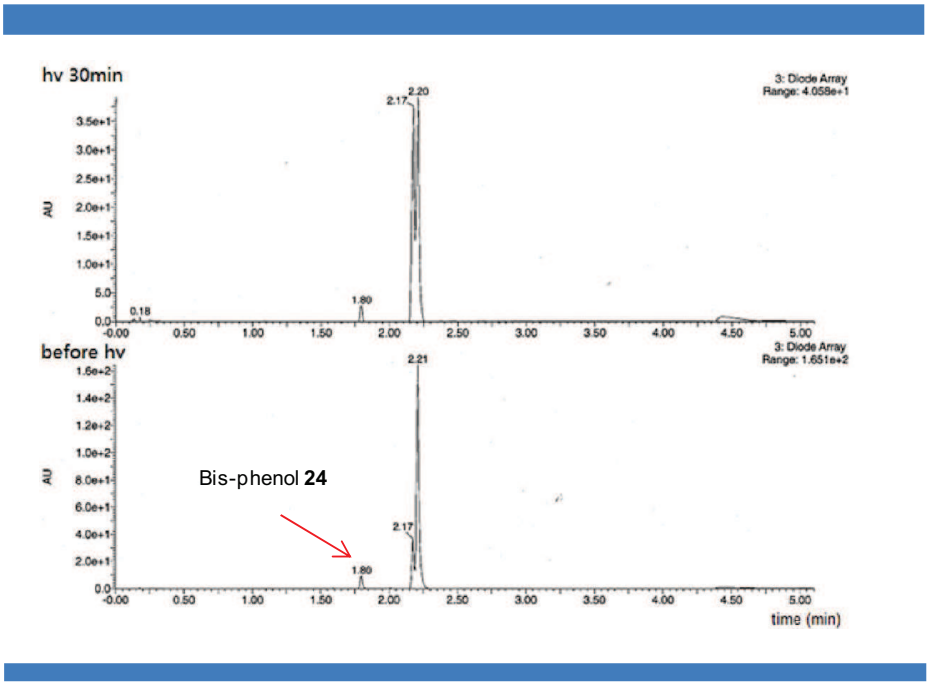

Figure 39 | Monitor of rotation process by UPLC-MS. Compound **27** (t_R=30.87 min) was used. Before UV irradiation (bottom); UV irradiation for 30 min (top)

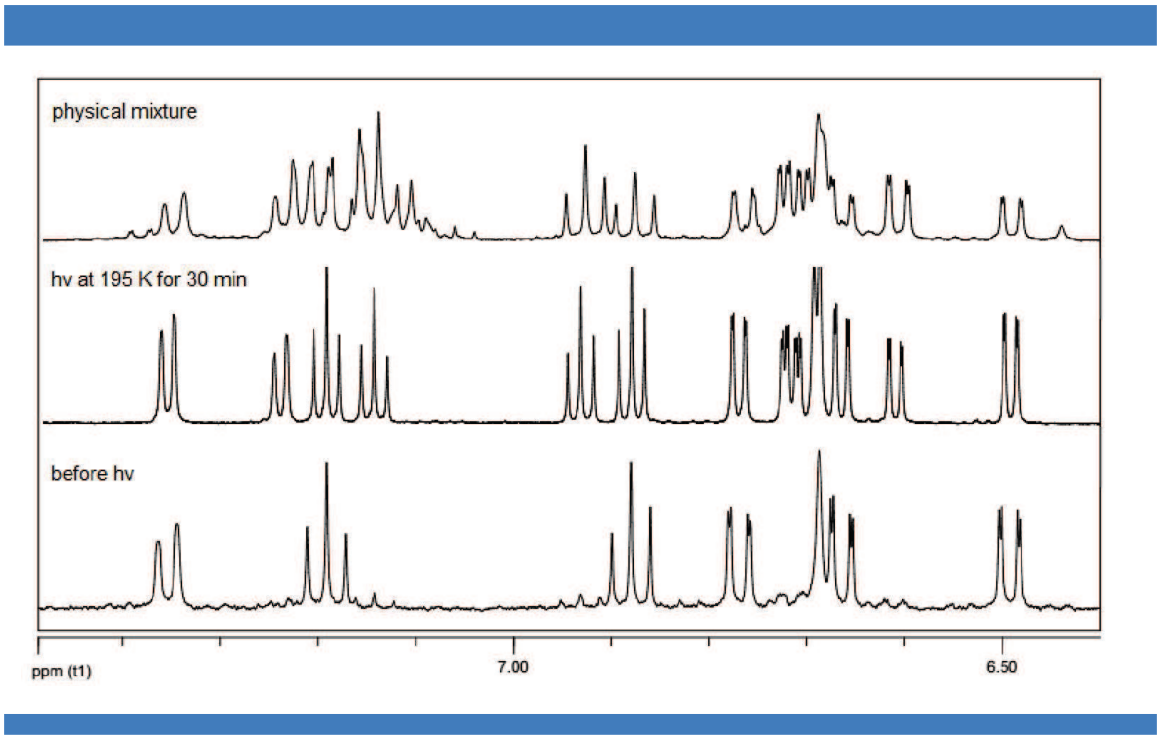

Figure 40 | ^{1}H NMR of asymmetric motor **27** (t_R=30.87 min) before irradiation (bottom), irradiation at -78 °C for 30min (middle, NMR was taken at room temperature) and physical mixture of two isomers (top). Solvent: CD_3OD

Meanwhile, we still performed the irradiation at -78 °C and analyzed by ^{1}H NMR at that temperature to verify the existence of the unstable form. Similarly, a mixture of only two stable isomers was obtained after the irradiation (Figure 40). On the NMR spectrum, only two isomers could be seen and distinguished. It is noteworthy that the chemical shift at low temperature was a slightly drift due the shimming problems, however, this phenomenon did not hamper our analysis and we were able to draw a reasonable conclusion.

6/ UV/Vis- and CD characterization

From low temperature NMR experiments, it is evident that the unstable form of the motor after the irradiation is difficult to trap. Alternatively, UV/Vis spectroscopy and CD spectroscopy can also provide structural information about the irradiation of the motor.

Compound **23**-(*M*)-(*S*) was used for UV/Vis characterization. Before irradiation in **23**-(*M*)-(*S*), the absorption at 294 nm could be explained as being due to the conjugation through the central double bond.[68] Upon the UV irradiation, no changes occurred in the UV spectra. This implies that either no photochemical isomerization occurred or that unstable form was already converted to the stable form at room temperature. Obviously the above NMR results confirmed the second possibility.

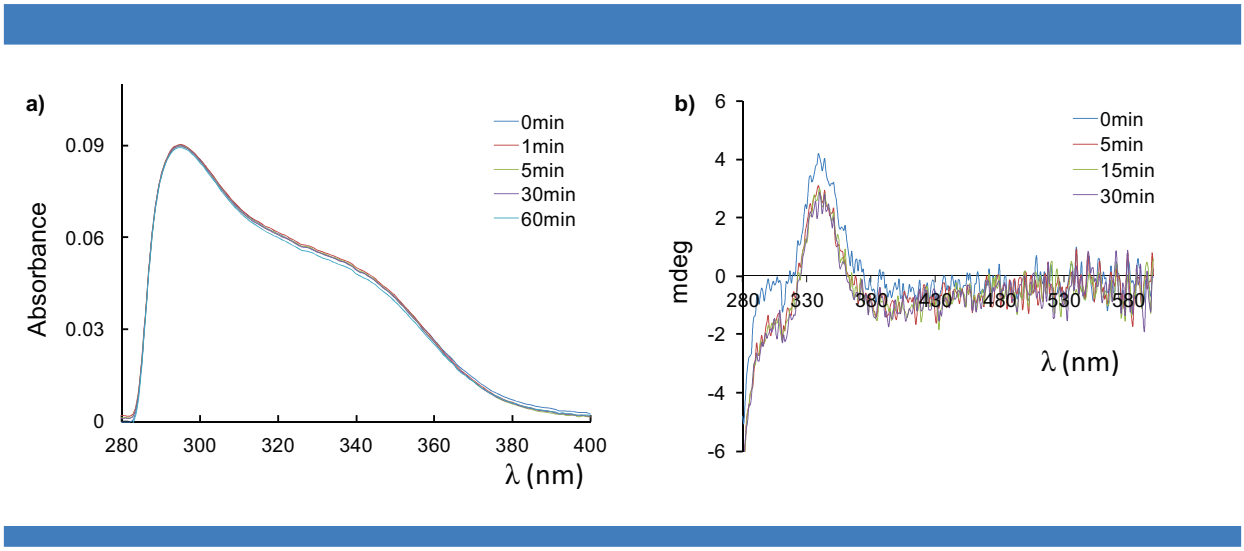

Figure 41 | a) UV/vis absorption spectrum of compound **23**-(*M*)-(*S*) after different irradiation time. b) CD spectrum of compound **23**-(*M*)-(*S*) after different irradiation time. Solvent: toluene

[68] W. F. Jager.; B. de Lange.; A. M. Schoevaars.; F. Bolhuis.; B. L. Feringa. *Tetrahedron: Asymmetry.* **4**, 1481-1497 (1993).

Meanwhile CD spectra were recorded in toluene and also led to the similar conclusions. The chirality of **23**-(*M*)-(*S*) didn't change upon the UV irradiation at room temperature (Figure 41b).

We also recorded CD spectra of the asymmetric motor **27**-(*P*)-(*R*) (t_R=30.87 min). Upon the irradiation of either **27**-(*P*)-(*R*) (t_R=30.87 min) with UV light (366 nm), no change in the chirality of **27**-(*P*)-(*R*) could be observed (Figure 42a).

Another important phenomenon is the opposite chiralities of compounds **23**-(*M*)-(*S*) and **27**-(*P*)-(*R*). As indicated in Figure 42, CD spectra of these two motors show a mirror image character, demonstrating the opposite molecular helicity which also confirms our previous structural elucidation for motor **23**.

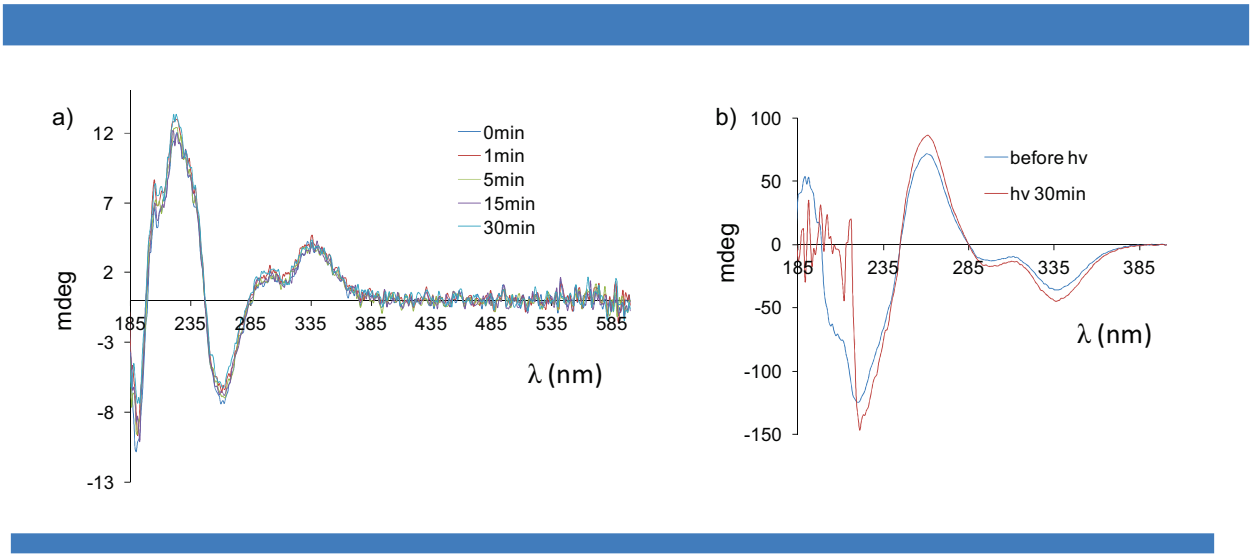

Figure 42 | a) CD spectrum of asymmetric motor **27**-(*P*)-(*R*) (t_R=30.87 min) before and after UV irradiation. b) CD spectrum of compound **23**-(*M*)-(*S*) after different irradiation time. Solvent: acetonitrile.

7/ Conclusion

In this chapter, we have synthesized a new second generation molecular motor **23**. Two different functional groups (ester and silyl) have been successfully introduced into the upper and lower parts of the molecular motor, which is a significant advantage compared with previous reported ones. Another achievement was the gram scale synthesis of this molecular motor as well as the easy access to enantiopure motors. In addition, these two functional groups can be removed in a selective manner, which will endow the molecule more ability to be integrated into more complicated systems to further perform useful tasks. Although direct proof of unidirectionality of this motor is limited by the

availability of cryogenic techniques and solubility issues, the current results have unambiguously proved our assumption for the rotation mechanism of the motor.

We also have successfully integrated this motor in a polymer system via peptide synthesis methods. The motor-polymer conjugates feature by azide and terminal alkyne groups, which will allow us to prepare novel polymeric material via click reaction. We will discuss the utility of these motor-conjugates towards exploring the applications of the molecular motors in Chapter 3.

Chapter 3: Applications of Highly Functionalized Rotary Molecular Motors

We have seen in chapter 2 the synthetic strategy employed to synthesize enantiopure molecular motors in large scale. The design described allowed the asymmetric functionalization with polymer chains. In key compound **38**, the lower part was functionalized with an alkyne terminated triethylene glycol whereas the upper part was linked to an azido-terminated PEG chain (PEG 5000 or PEG 10000). With this key compound in hand, one can envision two different synthetic strategies based on Huisgen cycloaddition (click chemistry). Indeed, working in diluted conditions should lead to an intramolecular cyclization yielding an 8-shaped molecule whereas working in concentrated conditions should lead to intermolecular connections between the motor units and a gel structure is expected. Both systems will be described in this chapter and the effect of motor's rotation will be described for each of them. Different techniques such as UV, CD, AFM, SAXS will be used to characterize the rotation process. This chapter will start with a brief introduction to the characterization techniques used to study the motor-bound polymers.

1/ Characterization methods used in this study

a) Atomic Force Microscopy

Atomic force microscopy (AFM) is a very powerful technique that allows to image directly a compound deposited on a surface such as glass or silicon wafers. In a typical AFM experiment, a tip scans the surface continuously. The topology is read by the deflection of a laser beam and the corresponding image is further reconstructed. Different scanning modes can be implemented. The most common one is the contact mode in which the AFM tip keeps in constant contact with the surface to analyze. Another useful mode is the tapping mode in which the tip is constantly oscillating on the surface. When it comes to analyzing soft materials, this mode is preferred as it generates less damage on the surface than the contact mode. Over the past years, AFM has provided qualitative structural information on many chemical systems down to the nanometer scale.

b) Small Angle X-Ray Scattering

Different scattering techniques are used by soft matter scientists in order to obtain structural information on objects in solution. In general, they consist in the illumination of a sample with a monochromatic ray followed by an analysis of the scattered radiations at different angles. In particular, SAXS concerns the small angle elastic scattering of X-ray photons by the electrons of the sample to analyze. The recorded scattering profile can then be used to determine the global structure as well as the radius of gyration (R_g) of the objects to study. In this study, we have chosen to use a Kratky representation of the scattered intensity. In polymer analyses, it allows to emphasize the Gaussian nature of the polymers. Since the form factor for Gaussian chains is proportional to $1/q^2$ at high q values, this plot tends to a horizontal asymptote.

2/ Synthesis of 8-shaped molecules

The first configuration of polymer-grafted motors that we envisioned consisted in an intramolecular cyclization through click chemistry that should afford an 8-shaped molecule. It was expected that upon irradiation with UV light, the chains would entangle leading to a collapse of the obtained molecule (Figure 43).

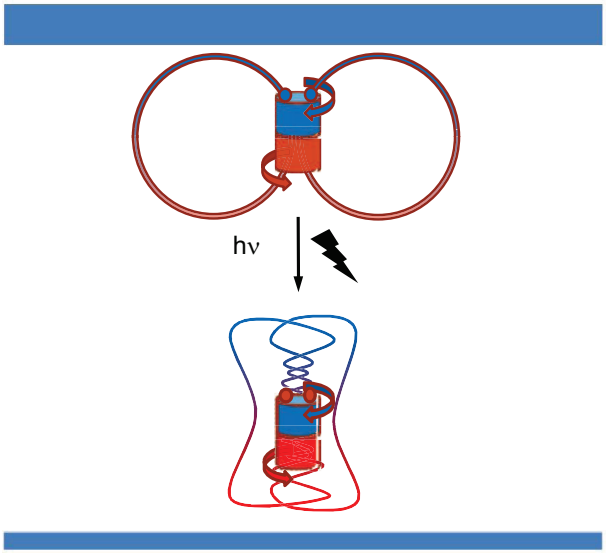

Figure 43 | Proposed scheme for the polymer entanglement

The attachment of two end points from one polymer chain seems to be quite challenging. However, a survey of literature shows that such cyclic polymer have been extensively

synthesized and studied (Figure 44). These large cyclic polymers are usually synthesized in highly diluted solutions with very good yield.

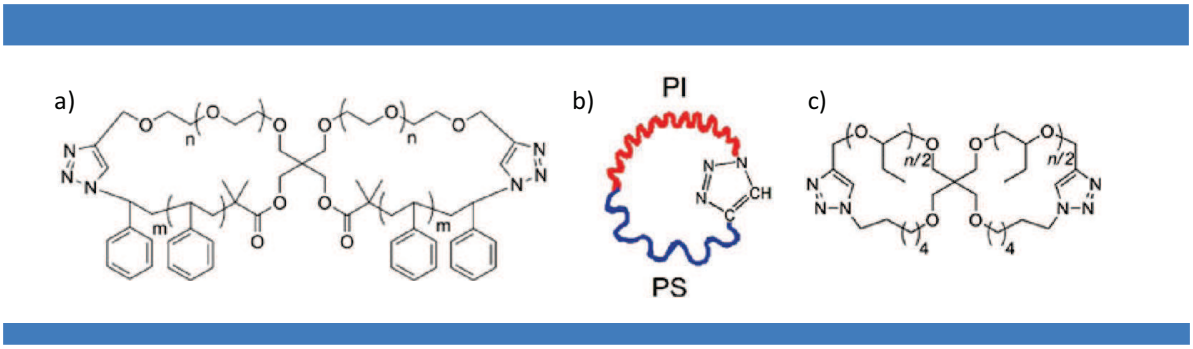

Figure 44 | Examples of large cyclic polymers made by click reactions: a) Cyclic Polystyrene.[69] b) Cyclic polystyrene-*block*-polyisoprenecopolymers.[70] c) 8-shaped poly-(butylene oxide)s.[71]

The conditions for the intramolecular cyclization were based on the conditions described in the literature. DMF was used as solvent and PMDETA as a ligand for copper. The temperature was set at 80˚C and the final concentration of the polymer-motor **38** was maintained at 10^{-5} M. A syringe pump was used to control the rate of addition of **38**, this addition rate was fixed at 1.5 mL/h. By slow addition of material in such highly diluted conditions, the intramolecular cyclization occurred in good yield (Scheme 20).

[69] X. Fan.; B. Huang.; G. Wang.; J. Huang. Synthesis of amphiphilic heteroeight-shaped polymer cyclic-[Poly(ethylene oxide)-*b*-polystyrene]$_2$ via "Click" chemistry. *Macromolecules* **45**, 3779-3786 (2012).
[70] A. Touris.; N. Hadjichristidis. Cyclic and multiblock polystyrene-block-polyisoprene copolymers by combining anionic polymerization and azide/alkyne "Click" chemistry. *Macromolecules* **44**, 1969-1976 (2011).
[71] T. Isono *et al*. Synthesis of star- and figure-eight-shaped polyethers by *t*-Bu-P$_4$-catalyzed ring-opening polymerization of butylene oxide. *Macromolecules* **46**, 3841-3849 (2013).

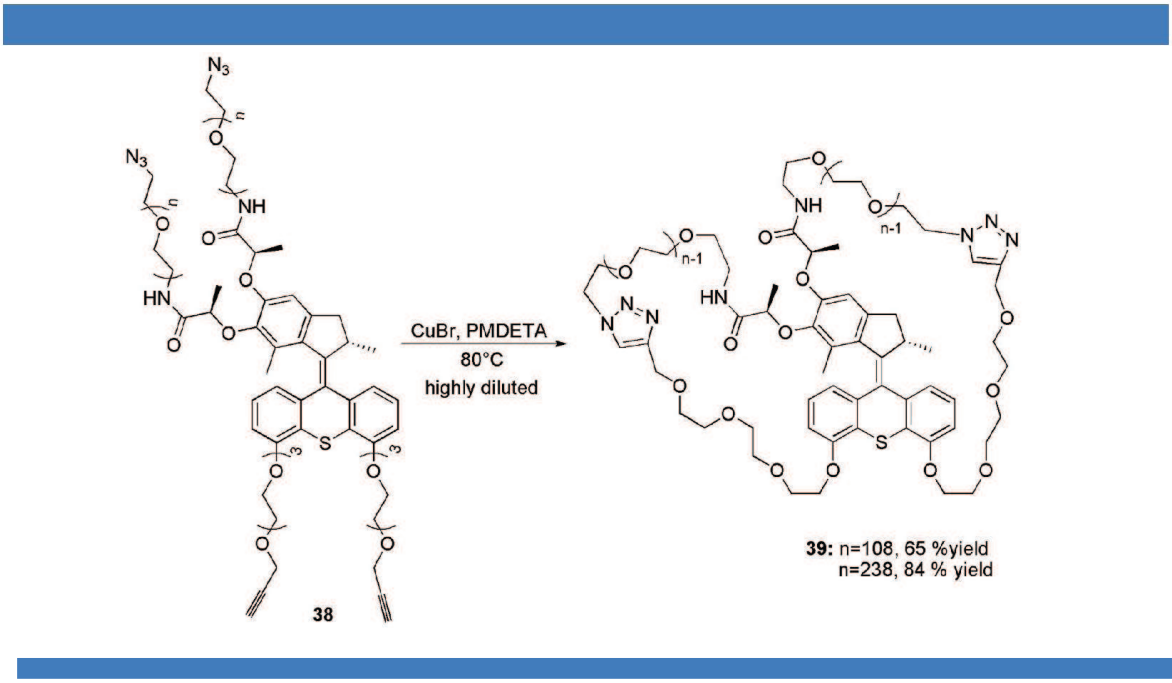

Scheme 20 | Synthesis of "8" shaped molecule

3/ Characterization of 8-shaped molecules

The structure of 8-shaped molecules was characterized unambiguously by ^{1}H NMR (Figure 45). Before the click reaction, the star shaped motor-polymer displayed a triplet signal at 2.80 ppm characteristic for the alkynes resonance H_1. In the 8.00-6.00 ppm range, seven aromatic protons from the motor could be clearly seen. After the cyclic click reaction, two triazole cycles were formed, which was evidenced by the new resonance appearing at 8.00 ppm H_2. Meanwhile the signal of the alkyne at 2.80 ppm disappeared. For PEG 10000 and 5000, the corresponding star and 8-shaped molecules showed a similar NMR spectrum and the only difference was the integration area of the PEG backbone, around 1800 protons for PEG_{10000} and around 900 protons for PEG_{5000}, respectively.

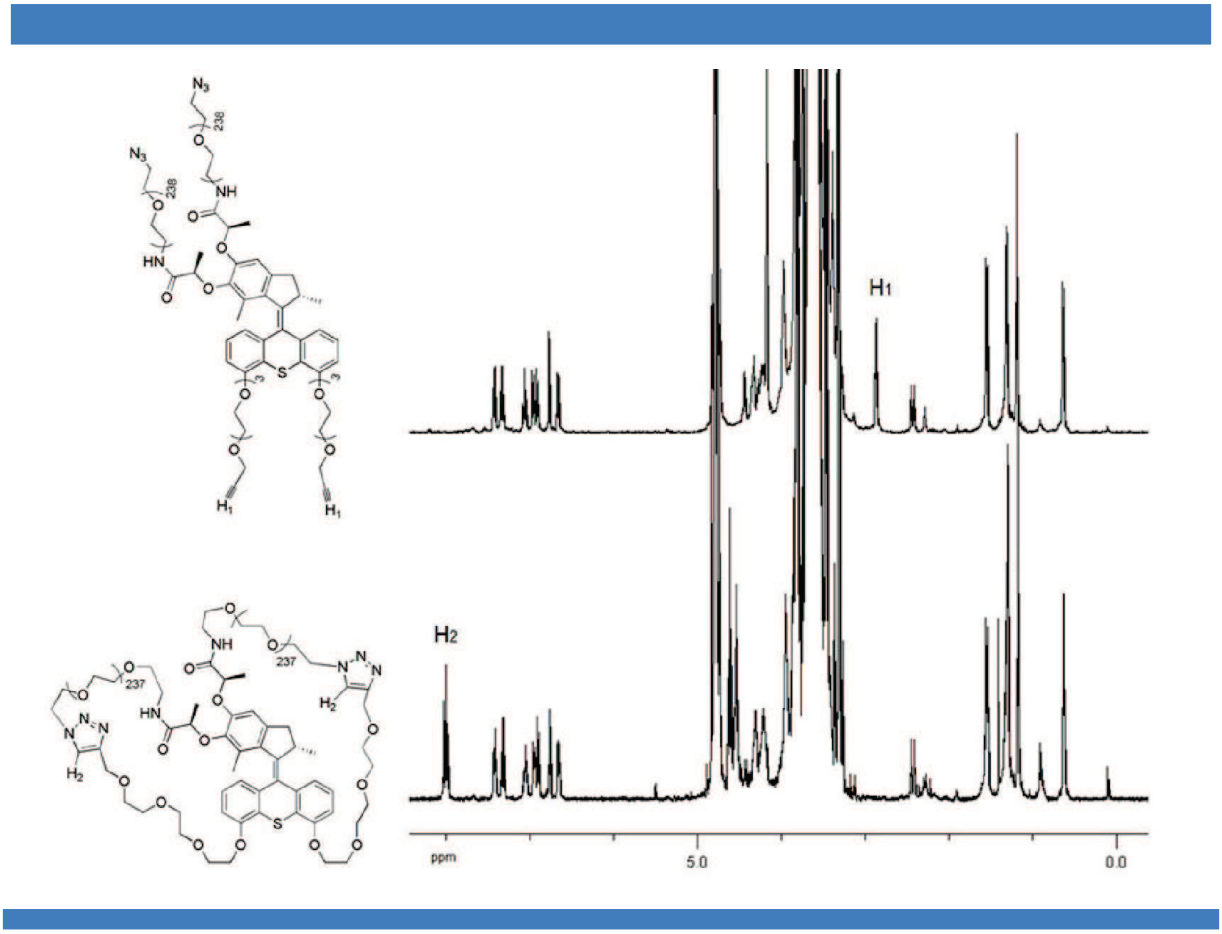

Figure 45 | ^{1}H NMR spectrum of compound **38** (top) and **39** (bottom) (for PEG_{10000}). Solvent: CD_3OD

The morphology of this 8-shaped cyclic motor-polymer was unambiguously observed by atomic force microscopy (AFM) using the peak force tapping mode (Figure 46). The AFM images of "8" shaped motor-polymers (for PEG_{10000}) showed that, the conformation of the molecules adsorbed in a 2D conformation on a mica surface is an almost double-circular shape with single circular ring radius of about 8 nm. This value is in agreement with the theoretical value of the PEG ring for a polymer chain having 230 monomers, $R=L/2\pi=10$ nm (L being the contour length of the chain).

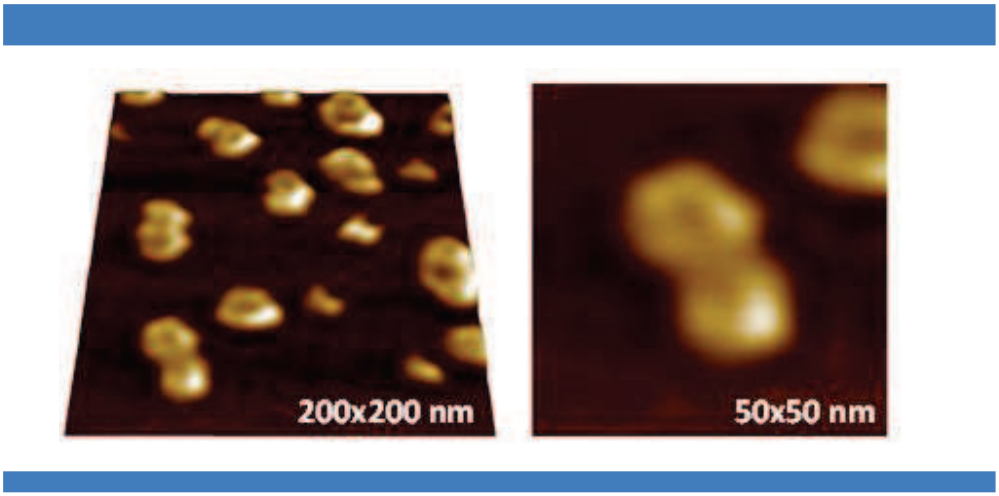

Figure 46 | AFM images of isolated 8-shaped **39** (n=238) on a mica surface before light irradiation.

4/ Irradiation and characterization of 8-shaped molecules in solution

With this 8-shaped molecule in hand, we first performed irradiation experiments. In acetonitrile, compounds **38** and **39** show similar absorptions as well as the non grafted motor **23** (Figure 47). Upon UV irradiation at 366 nm, no changes were observed for **38** and **39**. For **38**, this implies that when the motor is bound to the polymer chain, it still rotates too fast to trap the unstable form at room temperature. For **39**, since the polymer chains form a ring around the motor, the entanglement of the polymer chains upon the rotation of the motor does not change the electronic distribution on the motor, thus the UV/Vis spectrum remains unchanged. In toluene, compound **38** and **39** show a similar behavior compared with free motor **23** after UV irradiation (Figure 48).

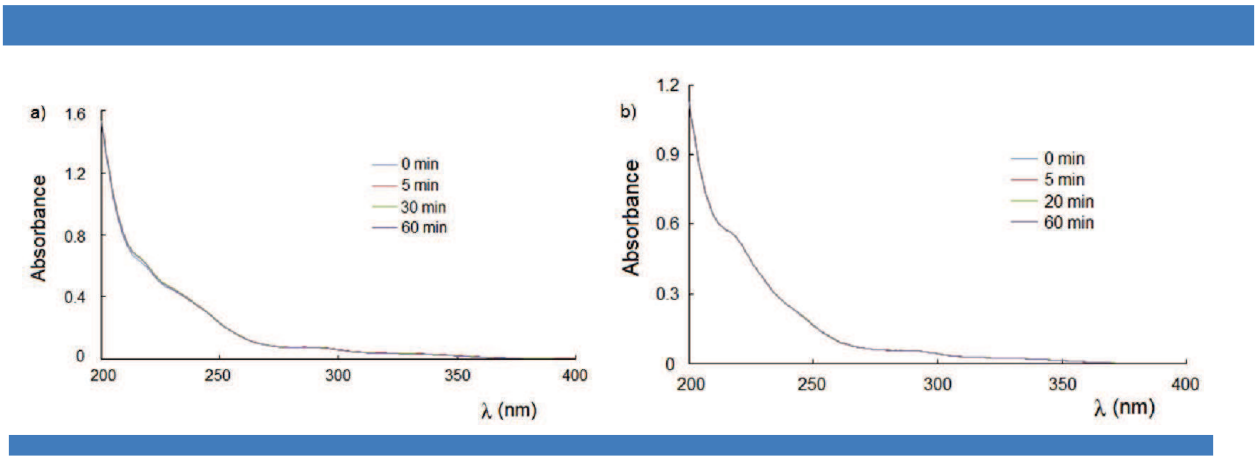

Figure 47 | UV/Vis spectrum of a) compound **38** (n=238) and b) **39** (n=238) in acetonitrile after different irradiation time

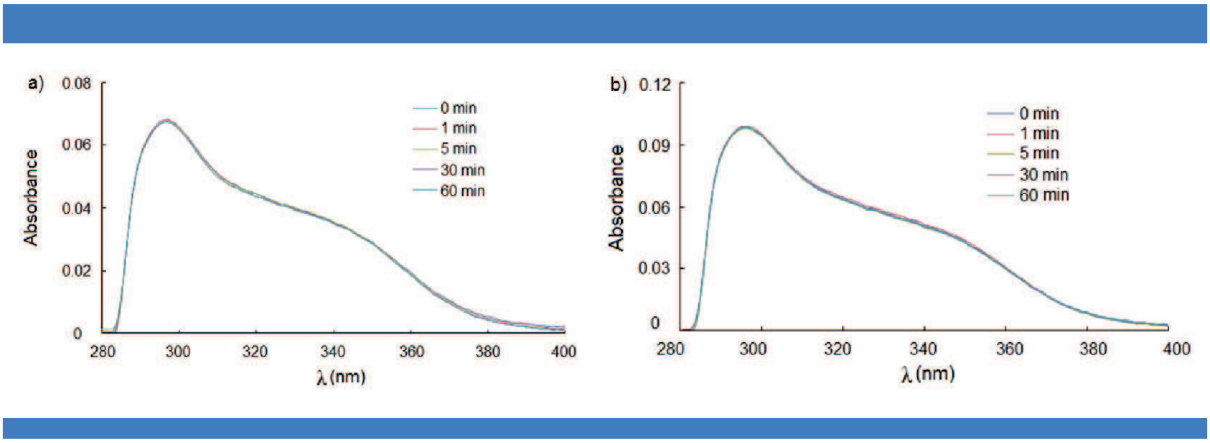

Figure 48 | UV/Vis spectrum of a) compound **38** (n=238) and b) **39** (n=238) in toluene after different irradiation time.

The chirality of **38** and **39** was evidenced by circular dichroism spectroscopy (CD) either in acetonitrile or toluene. However, after irradiation, The CD spectra of compounds **38** and **39** remained unchanged. This indicated that even when the polymer chain was entangled, the motor's unstable form generated by irradiation still could not be trapped (Figure 49 and Figure 50).

Atomic force microscopy was the first technique that allowed to characterize the effect of the motor's rotation occurring upon irradiation. Indeed, after 15 minutes exposure to UV light in toluene, no more 8-shaped morphologies were detected by AFM. Instead, one could only observe collapsed (spherical or more elongated) coils with smaller dimensions (Figure 51). The rotation of the motor triggered the self-entanglement of the polymer chains leading to the observed winded topology. This result is in good correlation with the expected morphology for the self-entangled motor (Figure 43).

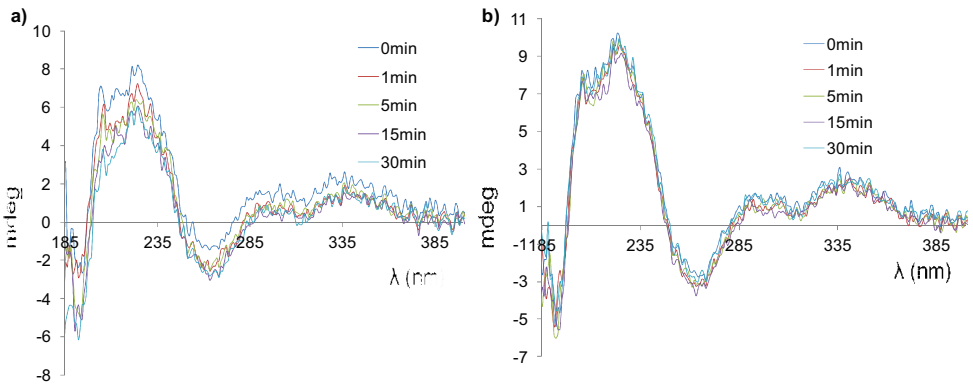

Figure 49 | CD spectrum of compound a) **38** (n=238) and b) **39** (n=238) in acetonitrile after different irradiation time.

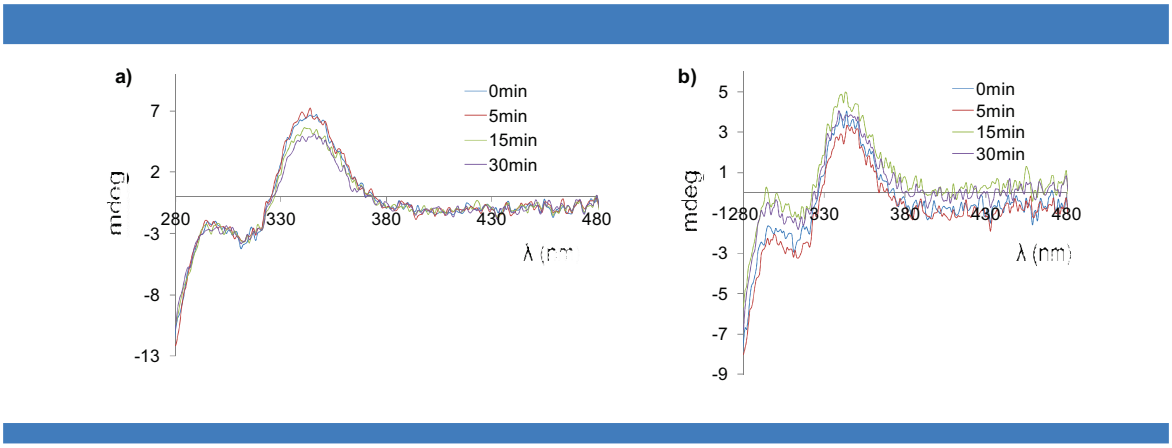

Figure 50 | CD spectrum of a) compound **38** (n=238) and b) **39** (n=238) in toluene after different irradiation time.

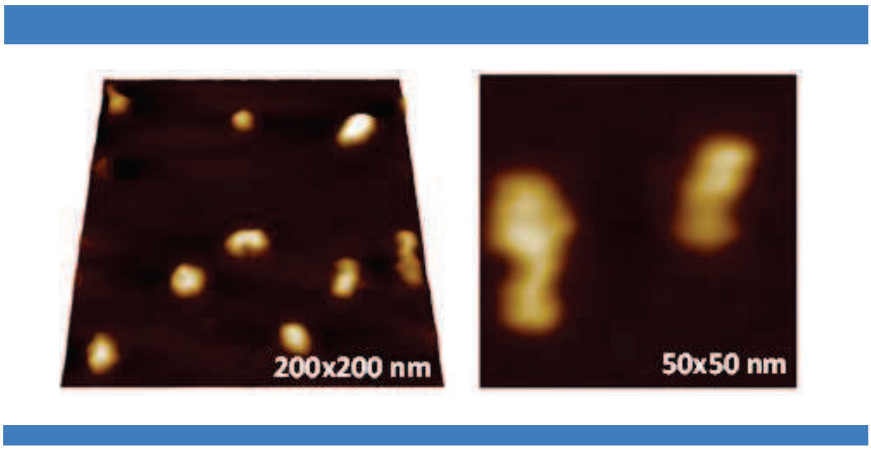

Figure 51 | AFM images of isolated entangled 8-shaped 39 (n=238) on a mica surface after 15 minutes of UV light irradiation.

To confirm this entanglement process, we further performed small angle X-ray scattering (SAXS) on compounds **39** (n=108, 238) in diluted toluene solutions (Figure 52). By using a Kratky representation of the scattered intensity, we can observe the presence of a characteristic bump for a figure-of-eight polymer.[72] The radius of gyration (R_g) associated to the position of the peak in the reciprocal space can be determined [R_g (PEG_{5000}) = 2.58 nm; R_g (PEG_{10000}) = 3.48 nm], these values are in good agreement with the expected values of Rg for such 8-shaped polymers (see experimental part).

When compound **39** (PEG_{5000}) is irradiated in toluene with a UV lamp of 6W working at 366 nm, the scattering peaks in the Kratky plot shift indicating an evolution towards smaller radius of gyration values (from 2.58 nm to 2.24 nm). In addition, the 50 % increase of the scattered intensity reveals that

[72] M. K.Shimamura.; K.Kamata.; A.Yao.; T. Degushi. Scattering functions of knotted ringpolymers. *Phys. Rev. E* **72**, 041804 (2005).

the internal density of the polymer is much higher after irradiation which is also consistent with a coiling of the particle. This global behavior is expected for a mechanically enforced coiling of the self-entangled polymer chains upon rotation of the motor.

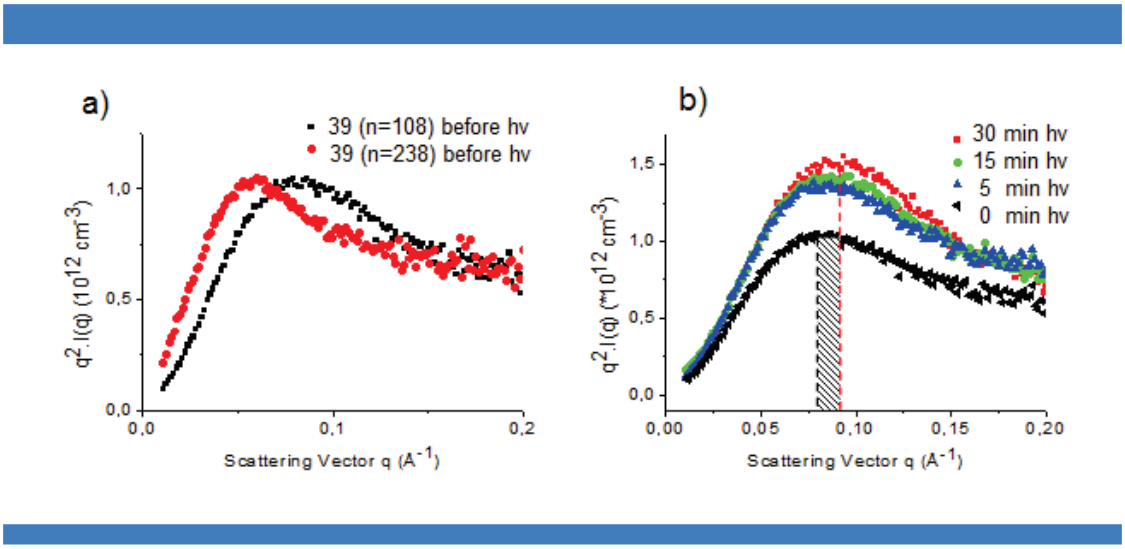

Figure 52 | a) Kratky plot representation of the scattered intensities of 8-shaped compounds **39** (n=108, 238) (c = 10^{-2} g·cm^{-3} in toluene) before UV light irradiation. b) Kratky plot representation of the scattered intensities of 8-shaped compound39 (n=108) upon UV light irradiation.

We have successfully integrated the molecular motor into polymeric system and synthesized a novel "8" shaped motor-polymer conjugate by using an efficient intramolecular"click" reaction. The structure of this "8" shaped motor-polymer conjugate was clearly evidenced by ^{1}H NMR, AFM and SAXS characterizations. In particular, upon UV irradiation, the polymer chain could be entangled due to the rotation of the motor, thus changing the morphology and dimension of this motor-polymer conjugate. This entanglement process was strongly proved by AFM and SAXS experiment. The rotation from the molecular motor was converted into mechanical entanglement of polymer chains thus producing useful work. Now, we are going to describe the next step of this study which consists in the integration of molecular motors in a gel in order to obtain a macroscopic signature of the motors rotation.

5/ Integration of molecular motors in a gel

Starting from the same key precursor **38**, one can imagine that working in concentrated conditions would favor the intermolecular click reaction thus yielding a chemical gel where molecular motors would be placed at the reticulating points of the gel. By performing the same UV irradiation, the polymer chains in the gel would be entangled due to the rotation of the motors, thus the whole gel would

be contracted in dimension, this contraction would be the macroscopic consequence of molecular rotations from the motors.

In fact, a similar "click" gel but without any motors inside has been reported by Craig J. *et al* (Figure 53).[73] In that case, diacetylene-functionalized and tetra azide-functionalized PEG derivatives were synthesized and then underwent a click reaction giving a crosslinked hydrogel. The crosslinking in these hydrogels is extremely high, and results in an ideal structure leading to improved properties when compared to traditional photochemically-crosslinked PEG hydrogels.

In our case, the conditions for the above intramolecular click were used except for the concentration (Scheme 21). Under high concentration conditions, the gel was formed quickly usually within 1 min after addition of copper [I]. By successive extensive washings with EDTA solution, water and methanol, a transparent gel was obtained (Figure 54).

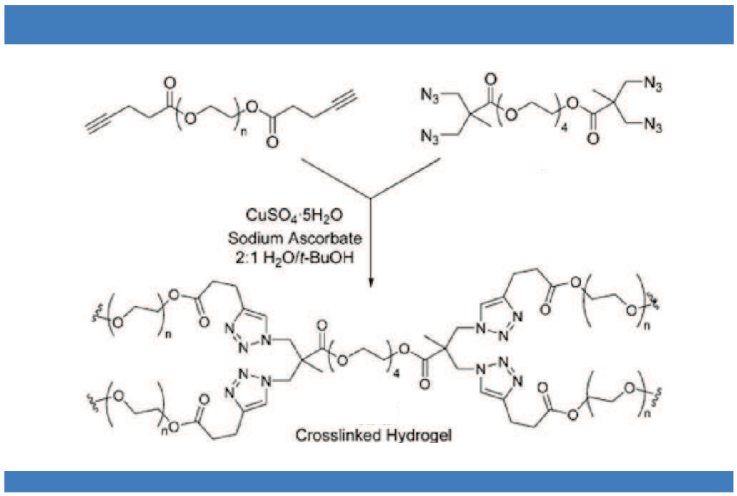

Figure 53 | Crosslinked click hydrogel made by Craig J. et al.[73]

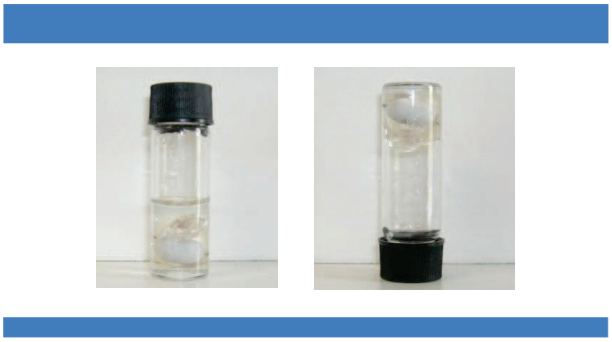

Figure 54 | Gel **40** (n=108) in toluene (a small stirring bar is seen inside)

[73] Craig J. Hawke *et al*. Synthesis of well-defined hydrogel networks using Click chemistry. *Chem. Commun*., 2774-2776 (2006).

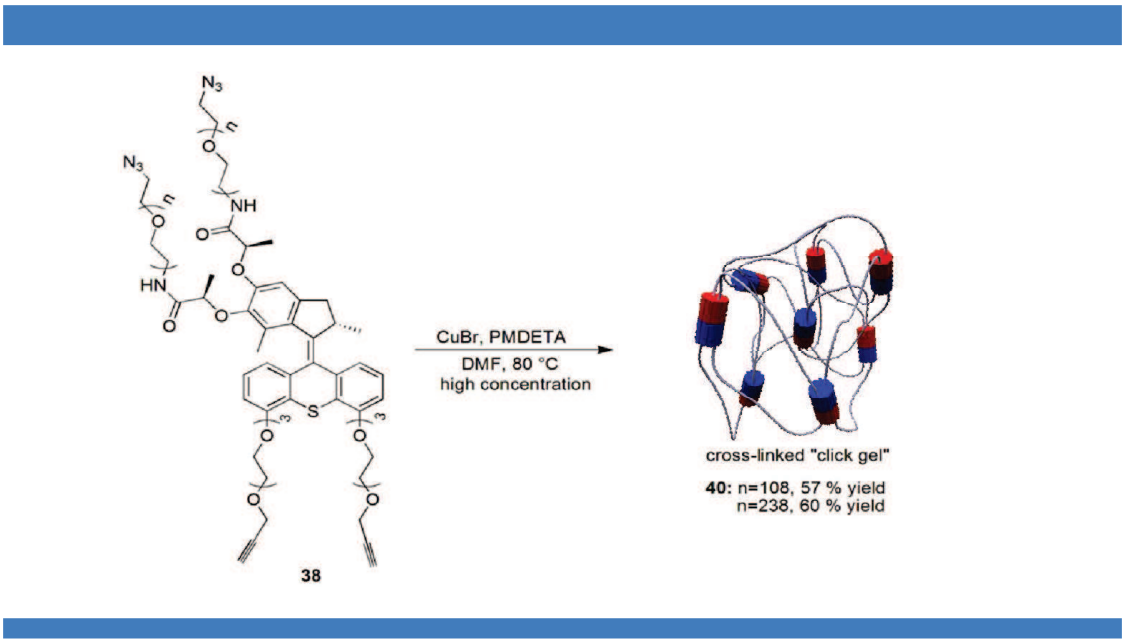

Scheme 21 | Synthesis of "click" gel.

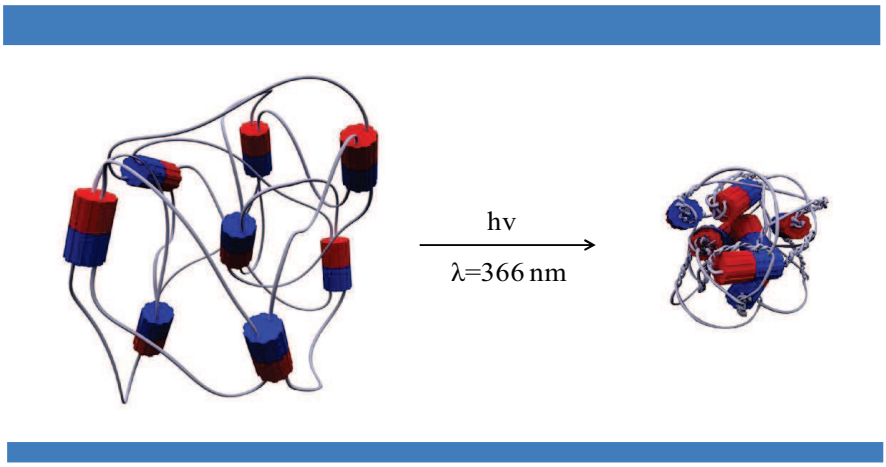

Figure 55 | Gel contraction by the rotation of the motor.

We then postulated that upon UV irradiation, the contraction of the gel would be observed because of the entanglement from the single polymer chains triggered by the rotation of the motor units (Figure 55).

To verify if the gel contraction is indeed due to the rotation of motor in which the central double bond plays a key role (*cis-trans* isomerization), we synthesized a similar gel but without motors to serve as a control experiment. Since the central double bond is essential for the rotation of motor, the precursor of motor-episulfide should not rotate as no isomerizations are expected for the episulfide.

Thus a non-motor gel was produced following the same procedure as gel **40** (Scheme 22). Starting from episulfide **22**, the bis-phenol **41** was obtained in quantitative yield by treatment with TBAF in THF for 5 minutes. This compound was then reacted with 3 equivalents of alkyne terminated triethyleneglycol bearing a tosylate in DMF. The obtained compound has not been purified by flash column chromatography and was used directly in the next step after a simple work up. Potassium hydroxide was used in a mixture of methanol and THF to perform the saponification leading to the bis-acid. Then, a classical peptide coupling was carried on this bis acid with azido terminated PEG to afford the episulfide-gel precursor **42**. This episulfide-polymer conjugate **42** was purified by reversed column chromatography and obtained with a yield of 11 % over three steps. ^{1}H NMR was used to demonstrate its structure unambiguously (Figure 56).

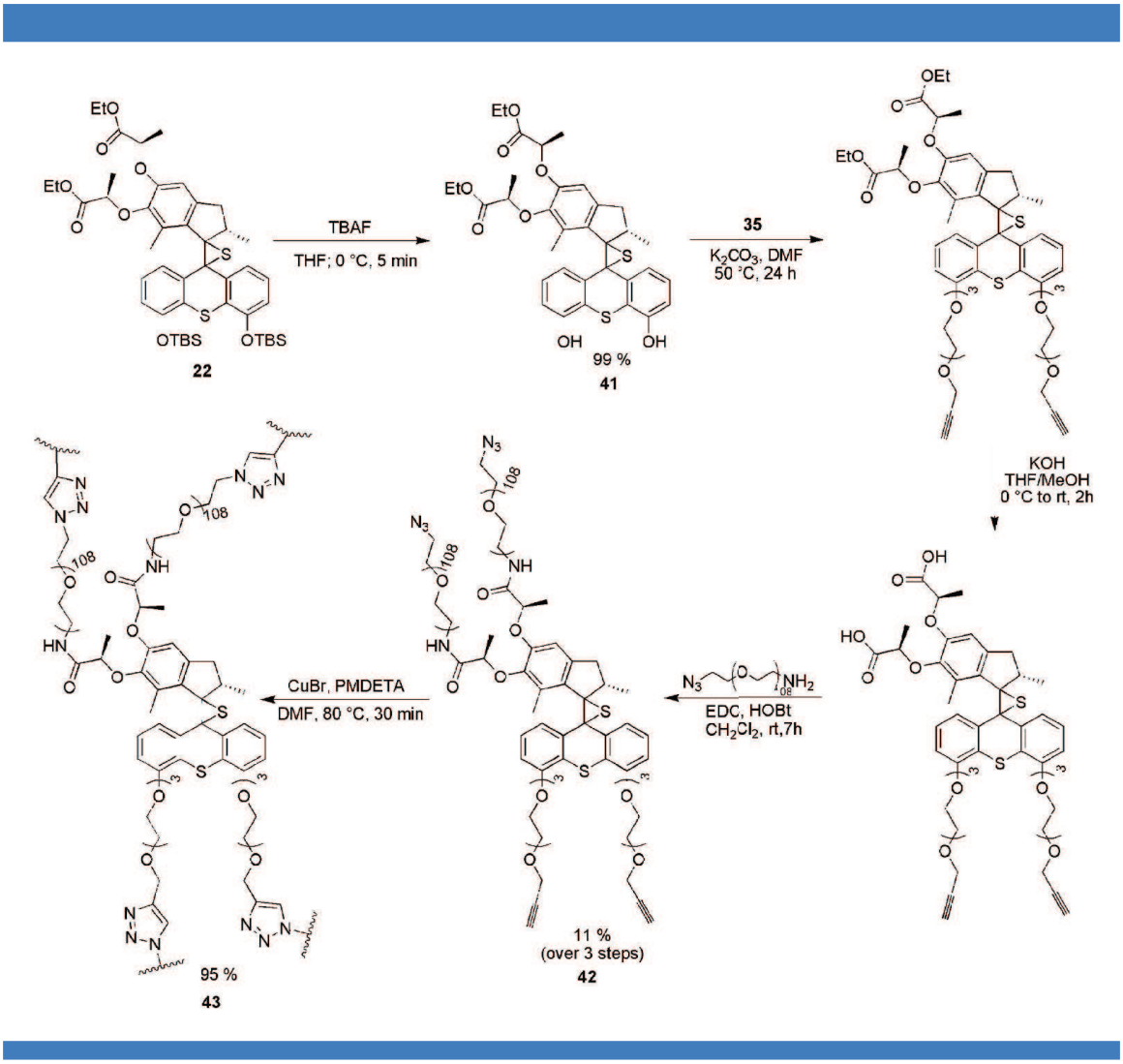

Scheme 22 | Synthesis of non-motor "click" control gel

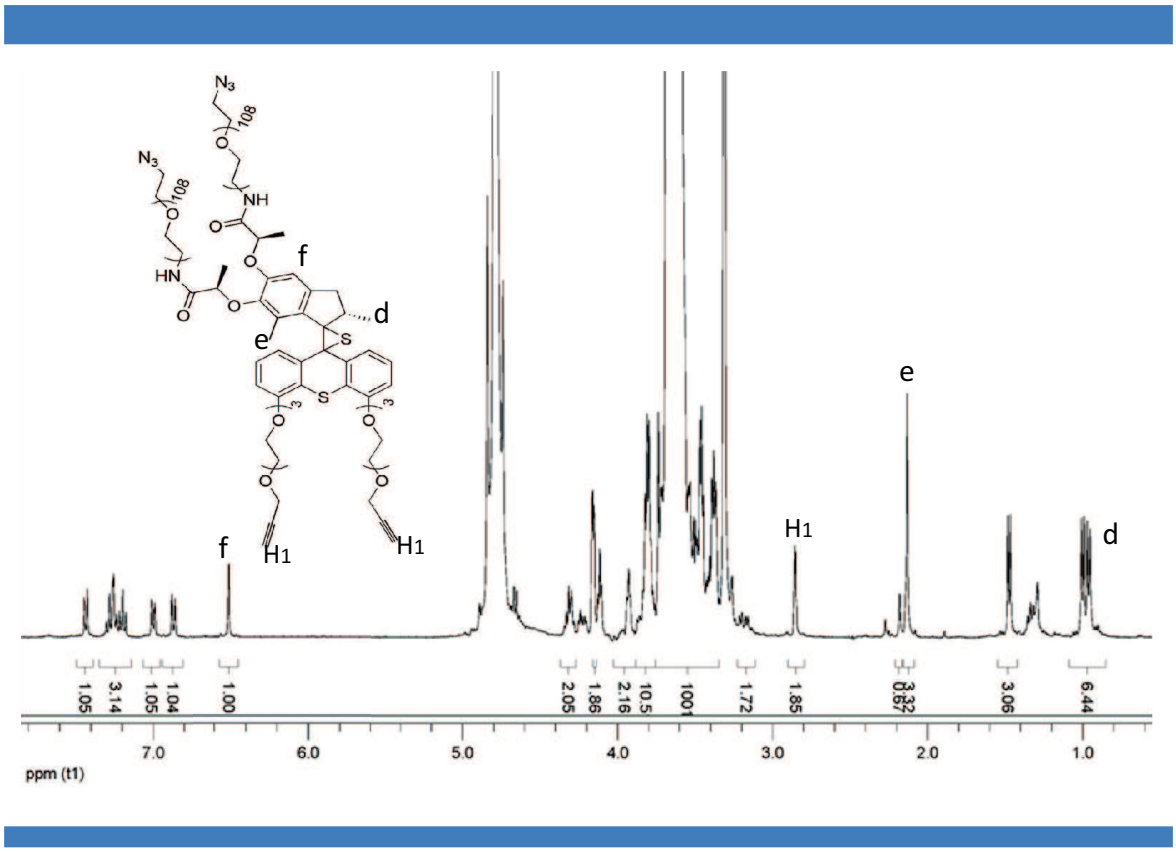

Figure 56 | ^{1}H NMR spectrum of episulfide-polymer conjugate **42**.

With episulfide-polymer conjugate **42** in hand, the control gel was produced efficiently by copper catalyzed "click" reaction. After successive washings with EDTA solution, water and methanol, a transparent gel was obtained (Figure 57).

Figure 57 | Control gel made from episulfide-polymer conjugate **42.** (The piece of gel was placed in a Petri dish)

6/ Characterization of gel contraction

Since the motor-polymer gel was prepared successfully, we decided to irradiate this gel with UV light (λ=366 nm) to induce the contraction of the gel and to observe its effect at the macroscopic scale.

We first used a digital camera to monitor the gel contraction (Figure 58). A small piece of gel **40** (n=108) was placed at the bottom of a small glass vial. Then, the gel was immersed in toluene (~0.15 mL) to keep it swollen during the entire experiment to preclude any contraction induced by deswelling. The vial was placed 1 cm above the lamp in order to avoid excessive heating, and with the camera on top of the vial. Under these conditions, we verified that the temperature in the vial remained unchanged upon UV irradiation.

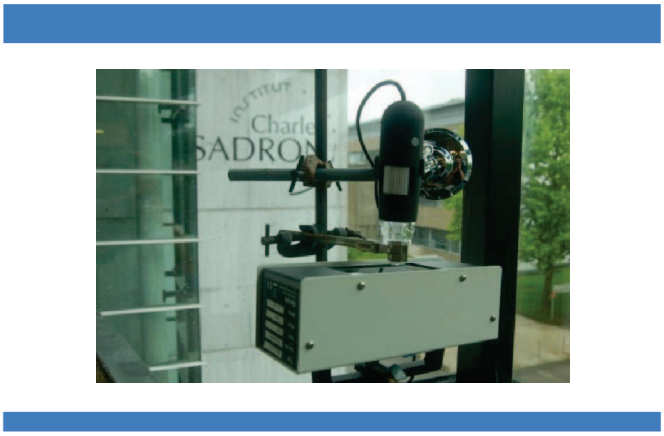

Figure 58 | Setup for the recording of the gel contraction. The gel contraction video was recorded using Video Velocity Free software and USB collected camera.

Upon the UV irradiation, the macroscopic contraction of the gel can be observed easily. For the first time, one could observe a macroscopic motion induced by the integration of different synthetic molecular motors. During the contraction process, the general shape of the gel was not significantly changed which indicates that the contraction occurred in an isotropic manner. A measurement of the surface from the gel after 2 hours exposure to UV light and assuming an isotropic effect on the volume, we could approximate that the contracted gel displayed a volume representing less than 20 % of the initial gel volume. After longer times of irradiation, we noticed that the gel was ruptured and recovered its initial volume and shape. This breaking up is concomitant with the loss of fluorescence in the broken regions (see differences between z_1 (not yet broken) and z_2 (broken) (t = 2 h 50 min) (Figure 59a), indicating a probable disruption by oxidation of the central double bond in motor and a loss of conjugation. Control experiments carried on individual motors allowed us to identify oxygen as the

cause of this rupture. Indeed, exposure of a single motor to UV light with bubbling oxygen revealed the presence of oxidation products such as the upper and lower part ketones. We explain this by the enhanced reactivity of the double bond when the gel becomes tensed upon chains entanglement, but it can be delayed for several hours by working under argon or by stopping the irradiation. When the double bonds from the motors are oxidized, there is no ratchet anymore (the rotation around a single bond is free) thus the polymer chains can disentangle by rotating in the opposite direction leading to a recovery of the initial gel shape and volume. In some experiments, we observed that the energy contained in the tensed gel was so high that this sudden rupture could lead to a jump of the entire piece of gel from the vial's bottom surface (Figure 59b).

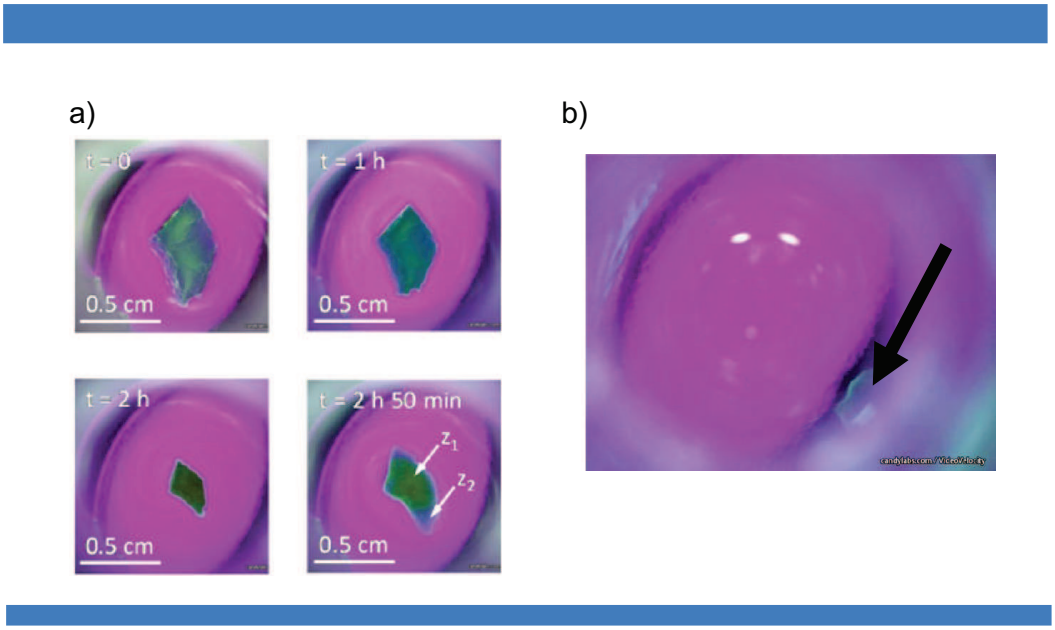

Figure 59 | a) Snapshots taken from the video showing time-dependent macroscopic contraction of a piece of gel immersed in toluene and upon UV light irradiation. At t=2h 50min, z_1 corresponds to a region still contracted and z_2 corresponds to a region which starts disrupting. b) Snapshot taken after the ruptured gel jumped away from the bottom surface. Black arrow indicates the position of the broken piece of gel.

In addition, this very strong macroscopic contraction was also probed at the microscopic scale through AFM imaging (Figure 60). The gel surface displays pores whose diameters are significantly increased upon the course of UV irradiation (increase from 8 to 20 nm). This pore size increase indicates that the macroscopic contraction is the result of the microscopic coiling of entangled polymer chains in the tensed gel, leaving more empty spaces (pores) between denser winded regions. After longer times of irradiation, the initial size of the pores is recovered as the gel breaks up due to the oxidation of the

motors double bonds, which is also in agreement with an uncoiling of the gel while the gel keeps its initial topology.

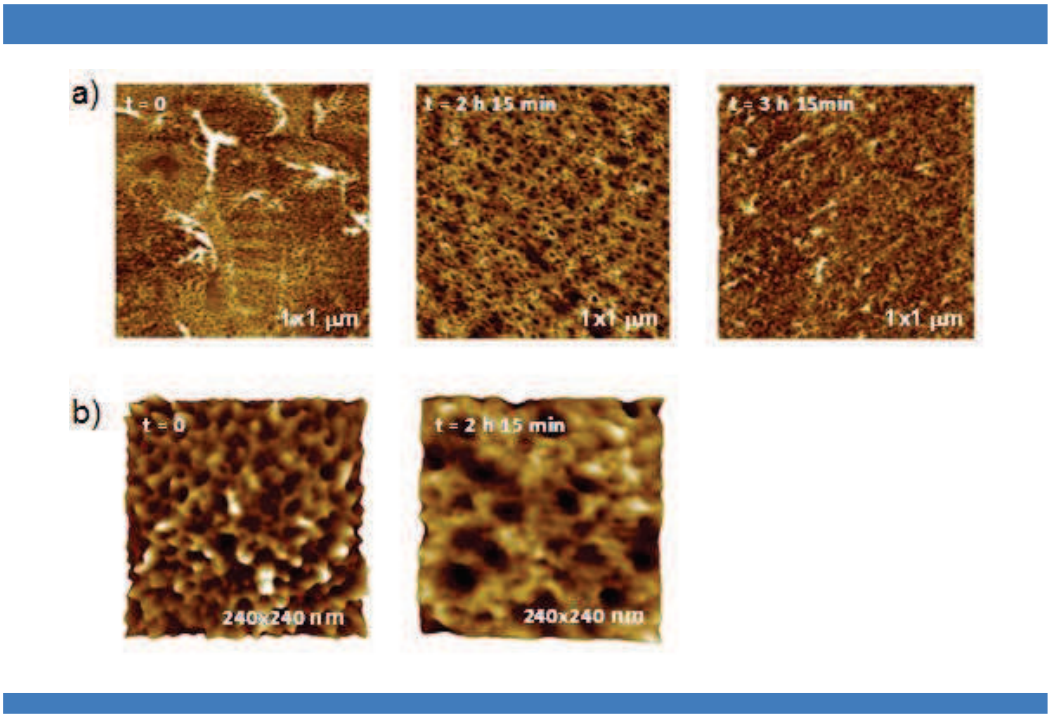

Figure 60 | a) AFM images of gel **40** (n=108) at different UV light irradiation times: before contraction (t=0 min), after contraction (t=2h 15min), and after rupture (t=3h 15min). b) Scaled AFM images of gel **40** (n=108) before and after contractionupon UV light irradiation, which showed an increase of the average pore sizes from 8 nm to 20 nm.

SAXS experiments were also carried on in order to confirm the above observations (Figure 61). As can be seen from Figure 61, the scattered intensity from gel **40** cannot be described by a Lorentzian analytical form prevailing for a semi-dilute polymer solution. Nevertheless, we measured a very strong increase of the scattered intensity upon irradiation, indicating a densification of the polymer chains by aggregation and shrinkage at maximum contraction. This correlates with macroscopic and AFM observations.

Meanwhile, the non-motor gel **43** was subjected to UV irradiation. Unlike gel **40**, no fluorescence was observed when this gel was placed on top of the UV light. Using the same camera set-up above, no contraction could be observed after long irradiation time, which strongly proved that the gel contraction originated from the rotation of the motors since the gel **43** only contained the precursor of motor-episulfide which could not undergo isomerization with UV light.

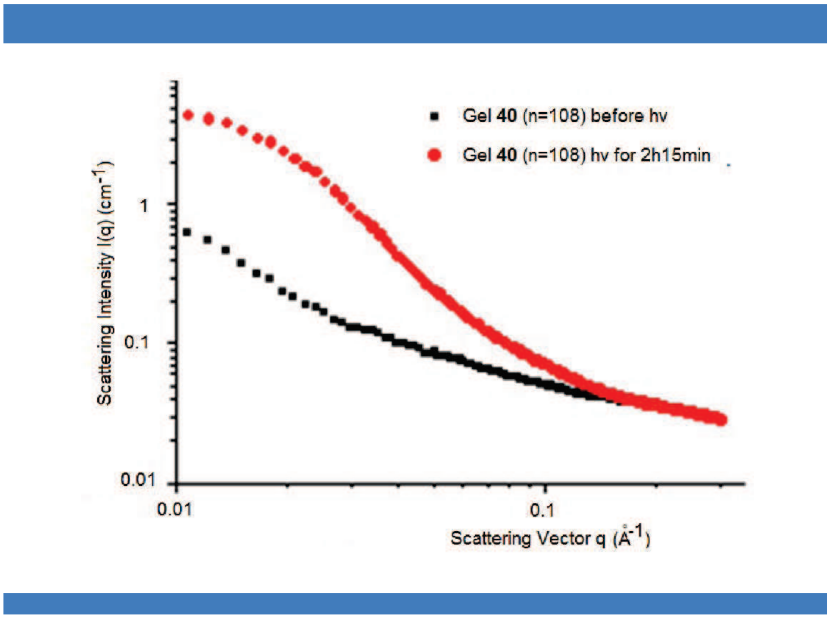

Figure 61 | SAXS data obtained before and after irradiation of gel **40** (n=108).

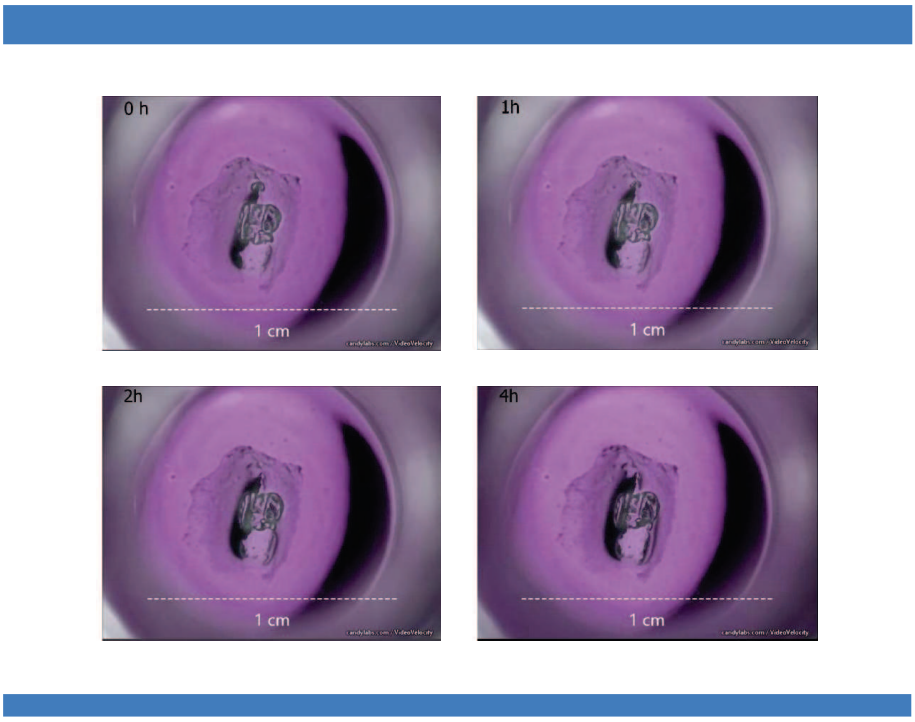

Figure 62 | Snapshots taken from the video showing the contraction of the control gel immersed in toluene upon UV light irradiation.

7/ DFT calculations

To gain more insight into the rotation mechanism of this motor, density functional theory studies (DFT) were performed to calculate the energy profile for the rotation process. Since the photoisomerization steps usually occur at an extremely fast picoseconds rate, the thermal helix inversion step becomes the rate limiting step during the whole rotation cycle. Thus our calculations mainly focused on this thermal helix inversion step. To simplify the calculation, the non-substituted molecular motor was used as a model compound.

DFT calculations show that the thermal helix inversion may undergo different multispets pathways (Figure 63). The unstable form is generated from the stable form upon UV irradiation. Meanwhile the methyl at the stereogenic center will adopt an energy-unfavored equatorial conformation due to the steric repulsion between this methyl and the lower benzene ring. The relative energy of this unstable form was calculated to be 32.6 kJ/mol after geometry optimization. This energy value represents the maximum energy that can be stored in the motor when it is used to perform tasks.

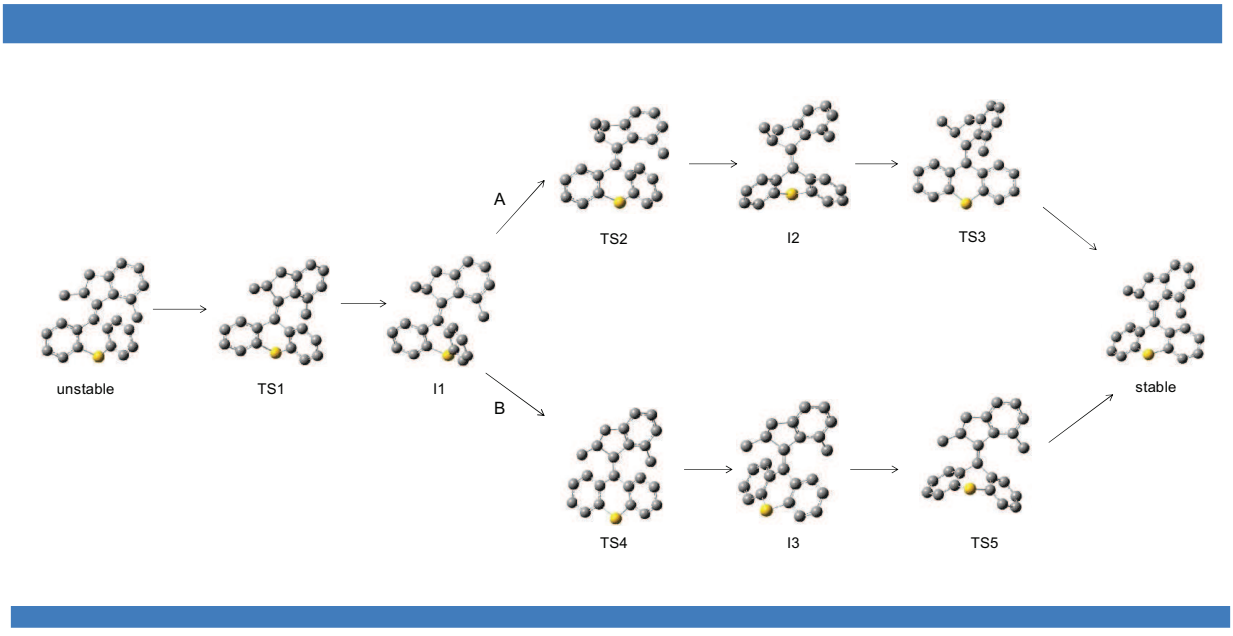

Figure 63 | Two different pathways (A and B) for thermal helix inversion step from unstable form to stable form

Then the methyl group re-adopts the favorable axial conformation concomitant with the ring flip in the cyclopentane affording an intermediate **I1**. Intermediate **I1** is common to both pathway A and B.

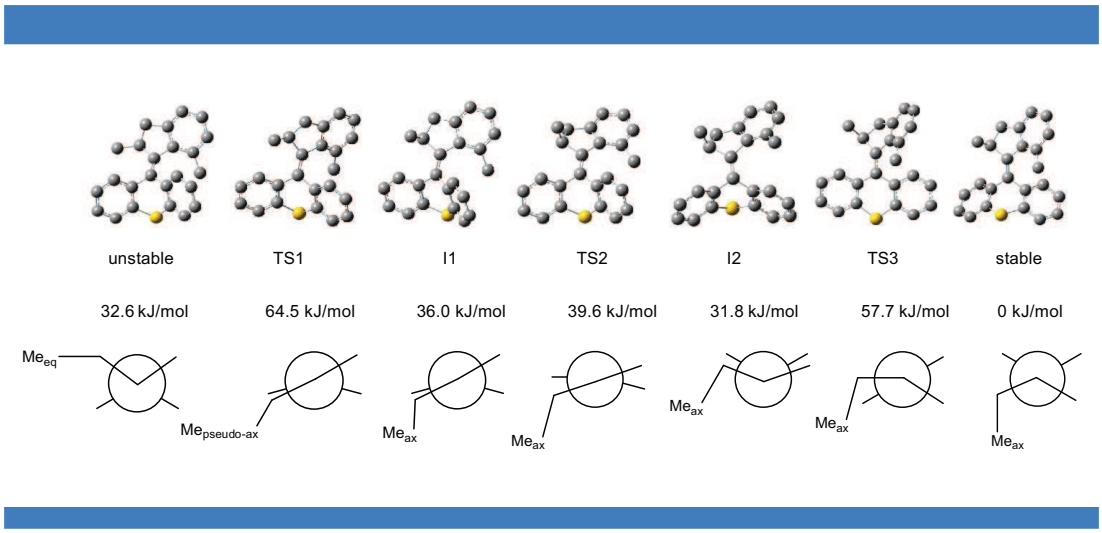

Figure 64 | Conformations of intermediate (I) and transition states (TS) of pathway A identified by DFT calculation at the B3LYP 6-31G (d,p) level for the thermal helix inversion step (top); Relative energies of each conformation (middle); Newman projection for each conformation (bottom).

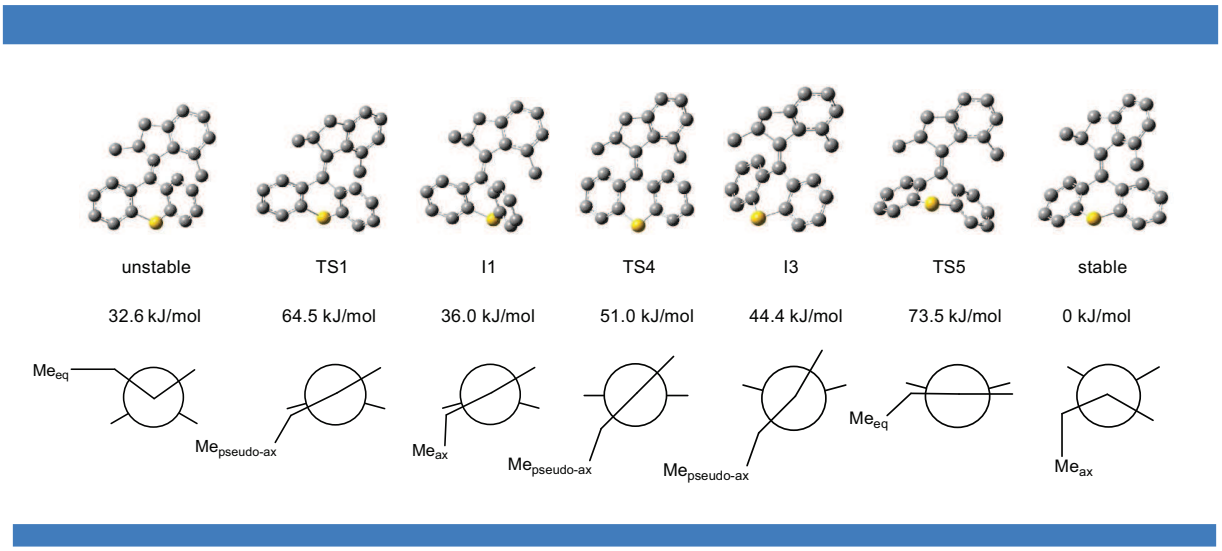

Figure 65 | Conformations of intermediate (I) and transition states (TS) of pathway B identified by DFT calculation at the B3LYP 6-31G (d,p) level for the thermal helix inversion step (top); Relative energies of each conformation (middle); Newman projection for each conformation (bottom).

The difference between pathways lies in the sequence of ring flips. For pathway A, the upper benzene ring first slips over the lower half via **TS2** affording a local minimum, *syn*-folded intermediate **I2**. And finally the lower half in **I2** undergoes a ring flip via **TS3** regenerating the *anti*-folded stable form. For pathway B, the sequence of ring flips is inverted: the lower half first slips over the upper half

via **TS4** giving a local minimum, *twisted* intermediate **I3**. Then the upper half undergoes a ring flip via **TS5** affording the stable form (Figure 64 and 65).

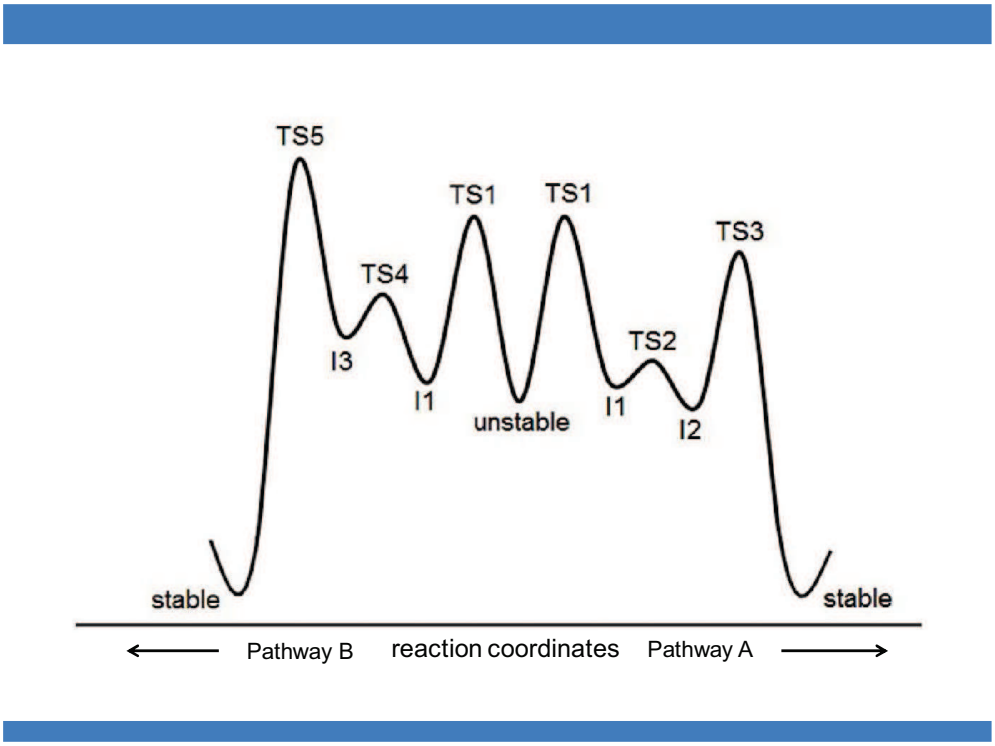

Figure 66 | Energy profile along the reaction coordinate for the thermal helix inversion step of the non-substituted motor

The energy profile along the reaction coordinate for this thermal helix inversion step can be established (Figure 66). For second generation motors, the thermal kinetic decay of unstable to stable isomer can be experimentally monitored by ^{1}H NMR, UV or CD techniques if the energy difference is sufficient large. Previous extensive studies have shown that this thermal decay process followed a first-order reaction kinetics. At a fixed temperature, the decay of unstable isomer as a function of time can give the Gibbs energy of activation ($\Delta G^{\neq}$) at that temperature using the following equations:

$$k = \ln 2/t_{1/2}; \quad \Delta G^{\neq} = -RT\ln(hk/k_BT)$$

where k is the rate constant of conversion (s^{-1}); $t_{1/2}$ is the half-life time for the thermal decay step (s); k_B being the Boltzmann constant (1.381×10^{-23} J K^{-1}); *h* being the Planck's constant (6.626×10^{-34} J s); R being the perfect gas constant (8.314 J $mol^{-1}K^{-1}$).

From figure 66, the energy profile shows that the pathway A would be preferred for the thermal helix inversion step. By calculating the free activation energy $\Delta G^{\neq}$ (31.9 kJ/mol), we can deduce the half

life for this thermal helix inversion step at room temperature (4.3×10^{-8} s), thus the rotation frequency of this motor is 8.05 MHz at room temperature.

8/ Energetic study of the gel

The energy difference between the motor's unstable and stable form represents the maximum of energy that can be stored in this gel through the twisting of polymer chains during the motor's rotation. By plotting the gel **40a** volume contraction against time, we obtained an overview of the gel contraction process (Figure 67).

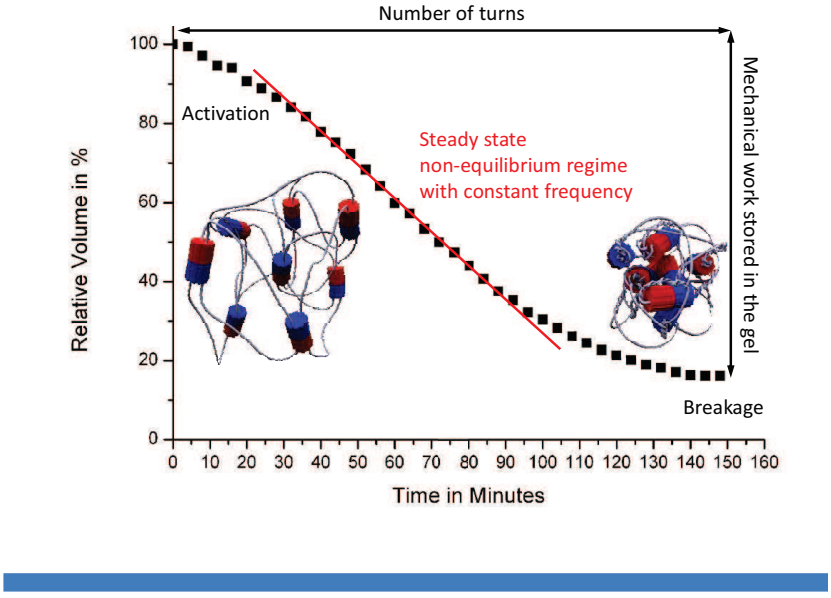

Figure 67 | Overview of the gel contraction (**40a**) during the UV irradiation experiment

As demonstrated in Figure 67, between 0 and 30 min, the gel contracted very slowly representing an activation stage for the motor to twist the polymer chains. Then in the following 60 min, the gel contraction entered an apparent linear regime. In this stage, the volume contraction against time showed a linear relationship, which indicated that the motor was rotating with a constant frequency and that a single process of twisting was involved. After this stage, the contraction slowed down and the gel

reached a very tensed state with highly twisted torsion of the polymer chains, leading to the breakage of motors double bonds representing an original type of chemical activation upon mechanical constraints.

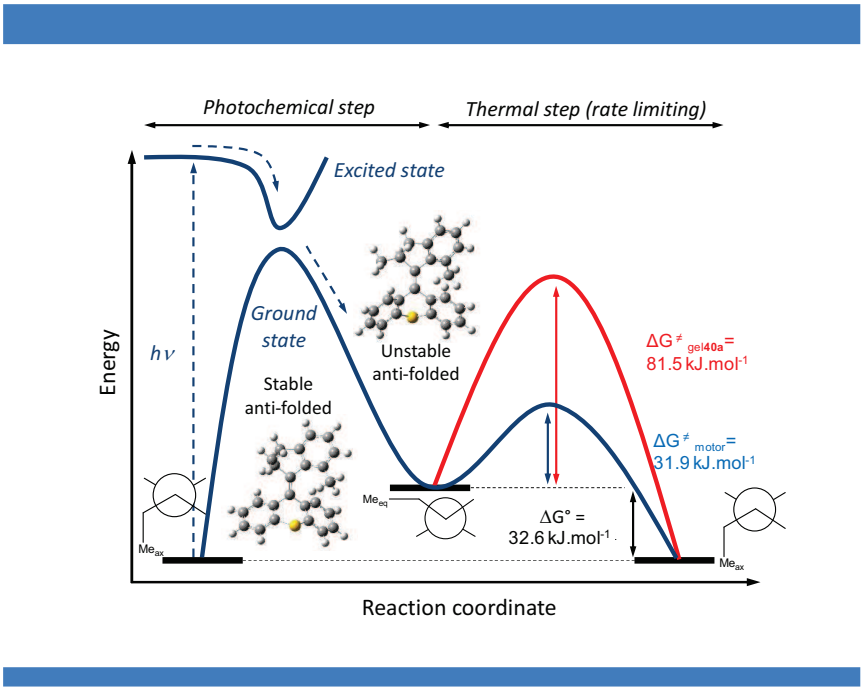

Figure 68 | General energy profile for non-substituted motor (blue line) and gel **40a** (red line) during 180 ° rotation process

The maximum number of turns (105) for the motor in this gel could be estimated as the ratio between the contour length (L_c, that is 40 nm) of PEG 5000 and its persistence length (L_p, which is 0.38 nm). From Figure 67, one can estimate that the maximum frequency for the motor in this gel is 3.16×10^{-2} Hz ($t_{1/2}$=22 s) at 25 ˚C, this frequency corresponds to an activation energy $\Delta G^{\neq}_{40a}$=81.5 kJ/mol for the thermal helix inversion step of the motor. This extra 50 kJ/mol energy represents the penalty for the motor to twist the reticulated polymer chains (Figure 68). It also indicates that the activation energy in such a gel will depend on the polymer chains length. Indeed, for the gel **40b** which was prepared from PEG10000, we could not observe any significant contraction at room temperature even after 8 hours of UV irradiation. However, when the temperature was increased to 50 ˚C, a significant contraction was observed after 18 hours indicating a slower rotation speed for the motor in gel **40b** (f=3.28×10^{-3} Hz, $t_{1/2}$=105 s) at this temperature. This rotation speed can be extrapolated at room temperature (f =1.74×10^{-3}Hz; $t_{1/2}$ = 200 s), the 100 % increase in polymer length results in a one order of magnitude reduced speed of rotation. Interestingly, gel **40b** also displayed a 75~80 % volume contraction similar to the

contraction observed for gel **40a**. This unexpected result prompted us to establish a simplified model for the contraction of polymer chains through twisting (Figure 69).

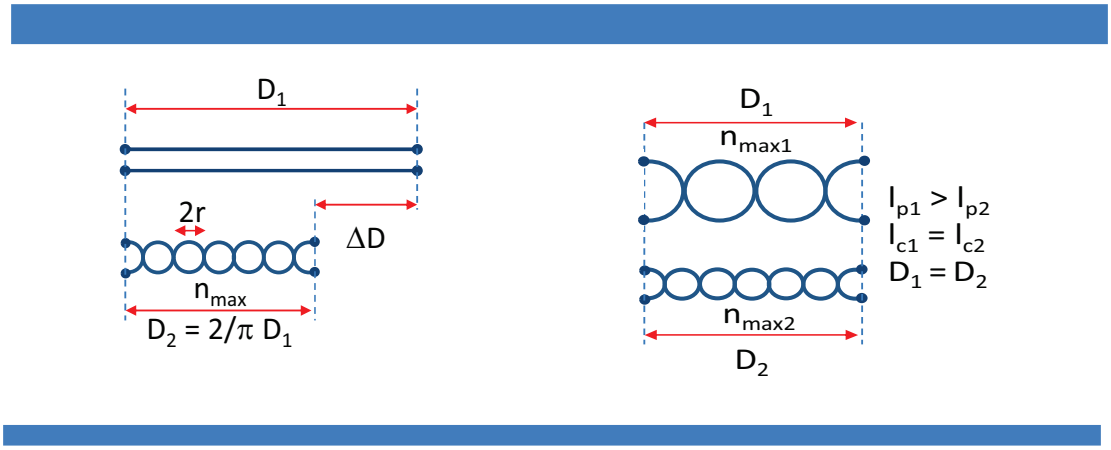

Figure 69 | Simplified model of polymer chain contraction.

The establishment of this simplified model begins with the determination of the maximum number of turns during the rotation process. This maximum number of turns will be determined by the maximum curvature that the polymer can locally stand before ongoing a supercoiled topology. Thus, the final topology for a twisted double chain can be approximated by a series of linked circles of radius r, which is dependent on the persistence length L_p. However, the contour length is invariant during the contraction process, this implies that the maximum number of turn n_{max} will tend to the ratio L_c/L_p. Considering that in the fully extended form, L_c is equal to D_1 (the distance between the end chains), after contraction this distance becomes $D_2 = 2rn_{max}$ while L_c is unchanged. For gel **40a** (M = 5 000 g·mol^{-1}), D_1=L_c = 40 nm and L_p = 0.38 nm, thus n_{max} = 105, and r = 0.12 nm. From the model depicted in Figure 69, we obtain a value for D_2, D_2 = 25.2 nm (63 % of D_1). In volume, this value corresponds to $(0.63)^3$ = 25 % for the contracted gel compared to the extended one. It is noteworthy that this value is independent on the polymer size because the ratio D_2/D_1 is independent of n_{max} and is equal to $2/\pi$ as $D_1 = \pi rn_{max}$, with a maximum gel contraction in volume before supercoiling of $(2/\pi)^3$. In addition, when using circles of various r for n_{max}, which would be the case for polymers of different L_p, one should have the same ratio D_2/D_1 and therefore the same contraction ratio. In our case, it correlates nicely with the experiments performed on gels **40a** and **40b**, respectively made from PEG 5 000 and PEG 10 000 where the relative volumes observed after contraction were around 20 %.

The efficiency for the conversion of light into mechanical work of gel **40a** was estimated by measuring the absorbance when it was submitted to irradiation with a lamp functioning at 366 nm and having a power of 959 $mW \cdot cm^{-2}$. By integrating the volume of the gel, we obtained an absorbed energy of 19 $mW \cdot cm^{-3}$. Then by estimating the number of motors in a given volume of gel, and taking into account the time of irradiation, we determined an energy conversion of 0.15 % for the gel contraction.

9/ Conclusion

In this chapter, we have successfully integrated molecular motors in polymer systems. First, we have synthesized an 8-shaped molecule through intramolecular Huisgen cycloaddition of compound **39**. As expected, upon UV irradiation, the entanglement of polymer chains led to a collapse of the initial 8-shaped molecule resulting in a coiled conformation and an increase in internal density. Then, working in concentrated conditions allowed us to synthesize a novel “click” gel with integrated molecular motors. This motor-gel demonstrated strong contracting properties upon UV irradiation. The contracting process could be characterized both at macroscopic scale by a digital recording camera and at microscopic scale by AFM and SAXS techniques. With the UV light energy input, the individual motions from single molecular motors at the nanoscale could be amplified to generate a macroscopic contraction in metastable materials.

Conclusions and Perspectives

The core of this work relies on organic synthesis. We have successfully developed a new synthetic route to unidirectional molecular motors based on Feringa's design of overcrowded alkenes. Thanks to the incorporation of a chiral auxiliary, this methodology allows to access enantiopure molecular motors without requiring the use of chiral chromatography techniques. Consequently, this synthetic route can be implemented to prepare an enantiopure molecular motor on gram scale. Furthermore, the synthesized molecular motor exhibits orthogonal reactive groups in its upper and lower parts (ester and ether, respectively) allowing an asymmetric functionalization which proved to be crucial for implementing these motors in material science. All the compounds described in the synthetic part have been systematically characterized thanks to NMR techniques (^{1}H, ^{13}C, 2D). The unidirectionality of the rotation process was probed thanks to the synthesis of an asymmetric version of the overcrowded alkene which allowed the visualization of two stable forms by NMR and LC-MS. The absolute configurations of the molecular motors have been determined by X-ray crystallography. Optical spectroscopy techniques such as UV and CD have been used to further characterize the final compounds. DFT studies have also been carried on in order to obtain further insight on the mechanism and the energetics of the rotation.

Then, we succeeded in implementing molecular motors in two different polymer systems thanks to intra- and intermolecular click chemistry. In the first case, 8-shaped molecules were successfully prepared whereas the second route led to a gel material. In both cases, a combination of AFM and SAXS allowed us to characterize the effect of the rotation from the rotating units. In the case of the gel, videos taken with a simple USB camera evidenced a strong gel contraction which is the macroscopic consequence of the molecular motions from molecular motors. For the first time, the work performed by unidirectional molecular motors was used to entangle polymer chains (instead of being dissipated). The nanorotations were integrated to yield a macroscopic contraction just like in natural systems (muscle contraction for instance which is the result of the integration of millions of nanoscopic motions leading to a macroscopic movement). Unlike machine based on switches that can only work between two thermodynamic minima, this system can operate continuously out of equilibrium in an isotropic medium submitted to Brownian motion with light being the only required stimulus. Upon the course of UV irradiation, the global free energy of the system increases, implying that this system could be used to

store energy from light by entangling polymer chains. This aspect is currently investigated in our research group. We envision that a dissipative unit would allow us to store light energy in a gel and to release it by disentangling the polymer chains on demand thanks to a second stimulus. This would lead to a new energy storage device that could pave the way for further applications. Another perspective of thiswork is to measure the torque exerted by the motor. For that, we are currently functionalizing surfaces with polymer grafted molecular motors, then we plan to adsorb the polymer to an AFM tip. A force analysis during UV irradiation should allow us to directly measure the pulling force exerted on the AFM tip by a single molecular motor. We also wish to complete the characterization of the contractile gel through rheology experiments in order to obtain mechanical information. In particular, we plan to study gels prepared with different polymer lengths and also to test other polymer motifs which will also require new synthetic efforts.

We believe that this work represents a major achievement in the field of molecular machines. The integration of machines which display motions out of equilibrium to movement to the macroscopic world will open very interesting prospects in nanotechnology for further developments.

Experimental Part

1/ General Procedures

a) Solvent and chemical reagents

All reagents and solvents were purchased at the highest commercial quality (sigma Aldrich, Acros, TCI) and used without further purification unless otherwise noted. Dry solvents were used from a double column SolvTech purification system. Water was deionized by using a milli-gradient system (Millipore, Molsheim, France). All reactions were carried out under argon atmosphere with dry solvents unless otherwise noted. Microwave reactions were carried out with a single mode cavity Discover Microwave Synthesizer (CEM Corporation, NC, USA), producing continuous irradiation at 2455 MHz and equipped with simultaneous external air-cooling system.

b) Chromatographic methods

Reactions were monitored by UPLC-MS (Waters, diode array as UV detector) or thin layer chromatography (TLC) carried out on 0.25 mm E. Merck silica gel plates (60F-254) by using UV light as visualizing agent and 10 % ethanolic phosphomolybdic acid or vanillin solution and heat as visualizing agents. Silica gel 60 (230-400 mesh, 40-63 µm, Merck) was used for flash column chromatography. Preparative thin layer chromatography (preparative TLC) was carried out on 0.25 mm E. Merck silica gel plate.

c) Analytical methods and instruments

I. Nuclear Magnetic Resonance (NMR)

^{1}H NMR spectra were recorded on a Bruker Avance 400 spectrometer at 400 MHz and ^{13}C spectra at 100 MHz and calibrated by using the the residual proton solvent signal ($CDCl_3$: 7.26 ppm, DMSO-d_6: 2.50 ppm, CD_3OD-d_4:3.31 ppm). For ^{1}H and ^{13}C NMR assignments, the chemical shifts (δ) are given in ppm. Coupling constants *J* are given in Hz. Peaks are described as singlet (s), doublet (d), triplet (t), quartet (q), multiplet (m) and broad (br).

II. Mass spectrometry

Ultra Performance Liquid Chromatographies coupled to Mass Spectroscopy (UPLC-MS) were carried out on a Waters Acquity UPLC-SQD apparatus equipped with a PDA detector (190-500 nm, 80 Hz), using a reverse phase column (Waters, BEH C_{18} 1.7 µm, 2.1 × 50 mm), the MassLynx 4.1 - XP software and a gradient (water-acetonitrile + 0.1% TFA) as eluent.

III. UV-vis and CD measurements

UV/VIS absorbance spectra were measured with a Varian Cary 500 spectrophotometer using a quartz cuvette with a 1 cm path length. The spectra were taken at a concentration of -2×10^{-5} M. Irradiation time points were carried out with a lamp placed 2-3 cm from the cuvette.

CD spectra were recorded on a JASCO J-715 spectropolarimeter using a quartz cuvette with a 1 mm path length. Irradiation time points were carried out with a lamp placed 2-3 cm from the cuvette.

IV. AFM characterization

Atomic force microscopy (AFM) images were obtained by scanning the samples using a Nanoscope 8 (Bruker) operated in Peak-Force tapping mode. Peak-Force AFM is based on Peak force tapping technology, during which the probe is oscillated in a similar fashion as it is in tapping mode, but at far below the resonance frequency. Each time the tip and the sample are brought together, a force curve is captured. These forces can be controlled at levels much lower than contact mode and even lower than tapping mode allowing operation on even the most delicate soft samples, as is the case here. Ultra-sharp silicon tip on nitride lever were used (Bruker, Scanasyst with spring constant of 0,4 N/m and tip radius of about 5 nm). During AFM imaging, the force was reduced in order to avoid dragging of molecules by the tip. Here the applied peak force is about 50 pN. All analyses of the images were conducted in integrated software.

V. Small Angle X-ray Scattering (SAXS)

SAXS experiments were performed in our laboratory by using a diffractometer developed by Molecular Metrology (Elexience in France). It operates with a pinhole collimation of the X-ray beam and a two-dimensional gas-filled multiwire detector. A monochromatic (λ=1.54Å with $\Delta\lambda/\lambda$ <4%) and focused X-ray beam is obtained through a multilayer optic designed and fabricated by Osmic. The size of the incident beam on the sample was close to 600 µm. The sample to detector distance was set at 0.70 m, allowing to explore scattering vectors ranging from q = 0.01 $Å^{-1}$ to 0.3 $Å^{-1}$. The magnitude of the

scattering vector is defined by $q=4\pi\sin(\theta/2)/\lambda$, where λ and θ are the wavelength of the incident beam and the scattering angle, respectively. The q-resolution related to the beam size on the sample and the beam divergence was close to 0.005 $Å^{-1}$. A quartz capillary of 1 mm diameter and cells of 1 mm thickness with calibrated Mica windows were used as sample holders for molecular motor solutions and gels, respectively. Measurements were performed at room temperature.

2/ Synthesis and Characterization of Compounds

Compound 1

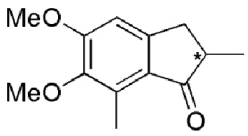

5,6-dimethoxy-2,7-dimethyl-indane-1-one (1): To mechanically stirred polyphosphoric acid (30 mL) heated at 70 ˚C, were added methacrylic acid (12.9 mL, 150 mmol) and 2,3-dimethoxytoluene (12 mL, 89 mmol). After stirring at 70 ˚C for 3 h, the mixture was poured onto ice and stirred overnight. The water layer was extracted with EtOAc (3 × 50 mL). The combined organic layers were washed with aqueous $NaHCO_3$ (30 mL), water (30 mL) and brine (30 mL) and dried (Na_2SO_4). The solution was concentrated in vacuum to a damp solid and then recrystallized from *n*-heptane (20 mL) giving brown crystals (10 g, 51 % yield). R_f=0.74 (cyclohexane:EtOAc=1:1);

^{1}H NMR ($CDCl_3$, 400 MHz, 298 K) δ 6.74 (s, 1H), 3.92 (s, 3H), 3.76 (s, 3H), 3.27-3.22 (m, 1H), 2.66-2.60 (m, 2H), 2.56 (s, 3H), 1.26 (d, *J*=7.2 Hz, 3H).

^{13}C NMR ($CDCl_3$, 100 MHz, 298 K) δ 208.9, 158.1, 151.8, 146.9, 132.1, 127.3, 105.9, 60.4, 55.8, 42.6, 34.5, 16.6, 10.6.

HRMS (*m/z*): calculated for $C_{13}H_{16}LiO_3$ $[M+Li]^+$ 227.1254, Found 227.1249.

Compound 2

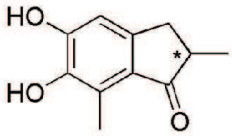

5,6-dihydroxy-2,7-dimethyl-indane-1-one (2): BBr_3 (1.9 mL, 20.0 mmol) was added slowly to a stirred solution of **1** (3.00 g, 13.4 mmol) in CH_2Cl_2 (10 mL) at 0 ˚C under Ar. After 3 h at this temperature, the reaction was quenched by adding water (20 mL) slowly. The water layer was extracted with ethyl acetate until the water phase became colorless. The combined organic layer was washed with water, brine and dried over Na_2SO_4. The solvent was evaporated under reduced pressure to give the crude product as a brown solid. The suspension of the solid in diethyl ether (2×20 mL) followed by filtration provided compound **2** as a grey powder (2.39 g, 90 % yield). R_f=0.5 (cyclohexane:EtOAc=1:1);

^{1}H NMR (CD_3OD, 400 MHz, 298 K) δ 6.69 (s, 1H), 3.19-3.17 (m, 1H), 2.62-2.50 (m, 2H), 2.47 (s, 3H), 1.20 (d, *J*=7.2 Hz, 3H).

^{13}C NMR (CD_3OD, 100 MHz, 298 K) δ 212.1, 153.7, 150.1, 144.2, 126.9, 125.3, 109.7, 43.9, 34.9, 17.1, 10.6.

HRMS (*m/z*): calculated for $C_{11}H_{12}LiO_3$ $[M+Li]^+$ 199.0941, Found 199.0944.

Compound 3

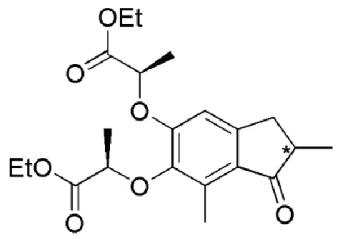

Ethyl 2-({6-[(1-ethoxy-1-oxopropan-2-yl)oxy]-2,7-dimethyl-1-oxo-2,3-dihydro-1H-inden-5-yl}oxy)propanoate (3): To a solution of compound **2** (500 mg, 2.6 mmol), (*S*)-lactic ethyl ester (0.75 mL, 6.5 mmol), PPh_3 (1.7 g, 6.5 mmol) in dry THF (13 mL) was added DIAD (1.4 mL, 6.5 mmol) dropwise at 0 ˚C. The mixture was stirred while allowed to reach room temperature for 16 h. The mixture was concentrated in vacuum and purified by flash column chromatography (silica gel, cyclohexane:EtOAc=6:1) affording compound **3** as a slight yellow oil (0.735 g, diasteriomeric mixture, 72 % yield). R_f=0.4 (cyclohexane:EtOAc=3:1);

^{1}H NMR [$(CD_3)_2CO$, 400 MHz, 298 K] δ 6.80 (s, 1H), 5.09 (q, *J*=6.8 Hz, 1H), 4.98 (q, *J*=6.8 Hz, 1H), 4.18-4.09 (m, 4H), 3.27-3.19 (m, 1H), 2.60-2.58 (m, 1H), 2.56 (s, 3H), 2.55-2.50 (m, 1H), 1.66 (d, *J*=6.8 Hz, 3H), 1.58 (d, *J*=6.8 Hz, 3H), 1.24 (t, *J*=6.8 Hz, 3H), 1.21 (t, *J*=6.8 Hz, 3H), 1.18 (d, *J*=7.2 Hz, 3H).

^{13}C NMR [$(CD_3)_2CO$, 100 MHz, 298 K] δ 208.5 (2C), 172.8, 171.8, 156.0, 152.0, 146.0 (2C), 132.9, 128.5, 108.3, 77.6, 73.3, 62.1, 61.4, 43.4 (2C), 35.0, 22.4, 19.3, 18.7, 16.8 (2C), 14.6, 11.7.

HRMS (*m/z*): calculated for $C_{21}H_{28}LiO_7$ $[M+Li]^+$ 399.1990, Found 399.1990.

Compound 4

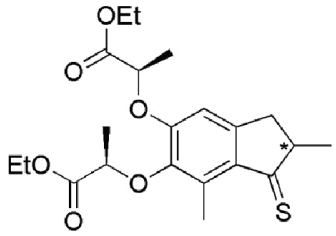

Ethyl 2-({6-[(1-ethoxy-1-oxopropan-2-yl)oxy]-2,7-dimethyl-1-sulfanylidene-2,3-dihydro-1H-inden-5-yl}oxy)propanoate (4): The mixture of ketone **3** (2.0 g, 5.1 mmol) and P_2S_5 (1.7 g, 7.6 mmol) in toluene (10 mL) was heated to 80 ˚C for 1 h. Then the mixture was filtered and washed with EtOAc (100 mL) until the eluent was colorless. Flash column chromatography (silica gel, EtOAc:cyclohexane=1:13) was then performed affording compound **4** as a purple oil (683 mg, 33 % yield). This compound is not stable towards air and is then directly used in the next step. ^{1}H NMR ($CDCl_3$, 400 MHz, 298 K) δ 6.61 (s, 1H), 4.88 (q, *J*=6.8 Hz, 1H), 4.82 (q, *J*=6.8 Hz, 1H), 4.26-4.18 (m, 4H), 3.33-3.26 (m, 1H), 3.00-2.96 (m, 1H), 2.77 (s, 3H), 2.71-2.66 (m, 1H), 1.69 (d, *J*=6.8 Hz, 3H), 1.62 (d, *J*=6.8 Hz, 3H), 1.39 (d, *J*=7.2 Hz, 3H), 1.27-1.24 (t, *J*=6.8 Hz, 6H).

^{13}C NMR ($CDCl_3$, 100 MHz, 298 K) δ 248.7, 172.1, 171.0, 154.6, 152.8, 145.2, 138.1, 135.1, 106.1, 77.2, 72.6, 60.9, 55.5, 43.4, 38.9, 21.6, 21.5, 18.6, 18.2, 14.0, 13.8.

MS (ESI): calculated for $C_{21}H_{29}O_6S$ $[M+H]^+$ 409.17, Found 409.28.

Compound 5

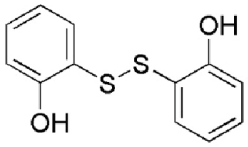

2-[(2-hydroxyphenyl) disulfanyl] phenol (5): To a stirred, biphasic solution of 2-mercaptophenol (1.0 g, 7.9 mmol) in H_2O (5.1 mL) was added, drop wise, a solution of iodine (1.0 g, 4.0 mmol) in methanol (3.5 mL). When the brown iodine color persisted the solution was diluted with ethyl acetate and water. The aqueous layer was removed and extracted with an additional portion of ethyl acetate. The combined organic layers were dried and washed with saturated aq. $Na_2S_2O_3$, brine then dried over (Na_2SO_4) and

concentrated to give compound **5** as a slightly yellow oil (0.9906 g, 99 % yield). R_f=0.45 (cyclohexane:Et_2O=6:1);

^{1}H NMR ($CDCl_3$, 400 MHz, 298 K) δ 7.35 (dt, *J*=7.6, 1.6 Hz, 2H), 7.22 (dd, *J*=8.0, 1.6 Hz, 2H), 7.00 (dd, *J*=8.4, 1.2 Hz, 2H), 6.83 (dt, *J*=7.6, 1.2 Hz, 2H), 6.22 (s, 2H).

^{13}C NMR ($CDCl_3$, 100 MHz, 298 K) δ 156.94, 136.22, 133.25, 121.05, 120.00, 115.77.

Compound 6

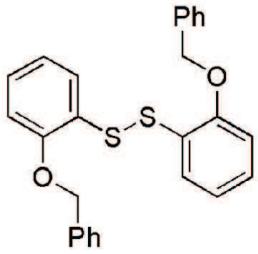

1-{[2-(benzyloxy)phenyl]disulfanyl}-2-(phenoxymethyl)benzene (6): To a solution of compound **5** (0.3044 g, 1.22 mmol) in DMF (7 mL) was added K_2CO_3 (0.4050 g, 2.93 mmol) and benzyl bromide (0.32 mL, 2.68 mmol) successively. The resulting mixture was stirred at 50 ˚C for 1.5 h. Then H_2O (20 mL) was added into the mixture which was then extracted by Et_2O (20 mL×3). The organic layer was washed with water (20 mL×3) and dried over Na_2SO_4. Flash column chromatography (silica gel, EtOAc:cyclohexane=1:10) was performed giving compound **6** as a white solid (0.4351 g, 83 % yield).

^{1}H NMR ($CDCl_3$, 400 MHz, 298 K) δ 7.57-7.55 (dd, *J*=7.8, 1.2 Hz, 2H), 7.49 (d, *J*=6.0 Hz, 4H), 7.38 (t, *J*=6.8 Hz, 4H), 7.30 (d, *J*=6.0 Hz, 2H), 7.15-7.11 (t, *J*=6.4 Hz, 2H), 6.91-6.87 (m, 4H), 5.18 (s, 4H).

^{13}C NMR ($CDCl_3$, 100 MHz, 298 K) δ 155.6, 136.7, 128.6, 127.9, 127.6, 127.5, 127.1, 125.4, 121.8, 112.3, 70.7.

MS (ESI): calculated for $C_{26}H_{23}O_2S_2$ $[M+H]^+$ 431.11, Found: 431.39.

Compound 7

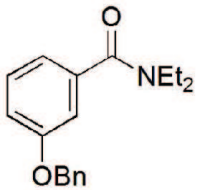

***N,N*-diethyl-3-benzyloxy-benzamide (7):** To a solution of 3-benzylbenzoic acid (1.25 g, 5.5 mmol) in CH_2Cl_2 (20 mL) containing pyridine (1.4 mL, 19.8 mmol) was slowly added oxalyl chloride (8.6 mL, 99 mmol) with stirring. After stirring for 2 h at room temperature, the excess oxalyl chloride was removed *in vacuo* and the remained oxalyl chloride was removed by co-distillation with toluene. The obtained acid chloride was dissolved in CH_2Cl_2 (20 mL) and diethyl amine (13 mL, 126.5 mmol) was added dropwise at 0 ˚C. The reaction mixture was washed with 10 % HCl (20 mL×2), 1M NaOH solution (20 mL×2) and brine successively. The organic layer was then subject to flash column chromatography (silica gel, EtOAc:cyclohexane=1:50→1:7) to give amide **7** as a slight yellow oil (0.986 g, 63 % yield).

^{1}H NMR ($CDCl_3$, 400 MHz, 298 K) δ 7.44-7.27 (m, 6H), 7.01-6.93 (m, 3H), 5.08 (s, 2H), 3.53 (br.s, 2H), 3.23 (br.s, 2H), 1.23 (br.s, 3H), 1.07 (br.s, 3H).

^{13}C NMR ($CDCl_3$, 100 MHz, 298 K) δ 170.84, 158.66, 138.53, 136.65, 129.54, 128.54, 127.95, 127.37, 118.67, 115.84, 112.64, 70.02, 42.21, 38.23, 13.92, 12.51.

MS (ESI): calculated for $C_{18}H_{22}O_2$ $[M+H]^+$ 284.16, Found: 284.06.

Compound 8

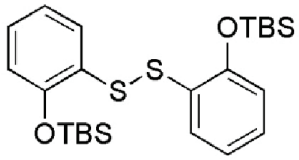

***tert*-butyl(2-({2-[(tert-butyldimethylsilyl)oxy]phenyl}disulfanyl)phenoxy)dimethylsilane (8):** To a solution of compound **5** (500 mg, 2 mmol) in 10 mL DMF was added TBDMS-Cl (0.83 g, 5.52 mmol) and and imidazole (376 mg, 5.52 mmol) under argon. The mixture was stirred at room temperature for 24 h. The mixture was then diluted with water (5 mL) and extracted with Et_2O (30 mL×3). The combined organic phase was dried over Na_2SO_4. Then the solvent was removed in vacuum and the residue was purified by flash column chromatography (cyclohaxane) to afford compound **8** as a white solid (919 mg, 96 % yield). R_f=0.9 (EtOAc:cyclohxane=1:2);

^{1}H NMR ($CDCl_3$, 400 MHz, 298 K) 7.45 (dd, *J*=8.0, 1.6 Hz, 2H), 7.06 (td, *J*=8.0, 1.6 Hz, 2H), 6.90 (td, *J*=8.0, 1.2 Hz, 2H), 6.78 (dd, *J*=8.0, 1.0 Hz, 2H), 1.07 (s, 18H), 0.29 (s, 12H).

^{13}C NMR ($CDCl_3$, 100 MHz, 298 K) 152.54, 127.62, 127.10, 126.94, 121.98, 118.40, 25.87, 18.43, -4.06.

MS (ESI): calculated for $C_{24}H_{38}NaO_2S_2Si_2$ $[M+Na]^+$ 501.17, Found: 501.30.

Compound 9

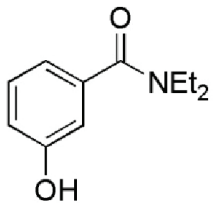

N,N-diethyl 3-hydroxyl benzamide (9): To 3-hydroxy benzoic acid (4.8 g, 34.75 mmol) was added $SOCl_2$ (32 mL) and one drop of dry DMF at room temperature under argon. The mixture was then refluxed at 70 ˚C for 1 h and then cool down to room temperature. The excess $SOCl_2$ was removed at vacuum and further azeotropped with toluene (5 mL). Then 20 mL dry CH_2Cl_2 was added and the solution was treated slowly with Et_2NH at 0 ˚C. The mixture was further stirred at 0 ˚C for 1 h. After the evaporation of CH_2Cl_2, the mixture was dispersed in H_2O (50 mL) and the pH was adjusted to 2-3 and then extracted with EtOAc (50 mL×3). The combined organic layers were dried over Na_2SO_4 and evaporated in vacuum. The crude product was then crystallized in EtOAc affording compound **9** as white crystals (4 g, 60 % yield). Flash column chromatography was performed when this reaction was reproduced (silica gel, CH_2Cl_2-Et_2O=5:1, 6.18 g white crystals, 92 % yield). R_f=0.13 (CH_2Cl_2-Et_2O=5:1);
^{1}H NMR ($CDCl_3$, 400 MHz, 298 K) δ 8.64 (br.s, 1H), 7.13 (t, 1H, *J*=8.0 Hz), 6.85-6.84 (m, 1H), 6.77-6.75 (m, 2H), 3.53 (br.s, 2H), 3.24 (br.s, 2H), 1.23 (br.s, 3H), 1.07 (br.s, 3H).
^{13}C NMR ($CDCl_3$, 100 MHz, 298 K) δ 172.14, 157.08, 137.08, 129.42, 117.09, 116.92, 114.02, 43.54, 39.54, 14.06, 12.77.
MS (ESI): calculated for $C_{11}H_{16}NO_2$ $[M+H]^+$ 194.12, Found: 193.98.

Compound 10

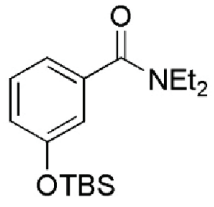

3-[(*tert*-butyldimethylsilyl)oxy]-N,N-diethylbenzamide (10): To a solution of compound **9** (500 mg, 2.6 mmol) in dry CH_2Cl_2 5 mL was added TBDMS-Cl (585 mg, 3.88 mmol) and imidazole (264 mg, 3.88 mmol) under argon. The mixture was stirred at room temperature for 16 h. Then the solvent was removed in vacuum and the residue was purified by flash column chromatography

(EtOAc:cyclohxane=1:5) to give compound **10** as a slight yellow oil (800 mg, 99 % yield). R_f=0.45 (EtOAc:cyclohexane=1:2);

^{1}H NMR ($CDCl_3$, 400 MHz, 298 K) δ 7.24 (t, *J*=8.0 Hz, 1H,), 6.94 (dt, *J*=7.6, 1.2 Hz, 1H,), 6.86-6.82 (m, 2H), 0.98 (s, 9H), 0.19 (s, 6H).

^{13}C NMR ($CDCl_3$, 100 MHz, 298 K) δ 170.8, 155.4, 138.3, 129.4, 120.7, 119.0, 117.8, 43.1, 39.1, 25.4(3C), 17.9, 14.0, 12.7, -4.6(2C).

MS (ESI): calculated for $C_{17}H_{30}NO_2Si$ $[M+H]^+$ 308.20, Found: 308.31.

Compound 11a

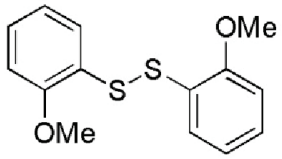

1-methoxy-2-[(2-methoxyphenyl) disulfanyl]benzene (11a): To a solution of compound **5** (3.59 g, 14.35 mmol), K_2CO_3 (5.94 g, 43.05 mmol) in acetone (40 mL) was added MeI (2.68 mL, 43.05 mmol) slowly. The mixture was stirred at room temperature overnight. The mixture was then filtrated and the fitration was collected. The solvent was removed in vacuum and the resulting residue was purified by flash column chromatography (silica gel, cyclohexane→cyclohexane-EtOAc=200:1) affording compound **11a** as a white solid (3.8 g, 95 % yield). R_f=0.4 (Et_2O:cyclohexane=1:6);

^{1}H NMR ($CDCl_3$, 400 MHz, 298 K) 7.53 (dd, *J*=7.6, 1.2 Hz, 2H), 7.19 (t, *J*=7.6 Hz, 2H), 6.93-6.89 (m, 2H), 6.85 (d, *J*=8.4 Hz, 2H), 3.90 (s, 6H).

^{13}C NMR ($CDCl_3$, 100 MHz, 298 K) δ 156.5, 127.7, 127.5, 124.5, 121.3, 110.4, 55.8.

MS (ESI): calculated for $C_{14}H_{15}O_2S_2$ $[M+H]^+$ 279.05, Found: 279.15

Compound 11b

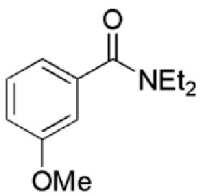

N,N-diethyl-3-methoxybenzamide (11b): To a solution of N,N-diethyl-3-hydroxybenzamide (1.2 g, 6.2 mmol) in acetone (10 mL) was added K_2CO_3 (1.7 g, 12.4 mmol) and MeI (0.78 mL, 12.4 mmol). The mixture was stirred at room temperature for 15 h. After the reaction, the solvent was evaporated and the residue was partitioned by water (10 mL) and EtOAc (20 mL×2). The organic phase was combined and dried over Na_2SO_4. After removal of the solvent in vacuum, the residue was purified by flash column chromatography (silica gel, EtOAc:cyclohexane=1:2) affording compound **11b** as a slight yellow oil (0.962 g, 75 % yield). R_f=0.3 (Et_2O:cyclohexane=1:2).

^{1}H NMR ($CDCl_3$, 400 MHz, 298 K) δ 7.29 (t, *J*=8.0 Hz, 1H), 6.94-6.90 (m, 3H), 3.82 (s, 3H), 3.54 (br.s, 2H), 3.26 (br.s, 2H), 1.24 (br.s, 3H), 1.12 (br.s, 3H).

^{13}C NMR ($CDCl_3$, 100 MHz, 298 K) δ 170.80, 159.39, 138.40, 129.35, 118.21, 114.80, 111.54, 55.12, 43.08, 39.03, 14.07, 12.72.

MS (ESI): calculated for $C_{12}H_{18}NO_2$ $[M+H]^+$ 208.13, Found: 208.19

Compound 11

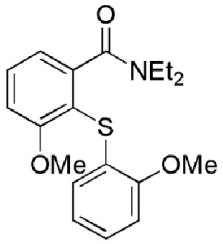

N,N-diethyl-3-methoxy-2-[(2-methoxyphenyl)sulfanyl]benzamide (11): To a solution of THF (50 mL) were added *s*-BuLi (2.75 mL, 3.3 mmol, 1.2 M in cyclohexane) and TMEDA (0.48 mL, 3.3 mmol) at -78 °C. After stirring for 30 min, a solution of **11b** (0.62 g, 3.0 mmol) dissolved in THF (10 mL) was added dropwise and the mixture continued being stirred for 1 h. Then the disulfide **11a** (1.52 g, 5.46 mmol) was added at -78 °C. The mixture was stirred at -78 °C while allowed to warm to room temperature. After 20 h, the mixture was diluted with Et_2O (100 mL) and wased with 1 M NaOH solution (2×100 mL). The organic layer was concentrated in vacuum and further purified by flash column chromatography (EtOAc:toluene=1:6) to give compound **11** as a white solid (0.768 g, 74 % yield). R_f=0.2 (toluene:EtOAc=2:1).

^{1}H NMR ($CDCl_3$, 400 MHz, 298 K) δ 7.43 (t, *J*=8.0 Hz, 1H), 7.06-7.02 (m, 1H), 6.95-6.93 (m, 2H), 6.78 (d, *J*=7.6 Hz, 1H), 6.75-6.67 (m, 2H), 3.87 (s, 3H), 3.74 (s, 3H), 3.73-3.64 (m, 1H), 3.39-3.30 (m, 1H), 3.15-3.06 (m, 1H), 3.04-2.95 (m, 1H), 1.18 (t, *J*=6.8 Hz, 3H), 0.98 (t, *J*=7.2 Hz, 3H).

^{13}C NMR ($CDCl_3$, 100 MHz, 298 K) δ 168.6, 160.5, 155.6, 145.2, 131.1, 127.0, 125.8, 125.4, 120.9, 118.7, 116.1, 111.2, 110.2, 56.1, 55.7, 42.6, 38.5, 13.8, 12.4.

HRMS (*m/z*): calculated for $C_{19}H_{23}LiNO_3S$ $[M+Li]^+$ 352.1554, Found 352.1553.

Compound 12

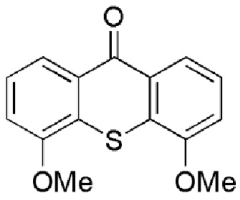

4,5-dimethoxy-9H-thioxanthen-9-one (12): To a solution of diisopropylamine (1.4 mL, 10 mmol) in THF (28 mL) was added *n*-BuLi (6.25 mL, 1.6 M solution in cyclohexane, 10 mmol) at -78 ˚C and after 30 min the dry ice bath was replaced by an ice water bath. Compound **11** (690 mg, 2 mmol) in THF (14 mL) was then added dropwise at 0 °C. The ice water bath was removed and the mixture was stirred at room temperature for 1 h. Then a saturated NH_4Cl solution (100 mL) was added and the mixture was extracted with Et_2O (100 mL×3). The combined organic phase was dried over Na_2SO_4, filtered and concentrated in vacuum. Further purification by flash column chromatography (silica gel, toluene) afforded compound **12** as a yellow solid (480 mg, 88 % yield). R_f=0.47 (toluene);

^{1}H NMR ($CDCl_3$, 400 MHz, 298 K) δ 8.25 (dd, *J*=8.0, 0.8 Hz, 2H), 7.45 (t, *J*=8.0 Hz, 2H), 7.13 (dd, *J*=8.0, 0.8 Hz, 2H), 4.06 (s, 6H).

^{13}C NMR ($CDCl_3$, 100 MHz, 298 K) δ 180.2, 154.9, 130.0, 127.7, 126.0, 121.5, 112.1, 56.4.

HRMS (*m/z*): calculated for $C_{15}H_{12}LiO_3S$ $[M+Li]^+$ 279.0662, Found 279.0664.

Compound 13a

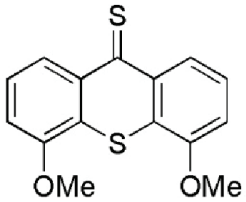

4,5-dimethoxy-9H-thioxanthene-9-thione (13a): To a solution of the ketone **12** (544 mg, 2 mmol) in toluene (25 mL) was added P_2S_5 (2.667 g, 12 mmol). The mixture was refluxed at 110 ˚C for 5 h. The mixture was then filtered by a short silica plug with toluene as eluent and washed with toluene until the

eluent was colorless. The crude product was used in the next step without further purification. R_f=0.45 (EtOAc:cyclohexane=1:4).

^{1}H NMR ($CDCl_3$, 400 MHz, 298 K) δ 8.66 (dd, *J*=8.4, 1.2 Hz, 2H), 7.39 (t, *J*=8.0 Hz, 2H), 7.12 (dd, *J*=8.0, 0.8 Hz, 2H), 4.06 (s, 6H).

^{13}C NMR ($CDCl_3$, 100 MHz, 298 K) δ 155.0, 138.4, 126.4, 126.0, 125.3, 111.2, 56.6.

Compound 13

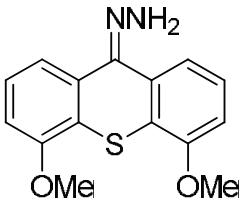

(4,5-dimethoxy-9H-thioxanthen-9-ylidene)hydrazone (13): To a hot solution of the above thioketone in EtOH (5 mL) was added hydrazine monohydrate dropwise (2 mL). The mixture was stirred at 80 °C for 4 h. The solvent was then evaporated and the residue was purified by flash column chromatography (silica gel, toluene→toluene:EtOAc=100:1) affording compound **13** as a orange solid (484 mg, 85 % yield over two steps). R_f=0.5 (EtOAc:toluene=1:6);

^{1}H NMR ($CDCl_3$, 400 MHz, 298 K) δ 7.65 (dd, *J*=8.4, 1.0 Hz, 1H), 7.45 (dd, *J*=8.0, 1.2 Hz, 1H), 7.32 (t, *J*=8.0 Hz, 1H), 7.27 (t, *J*=8.0 Hz, 1H), 6.90 (dd, *J*=8.0, 1.0 Hz, 1H), 6.84 (dd, *J*=8.0, 1.0 Hz, 1H).

^{13}C NMR ($CDCl_3$, 100 MHz, 298 K) δ 156.1, 154.6, 141.4, 135.3, 126.9, 126.7, 125.7, 124.3, 120.7, 120.0, 118.3, 109.9, 108.7, 56.1, 56.0.

MS (ESI): calculated for $C_{15}H_{15}N_2O_2S$ $[M+H]^+$ 287.09, Found 287.18.

Compound 14

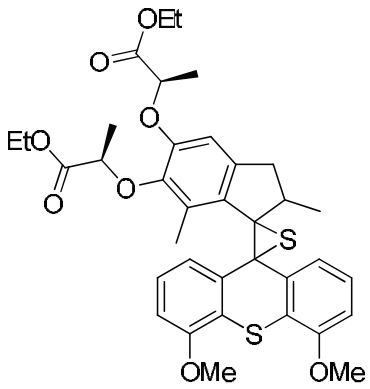

Episulfide (14): Typical procedure: to a solution of hydrazone **13** (345 mg, 1.2 mmol) in dry THF (5 mL) was added Na_2SO_4 (1.0 g, 7.0 mmol) and MnO_2 (522 mg, 6.0 mmol) at room temperature under argon. After 40 min the solution was filtered and washed with THF (5 mL) under argon to remove MnO_2. To the filtrate under argon was added a solution of thioketone **4** (334 mg, 0.82 mmol) dropwise in THF (5 mL) at room temperature. The evolution of nitrogen gas was observed. The mixture was stirred at room temperature for 19 h. The solvent was evaporated in vacuum and the residue was purified by flash column chromatography (silica gel, toluene→EtOAc:toluene=1:100→EtOAc:toluene=1:50) affording compound **14** as yellow solid (460 mg, 84 % yield totally based on thioketone **4**, 230 mg for each isomer).

For *R,R,S*-isomer: R_f=0.7 (toluene:EtOAc=6:1);

^{1}H NMR ($CDCl_3$, 400 MHz, 298 K) δ 7.40 (dd, *J*=7.6, 0.8 Hz, 1H), 7.25 (dd, *J*=7.6, 1.6 Hz, 1H), 7.21 (t, *J*=7.6 Hz, 1H), 7.11 (t, *J*=8.0 Hz, 1H), 6.78 (dd, *J*=8.0, 1.2 Hz, 1H), 6.63 (dd, *J*=8.0, 0.8 Hz, 1H), 6.30 (s, 1H), 4.68 (q, *J*=6.8 Hz, 1H), 4.62 (q, *J*=6.8 Hz, 1H), 4.21-4.11 (m, 4H), 3.91 (s, 3H), 3.78 (s, 3H), 3.19-3.14 (m, 1H), 2.09 (s, 3H), 2.05 (d, *J*=14.8 Hz, 1H), 1.52 (d, *J*=6.8 Hz, 3H), 1.34-1.30 (m, 1H), 1.24 (t, *J*=6.8 Hz, 3H), 1.20 (d, *J*=6.8 Hz, 3H), 1.17 (t, *J*=6.8 Hz, 3H), 0.93 (d, *J*=6.8 Hz, 3H).

^{13}C NMR ($CDCl_3$, 100 MHz, 298 K) δ 172.5, 172.0, 155.4, 155.3, 149.0, 143.7, 140.1, 136.3, 131.8, 128.6, 126.7, 126.0, 124.7, 124.3, 123.2, 121.1, 108.9, 108.7, 108.5, 76.1, 72.8, 71.4, 61.4, 61.1, 60.7, 56.1, 55.9, 41.2, 37.6, 21.2, 18.2, 17.9, 14.1, 14.0, 12.4.

MS (ESI): calculated for $[M+H]^+$ $C_{36}H_{41}O_8S_2$ 665.22, Found: 665.38.

For *R,R,R*-isomer: R_f=0.65 (toluene:EtOAc=6:1);

^{1}H NMR ($CDCl_3$, 400 MHz, 298 K) δ 7.39 (dd, *J*=8.0, 0.8 Hz, 1H), 7.25 (dd, *J*=7.6, 1.6 Hz, 1H), 7.21 (t, *J*=8.0 Hz, 1H), 7.11 (t, *J*=8.0 Hz, 1H), 6.78 (dd, *J*=8.0, 1.2 Hz, 1H), 6.65 (dd, *J*=8.0, 1.2 Hz, 1H), 6.33 (s, 1H), 4.64 (q, *J*=6.8 Hz, 1H), 4.24-4.19 (m, 2H), 4.14-4.10 (m, 1H), 3.91 (s, 3H), 3.77 (s, 3H), 3.20-3.14 (m, 1H), 2.11 (s, 3H), 2.07 (d, *J*=14.8 Hz, 1H), 1.52 (d, *J*=6.8 Hz, 3H), 1.36 (d, *J*=6.8 Hz, 3H), 1.31 (t, *J*=7.2 Hz, 3H), 1.18 (t, *J*=7.2 Hz, 3H), 0.95 (d, *J*=7.2 Hz, 3H).

^{13}C NMR ($CDCl_3$, 100 MHz, 298 K) δ 172.5, 172.2, 155.4, 155.2, 149.6, 144.3, 140.2, 139.9, 136.2, 131.3, 128.7, 126.6, 125.9, 124.6, 124.3, 123.0, 121.2, 108.8, 108.7, 108.5, 73.1, 71.2, 61.6, 61.1, 60.6, 56.0, 55.9, 41.0, 37.7, 21.2, 18.5, 18.3, 14.2, 14.1, 12.4.

HRMS (*m/z*): calculated for $C_{36}H_{40}LiO_8S_2$ $[M+Li]^+$ 671.2320, Found: 671.2324.

Compound 15

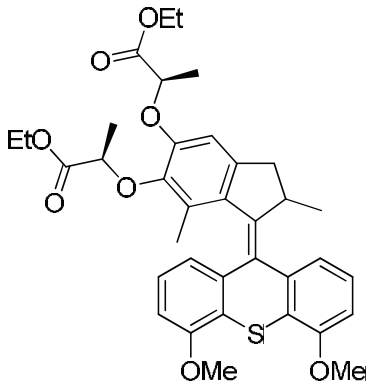

Methoxy-protected motor 15: Typical procedure: to a solution of the episulfide **14** (224 mg, 0.34 mmol) (from this stage, we start to work with single isomer) in toluene (10 mL) was added PPh_3 (900 mg, 3.4 mmol). The mixture was heated to 130 ˚C for 23 h until consumption of starting materials. After evaporation of solvent under vacuum, the residue was purified by flash column chromatography (silica gel, toluene→EtOAc:toluene=1:100→EtOAc:toluene=1:50) affording compound **15** as a yellow solid (202 mg, 95 % yield).

For *R,R,S*-isomer: R_f=0.65 (toluene:EtOAc=6:1);

^{1}H NMR ($CDCl_3$, 400 MHz, 298 K) δ 7.32 (d, *J*=7.2 Hz, 1H), 7.24 (t, *J*=8.0 Hz, 1H), 6.96 (t, *J*=8.0 Hz, 1H), 6.74 (dd, *J*=8.0, 0.8 Hz, 1H), 6.66 (dd, *J*=7.2, 0.8 Hz, 1H), 6.63 (dd, *J*=7.6, 1.2 Hz, 1H), 6.54 (s, 1H), 4.77 (q, *J*=6.8 Hz, 2H), 4.27-4.08 (m, 4H), 3.94 (s, 3H), 3.92 (s, 3H), 3.38-3.32 (m, 1H), 2.32 (d, *J*=14.8 Hz, 1H), 1.61 (d, *J*=6.8 Hz, 3H), 1.46 (d, *J*=6.8 Hz, 3H), 1.22 (t, *J*=6.8 Hz, 3H), 1.20 (s, 3H), 1.18 (t, *J*=6.8 Hz, 3H), 0.62 (d, *J*=6.8 Hz, 3H).

^{13}C NMR ($CDCl_3$, 100 MHz, 298 K) δ 172.53, 171.99, 156.56, 156.12, 149.62, 145.95, 144.45, 141.92, 141.78, 138.32, 133.38, 131.06, 127.65, 126.88, 126.53, 124.01, 123.81, 120.48, 119.96, 107.98, 107.60, 107.37, 76.69, 72.91, 61.21, 60.68, 55.93(2C), 39.48, 38.12, 18.96, 18.55, 18.41, 14.48, 14.07, 14.05.

MS (ESI): calculated for $[M+H]^+$ $C_{36}H_{41}O_8S$ 633.25, Found: 633.39.

For *R,R,R*-isomer: R_f=0.55 (toluene:EtOAc=6:1);

^{1}H NMR ($CDCl_3$, 400 MHz, 298 K) δ 7.31 (d, *J*=7.6 Hz, 1H), 7.24 (t, *J*=8.0 Hz, 1H), 6.99 (t, *J*=8.0 Hz, 1H), 6.74 (dd, *J*=8.0, 0.8 Hz, 1H), 6.68 (dd, *J*=6.4, 0.8 Hz, 1H), 6.66 (dd, *J*=6.4, 1.2 Hz, 1H), 6.57 (s, 1H), 4.77 (q, *J*=6.8 Hz, 1H), 4.50 (q, *J*=6.8 Hz, 1H), 4.28-4.16 (m, 4H), 4.13-4.10 (m, 1H), 3.94 (s, 3H),

3.91 (s, 3H), 3.38-3.32 (m, 1H), 2.34 (d, *J*=15.2 Hz, 1H), 1.61 (d, *J*=6.4 Hz, 3H), 1.51 (d, *J*=6.8 Hz, 3H), 1.29 (t, *J*=7.2 Hz, 3H), 1.27 (t, *J*=7.2 Hz, 3H), 1.19 (s, 3H), 0.62 (d, *J*=6.8 Hz, 3H).

^{13}C NMR ($CDCl_3$, 100 MHz, 298 K) δ 172.51, 172.11, 156.55, 156.12, 150.23, 145.88, 144.81, 142.29, 141.77, 138.32, 133.39, 131.08, 127.67, 126.98, 126.53, 123.90, 123.77, 120.52,120.01, 108.20, 107.52, 107.38, 77.31, 72.94, 61.17, 60.65, 55.92(2C), 39.56, 38.15, 18.97, 18.75, 18.48, 14.58, 14.21, 14.12.

HRMS (*m/z*): calculated for $C_{36}H_{40}LiO_8S$ $[M+Li]^+$ 639.2599, Found 639.2588.

Compound 16

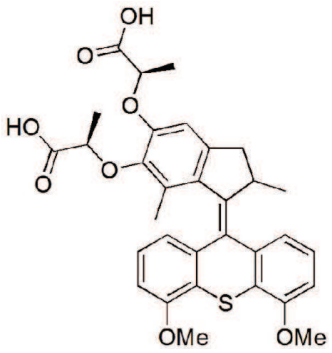

Acid 16: To a solution of the ester protected motor **15** (166 mg, 0.26 mmol) in THF/MeOH (0.72 mL/0.72 mL) was added 2M NaOH solution (0.72 mL) dropwise. The mixture was stirred at room temperature for 12 h. Then the mixture was cooled at 0 °C and 2 mL 1N HCl solution was added slowly. The mixture was extracted with EtOAc for several times. The combined organic layers were dried over Na_2SO_4 and evaporated in vacuum affording **16** as a brown solid (170 mg, >99 % yield).

For (*R,R,S*)-isomer:

^{1}H NMR ($CDCl_3$, 400 MHz, 298 K) δ 7.34 (d, *J*=7.6 Hz, 1H), 7.25 (t, *J*=7.8 Hz, 1H), 6.99 (t, *J*=7.8 Hz, 1H), 6.77 (d, *J*=8.0 Hz, 1H), 6.71 (d, *J*=8.0 Hz, 1H), 6.70 (s, 1H), 6.65 (dd, *J*=7.6, 0.8 Hz, 1H), 4.84 (q, *J*=6.8 Hz, 1H), 4.40 (q, *J*=6.4 Hz, 1H), 4.16-4.13 (m, 1H), 3.95 (s, 3H), 3.94 (s, 3H), 3.39-3.34 (m, 1H), 2.39 (d, *J*=15.2 Hz, 1H), 1.68 (d, *J*=6.8 Hz, 3H), 1.45 (d, *J*=6.8 Hz, 3H), 0.65 (d, *J*=6.4 Hz, 3H).

^{13}C NMR ($CDCl_3$, 100 MHz, 298 K) δ 176.49, 176.09, 156.71, 156.03, 148.94, 145.34, 145.16, 142.90, 141.34, 137.73, 135.20, 131.04, 128.43, 126.68, 126.58, 124.07, 123.43, 120.41, 119.74, 110.72, 107.59, 107.52, 77.89, 74.02, 55.96, 55.92, 39.46, 37.99, 18.82, 18.24, 17.99, 14.91.

MS (ESI): calculated for $[M+H]^+$ $C_{32}H_{33}O_8S$ 577.19, Found: 577.39.

For (*R,R,R*)-isomer:

^{1}H NMR ($CDCl_3$, 400 MHz, 298 K) δ 7.31 (d, *J*=7.2 Hz, 1H), 7.25 (t, *J*=7.6 Hz, 1H), 7.01 (t, *J*=8.0 Hz, 1H), 6.76 (dd, *J*=8.0, 0.8 Hz, 1H), 6.70 (m, 2H), 6.64 (dd, *J*=7.6, 1.2 Hz, 1H), 4.88 (q, *J*=6.8 Hz, 1H), 4.68 (q, *J*=6.8 Hz, 1H), 4.17-4.10 (m, 1H), 3.95 (s, 3H), 3.93 (s, 3H), 3.40-3.34 (m, 1H), 2.36 (d, *J*=14.8 Hz, 1H), 1.66 (d, *J*=6.8 Hz, 3H), 1.44 (d, *J*=6.8Hz, 3H), 1.19 (s, 3H), 0.65 (d, *J*=6.8 Hz, 3H).

^{13}C NMR ($CDCl_3$, 100 MHz, 298 K) δ 176.89, 176.24, 156.57, 156.13, 148.67, 145.36, 144.18, 142.75, 141.51, 138.11, 134.50, 130.90, 128.46, 127.24, 126.65, 123.88, 123.67, 120.35, 119.91, 109.93, 107.76, 107.48, 76.68, 73.19, 55.97 (2C), 39.45, 38.11, 18.95, 18.33, 17.88, 14.67.

MS (ESI): calculated for $[M+H]^+$ $C_{32}H_{33}O_8S$ 577.19, Found: 577.39.

Compound 17a

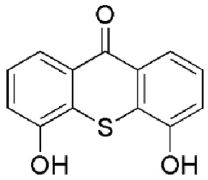

4,5-dihydroxy-9H-thioxanthen-9-one (17a): To a solution of compound **12** (909 mg, 3.34 mmol) in dry CH_2Cl_2 (20 mL) was added BBr_3 (13.4mL, 1M in CH_2Cl_2, 13.4 mmol) at 0 °C slowly. The mixture was stirred overnight while allowed to warm to room temperature. Cold water was then added slowly at 0 °C. The mixture was extracted extensively with EtOAc. The combined organic phase was dried over Na_2SO_4 and further evaporation of the solvent afforded crude compound **17a** (bis-phenol) as a brown powder (926 mg). This crude product was used in the next step without further purification. For analytical reasons, a small amount of crude product was purified by flash column chromatography (silica gel, EtOAc:cyclohexane=1:5) giving the compound **17a** as a green solid. R_f=0.25 (EtOAc:cyclohexane=1:5);

^{1}H NMR (d_6-DMSO, 400 MHz, 298 K) δ 10.97 (s, 2H), 7.95 (dd, *J*=8.0, 1.2 Hz, 2H), 7.39 (t, *J*=8.0 Hz, 2H), 7.21 (dd, *J*=8.0, 1.2 Hz, 2H).

^{13}C NMR (d_6-DMSO, 100 MHz, 298 K) δ 179.3, 153.0, 129.2, 126.3, 125.3, 119.2, 116.4.

MS (ESI): calculated for $C_{15}H_{13}O_3S$ $[M+H]^+$ 245.03, Found 245.14.

Compound 17

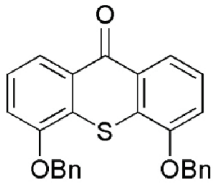

Keone 17: To a solution of **17a** (20 mg, 0.082 mmol) in acetone (5 mL) was added K_2CO_3 (34 mg, 0.25 mmol), benzyl bromide (0.03 mL, 0.25 mmol). The mixture was stirred at room temperature overnight. After the reaction, 15 mL water was added and the mixture was extracted with EtOAc (25 mL×2). The combined organic phase was purified by flash column chromatography (silica gel, cyclohexane:EtOAc=20:1) affording compound **17** as a slight yellow solid (33 mg, 95 % yield). R_f=0.2 (EtOAc:cyclohexane=1:20).

^{1}H NMR ($CDCl_3$, 400 MHz, 298 K) δ 8.27 (dd, *J*=8.4, 0.8 Hz, 2H), 7.55-7.53 (m, 2H), 7.43-7.40 (m, 6H), 7.38-7.36 (m, 2H,), 7.20 (dd, *J*=8.0, 1.2 Hz, 2H), 5.34 (s, 4H).

^{13}C NMR ($CDCl_3$, 100 MHz, 298 K) δ 180.2, 153.8, 136.2, 130.13, 128.6, 128.5, 128.1, 127.0, 125.9, 121.8, 113.9, 71.1.

Compound 18a

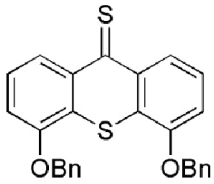

Thioketone 18a: To a solution of the ketone **17** (137 mg, 0.33 mmol) in toluene (10 mL) was added P_2S_5 (440 mg, 1.98 mmol). The mixture was heated to 110 ˚C for 1 h. The mixture was filtered through a short plug (packed with celite) and washed with $CHCl_3$ until the eluent is colorless. The filtration was evaporated and purified by flash column chromatography (silica gel, cyclohexane-toluene=1:20) affording the desired compound as a light green solid (80 mg, 56 % yield). ^{1}H NMR ($CDCl_3$, 400 MHz, 298 K) δ 8.68 (dd, *J*=8.4, 0.8 Hz, 2H), 7.54 (m, 4H), 7.34-7.43 (m, 8H), 7.18 (dd, *J*=7.6, 1.0 Hz, 2H), 5.34 (s, 4H). Comments: this product is quite smelly and active toward air. Usually we only check the ^{1}H NMR for this compound. In addition, try to avoid column purification because under the UV lamp, there is only a weak absorbance. In fact, the crude product can be used for the next step. Finally, for this type reaction, try to perform everything inside the fume hood, any stuffs touched with P_2S_5 strongly suggested being stand in the fume hood for at least one day.

Compound 18

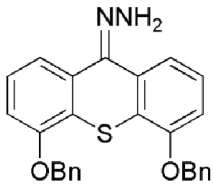

Hydrazone 18: The solution of the thioketone **18a** (80 mg, 0.18 mmol) in EtOH (5 mL) was heated up to 80 ˚C. Then to this hot solution was added $NH_2NH_2 \bullet H_2O$ (1 mL) dropwise. After stirring at 80 ˚C for 1 h, the solvent was removed in vacuum and purified by flash column chromatography (silica gel, EtOAc-cyclohexane=1:8) affording the compound **18** as a slight yellow solid (23 mg, 29 % yield).

^{1}H NMR ($CDCl_3$, 400 MHz, 298 K) δ 7.68 (dd, *J*=8.0, 0.8 Hz, 1H), 7.55-7.51 (m, 4H), 7.47 (dd, *J*=7.6, 1.0 Hz, 1H), 7.41-7.32 (m, 4H), 7.29 (m, 1H), 7.22 (m, 1H), 6.95 (dd, *J*=8.4, 1.2 Hz, 1H), 6.89 (dd, *J*=8.0, 1.2 Hz, 1H), 5.86 (br.s, 2H), 5.26 (s, 2H), 5.23 (s, 2H).

^{13}C NMR ($CDCl_3$, 100 MHz, 298 K) δ 155.16, 153.60, 141.39, 136.83, 136.58, 135.30, 128.58, 128.52, 127.89, 127.77, 126.95, 126.85, 126.71, 125.58, 125.43, 121.80, 120.44, 118.76, 111.87, 110.84, 70.83, 70.75.

MS (ESI): calculated for $[M+H]^+$ $C_{27}H_{23}N_2O_2S$ 439.15, Found: 439.39.

Compound 20

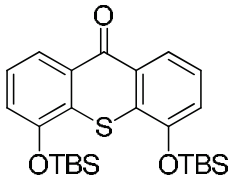

4,5-bis[(tert-butyldimethylsilyl)oxy]-9H-thioxanthen-9-one (20): To a solution of the crude bis-phenol **17a** (926 mg, 3.79 mmol) in dry THF (20 mL) was added imidazole (776 mg, 11.37 mmol), TBDMS-Cl (1.72 g, 11.37 mmol) at room temperature under argon. The mixture was stirred at room temperature for 3 h and then filtered, washed with tetrahydrofuran. After evaporation of the solvent, the resulting residue was purified by flash column chromatography (silica gel, toluene) affording compound **20** as a yellow solid (1.42 g, 90 % yield over two steps). R_f=0.7 (toluene:EtOAc=6:1);

^{1}H NMR ($CDCl_3$, 400 MHz, 298 K) δ 8.25 (dd, *J*=8.0, 1.2 Hz, 2H), 7.35 (t, *J*=8.0 Hz, 2H), 7.10 (dd, *J*=8.0, 1.4 Hz, 2H), 1.11 (s, 18H), 0.35 (s, 12H).

^{13}C NMR ($CDCl_3$, 100 MHz, 298 K) δ 180.6, 151.3, 130.60, 130.4, 125.7, 122.0, 119.7, 25.9, 18.5, -4.1.

HRMS (*m/z*): calculated for $C_{25}H_{36}LiO_3SSi_2$ $[M+Li]^+$ 479.2079, Found: 479.2071.

Compound 21a

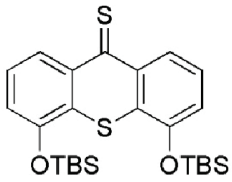

{4,5-bis[(tert-butyldimethylsilyl)oxy]-9H-thioxanthen-9-ylidene}hydrazone (21a): To a solution of ketone **20** (1.41 g, 2.98 mmol) in THF (20 mL) was added P_2S_5 (1.99 g, 8.94 mmol). The mixture was stirred at 60-65 ˚C for 1 h and then filtered through a short silica plug and the residue was washed with CH_2Cl_2 until the eluent became colorless. The solvent was evaporated and a light red solid was obtained. This crude product **21a** (thioketone) was used directly in the next step without any further purification. R_f=0.3 (*n*-pentane);

^{1}H NMR ($CDCl_3$, 400 MHz, 298 K) δ 8.68 (d, *J*=8.0 Hz, 2H), 7.30 (t, *J*=8.0 Hz, 2H), 7.09 (d, *J*=8.0 Hz, 2H), 1.09 (s, 18H), 0.28 (s, 12H).

^{13}C NMR (100 MHz, $CDCl_3$, 298 K) δ 211.3, 151.3, 138.7, 126.2, 126.1, 125.8, 118.6, 25.4, 18.4, -4.1.

MS (ESI): calculated for $C_{25}H_{37}O_2S_2Si_2$ $[M+H]^+$ 489.18, Found 489.27.

Compound 21

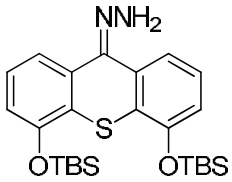

{4,5-bis[(tert-butyldimethylsilyl)oxy]-9H-thioxanthen-9-ylidene}hydrazine (21): To a crude thioketone **21a** solution in EtOH (30 mL) was added hydrazine monohydrate (2.5 mL) dropwise. The mixture was stirred at 80 ˚C for 1 h. After evaporation of the solvent, the crude residue was purified by flash column chromatography (silica gel, toluene→toluene:EtOAc=100:1) affording compound **21** as a orange solid (1.17 g, 81 % yield over two steps).

^{1}H NMR ($CDCl_3$, 400 MHz, 298 K) δ 7.65 (dd, *J*=8.0, 1.2 Hz, 1H), 7.44 (dd, *J*=8.0, 1.0 Hz, 1H), 7.21 (t, *J*=8.0 Hz, 1H), 7.17 (t, *J*=8.0 Hz, 1H), 6.84 (dd, *J*=8.0, 1.0 Hz, 1H), 6.79 (dd, *J*=8.0, 1.2 Hz, 1H), 1.09 (s, 9H), 1.07 (s, 9H), 0.32 (s, 6H), 0.28 (s, 6H).

^{13}C NMR ($CDCl_3$, 100 MHz, 298 K) δ 152.5, 150.7, 142.0, 135.2, 127.6, 126.6, 126.6, 125.2, 124.1, 120.5, 118.7, 117.7, 116.7, 25.9, 25.8, 18.4, -4.1.

MS (ESI): calculated for $C_{25}H_{39}N_2O_2SSi_2$ $[M+H]^+$ 487.23, Found 487.31.

Compound 22

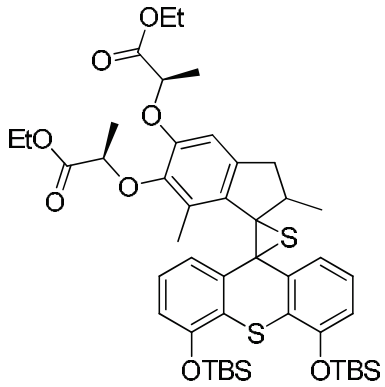

Episulfide **22**: To a solution of the freshly prepared hydrazone **21** (1.13 g, 2.32 mmol) in THF (5 mL) was added Na_2SO_4 (1.5 g, 10.6 mmol) and MnO_2 (1.0 g, 11.6 mmol) at 0 ˚C. The mixture was stirred at 0 ˚C for 40 min. Then the mixture was filtered under argon and the residue was washed with THF (5 mL). To the filtration was added a solution of the thioketone **4** (805 mg, 1.97 mmol) in THF (9 mL) at 0 ˚C dropwise. The mixture was then stirred at room temperature for 19 h. The solvent was evaporated under reduced pressure and the mixture was then purified by flash column chromatography (silica gel, toluene→toluene:EtOAc=1000:1→200:1) affording compound **22** as a yellow solid (1.262 g, 74 % yield based on thioketone **4**; 540 mg of each isomer, 180 mg of mixture of both isomers).

For *R,R,R*-isomer: R_f=0.7 (toluene:EtOAc=6:1);

^{1}H NMR ($CDCl_3$, 400 MHz, 298 K) δ 7.39 (dd, *J*=8.0, 0.8 Hz, 1H), 7.24 (dd, *J*=7.6, 1.2 Hz, 1H), 7.10 (t, *J*=8.0 Hz, 1H), 7.01 (t, *J*=8.0 Hz, 1H), 6.73 (dd, *J*=8.0, 1.2 Hz, 1H), 6.60 (dd, *J*=8.0, 1.2 Hz, 1H), 6.35 (s, 1H), 4.61 (q, *J*=6.8 Hz, 1H), 4.22-4.15 (m, 5H), 3.22-3.17 (m, 1H), 2.16 (s, 3H), 2.07 (d, *J*=14.8 Hz, 1H), 1.52 (d, *J*=6.8 Hz, 3H), 1.42 (d, *J*=6.8 Hz, 3H), 1.35-1.32 (m, 1H), 1.31 (t, *J*=6.8 Hz, 3H), 1.23 (t, *J*=7.2 Hz, 3H), 1.05 (s, 9H), 0.98 (s, 9H), 0.92 (d, *J*=6.8 Hz, 3H), 0.26 (s, 3H), 0.24 (s, 3H), 0.09 (s, 3H), -0.07 (s, 3H).

^{13}C NMR ($CDCl_3$, 100 MHz, 298 K) δ 172.5, 171.9, 151.6, 151.5, 149.7, 144.7, 140.3, 139.9, 136.1, 131.6, 128.9, 127.9, 127.8, 126.2, 125.5, 123.5, 121.7, 117.5, 116.9, 108.9, 77.5, 77.2, 73.2, 71.6, 61.9, 60.9, 60.6, 41.1, 37.7, 25.9, 25.8, 21.1, 18.9, 18.4, 18.3, 18.2, 14.2, 14.1, 12.4, -3.9, -4.2, -4.3, -4.7.

MS (ESI): calculated for $C_{46}H_{65}O_8S_2Si_2$ $[M+H]^+$ 865.37, Found 865.46.

For *R,R,S*-isomer: R_f=0.65 (toluene:EtOAc=6:1);

^{1}H NMR ($CDCl_3$, 400 MHz, 298 K) δ 7.38 (dd, *J*=8.0, 1.2 Hz, 1H), 7.24 (dd, *J*=8.0, 1.2 Hz, 1H), 7.09 (t, *J*=8.0 Hz, 1H), 7.00 (t, *J*=8.0 Hz, 1H), 6.73 (dd, *J*=8.0, 1.2 Hz, 1H), 6.59 (dd, *J*=8.0, 1.2 Hz, 1H), 6.26 (s, 1H), 4.59 (q, *J*= 6.8 Hz, 2H), 4.22-4.12 (m, 4H), 3.23-3.18 (m, 1H), 2.13 (s, 3H), 2.04 (d, *J*=14.8 Hz, 1H), 1.52 (d, *J*=6.8 Hz, 3H), 1.35-1.32 (m, 1H), 1.28 (d, *J*=6.8 Hz, 3H), 1.24 (t, *J*=6.8 Hz, 3H), 1.18 (t,

J=7.2 Hz, 3H), 1.06 (s, 9H), 0.95 (s, 9H), 0.92 (d, *J*=7.2 Hz, 3H), 0.26 (s, 3H), 0.24 (s, 3H), 0.07 (s, 3H), -0.09 (s, 3H).

^{13}C NMR ($CDCl_3$, 100 MHz, 298 K) δ 172.7, 171.9, 151.5, 151.4, 149.1, 143.8, 140.0, 139.7, 136.1, 131.5, 128.8, 127.9 (2C), 126.2, 125.5, 123.6, 121.7, 117.5, 116.9, 107.8, 77.2, 76.5, 72.5, 71.4, 61.7, 61.1, 60.6, 40.9, 37.6, 25.9, 25.8, 21.1, 18.6, 18.4, 18.3, 18.2, 14.1, 14.0, 12.4, -4.0, -4.2, -4.3, -4.8.

HRMS (*m/z*): calculated for $C_{46}H_{64}O_8LiS_2Si_2$ $[M+Li]^+$ 871.3739, Found 871.3738.

Compound 23

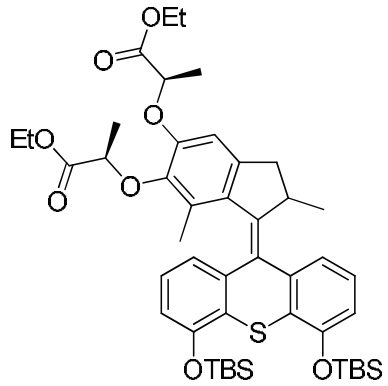

Motor **23**: To a solution of episulfide **22** (51 mg, 0.058 mmol) in toluene (2 mL) was added PPh_3 (75 mg, 0.29 mmol). The mixture was stirred at 120 ˚C for 20 h and then another batch of PPh_3 (75 mg, 0.29 mmol) was added. After 27 h, the mixture was concentrated in vacuum and further purified by flash column chromatography (silica gel, toluene→toluene:EtOAc=50:1) affording compound **23** as a yellow solid (48 mg, 98 % yield).

For *R,R,R*-isomer: R_f=0.68 (toluene:EtOAc=6:1);

^{1}H NMR ($CDCl_3$, 400 MHz, 298 K) δ 7.28 (d, *J*=7.2 Hz, 1H), 7.12 (t, *J*=8.0 Hz, 1H), 6.88 (t, *J*=8.0 Hz, 1H), 6.68 (dd, *J*=8.0, 0.8 Hz, 1H), 6.65 (t, *J*=7.6 Hz, 2H), 6.56 (s, 1H), 4.77 (q, *J*=6.8 Hz, 1H), 4.44 (q, *J*=6.8 Hz, 1H), 4.28-4.16 (m, 4H), 4.11-4.08 (m, 1H), 3.35-3.29 (m, 1H), 2.32 (d, *J*=14.8 Hz, 1H), 1.62 (d, *J*=6.4 Hz, 3H), 1.51 (d, *J*=6.8 Hz, 3H), 1.28 (t, *J*=7.2 Hz, 3H), 1.27 (t, *J*=7.2 Hz, 3H), 1.19 (s, 3H), 1.09 (s, 9H), 1.08 (s, 9H), 0.61 (d, *J*=6.8 Hz, 3H), 0.29 (s, 3H), 0.28 (s, 3H), 0.27 (s, 3H), 0.25 (s, 3H).

^{13}C NMR ($CDCl_3$, 100 MHz, 298 K) δ 172.4, 172.2, 152.7, 152.2, 150.2, 145.4, 144.9, 142.3, 141.8, 138.4, 133.5, 130.9, 128.2, 127.6, 127.2, 126.5, 126.1, 121.0, 120.3, 116.3, 115.5, 108.2, 77.4, 73.0, 61.2, 60.7, 39.5, 38.0, 25.9 (6C), 18.9, 18.7, 18.5, 18.4 (2C), 14.4, 14.2, 14.1, -3.9, -4.0, -4.3, -4.4.

MS (ESI): calculated for $C_{46}H_{65}O_8SSi_2$ $[M+H]^+$ 833.39, Found 833.41.

For *R,R,S*-isomer: R_f=0.63 (toluene:EtOAc=6:1);

^{1}H NMR ($CDCl_3$, 400 MHz, 298 K) δ 7.29 (d, *J*=7.2 Hz, 1H), 7.13 (t, *J*=8.0 Hz, 1H), 6.86 (t, *J*=8.0 Hz, 1H), 6.69 (dd, *J*=8.0, 1.2 Hz, 1H), 6.64 (dd, *J*=7.6, 1.2 Hz, 1H), 6.63 (dd, *J*=7.6, 1.2 Hz, 1H), 6.54 (s, 1H), 4.78-4.72 (m, 2H), 4.27-4.09 (m, 5H), 3.38-3.31 (m, 1H), 2.32 (d, *J*=15.2 Hz, 1H), 1.61 (d, *J*=6.8 Hz, 3H), 1.44 (d, *J*=6.8 Hz, 3H), 1.22 (t, *J*=7.2 Hz, 3H), 1.21 (t, *J*=7.2 Hz, 3H), 1.21 (s, 3H), 1.09 (s, 9H), 1.08 (s, 9H), 0.62 (d, *J*=6.8 Hz, 3H), 0.29 (s, 3H), 0.27 (s, 6H), 0.25 (s, 3H).

^{13}C NMR ($CDCl_3$, 100 MHz, 298 K) δ 172.4, 172.0, 152.7, 152.2, 149.6, 145.5, 144.4, 142.0, 141.8, 138.3, 133.4, 130.9, 128.1, 127.7, 127.1, 126.4, 126.1, 121.0, 120.2, 116.3, 115.5, 108.1, 76.9, 73.0, 61.2, 60.6, 39.4, 38.0, 25.9 (6C), 18.9, 18.5, 18.4 (3C), 14.4, 14.1, 14.0, -3.9, -4.0, -4.3, -4.4.

HRMS (*m/z*): calculated for $C_{46}H_{64}LiO_8SSi_2$ $[M+Li]^+$ 839.4016, Found 839.4006.

Compound 24

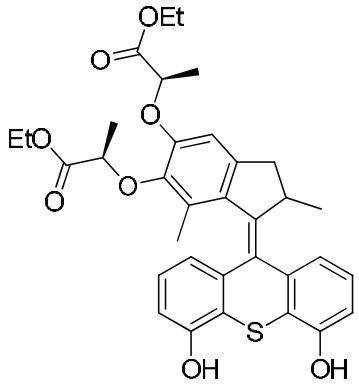

Bis-phenol 24: To a solution of motor **23** (164 mg, 0.19 mmol) in THF (5 mL) was added TBAF (0.44 mL, 1M in THF) at 0 ˚C and the mixture was stirred at 0 ˚C for 5 min. Then a saturated solution of NH_4Cl (10 mL) was added and the mixture was extracted with CH_2Cl_2 (3×20 mL). The combined organic layer was dried over Na_2SO_4 and concentrated in vacuum. Further purification by flash column chromatography (silica gel, CH_2Cl_2→CH_2Cl_2:MeOH=100:1→10:1) afforded compound **24** as a yellow solid (128 mg, 99 % yield).

For *R,R,R*-isomer: R_f=0.2 (CH_2Cl_2:MeOH=20:1);

^{1}H NMR ($CDCl_3$, 400 MHz, 298 K) δ 7.30 (dd, *J*=7.6, 0.8 Hz, 1H), 7.22 (t, *J*=8.0 Hz, 1H), 6.98 (t, *J*=8.0 Hz, 1H), 6.82 (dd, *J*=8.0, 1.2 Hz, 1H), 6.75 (dd, *J*=8.0, 1.2 Hz, 1H), 6.67 (dd, *J*=8.0, 1.0 Hz, 1H), 6.59 (s, 1H), 5.57-5.45 (br.m, 2H), 4.79 (q, *J*=6.8 Hz, 1H), 4.53 (q, *J*=6.8 Hz, 1H), 4.27-4.15 (m, 4H), 4.14-4.10 (m, 1H), 3.38-3.32 (m, 1H), 2.37 (d, *J*=15.2 Hz, 1H), 1.63 (d, *J*=6.8 Hz, 3H), 1.52 (d, *J*=6.8 Hz, 3H), 1.29 (t, *J*=6.8 Hz, 6H), 1.26 (s, 3H), 0.70 (d, *J*=6.8 Hz, 3H).

^{13}C NMR ($CDCl_3$, 100 MHz, 298 K) δ 172.5, 172.0, 153.0, 152.8, 150.5, 146.7, 145.0, 144.1, 142.5, 141.0, 132.8, 131.0, 128.3, 128.0, 120.5 (2C), 120.4, 120.3, 112.8, 112.7, 108.1, 77.2, 72.9, 61.2, 60.8, 39.5, 38.2, 19.2, 18.8, 18.5, 15.0, 14.2, 14.1.

MS (ESI): calculated for $C_{34}H_{37}O_8S$ $[M+H]^+$ 605.22, Found 605.41.

For *R,R,S*-isomer: R_f=0.2 (CH_2Cl_2:MeOH=20:1);

^{1}H NMR (CD_3OD, 400 MHz, 298 K) δ 7.24 (d, *J*=7.2 Hz, 1H), 7.15 (t, *J*=8.0 Hz, 1H), 6.86 (t, *J*=8.0 Hz, 1H), 6.72 (dd, *J*=8.0, 1.2 Hz, 1H), 6.66 (dd, *J*=8.0, 1.0 Hz, 1H), 6.64 (s, 1H), 6.64 (dd, *J*=7.6, 0.8 Hz, 1H), 4.86 (q, *J*=6.8 Hz, 1H), 4.78 (q, *J*=6.8 Hz, 1H), 4.22-4.09 (m, 5H), 3.40-3.35 (m, 1H), 2.35 (d, *J*=14.8 Hz, 1H), 1.57 (d, *J*=6.8 Hz, 3H), 1.38 (d, *J*=6.8 Hz, 3H), 1.23 (t, *J*=6.8 Hz, 3H), 1.20 (t, *J*=6.8 Hz, 3H), 1.20 (s, 3H), 0.62 (d, *J*=6.4 Hz, 3H).

^{13}C NMR (CD_3OD, 100 MHz, 298 K) δ 174.2, 173.5, 155.7, 155.2, 151.1, 146.5, 145.5, 143.8, 143.5, 140.2, 134.7, 131.9, 130.2, 127.9, 127.8, 124.0, 123.3, 120.5, 120.0, 113.2, 113.1, 109.4, 77.9, 74.1, 62.4, 62.0, 40.4, 39.3, 19.3, 18.9, 18.7, 15.0, 14.5, 14.4.

HRMS (*m/z*): calculated for $C_{34}H_{36}LiO_8S$ $[M+Li]^+$ 611.2286, Found 611.2284.

Compound 25

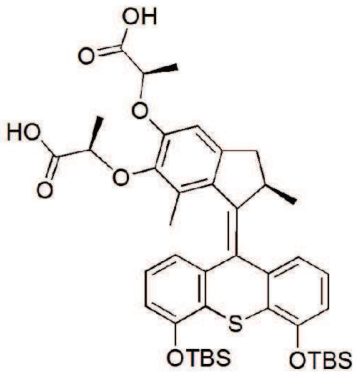

Acid 25: Typical procedure for the saponification of the motor: A mixture of bis-ester **23** (*R,R,R*-isomer) (70 mg, 0.084 mmol), $(CH_3)_3SnOH$ (76 mg, 0.42) in DCE (2 mL) was reacted under microwave conditions (100 ˚C, 300 w, fixed power) for 5 h. Then DCE was removed and the mixture was diluted with EtOAc (20 mL), washed with H_2O (20 mL×5) (to remove Sn species). The organic layer was dried over Na_2SO_4 and evaporated in vacuum affording the crude product as a slight gray solid in quantitative yield.

^{1}H NMR (CD_3OD, 400 MHz, 298 K) δ 7.36 (d, *J*=7.6 Hz, 1H), 7.20 (t, *J*=8.0 Hz, 1H), 6.93 (t, *J*=8.0 Hz, 1H), 6.77 (dd, *J*=8.0, 0.8 Hz, 1H), 6.71 (dd, *J*=8.0, 0.8 Hz, 1H), 6.63 (s, 1H), 6.61 (dd, *J*=7.6, 1.2 Hz,

1H), 4.80 (q, *J*=6.8 Hz, 1H,), 4.66 (q, *J*=6.8 Hz, 1H), 4.15-4.09 (m, 1H), 3.36-3.33 (m, 1H), 2.37 (d, *J*=14.8 Hz, 1H), 1.55 (d, *J*=6.8 Hz, 3H), 1.47 (d, *J*=6.8 Hz, 3H), 1.17 (s, 3H), 1.10 (s, 18H), 0.61 (d, *J*=6.4 Hz, 3H), 0.31 (s, 3H), 0.30 (s, 3H), 0.28 (s, 3H), 0.27 (s, 3H).

^{13}C NMR (CD_3OD, 100 MHz, 298 K) δ 178.5 (2C), 154.1, 153.5, 152.5, 147.1, 146.1, 143.5, 143.4, 139.9, 133.7, 131.5, 129.3, 129.0, 128.2, 127.8, 127.6, 122.3, 121.7, 117.8, 117.1, 109.4, 79.4, 75.4, 40.4, 39.2, 26.6 (6C), 19.7, 19.4 (2C), 19.3, 19.2, 15.2, -3.5, -3.7, -3.8, -4.0.

MS (ESI): calculated for $C_{42}H_{57}O_8SSi_2$ $[M+H]^+$ 777.33, Found: 776.32.

Compound 26

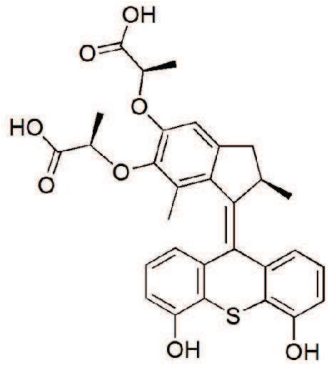

Fully deprotected motor 26: To a solution of the bis-ester phenol **24** (*R,R,R*-isomer) 7.7 mg (0.013 mmol) in MeOH/THF (0.1 mL/0.1 mL) was added a NaOH solution (5 mg in 0.1 mL H_2O). The mixture was stirred at room temperature for 16 h. Then 2N HCl solution was added at 0 ˚C. The mixture was extracted with EtOAc until the water layer becomes colorless. The combined organic phase was dried over Na_2SO_4 and evaporated in vacuum affording a green solid 3.2 mg (45 % yield).

^{1}H NMR (CD_3OD, 400 MHz, 298 K) δ 7.24 (d, *J*=8.0 Hz, 1H), 7.15 (t, *J*=8.0 Hz, 1H), 6.88 (t, *J*=8.0 Hz, 1H), 6.72 (dd, *J*=8.0, 1.2 Hz, 1H), 6.71 (s, 1H), 6.67 (dd, *J*=8.0, 1.2 Hz, 1H), 6.51 (dd, *J*=7.6, 1.2 Hz, 1H), 4.84 (q, *J*=6.8 Hz, 1H), 4.46 (q, *J*=6.8 Hz, 1H), 4.18-4.14 (m, 1H), 3.39-3.35 (m, 1H), 2.38 (d, *J*=15.2 Hz, 1H), 1.61 (d, *J*=6.8 Hz, 3H), 1.48 (d, *J*=6.8 Hz, 3H), 1.22 (s, 3H), 0.63 (d, *J*=6.8 Hz, 3H).

^{13}C NMR (CD_3OD, 100 MHz, 298 K) δ 176.62, 175.79, 155.63, 155.17, 151.63, 146.48, 145.87, 143.81, 143.71, 140.33, 134.46, 131.82, 130.14, 128.08, 127.78, 23.85, 123.36, 120.47, 120.07, 113.41, 113.07, 109.23, 78.57, 74.04, 40.38, 39.28, 19.31(2C), 18.90, 15.09.

MS (ESI): calculated for $C_{30}H_{29}O_8S$ $[M+H]^+$ 549.16, Found: 549.31.

Compound 27

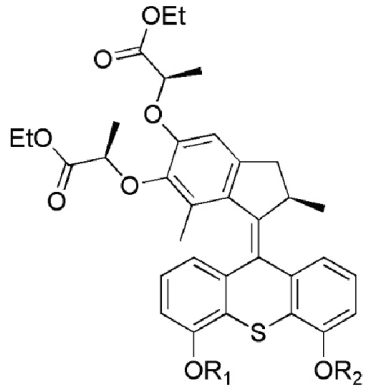

trans: R_1=H, R_2=TBS
cis: R_1=TBS, R_2=H

To a solution of bis-phenol **24** (20 mg, 0.033 mmol) in CH_2Cl_2 (1 mL) was added imidazole (3.35 mg, 0.049 mmol) and TBSCl (7.5 mg, 0.049 mmol) at room temperature. The mixture was stirred at room temperature for 2 h. The mixture was filtered and washed with CH_2Cl_2. The filtration was collected. After removal of the solvent in vacuum, the resulting residue was purified either by preparative TLC (toluene:EtOAc=6:1) or by preparative HPLC affording two isomers as slightly yellow solid. (Column conditions: C18, 5 μm, 19×150 mm; eluant 5:95 MeOH/H_2O; flow rate 2 mL/min; λ= 300 nm; t_{R1}= 30.17 min, t_{R2}=30.87 min.)

First fraction from the HPLC (t_{R1}= 30.17 min): ^{1}H NMR (CD_3OD, 400 MHz, 298 K) δ 7.24 (dd, *J*=8.0, 0.8 Hz, 1H), 7.14 (t, *J*=8.0 Hz, 1H), 6.93 (t, *J*=8.0 Hz, 1H), 6.72 (dd, *J*=8.0, 1.2 Hz, 1H), 6.71 (dd, *J*=8.0, 1.6 Hz, 1H), 6.69 (s, 1H), 6.61 (dd, *J*=7.6, 1.2 Hz, 1H), 4.94 (q, *J*=6.8 Hz, 1H), 4.52 (q, *J*=6.8 Hz, 1H), 4.25-4.16 (m, 5H), 3.38-3.35 (m, 1H), 2.38 (d, *J*=15.2 Hz, 1H), 1.60 (d, *J*=6.8 Hz, 3H), 1.50 (d, *J*=6.8 Hz, 3H), 1.29 (t, *J*=7.2 Hz, 3H), 1.26 (t, *J*=7.2 Hz, 3H), 1.17 (s, 3H), 1.12 (s, 9H), 0.62 (d, *J*=6.8 Hz, 3H), 0.29 (s, 3H), 0.26 (s, 3H).

HRMS (*m/z*): calculated for $C_{40}H_{50}LiO_8SSi$ $[M+Li]^+$ 725.3151, Found 725.3141.

Second fraction from the HPLC (t_{R2}=30.87 min): ^{1}H NMR (CD_3OD, 400 MHz, 298 K) δ 7.35 (d, *J*=7.2 Hz, 1H), 7.19 (t, *J*=8.0 Hz, 1H), 6.87 (t, *J*=8.0 Hz, 1H,), 6.76 (dd, *J*=8.0, 0.8 Hz, 1H), 6.68 (s, 1H), 6.66 (dd, J=8.0, 1.2 Hz, 1H), 6.48 (dd, J=7.6, 1.2 Hz, 1H), 4.92 (q, J=6.8 Hz, 1H), 4.52 (q, J=6.8 Hz, 1H), 4.24-4.14 (m, 5H), 3.38-3.33 (m, 1H), 2.37 (d, J=15.2 Hz, 1H), 1.59 (d, J=6.8 Hz, 3H), 1.49 (d, J=6.8 Hz, 3H), 1.28 (t, J=7.2 Hz, 3H), 1.26 (t, J=6.8 Hz, 3H), 1.18 (s, 3H), 1.11 (s, 9H), 0.60 (d, J=6.8 Hz, 3H), 0.29 (s, 3H), 0.26 (s, 3H).

^{13}C NMR (CD_3OD, 100 MHz, 298 K) δ 174.4, 173.6, 155.9, 153.7, 151.6, 146.5, 146.1, 143.9, 143.6, 140.3, 134.5, 131.9, 130.1, 128.8, 128.0, 127.5, 124.0, 121.8, 120.3, 117.4, 113.2, 109.3, 78.8, 74.0, 62.4, 62.1, 40.4, 39.3, 26.5, 19.5, 19.3, 19.2, 18.8, 15.1, 14.5 (2C), -4.00 (2C).

MS (ESI): calculated for $C_{40}H_{51}O_8SSi$ $[M+H]^+$ 719.31, Found 719.32.

Compound 28

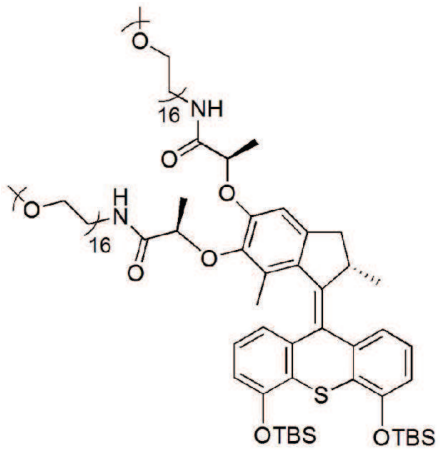

To a solution of acid **25** (10 mg, 0.0128 mmol), HOBt (2 mg, 0.013 mmol), EDC (5 mg, 0.025 mmol) in CH_2Cl_2 (1 mL) was added PEG_{750}-NH_2 (10 mg, 0.025 mmol) and the mixture was stirred at room temperature. After 1 h, HOBt (2 mg, 0.013 mmol), EDC (5 mg, 0.025 mmol), PEG_{750}-NH_2 (3.6 mg, 0.005 mmol) was added. After 2 h, HOBt (2 mg, 0.013 mmol), EDC (5 mg, 0.025 mmol), PEG_{750}-NH_2 (5 mg, 0.013 mmol) was added. After 12 h, 10 mL CH_2Cl_2 was added, this mixture was washed with 1N HCl solution (10 mL), sat.K_2CO_3 solution (10 mL) and brine (10 mL). The organic layer was evaporated in vacuum and the residue was purified by flash column chromatography (silica gel, CH_2Cl_2→CH_2Cl_2:MeOH=20:1→10:1) affording compound **28** as a slight yellow solid (22.4 mg, 76 % yield). R_f=0.4 (CH_2Cl_2:MeOH=10:1);

^{1}H NMR ($CDCl_3$, 400 MHz, 298 K) δ 7.30 (d, *J*=8.4 Hz, 1H), 7.14 (t, *J*=8.0 Hz, 1H), 6.88 (t, *J*=8.0 Hz, 1H), 6.70 (dd, *J*=8.0, 0.8 Hz, 1H), 6.65 (dd, *J*=8.0, 1.2 Hz, 1H), 6.65 (s, 1H), 6.64 (dd, *J*=7.6, 1.2 Hz), 4.62 (q, *J*=6.8 Hz, 1H), 4.35 (q, *J*=6.8 Hz, 1H), 4.14-4.0 (m, 1H), 3.68-3.53 (m, 168 H), 3.37 (s, 6H), 3.34-3.30 (m, 1H), 2.36 (d, *J*=15.2 Hz, 1H), 1.57 (d, *J*=6.8 Hz, 3H), 1.34 (d, *J*=7.2 Hz, 3H), 1.14 (s, 3H), 1.08 (s, 9H), 1.07 (s, 9H), 0.62 (d, *J*=6.8 Hz, 3H), 0.29 (s, 3H), 0.27 (s, 3H), 0.26 (s, 3H), 0.24 (s, 3H).

Compound 29

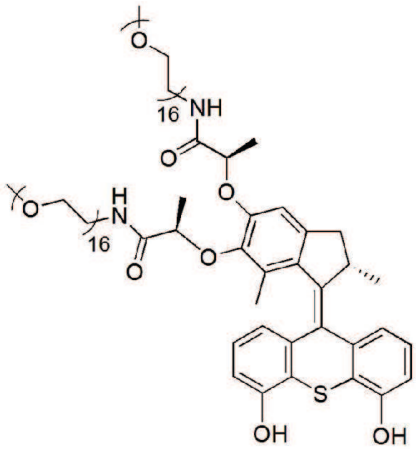

To a solution of compound **28** (5 mg, 0.0022 mmol) in THF (1 mL) was added TBAF (0.005 mL, 0.005 mmol, 1M in THF) at 0 ˚C. The mixture was stirred at 0 ˚C for 10 min. Then THF was evaporated and the mixture was redissolved in CH_2Cl_2 (10 mL), washed with water (10 mL) and brine (10 mL). The organic layer was evaporated in vacuum and the residue was purified by flash column chromatography (silica gel, $CH_2Cl_2 \rightarrow CH_2Cl_2$:MeOH=20:1→6:1) affording a slight yellow solid (9 mg, >99 % yield).
^{1}H NMR ($CDCl_3$, 400 MHz, 298 K) δ 7.27 (dd, *J*=7.2, 1.2 Hz, 1H), 7.17 (t, *J*=8.0 Hz, 1H), 6.91 (t, *J*=8.0 Hz, 1H), 6.82 (t, *J*=8.0 Hz, 2H), 6.69 (s, 1H), 6.57 (dd, *J*=7.6, 0.8 Hz, 1H), 4.70-4.63 (m, 2H), 4.19-4.15 (m, 1H), 3.67-3.53 (m, 195H), 3.38 (s, 6H), 3.34-3.30 (m, 1H), 2.38 (d, *J*=15.2 Hz, 1H), 1.59 (d, *J*=6.8 Hz, 3H), 1.29 (d, *J*=6.8 Hz, 3H), 1.28 (s, 3H), 0.68 (d, *J*=6.8 Hz, 3H).

Compound 30

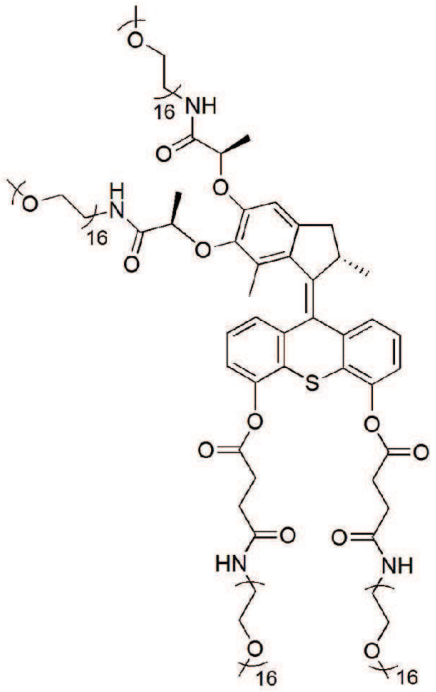

To a solution of compound **29** (8 mg, 0.004 mmol) in CH_2Cl_2 (1 mL) was added *O*-[(*N*-Succinimidyl) succinyl-aminoethyl]-*O'*-methylpolyethylene glycol (Mw=750 g·mol^{-1}) (13.2 mg, 0.018 mmol), DMAP (3.6 mg, 0.03 mmol). The mixture was stirred at room temperature for 7 days and then the solvent was evaporated in vacuum. The residue was purified by flash column chromatography (silica gel, CH_2Cl_2→CH_2Cl_2:MeOH=20:1→6:1) affording a slight yellow solid (14 mg, 99 % yield).

^{1}H NMR ($CDCl_3$, 400 MHz, 298 K) δ 7.26 (1H, overlap with solvent signal), 7.18 (t, *J*=8.0 Hz, 1H), 6.92 (t, *J*=8.0 Hz, 1H), 6.81 (t, *J*=7.6 Hz, 1H), 6.70 (d, *J*=7.2 Hz, 1H), 6.69 (s, 1H), 6.57 (dd, *J*=7.6, 1.0 Hz, 1H), 4.69-4.62 (m, 2H), 4.24-4.15 (m, 1H), 3.88-3.45 (m, 311H), 3.38 (s, 6H), 3.34-3.32 (m, 1H), 3.23 (s, 6H), 2.68-2.65 (m, 1H), 2.51-2.48 (m, 1H), 2.41-2.32 (m, 2H), 1.59 (d, *J*=6.8 Hz, 3H), 1.29 (d, *J*=7.6 Hz, 3H), 1.28 (s, 3H), 0.69 (d, *J*=6.8 Hz, 3H).

Compound 31

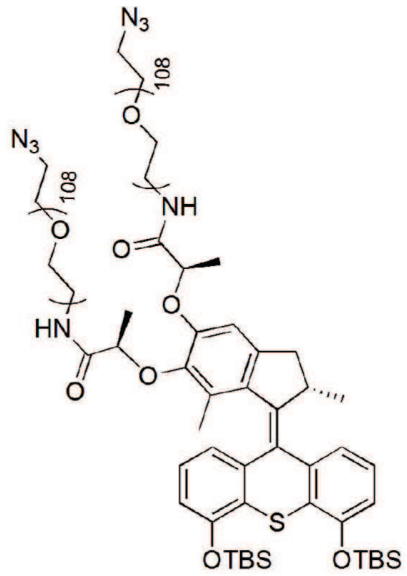

To a solution of acid **25** (5 mg, 0.0064 mmol) in CH_2Cl_2 (0.5 mL) was added HOBt (2 mg, 0.013 mmol), EDC (10 mg, 0.064 mmol). The mixture was stirred at room temperature for 10 min, then a solution of N_3-PEG_{5000}-NH_2 (63 mg, 0.013 mmol) in CH_2Cl_2 (0.5 mL) was added dropwise. Then after 120 h, another portion of HOBt (1 mg), EDC (5 mg), N_3-PEG_{5000}-NH_2 (32 mg) was added. After stirring for more 43 h, CH_2Cl_2 (10 mL) was added and the mixture was washed with sat.K_2CO_3 solution (10 mL), sat.NH_4Cl (10 mL) solution. The organic layer was evaporated in vacuum and around 70 mg crude product was obtained. This crude product was purified by preparative HPLC affording compound **31** as a slight yellow solid (24 mg, 36 % yield).

^{1}H NMR (CD_3OD, 400 MHz, 298 K) δ 7.39 (d, *J*=8.0 Hz, 1H), 7.24 (t, *J*=8.0 Hz, 1H), 6.95 (t, *J*=8.0 Hz, 1H), 6.80 (d, *J*=8.0 Hz, 1H), 6.77 (s, 3H), 6.75 (d, *J*=8.0 Hz, 1H), 6.61 (d, *J*=7.6 Hz, 1H), 4.74 (q, *J*=6.8 Hz, 1H), 4.35 (q, *J*=6.8 Hz, 1H), 4.19-4.16 (m, 1H), 3.82-3.59 (m, 1004H), 3.47-3.34 (m, 22H), 2.41 (d, *J*=15.2 Hz, 1H), 1.54 (d, *J*=6.8 Hz, 3H), 1.40 (d, *J*=6.8 Hz, 3H), 1.20 (s, 3H), 1.11 (s, 18H), 0.63 (d, *J*=6.8 Hz, 3H), 0.32 (s, 3H), 0.31 (s, 3H), 0.29 (s, 3H), 0.28 (s, 3H).

Compound 32

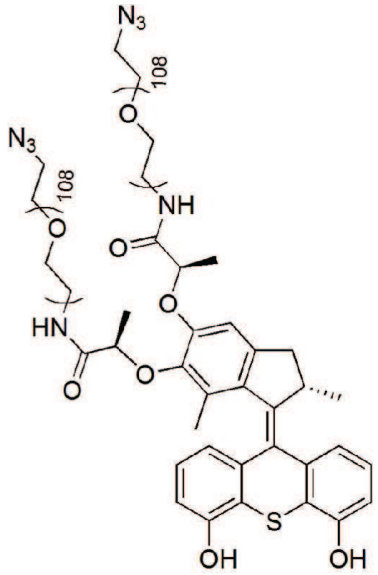

To a solution of compound **31** (100 mg, 9.6 µmol) in CH_2Cl_2 (2 mL) was added TBAF (86 µL, 86 µmol) at 0 ˚C. The mixture was stirred at 0 ˚C for 70 min. After removal of solvent in vacuum, around 120 mg crude product was obtained and this crude product was purified by preparative HPLC affording compound **32** as slight yellow solid (40 mg, 41 % yield).

^{1}H NMR (CD_3OD, 400 MHz, 298 K) δ 7.27 (d, *J*=8.0 Hz, 1H), 7.17 (t, *J*=8.0 Hz, 1H), 6.87 (t, *J*=7.6 Hz, 1H), 6.77 (s, 1H), 6.74 (dd, *J*=8.0, 0.8 Hz, 1H), 6.69 (dd, *J*=8.0, 1.2 Hz, 1H), 4.73 (q, *J*=6.8 Hz, 1H), 4.40 (q, *J*=6.8 Hz, 1H), 3.82-3.50 (m, 994H), 3.49-3.34 (m, 18H), 2.41 (d, *J*=15.2 Hz, 1H), 1.54 (d, *J*=6.8 Hz, 3H), 1.39 (d, *J*=6.8 Hz, 3H), 1.24 (s, 3H), 0.64 (d, *J*=6.8 Hz, 3H).

Compound 34

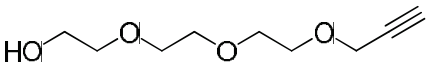

2-{2-[2-(prop-2-yn-1-yloxy)ethoxy]ethoxy}ethan-1-ol (34): To a solution of triethylene glycol (0.49 mL, 3.7 mmol) in THF (15 mL) was added *t*-BuOK (230 mg, 1.98 mmol, 97 %) under argon at room temperature. The mixture was stirred for 30 min at room temperature and then a solution of propargyl bromide (0.212 mL, 1.97 mmol, 80 % in toluene) in THF (6 mL) was added dropwise. The final mixture was stirred at room temperature for 15 h. Then the mixture was filtered through celite and washed with dichloromethane. After removal of the solvent, the residue was purified by flash column

chromatography (silica gel, EtOAc) affording product **34** as a slight yellow oil 275 mg (74 % based on propargyl bromide). R_f=0.3 (EtOAc);

^{1}H NMR ($CDCl_3$, 400 MHz, 298 K) δ 4.03-4.02 (m, 2H), 3.52-3.47 (m, 10H), 3.42-3.40 (m, 2H), 3.18 (br.s, 1H), 2.37-2.36 (m, 1H).

^{13}C NMR ($CDCl_3$, 100 MHz, 298 K) δ 79.2, 74.4, 72.1, 70.1-69.8 ($4CH_2$), 61.0, 57.8.

MS (ESI): calculated for $C_9H_{17}O_4$ $[M+H]^+$ 189.11, Found 189.33.

Compound 35

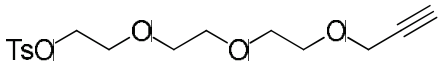

2-{2-[2-(prop-2-yn-1-yloxy)ethoxy]ethoxy}ethyl 4-methylbenzene-1-sulfonate (35): To a solution of **34** (153 mg, 0.81 mmol) in THF (0.6 mL) was added NaOH (97 mg, 2.43 mmol) solution (0.6 mL H_2O) at 0 ˚C. Then a solution of TsCl (200 mg, 1.05 mmol) in THF (0.4 mL) was added dropwise. The mixture was stirred at 0 ˚C while allowed to reach room temperature for 5 h. The mixture was diluted with water (10 mL) and extracted with Et_2O (3×20 mL). The combined organic phase was dried over Na_2SO_4. The solvent was removed in vacuum affording compound **35** as a colorless oil (270 mg, 97 % yield). R_f=0.45 (*n*-hexane:EtOAc=1:1);

^{1}H NMR ($CDCl_3$, 400 MHz, 298 K) δ 7.80 (d, *J*=8.4 Hz, 2H), 7.34 (d, *J*=8.0 Hz, 2H), 4.19 (d, *J*=2.4 Hz, 2H), 4.16 (t, *J*=4.8 Hz, 2H), 3.70-3.67 (m, 4H), 3.65-3.63 (m, 2H), 3.60 (s, 4H), 2.45 (s, 3H), 2.42 (t, *J*=2.4 Hz, 1H).

^{13}C NMR ($CDCl_3$, 100 MHz, 298 K) δ 144.7, 133.0, 129.7, 127.9, 79.6, 74.5, 70.6, 70.5, 70.4, 69.2, 69.0, 68.6, 58.3, 21.6.

HRMS (*m/z*): calculated for $C_{16}H_{22}LiO_6S$ $[M+Li]^+$ 349.1292, Found 349.1285.

Compound 36

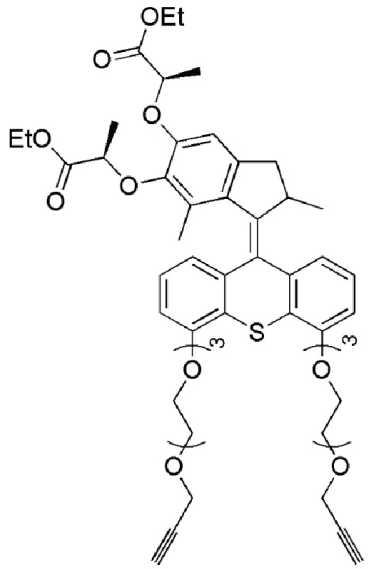

Compound 36: To a mixture of bis-phenol **24** (64 mg, 0.11 mmol) and K_2CO_3 (46 mg, 0.33 mmol) in DMF (4 mL) was added a solution of compound **35** (113 mg, 0.33 mmol) in DMF (1 mL). The mixture was stirred at 45 ˚C for 48 h. Then the mixture was diluted with water (10 mL) and extracted with CH_2Cl_2 (3×20 mL). The combined organic phase was dried over Na_2SO_4, concentrated in vacuum and further purified by flash column chromatography (silica gel, *n*-hexane:EtOAc=5:1→1:1) affording compound **36** as a yellowish solid (84 mg, 81 % yield).

For *R,R,S*-isomer: R_f=0.4 (*n*-hexane:EtOAc=1:1);

^{1}H NMR ($CDCl_3$, 400 MHz, 298 K) δ 7.32 (d, *J*=7.6 Hz, 1H), 7.21 (t, *J*=8.0 Hz, 1H), 6.93 (t, *J*=8.0 Hz, 1H), 6.76 (d, *J*=7.6 Hz, 1H), 6.69 (dd, *J*=8.0, 1.0 Hz, 1H), 6.64 (dd, *J*=7.6, 1.2 Hz, 1H), 6.54 (s, 1H), 4.79 (q, *J*=6.8 Hz, 1H), 4.76 (q, *J*=6.8 Hz, 1H), 4.31-4.08 (m, 13H), 3.98-3.93 (m, 4H), 3.85-3.82 (m, 4H), 3.72-3.67 (m, 12H), 3.37-3.32 (m, 1H), 2.42 (t, *J*=2.4 Hz, 1H), 2.41 (t, *J*=2.4 Hz, 1H), 2.32 (d, *J*=14.8 Hz, 1H), 1.61 (d, *J*=6.8 Hz, 3H), 1.46 (d, *J*=6.8 Hz, 3H), 1.22 (t, *J*=7.2 Hz, 3H), 1.20 (s, 3H), 1.19 (t, *J*=7.2 Hz, 3H), 0.62 (d, *J*=6.8 Hz, 3H).

^{13}C NMR ($CDCl_3$, 100 MHz, 298 K) δ 172.5, 172.0, 155.8, 155.3, 149.6, 145.9, 144.4, 141.9, 141.7, 138.2, 133.4, 131.0, 127.6, 126.7, 126.4, 124.9, 124.6, 120.9, 120.3, 109.5, 109.0, 108.0, 79.7(-C≡*C*H), 77.2, 76.8, 74.5(-C≡*C*H), 72.9, 71.1, 70.8, 70.4, 69.7, 69.6, 69.1, 68.8, 61.2, 60.7, 58.4, 39.5, 38.1, 18.9, 18.6, 18.4, 14.5, 14.1, 14.0.

HRMS (*m/z*): calculated for $C_{52}H_{64}LiO_{14}S$ $[M+Li]^+$ 951.4172, Found 951.4147.

For *R,R,R*-isomer: R_f=0.4 (*n*-hexane:EtOAc=1:1);

^{1}H NMR ($CDCl_3$, 400 MHz, 298 K) δ 7.31 (d, *J*=7.6 Hz, 1H), 7.21 (t, *J*=8.0 Hz, 1H), 6.97 (t, *J*=8.0 Hz, 1H), 6.76 (d, *J*=8.0 Hz, 1H), 6.70 (d, *J*=7.6 Hz, 1H), 6.67 (d, *J*=7.6 Hz, 1H), 6.57 (s, 1H), 4.77 (q, *J*=6.8

Hz, 1H), 4.50 (q, *J*=6.8 Hz, 1H), 4.31-4.14 (m, 12H), 4.12-4.08 (m, 1H), 3.98-3.93 (m, 4H), 3.85-3.82 (m, 4H), 3.72-3.68 (m, 12H), 3.35-3.30 (m, 1H), 2.42 (t, *J*=2.4 Hz, 1H), 2.41 (t, *J*=2.4 Hz, 1H), 2.34 (d, *J*=14.8 Hz, 1H), 1.61 (d, *J*=6.8 Hz, 3H), 1.50 (d, *J*=6.8 Hz, 3H), 1.29 (t, *J*=6.8 Hz, 3H), 1.28 (t, *J*=6.8 Hz, 3H), 1.18 (s, 3H), 0.62 (d, *J*=6.8 Hz, 3H).

^{13}C NMR ($CDCl_3$, 100 MHz, 298 K) δ 172.5, 172.1, 155.8, 155.3, 150.2, 145.8, 144.8, 142.3, 141.7, 138.2, 133.4, 131.0, 127.7, 126.9, 126.4, 124.8, 124.6, 120.9, 120.3, 109.4, 109.0, 108.2, 79.7 (-C≡*C*H), 77.2, 74.5(-C≡*C*H), 72.9, 71.1, 70.8, 70.4, 69.7, 69.6, 69.1, 68.8, 68.7, 61.2, 60.7, 58.4, 39.5, 38.1, 19.0, 18.7, 18.5, 14.6, 14.2, 14.1.

MS (ESI): calculated for $C_{52}H_{65}O_{14}S$ $[M+H]^+$ 945.41, Found 945.51.

Compound 37

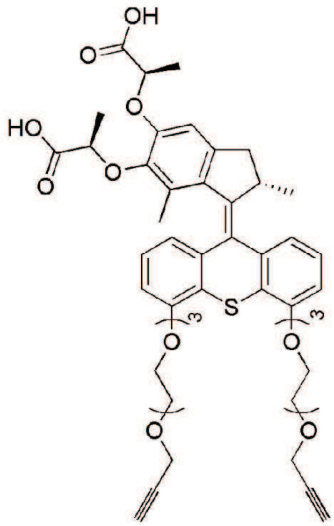

Compound 37: To a solution of bis-ester **36** (80 mg, 0.085 mmol) in THF/MeOH (0.25 mL/0.25 mL) was added NaOH (17 mg, 0.43 mmol) solution (0.25 mL H_2O). The mixture was stirred at room temperature for 3 h and then quenched with 0.2 M HCl (5 mL) at 0 ˚C. The mixture was then washed with CH_2Cl_2 (3×10 mL). The combined organic phase was dried over Na_2SO_4, concentrated in vacuum and further purified by flash column chromatography (silica gel, CH_2Cl_2→CH_2Cl_2:MeOH=100:1→20:1) affording compound **37** as a slightly yellow solid (45 mg, 60 % yield). R_f=0.1 (CH_2Cl_2:MeOH=100:1);

^{1}H NMR (CD_3OD, 400 MHz, 298 K) δ 7.37 (d, *J*=7.6 Hz, 1H), 7.27 (t, *J*=8.0 Hz, 1H), 6.98 (t, *J*=8.0 Hz, 1H), 6.87 (d, *J*=7.6 Hz, 1H), 6.81 (d, *J*=7.6 Hz, 1H), 6.67 (s, 1H), 6.60 (dd, *J*=8.0, 1.2 Hz, 1H), 4.81 (q, *J*=7.2 Hz, 1H), 4.62 (q, *J*=6.8 Hz, 1H), 4.30-4.10 (m, 9H), 3.92-3.89 (m, 4H), 3.78-3.77 (m, 4H), 3.66-

3.60 (m, 12H), 3.40-3.35 (m, 1H), 2.80 (t, *J*=2.4 Hz, 1H), 2.79 (t, *J*=2.4 Hz, 1H), 2.36 (d, *J*=15.2 Hz, 1H), 1.60 (d, *J*=6.8 Hz, 3H), 1.38 (d, *J*=6.8 Hz, 3H), 1.17 (s, 3H), 0.60 (d, *J*=6.8 Hz, 3H).

^{13}C NMR (CD_3OD, 100 MHz, 298 K) δ 176.1, 175.5, 157.4, 156.8, 151.5, 147.2, 145.5, 143.8, 143.2, 139.5, 134.5, 131.9, 129.3, 128.0 (2C), 126.4, 125.6, 122.0, 121.3, 110.8, 110.6, 109.5, 80.7, 78.4, 76.0, 74.3, 73.7, 72.1, 71.7, 71.6, 71.4, 70.9, 70.8, 70.2, 70.1, 62.3, 59.1, 40.4, 39.3, 19.3, 19.1, 18.8, 15.2.

HRMS (*m/z*): calculated for $C_{48}H_{56}LiO_{14}S$ $[M+Li]^+$ 895.3546, Found 895.3542.

Compound 38

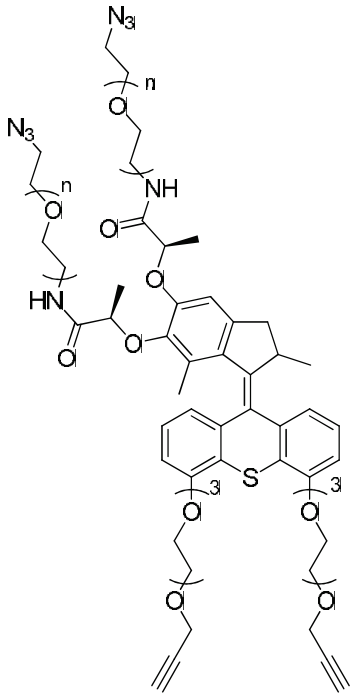

Polymer-motor conjugate 38 (n=108): To a solution of bis-acid **37** (10 mg, 0.012 mmol) in CH_2Cl_2 (0.4 mL) was added HOBt (5 mg, 0.028 mmol) and EDC (18 mg, 0.09 mmol) at room temperature. After 15 min, a solution of N_3-PEG_{5000}-NH_2 (Mw=4847 g·mol^{-1}, 109 mg, 0.022 mmol) in CH_2Cl_2 (0.6 mL) was added. The mixture was stirred at room temperature for 16 h. After removal of the solvent, the residue was then purified by reversed phase column chromatography (C18, Merck, MeOH:water=3:7→8:2) affording the desired compound as a slightly yellow solid (70 mg, 60 % yield).

^{1}H NMR (CD_3OD, 400 MHz, 298 K) δ 7.41 (d, *J*=7.6 Hz, 1H), 7.32 (t, *J*=8.0 Hz, 1H), 7.05 (t, *J*=8.0 Hz, 1H), 6.94 (d, *J*=8.0 Hz, 1H), 6.89 (d, *J*=8.0 Hz, 1H), 6.76 (s, 1H), 6.65 (d, *J*=7.6 Hz, 1H), 4.73 (q, *J*=6.8 Hz, 1H), 4.43 (q, *J*=6.8 Hz, 1H), 4.34-4.16 (m, 9H), 3.98-3.94 (m, 4H), 3.84-3.79 (m, 12H), 3.74-3.36(m, 1084H), 2.85 (t, *J*=2.4 Hz, 1H), 2.84 (t, *J*=2.4 Hz, 1H), 2.42 (d, *J*=15.2 Hz, 1H), 1.54 (d, *J*=6.8 Hz, 3H), 1.30 (d, *J*=6.8 Hz, 3H), 1.18 (s, 3H), 0.63 (d, *J*=6.8 Hz, 3H).

MS (ESI):

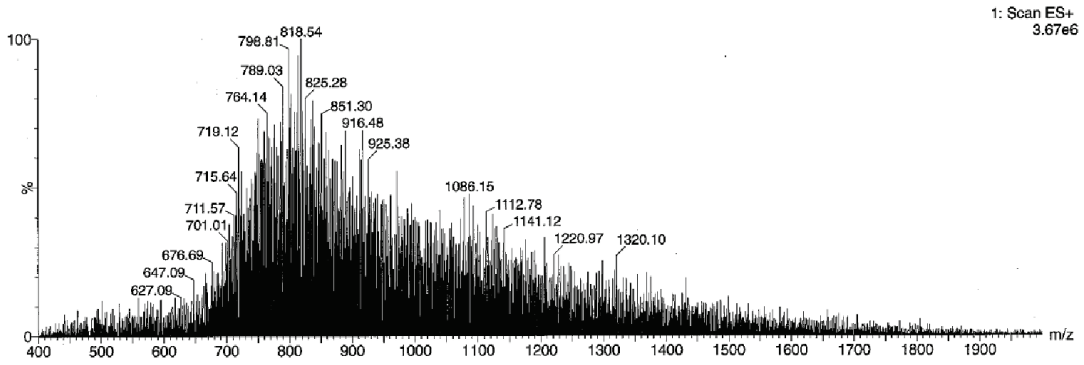

Polymer-motor conjugate 38 (n=238): To a solution of bis-acid **37** (10 mg, 0.012 mmol) in CH_2Cl_2 (0.4 mL) was added HOBt (5 mg, 0.028 mmol) and EDC (18 mg, 0.09 mmol) at room temperature. After 15 min, a solution of N_3-PEG_{10000}-NH_2 (Mw=10526 g·mol^{-1}, 246 mg, 0.023 mmol) in CH_2Cl_2 (0.6 mL) was added. The mixture was stirred at room temperature for 18 h. After removal of the solvent, the residue was then purified by reversed phase column chromatography (C18, Merck, MeOH:water=3:7→8:2) affording compound 3 as a slightly yellow solid (90 mg, 37 % yield).

^{1}H NMR (CD_3OD, 400 MHz, 298 K) δ 7.41 (d, *J*=7.6 Hz, 1H), 7.32 (t, *J*=8.0 Hz, 1H), 7.05 (t, *J*=8.0 Hz, 1H), 6.94 (d, *J*=8.0 Hz, 1H), 6.89 (d, *J*=8.0 Hz, 1H), 6.76 (s, 1H), 6.65 (d, *J*=7.6 Hz, 1H), 4.74 (q, *J*=6.8 Hz, 1H), 4.43 (q, *J*=6.8 Hz, 1H), 4.34-4.16 (m, 9H), 3.96-3.36 (m, 1864H), 2.87 (t, *J*=2.4 Hz, 1H), 2.86 (t, *J*=2.4 Hz, 1H), 2.42 (d, *J*=15.2 Hz, 1H), 1.54 (d, *J*=6.8 Hz, 3H), 1.30 (d, *J*=6.8 Hz, 3H), 1.18 (s, 3H), 0.63 (d, *J*=6.4 Hz, 3H).

MS (ESI):

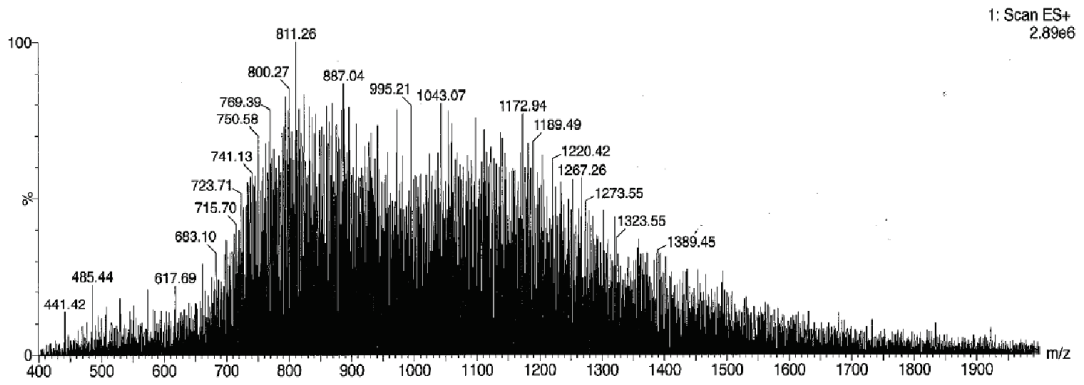

Compound 39

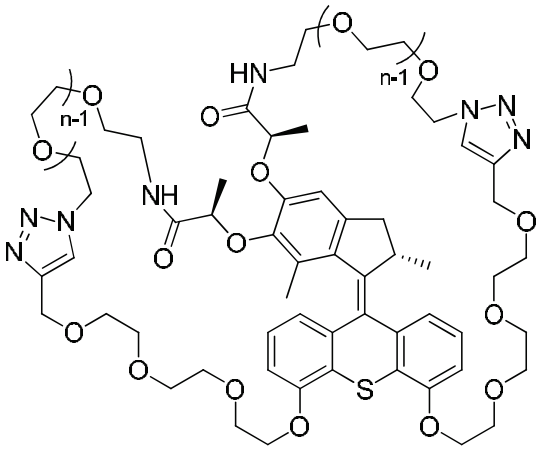

8-shaped motor-polymer 39 (n=108): To DMF (90 mL, degassed with freeze-pump-thaw cycles) was added PMDETA (210 µL, 0.97 mmol) and CuBr (140 mg, 0.97 mmol). The temperature was increased to 80 ˚C. Then a solution of compound **38 (n=108)** (34 mg, 3.22 µmol) in degassed DMF (10 mL) was added dropwise using a syringe pump at a rate of 1.5 mL/h. After 7 h, DMF was evaporated in vacuum and the mixture was suspended in dichloromethane, washed with 1M EDTA solution to remove copper. Then the organic phase was dried over Na_2SO_4. After removal of the solvent, the residue was purified by reversed phase column chromatography (C18, Merck, MeOH:water=3:7→8:2) affording compound **39 (n=108)** as a slightly yellow solid (22 mg, 65 % yield).

^{1}H NMR (CD_3OD, 400 MHz, 298 K) δ 8.03-7.98 (m, 2H), 7.41 (d, *J*=7.6 Hz, 1H), 7.31 (t, *J*=8.0 Hz, 1H), 7.07-7.02 (m, 1H), 6.96-6.93 (m, 1H), 6.89 (d, *J*=8.0 Hz, 1H), 6.76 (s, 1H), 6.66-6.64 (m, 1H), 4.64-4.52 (m, 7H), 4.43-4.16 (m, 4H), 3.96-3.40 (m, 982H), 2.42 (d, *J*=17.6 Hz, 1H), 1.56-1.53 (m, 3H), 1.31-1.29 (m, 3H), 1.17 (s, 3H), 0.62 (d, *J*=6.8 Hz, 3H).

MS (ESI):

8-shaped motor-polymer 39 (n=238): To DMF (110 mL, degassed with freeze-pump-thaw cycles) was added PMDETA (144 μL, 0.68 mmol) and CuBr (97 mg, 0.68 mmol). The temperature was increased to 80 ˚C. Then a solution of compound **38 (n=238)** (50 mg, 2.27 μmol) in degassed DMF (10 mL) was added dropwise using a syringe pump at a rate of 1.5 mL/h. After 7 h, DMF was evaporated in vacuum and the mixture was suspended in dichloromethane, washed with 1M EDTA solution to remove copper. Then the organic phase was dried over Na_2SO_4. After removal of the solvent, the residue was purified by reversed phase column chromatography (C18, Merck, MeOH:water=3:7→8:2) affording compound compound **39 (n=238)** as a slightly yellow solid (42 mg, 84 % yield).

^{1}H NMR (CD_3OD, 400 MHz, 298 K) δ 8.02-7.98 (m, 2H), 7.41 (d, *J*=7.6 Hz, 1H), 7.31 (t, *J*=8.0 Hz, 1H), 7.07-7.02 (m, 1H), 6.95 (dd, *J*=8.0 Hz, 2.4 Hz, 1H), 6.89 (d, *J*=8.4 Hz, 1H), 6.75 (s, 1H), 6.65 (d, *J*=7.6 Hz, 1H), 4.64-4.52 (m, 10H), 4.43-4.16 (m, 9H), 3.96-3.40 (m, 1888H), 2.42 (d, *J*=15.2 Hz, 1H), 1.56-1.53 (m, 3H), 1.31-1.29 (m, 3H), 1.17 (s, 3H), 0.62 (d, *J*=6.4 Hz, 3H).

MS (ESI):

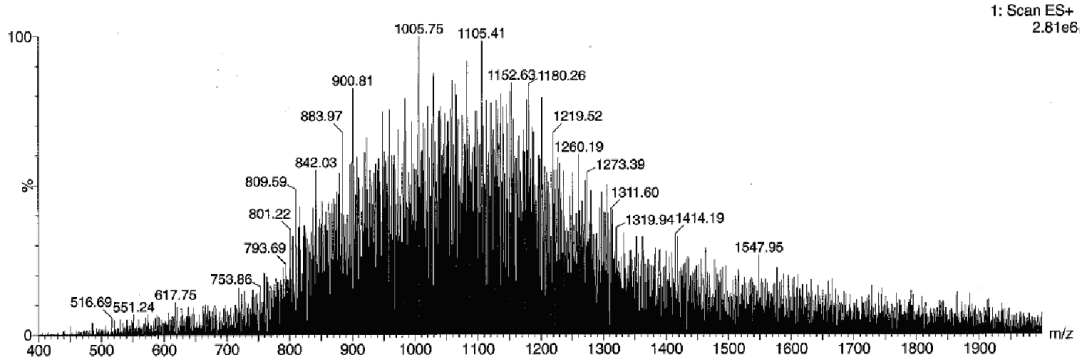

Gel-40 (n=108): To a solution of compound **38 (n=108)** (35 mg, 3.32 μmol) in degassed DMF (0.3 mL) was added PMDETA (210 μL, 0.97 mmol) and CuBr (140 mg, 0.97 mmol) at 80 ˚C. The gel was formed very quickly within 1 min. Then degassed DMF (0.5 mL) was added and the mixture was stirred at 80 ˚C for further 30 min. The gel was washed extensively with 1M EDTA solution, water and methanol. Finally, a colorless and transparent gel was obtained (20 mg dry gel, 57 % yield).

Gel-40 (n=238): To a solution of compound **38 (n=238)** (60 mg, 2.73 μmol) in degassed DMF (0.2 mL) was added PMDETA (5 μL, 23 μmol) and CuBr (9 mg, 23 μmol) at 80 ˚C. The gel was formed very quickly within 1 min. Then degassed DMF (0.5 mL) was added and the mixture was stirred at 80 ˚C for further 30 min. The gel was then washed extensively with 1M EDTA solution, water and methanol. Finally, a colorless and transparent gel was obtained (36 mg dry gel, 60 % yield).

Compound 41

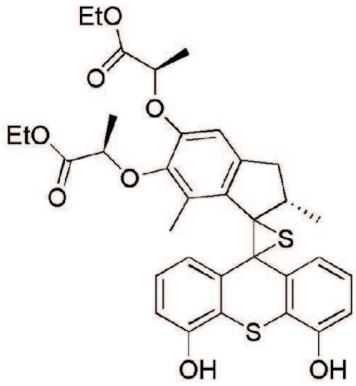

Episulfide 41: To a solution of **episulfide 22**-(*R,R,S*) (30 mg, 0.035 mmol) in THF (1 mL) was added TBAF (72 µL, 72 µmol) at 0 ˚C. The mixture was stirred at 0 ˚C for 5 min and then solvent was removed under vacuum. The residue was purified by flash column chromatography (silica gel, toluene:EtOAc=4:1) affording **41** as a yellow solid (24 mg, 99 % yield). R_f=0.3 (toluene:EtOAc=4:1);

^{1}H NMR (CD_3OD, 400 MHz, 298 K) δ 7.27 (dd, *J*=7.6, 1.2 Hz, 1H), 7.10 (dd, *J*=5.2, 0.8 Hz, 2H), 7.00 (t, *J*=8.0 Hz, 1H), 6.76 (t, *J*=4.4 Hz, 1H), 6.62 (dd, *J*=8.0, 0.8Hz, 1H), 6.39 (s, 1H), 4.76 (q, *J*=6.8 Hz, 1H), 4.61 (q, *J*=6.8 Hz, 1H), 4.19-4.07 (m, 4H), 3.26-3.21 (m, 1H), 2.10 (d, *J*=15.2 Hz, 1H), 2.09 (s, 3H), 1.49 (d, *J*=6.8 Hz, 3H), 1.38-1.35 (m, 1H), 1.23 (t, *J*=7.2 Hz, 3H), 1.19 (d, *J*=7.2 Hz, 3H), 1.16 (t, *J*=7.2 Hz, 3H), 0.94 (d, *J*=6.8 Hz, 3H).

^{13}C NMR (CD_3OD, 100 MHz, 298 K) δ 174.3, 173.5, 154.6 (2C), 150.7, 144.6, 141.8, 141.6, 138.1, 132.8, 129.8, 127.7, 127.0, 124.4, 124.2, 123.2, 120.9, 114.3 (2C), 109.6, 77.4, 73.9, 72.8, 63.4, 62.3, 62.1, 42.3, 38.5, 26.2, 21.6, 18.6, 18.5, 14.5, 13.2.

MS (ESI): calculated for $[M+H]^+$ $C_{34}H_{37}O_8S_2$ 637.19, Found: 637.42.

Compound 42

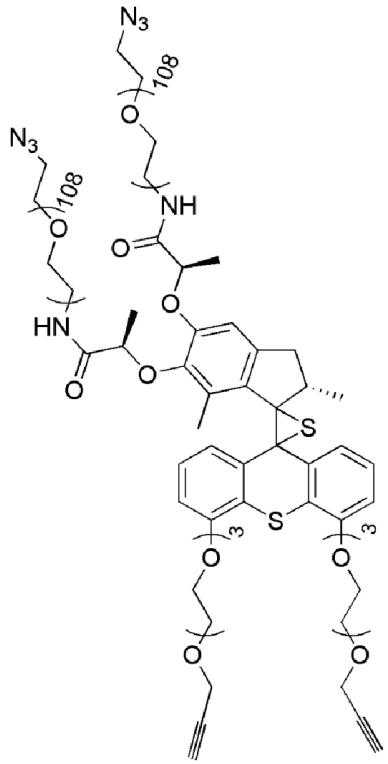

Episulfide-polymer conjugate 42: To a solution of phenol **41** (12 mg, 0.019 mmol) in DMF (0.7 mL) was added K_2CO_3 (8 mg, 0.058 mmol). Then a solution of compound **35** (20 mg, 0.058 mmol) in DMF (0.3 mL) was added and the mixture was stirred at 50 ˚C for 24 h. Then water (15 mL) was added and the mixture was extracted with dichloromethane (15 mL×3). The combined organic layers were dried over Na_2SO_4 and evaporated in vacuum. This crude product was used in the next step without further purification.

To this crude product in THF/H_2O (1 mL/1 mL) was added KOH solution (2.8 mg in 1 mL H_2O, 0.05 M). The mixture was stirred at 0 ˚C while allowed to reach room temperature for 2 h. Then 1M HCl solution (0.1 mL) was added at 0 ˚C to quench the reaction. Water (20 mL) was added and the mixture was extracted with dichloromethane (20 mL×3). The combined organic layers were dried over Na_2SO_4 and evaporated in vacuum affording around 6 mg crude product. This crude product was used in the next step without further purification.

To the above crude product (6 mg) in DCM (0.5 mL) was added HOBt (3 mg, 0.016 mmol), EDC (11 mg, 0.052 mmol) at room temperature. After 10 min, a solution of N_3-PEG_{5000}-NH_2 (60 mg, 0.013 mmol) in DCM (0.3 mL) was added. The mixture was stirred at room temperature for 7 h. After removal of the

solvent in vacuum, the residue was purified by reversed column chromatography (C18, Merck, MeOH:water=3:7→8:2) affording a slight yellow solid (22 mg, 11 % yield over 3 steps).

^{1}H NMR (CD_3OD, 400 MHz, 298 K) δ 7.43 (d, *J*=8.0 Hz, 1H), 7.28 (t, *J*=7.6 Hz, 1H), 7.24 (d, *J*=7.6 Hz, 1H), 7.20 (t, *J*=8.0 Hz, 1H), 7.00 (d, *J*=7.6 Hz, 1H), 6.87 (d, *J*=8.4 Hz, 1H), 6.51 (s, 1H), 4.67 (q, *J*=6.4 Hz, 1H), 4.30 (q, *J*=6.8 Hz, 1H), 4.25-4.20 (m, 1H), 4.16 (d, *J*=2.4 Hz, 2H), 4.15-4.10 (m, 4H), 3.94-3.36 (m, 1014H), 3.21-3.16 (m, 1H), 2.85 (t, *J*=2.0 Hz, 2H), 2.16 (d, *J*=14.4 Hz, 1H), 2.13 (s, 3H), 1.47 (d, *J*=6.8 Hz, 3H), 1.00 (d, *J*=6.8 Hz, 3H), 0.96 (d, *J*=6.8 Hz, 3H).

Gel-43: To a solution of compound **42** (20 mg, 1.89 μmol) in degassed DMF (0.3 mL) was added PMDETA (21 μL, 97 μmol) and CuBr (14 mg, 97 μmol) at 80 ˚C (This reaction was performed in a vial with 2.2 cm diameter at the bottom). The vial was shaken for a few seconds and continue to been heated at 80 ˚C. The gel was formed very quickly within 1 min. Then 0.5 mL degassed DMF was added and the mixture was heated at 80 ˚C for further 30 min. The gel was then washed extensively with 1M EDTA solution, water and methanol. Finally, a colorless and transparent gel was obtained (19 mg dry gel, 95 % yield).

Compound 44

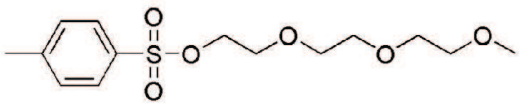

2-[2-(2-methoxyethoxy)ethoxy]ethyl 4-methylbenzene-1-sulfonate (42): To a solution of tri-ethylene glycol monomethyl ether (0.5 g, 3 mmol) in THF (1.8 mL) was added an aq. NaOH (360 mg, 9 mmol) solution (1.8 mL) at 0 ˚C. Then a solution of TsCl (744 mg, 3.9 mmol) in THF (1.3 mL) was added dropwise. The mixture was stirred at 0 ˚C while allowed to reach room temperature overnight. The organic layer was separated and the water layer was extracted with Et_2O. The combined organic layers were washed with 10 % NaOH (w/v), brine and dried over Na_2SO_4. Evaporation of the solvent afforded the desired compound as a colorless oil 0.92 g (95 % yield).

^{1}H NMR ($CDCl_3$, 400 MHz, 298 K) δ 7.78 (d, *J*=8.4 Hz, 1H), 7.33 (d, *J*=8.0 Hz, 1H), 4.15 (t, *J*=4.8 Hz, 2H), 3.68 (t, *J*=4.8 Hz, 2H), 3.58-3.61 (m, 6H), 3.52 (m, 2H), 3.36 (s, 3H), 2.44 (s, 3H).

^{13}C NMR ($CDCl_3$, 100 MHz, 298 K) δ 144.48, 132.64, 129.50 (2C), 127.55 (2C), 71.49, 70.29, 70.12 (2C), 68.97, 68.24, 58.56, 21.21.

MS (ESI): calculated for $[M+H]^+$ $C_{14}H_{23}O_6S$ 319.12, Found: 319.29.

Compound 45

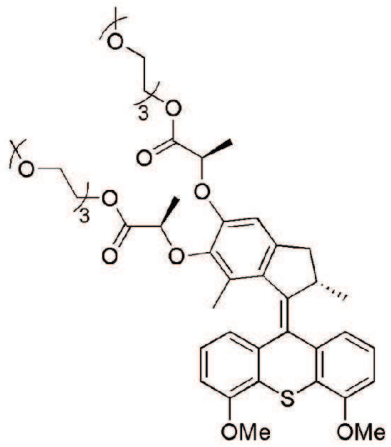

Compound 45: To a solution of the (*R,R,S*)-bis-acid motor **16** (20 mg, 0.034 mmol), triethylene glycol monomethyl ether (13 mg, 0.075 mmol), tris(3-chlorophenyl) phophine (51 mg, 0.14 mmol) in dry toluene (2 mL) was added DIAD (0.03 mL, 0.14 mmol) dropwise. The mixture was stirred at room temperature for 6 h. The mixture was purified by flash column chromatography (silica gel, toluene→toluene:EtOAc=1:100→EtOAc, then CH_2Cl_2→CH_2Cl_2:EtOAc=8:1). We found there are still some impurities (triethylene glycol monomethyl ether). Then the sample was dissolved in CH_2Cl_2 and washed with water affording the desired ester **41** as a deep green solid 21 mg (70 % yield). R_f=0.18 (EtOAc);

^{1}H NMR ($CDCl_3$, 400 MHz, 298 K) δ 7.32 (m, 1H), 7.24 (t, *J*=8.0 Hz, 1H), 6.96 (t, *J*=8.0 Hz, 1H), 6.74 (d, *J*=8.4 Hz, 1H), 6.66 (dd, *J*=8.4, 0.8 Hz, 1H), 6.63 (dd, *J*=8.0, 0.8 Hz, 1H), 6.54 (s, 1H), 4.78 (q, *J*=6.8 Hz, 2H), 4.35-4.16 (m, 4H), 4.15-4.10 (m, 1H), 3.94 (s, 3H), 3.91 (s, 3H), 3.69-3.50 (m, 20H), 3.36 (s, 3H), 3.35 (s, 3H), 2.33 (d, *J*=15.20 Hz, 1H), 1.62 (d, *J*=6.8 Hz, 3H), 1.47 (d, *J*=6.8 Hz, 3H), 1.20 (s, 3H), 0.64 (d, *J*=6.8 Hz, 3H).

^{13}C NMR ($CDCl_3$, 100 MHz, 298 K) δ 172.42, 171.79, 156.56, 156.12, 149.66, 145.89, 144.53, 141.94, 141.77, 138.29, 133.44, 130.99, 127.69, 126.87, 126.53, 124.02, 123.81, 120.46, 119.94, 108.10, 107.60, 107.38, 72.83, 71.92, 70.54, 68.90, 64.13, 63.74, 58.99, 55.92, 39.44, 38.04, 19.03, 18.69, 18.44, 14.49.

Compound 46

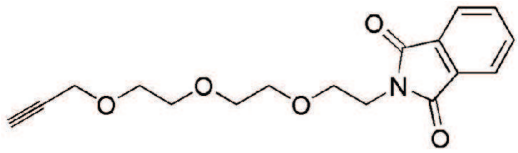

2-(2-(2-(2-(prop-2-yn-1-yloxy)ethoxy)ethoxy)ethyl)isoindoline-1,3-dione (46): To a solution of compound **35** (50 mg, 0.15 mmol) in DMF (1 mL) was added K_2CO_3 (25 mg, 0.18 mmol) and phthalimide (28 mg, 0.19 mmol). The mixture was stirred at 110 ˚C overnight. Then CH_2Cl_2 (15 mL) was added, washed with H_2O (15 mL×3). The connected organic layer was evaporated under vacuum affording a slightly yellow oil 40 mg (86 % yield) without further purification.

^{1}H NMR ($CDCl_3$, 400 MHz, 298 K) δ 7.86-7.84 (m, 2H), 7.72-7.70 (m, 2H), 4.16 (d, *J*=2.4 Hz, 2H), 3.90 (t, *J*=6.0 Hz, 2H), 3.74 (t, *J*=6.0 Hz, 2H), 3.66-3.59 (m, 8H), 2.41 (t, *J*=2.4 Hz, 1H).

^{13}C NMR ($CDCl_3$, 100 MHz, 298 K) δ 168.2 (2C), 133.9 (2C), 132.2 (2C), 123.2 (2C), 79.7, 74.4, 70.6, 70.4, 70.1, 69.1, 67.9, 58.3, 37.3.

MS (ESI): calculated for $[M+H]^+$ $C_{17}H_{20}NO_5$ 318.13, Found: 318.36.

Compound 47

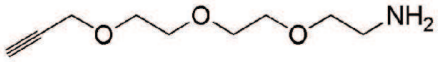

2-(2-(2-(prop-2-yn-1-yloxy)ethoxy)ethoxy)ethanamine (47): To a solution of compound **46** (10 mg, 0.032 mmol) in dry THF (1 mL) was added $NH_2NH_2 \cdot H_2O$ (0.1 mL). The mixture was stirred at room temperature for 24 h. The solvent was then evaporated under vacuum and water (10 mL) was added. The water phase was wased with $CHCl_3$ (15 mL×3) and the combined organic layers were dried over Na_2SO_4. Evaporation of the solvent affording a slightly yellow oil 5 mg (84 % yield).

^{1}H NMR ($CDCl_3$, 400 MHz, 298 K) δ 4.20 (d, *J*=2.4 Hz, 2H), 3.72-3.62 (m, 8H), 3.51 (t, *J*=5.2 Hz, 2H), 2.87 (t, *J*=4.8 Hz, 2H), 2.42 (t, *J*=2.4 Hz, 1H), 1.61 (br s, 2H).

^{13}C NMR ($CDCl_3$, 100 MHz, 298 K) δ 79.6, 74.5, 73.4, 70.6, 70.4, 70.3, 69.1, 58.4, 41.8.

Compound 48

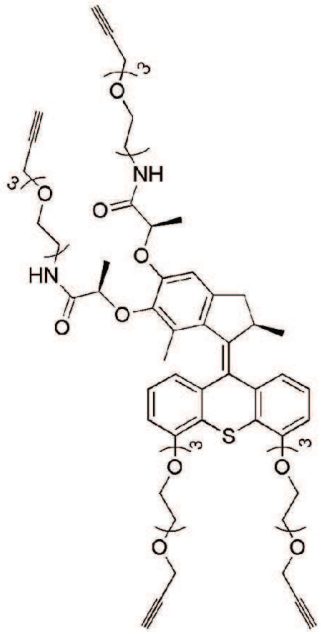

Tetra-alkyne (48): To a solution of compound **37** (10 mg, 0.011 mmol) in CH_2Cl_2 (0.5 mL) was added HOBt (5 mg, 0.027 mmol) and EDC (17 mg, 0.088 mmol). The mixture was stirred at room temperature for 5 min, and then a solution of the amine **47** (5 mg, 0.026 mmol) in CH_2Cl_2 (0.5 mL) was added. After 24 h, the solvent was evaporated under vacuum and the residue was purified by flash column chromatography (silica gel, EtOAc→EtOAc:MeOH=10:1) affording a slightly brown solid (10 mg, 74 % yield). R_f=0.55 (EtOAc: MeOH=10:1);

^{1}H NMR ($CDCl_3$, 400 MHz, 298 K) δ 7.33 (d, *J*=7.6 Hz, 1H), 7.23 (t, *J*=8.0 Hz, 1H), 6.97 (t, *J*=8.0 Hz, 1H), 6.78 (d, *J*=7.9 Hz, 1H), 6.73 (dd, *J*=7.6, 1.2 Hz, 1H), 6.66 (s, 1H), 6.65 (dd, *J*=7.6, 0.8 Hz, 1H), 4.63 (q, *J*=6.8 Hz, 1H), 4.38 (q, *J*=6.8 Hz, 1H), 4.31-4.26 (m, 2H), 4.24-4.14 (m, 9H), 4.00-3.93 (m, 4H), 3.85-3.83 (m, 4H), 3.72-3.40 (m, 40H), 3.38-3.32 (m, 1H), 2.43 (t, *J*=2.4 Hz, 2H), 2.41 (t, *J*=2.4 Hz, 2H), 2.37 (d, *J*=15.2 Hz, 1H), 1.58 (d, *J*=6.8 Hz, 3H), 1.34 (d, *J*=6.8 Hz, 3H), 1.15 (s, 3H), 0.64 (d, *J*=6.8 Hz, 3H).

^{13}C NMR ($CDCl_3$, 100 MHz, 298 K) δ 172.6, 172.1, 160.0, 155.4, 149.8, 145.5, 143.2, 142.9, 141.6, 137.9, 134.1, 130.7, 128.3, 126.7, 126.6, 125.0, 124.4, 120.6, 120.2, 109.6, 109.2, 109.1, 79.7, 79.6, 77.2, 76.1, 74.6, 74.5, 71.0, 70.8, 70.5, 70.4, 70.3, 69.7, 69.6, 69.1, 68.7, 58.4, 58.3, 39.5, 38.1, 19.1, 18.9, 18.3, 14.8.

MS (ESI): calculated for $[M+H]^+$ $C_{66}H_{87}N_2O_{18}S$ 1227.57, Found: 1227.84.

Compound 49

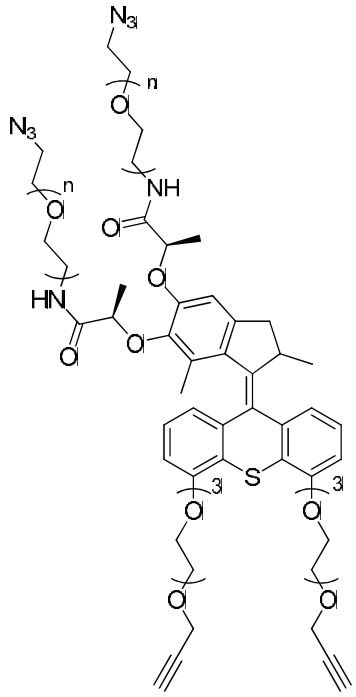

Polymer-motor conjugate 49 (n=35): To a solution of bis-acid **37** (13 mg, 0.015 mmol) in CH_2Cl_2 (0.4 mL) was added HOBt (7 mg, 0.036 mmol) and EDC (24 mg, 0.12 mmol) at room temperature. After 10 min, a solution of N_3-PEG_{1600}-NH_2 (Mw=1600 g·mol^{-1}, 48 mg, 0.03 mmol) in CH_2Cl_2 (0.6 mL) was added. The mixture was stirred at room temperature for 16 h. After removal of the solvent, the residue was then purified by reversed phase column chromatography (C18, Merck, MeOH:water=3:7→8:2) affording the desired compound as a slightly yellow solid (22 mg, 37 % yield).

^{1}H NMR (CD_3OD, 400 MHz, 298 K) δ 7.41 (d, *J*=7.6 Hz, 1H), 7.31 (t, *J*=8.0 Hz, 1H), 7.05 (t, *J*=8.0 Hz, 1H), 6.94 (d, *J*=7.6 Hz, 1H), 6.89 (d, *J*=8.0 Hz, 1H), 6.75 (s, 1H), 6.65 (dd, *J*=7.6, 0.8 Hz, 1H), 4.73 (q, *J*=6.8 Hz, 1H), 4.43 (q, *J*=6.8 Hz, 1H), 4.34-4.16 (m, 9H), 3.98-3.94 (m, 4H), 3.84-3.79 (m, 6H), 3.74-3.36(m, 321H), 2.85 (t, *J*=2.4 Hz, 1H), 2.84 (t, *J*=2.4 Hz, 1H), 2.42 (d, *J*=15.2 Hz, 1H), 1.54 (d, *J*=6.8 Hz, 3H), 1.30 (d, *J*=6.8 Hz, 3H), 1.18 (s, 3H), 0.63 (d, *J*=6.8 Hz, 3H).

Compound 50

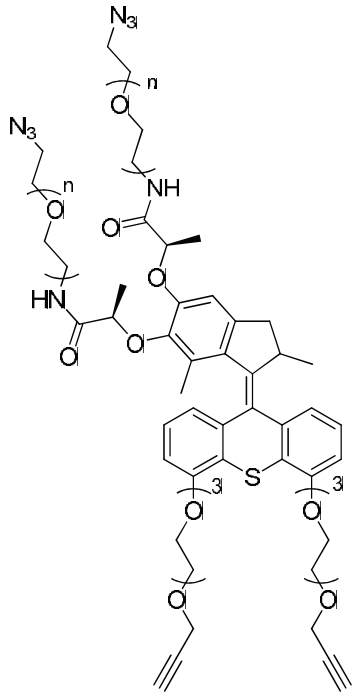

Polymer-motor conjugate 50 (n=64): To a solution of bis-acid **37** (10 mg, 0.011 mmol) in CH_2Cl_2 (0.4 mL) was added HOBt (5 mg, 0.027 mmol) and EDC (18 mg, 0.088 mmol) at room temperature. After 10 min, a solution of N_3-PEG_{3000}-NH_2 (Mw=3000 g·mol^{-1}, 68 mg, 0.022 mmol) in CH_2Cl_2 (0.6 mL) was added. The mixture was stirred at room temperature for 21 h. After removal of the solvent, the residue was then purified by reversed phase column chromatography (C18, Merck, MeOH:water=3:7→8:2) affording the desired compound as a slightly yellow solid (30 mg, 40 % yield).

^{1}H NMR (CD_3OD, 400 MHz, 298 K) δ 7.41 (d, *J*=7.6 Hz, 1H), 7.32 (t, *J*=8.0 Hz, 1H), 7.05 (t, *J*=8.0 Hz, 1H), 6.94 (d, *J*=8.0 Hz, 1H), 6.89 (d, *J*=8.4 Hz, 1H), 6.75 (s, 1H), 6.65 (d, *J*=7.2 Hz, 1H), 4.73 (q, *J*=6.8 Hz, 1H), 4.43 (q, *J*=6.8 Hz, 1H), 4.34-4.16 (m, 7H), 3.98-3.94 (m, 2H), 3.84-3.79 (m, 6H), 3.74-3.36(m, 625H), 2.86 (t, *J*=2.4 Hz, 1H), 2.85 (t, *J*=2.4 Hz, 1H), 2.42 (d, *J*=15.2 Hz, 1H), 1.54 (d, *J*=6.8 Hz, 3H), 1.30 (d, *J*=6.8 Hz, 3H), 1.18 (s, 3H), 0.63 (d, *J*=6.8 Hz, 3H).

3/ NMR Characterization of Key Compounds

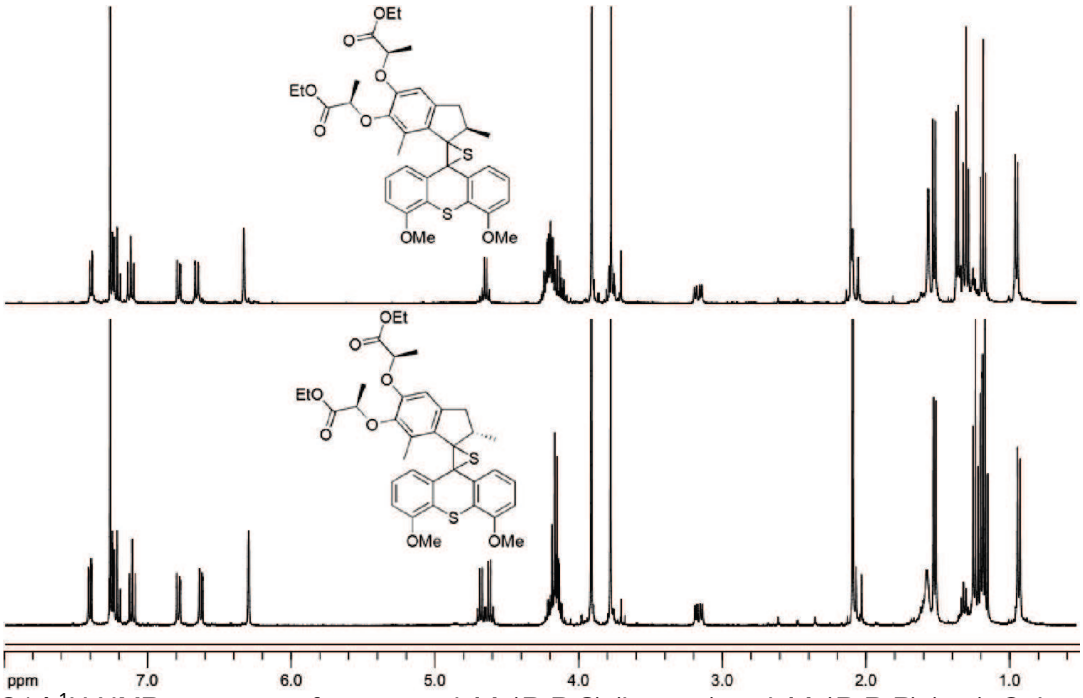

Figure S1 | ^{1}H NMR spectrum of compound **14**-(*R,R,S*) (bottom) and **14**-(*R,R,R*) (top). Solvent: $CDCl_3$

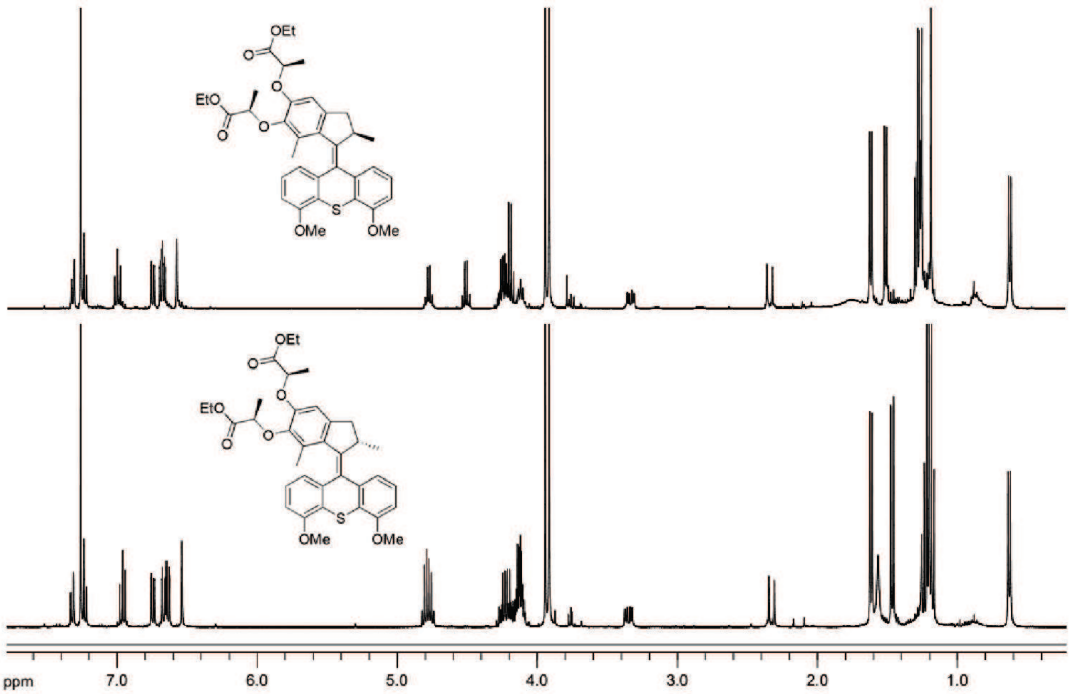

Figure S2 | ^{1}H NMR spectrum of motor **15**-(*R,R,S*) (bottom) and motor **15**-(*R,R,R*) (top). Solvent: $CDCl_3$

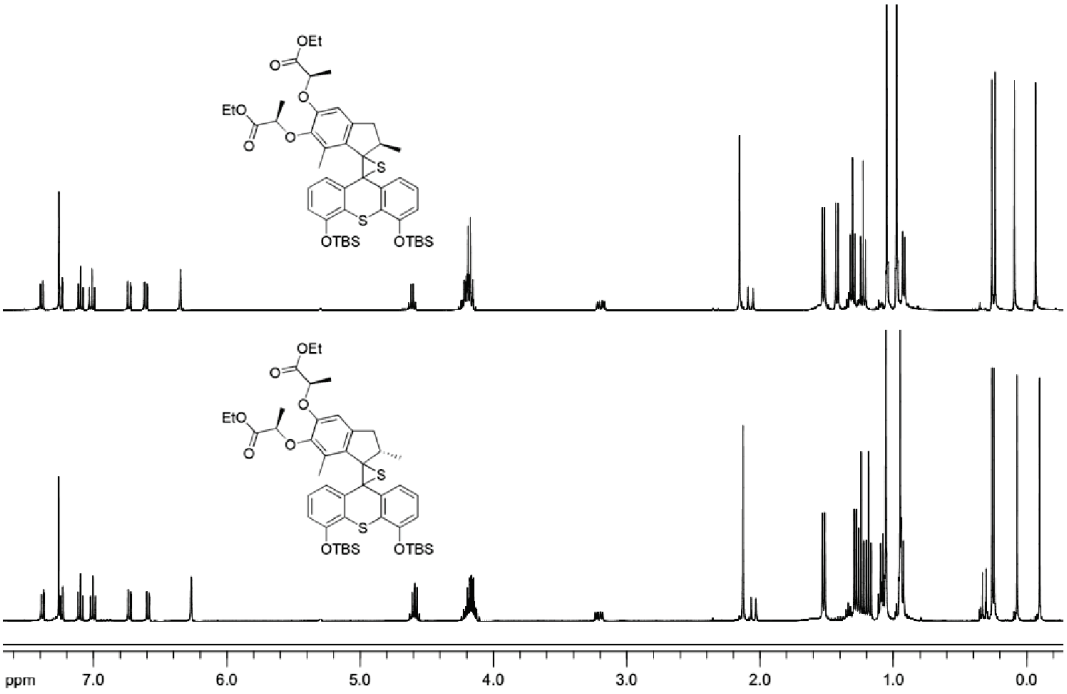

Figure S3 **|** ^{1}H NMR spectrum of episulfide **22**-(*R,R,S*) (bottom) and motor **22**-(*R,R,R*) (top). Solvent: $CDCl_3$

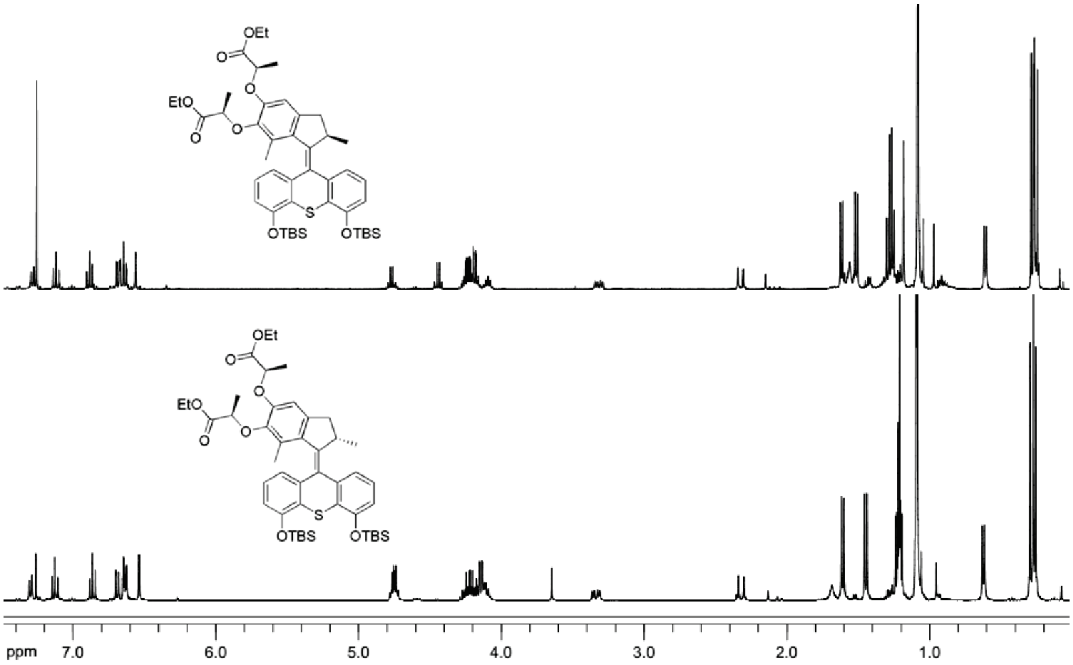

Figure S4 | ^{1}H NMR spectrum of motor **23**-(*R,R,S*) (bottom) and motor **23**-(*R,R,R*) (top). Solvent: $CDCl_3$

4/ Single X-ray diffraction data of episulfide 14-(*R*,*R*,*R*), motor 15-(*R*,*R*,*S*), episulfide 22-(*R*,*R*,*R*).

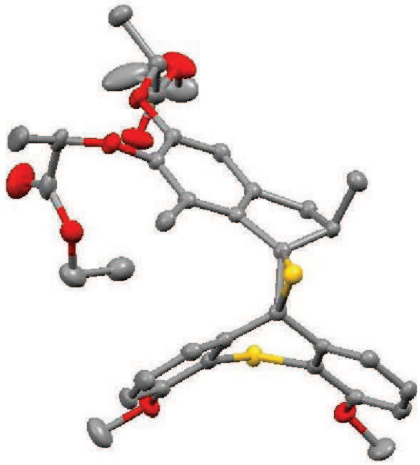

Table S1 | X-ray crystallographic data for 14-(*R*,*R*,*R*)

Chemical formula	$C_{36}H_{40}O_8S_2$	Crystal description	prism, colorless
Chemical formula weight ($g \cdot mol^{-1}$)	664.80	ρ ($g \cdot cm^{-3}$)	1.322
Symmetry cell setting	Orthorhombic	T(K)	173(2)
crystal dimension (mm)	0.30×0.20×0.12	μ (cm^{-1})	18.73
Space group	$P\ 2_12_12_1$	number of reflections	12991
a (Å)	8.8466(3)	number of refined parameters	423
b (Å)	11.2925(3)	$wR(F^2)$	0.0753
c (Å)	33.4252(10)	R factor	0.0296
β (°)	90.00	GooF	1.042
V ($Å^3$)	3339.19	Flack's refinement	0.016(11)
Z	4		

CCDC number: 1016699

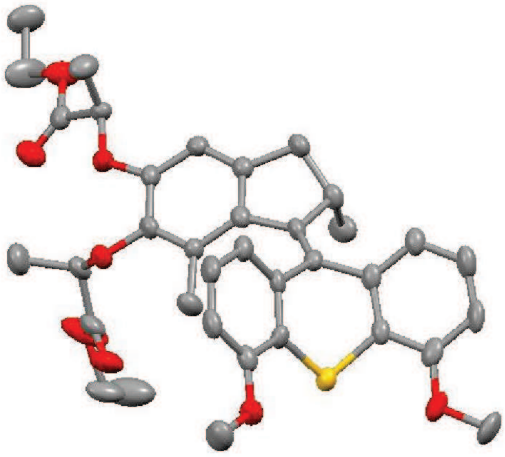

Table S2 | X-ray crystallographic data for motor 15-(*R,R,S*)

Chemical formula	C_{36} H_{40} O_8 S	Crystal description	prism, colorless
Chemical formula weight (g•mol^{-1})	632.24	ρ (g•cm^{-3})	1.169
Symmetry cell setting	Orthorhombic	T(K)	173(2)
Space group	P 2_1	μ (cm^{-1})	11.78
a (Å)	8.4338(2)	number of reflections	44652
b (Å)	40.6995(11)	number of refined parameters	423
c (Å)	19.9343(5)	wR(F^2)	0.0920
β (°)	93.540(2)	R factor	0.082
V (Å^3)	6829.42	GooF	1.050
Z	2	Flack's refinement	0.035(18)

CCDC number: 1016700

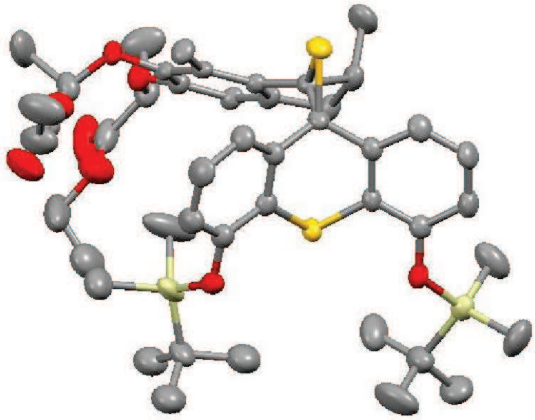

Table S3 | X-ray crystallographic data for 22-(*R*,*R*,*R*)

Chemical formula	$C_{46}H_{64}O_8S_2Si_2$	Crystal description	prism, yellow
Chemical formula weight ($g \cdot mol^{-1}$)	865.36	ρ ($g \cdot cm^{-3}$)	1.188
Symmetry cell setting	Orthorhombic	T(K)	173(2)
crystal dimension (mm)	0.40×0.30×0.20	μ (cm^{-1})	2.08
Space group	P $2_12_12_1$	number of reflections	83463
a (Å)	11.8751(7)	number of refined parameters	1101
b (Å)	18.7850(12)	wR(F^2)	0.1725
c (Å)	43.388(3)	R factor	0.0707
β (°)	90	GooF	1.070
V ($Å^3$)	9678.72	Flack's refinement	0.018(11)
Z	8		

CCDC number: 1016698

5/ DFT calculations

All the intermediates and transition states of the polymer free motors were determined by using Gaussian 09 program package with density functional theory (DFT) (B3LYP).[74] Initial geometry optimizations were performed by Avogadro software, and then refined by using 6-31 G (d,p) basis set using tight convergence criteria. Transition state (TS) was searched by QST2 method. The frequency and vibration were also analyzed to confirm that minima and TS had been reached.

[74] *Gaussian 09, Revision B.01,* Frisch, M. J., Trucks, G. W., Schlegel, H. B., Scuseria, G. E., Robb, M. A., Cheeseman, J. R., Scalmani, G., Barone, V., Mennucci, B., Petersson, G. A., Nakatsuji, H., Caricato, M., Li, X., Hratchian, H. P., Izmaylov, A. F., Bloino, J., Zheng, G., Sonnenberg, J. L., Hada, M., Ehara, M., Toyota, K., Fukuda, R., Hasegawa, J., Ishida, M., Nakajima, T., Honda, Y., Kitao, O., Nakai, H., Vreven, T., Montgomery, Jr., J. A., Peralta, J. E., Ogliaro, F., Bearpark, M., Heyd, J. J., Brothers, E., Kudin, K. N., Staroverov, V. N., Kobayashi, R., Normand, J., Raghavachari, K., Rendell, A., Burant, J. C., Iyengar, S. S., Tomasi, J., Cossi, M., Rega, N., Millam, J. M., Klene, M., Knox, J. E., Cross, J. B., Bakken, V., Adamo, C., Jaramillo, J., Gomperts, R., Stratmann, R. E., Yazyev, O., Austin, A. J., Cammi, R., Pomelli, C., Ochterski, J. W., Martin, R. L., Morokuma, K., Zakrzewski, V. G., Voth, G. A., Salvador, P., Dannenberg,J.J., Dapprich,S.,Daniels,A.D., Farkas,Ö., Foresman, J. B., Ortiz, J. V., Cioslowski, J., Fox, D. J. *Gaussian, Inc.: Wallingford, CT, 2009*.

6/ Theoretical radius of gyration for 8-shaped 39a and 39b

Determinations of theoretical radius of gyration for figure of eight polymers have been made as follow:

Considering a constant polymer molecular weight, we know that: [75,76]

$R_g^{2}{}_{(8\text{-shaped})} = 0.77\ R_g^{2}{}_{(\text{simple ring})} = 0.5 * 0.77 * R_g^{2}{}_{(\text{linear polymer})}$

$R_g^{2}{}_{(\text{linear polymer})} = 1/3 * L_c * L_p$,

L_c being the contour length of the polymer and L_p its persistence length.

Using a L_p value of 3.8 Å, [77] we obtain: $R_{g\ (8\text{-shaped } \mathbf{39a})} = 19.7$ Å and $R_{g\ (8\text{-shaped } \mathbf{39b})} = 27.3$ Å These values should be corrected by the excluded volume, which can be as high as 20 %, and are thus in good agreement with the experiments.

[75] M. Rubinstein.; R. H. Colby. Polymer Physics, Oxford University Press, New York, 53 (2003).
[76] E. Uehara.; T. Deguchi. Statistical and hydrodynamic properties of doublering polymers with a fixed linking number between twin rings. *J. Chem. Phys*.**140**, 044902 (2014).
[77] J. Brandrup and E. H. Immergut. Polymer Handbook, 3rd Edition, J Wiley & Sons (New York) (1989).